The Exploitation of Selected Environmental Bacteria in the Removal of 5-Nitrofuran Derivatives

Amanda Pacholak

Dissertation Presented for the Degree
Doctor of Philosophy

Supervised by
Professor Ewa Kaczorek

Institute of Chemical Technology and Engineering
Poznań University of Technology
Poland 2023

NATIONAL SCIENCE CENTRE
POLAND

Research conducted within this dissertation was supported by the National Science Centre in Poland, OPUS project entitled *Biodegradation of nitrofuran derivatives by environmental bacteria – from metabolic pathways to changes in genome and proteome*. Grant number: 2017/27/B/NZ9/01603.

Principal investigator: Professor Ewa Kaczorek

Acknowledgments

It is hard to believe that the time to write this section of my dissertation has finally arrived. For years this particular moment has seemed so incredibly far away. Many people have supported me in my pursuit of a Doctor of Philosophy degree. Thus, I would like to take this opportunity to express my gratitude.

The person I want to acknowledge first and foremost is my advisor, prof. Ewa Kaczorek. I will be eternally thankful to her for mentorship, exceptional patience, and for the space that I needed to grow as a scientist. I deeply appreciate the time and effort she has contributed to my development since the very beginning of my adventure with science.

I would like to express the sincere gratitude to my collaborators and each co-author of my publications for sharing with me their time, knowledge and ideas. A special thank you goes to prof. Agnieszka Zgoła – Grześkowiak (Poznan University of Technology) and prof. Wojciech Juzwa (Poznan University of Life Sciences).

My sincere gratitude to close colleagues and friends that I have worked with, especially Wojciech Smułek and Natalia Burlaga, who have been both a good co-workers and wonderful friends to me in the last several years. I would like to thank my colleagues from the Department of Organic Chemistry at the Institute of Chemical Technology and Engineering, especially Ewa Dziurla, Jerzy Maciejewski, Adam Grzywaczyk, and Mariusz Sandomierski. I am also grateful to my teachers and students with whom I had a pleasure to work with.

Finally, and most importantly, I want to thank my Mom for her constant support and interest in my progress and success. To Grandma Daniela, thank you for always being there for me. And then, there is Daniel – thank you for being an amazing brother, and Hela – my best four-legged friend – thank you for your constant presence during the writing of this dissertation and for supporting me in your own doggy way.

Because everything else in this document is way too long, I will keep this final dedication short: a big thank you to everyone who has contributed to my dissertation. The work that I have accomplished would not have been possible without all of you.

Podziękowania

Trudno mi uwierzyć, że wreszcie nadszedł czas na napisanie tej części mojej rozprawy doktorskiej. Przez lata ta szczególna chwila wydawała się niewiarygodnie odległa. Wiele osób wspierało mnie podczas studiów doktoranckich, dlatego chciałbym w tym miejscu wyrazić swoją wdzięczność.

Osobą, której pragnę przede wszystkim podziękować, jest moja promotor, prof. Ewa Kaczorek. Jestem i będę Jej dozgonnie wdzięczna za opiekę i wyjątkową cierpliwość. Dziękuję za przyjaźń, a także za czas i wysiłek, jaki wkładała w mój rozwój od samego początku mojej przygody z nauką.

Pragnę serdecznie podziękować wszystkim, z którymi miałam przyjemność współpracować. Dziękuję każdemu współautorowi publikacji za dzielenie się ze mną swoim czasem, wiedzą i pomysłami. Szczególne podziękowania kieruję do prof. Agnieszki Zgoła – Grześkowiak (Politechnika Poznańska) oraz prof. Wojciecha Juzwy (Uniwersytet Przyrodniczy w Poznaniu).

Serdecznie dziękuję bliskim współpracownikom, koleżankom i kolegom, z którymi współpracowałam, zwłaszcza Wojciechowi Smułkowi i Natalii Burladze, którzy byli dla mnie zarówno wspaniałymi współpracownikami, jak i dobrymi przyjaciółmi przez ostatnich kilka lat. Dziękuję wszystkim moim koleżankom i kolegom z Zakładu Chemii Organicznej Instytutu Technologii i Inżynierii Chemicznej, w szczególności pani Ewie Dziurli, panu Jerzemu Maciejewskiemu, Adamowi Grzywaczykowi i Mariuszowi Sandomierskiemu. Dziękuję również wszystkim moim nauczycielom i studentom, z którymi miałam przyjemność współpracować.

Na koniec, szczególne podziękowania dla mojej Mamy za nieustanne wsparcie i wiarę w to, że wszystko będzie dobrze. Dziękuję również Babci Danieli za to, że jest najlepszą babcią na świecie. Daniel – dziękuję za to, że jesteś wspaniałym bratem. Hela – mój najlepszy czworonożny przyjacielu – dziękuję za stałą obecność podczas pisania tej pracy i wspieranie mnie na swój szczególny pieskowy sposób.

Ponieważ wszystko inne w tej pracy jest o wiele za długie, chciałabym krótko podziękować wszystkim, którzy przyczynili się do powstania tej pracy. Praca, którą wykonałam, nie byłaby bez Was możliwa.

Contents

Abstract

Nitrofuran derivatives are synthetic, broad-spectrum antibiotics. Their excessive consumption poses a risk of environmental pollution which can be dangerous for organisms at various trophic levels. To minimize these adverse effects, understanding of their environmental impact and development of efficient strategies of their removal is essential. The overall purpose of this dissertation is to explore the biodegradation of selected nitrofurans by bacteria and to understand how they affect the properties of environmental strains. Results are based on five full length research articles published in journals indexed by the Journal Citation Reports. The experiments performed were focused on the single bacterial cells and microbial communities in terms of their short-time exposure to nitrofurantoin (NFT) (P1, P3, P5) as well as single strains subjected to prolonged exposure to nitrofurantoin and furaltadone (FTD) (P2, P4).

Publication P1 describes (i) the isolation of pure bacterial strains from the municipal and rural activated sludge, (ii) the ability of these novel strains to degrade NFT, and (iii) the effect of NFT on the cell properties. The results indicate that both sources of wastewater contain the strains capable of using NFT as a source of carbon and energy. Nitrofurantoin affects the properties of the strains; however, the cells response is not unequivocal.

Publication P3 focus on (i) efficiency of biodegradation of NFT by microbial consortia collected from two aqueous environmental niches, (ii) detection of products of NFT transformation, and (iii) analysis of shifts in microbial communities during biodegradation. Results of experiments revealed that aqueous bacterial communities are influenced by NFT. The results also show that increase in biodiversity of microbial community does not have to be correlated with increased ability to biodegradation. The primary biodegradation of NFT led to formation of stable transformation products, such as 1-aminohydantoin, semicarbazide, and hydrazine.

Publication P5 investigates (i) removal of NFT by three novel bacterial species, (ii) dynamic changes within the cells during biodegradation, and (iii) effect of transformation products on the bacterial cells. Results indicate, among others, that the fewest variations in cell properties were observed for the bacteria that efficiently degrade NFT.

Publications P2 and P4 are related with the response of single bacterial strains to the 12-month continuous exposure to NFT and FTD. The results indicate that prolonged exposure of strains to nitrofurans contributed to morphological changes within the cells, altered metabolomic characteristics, disrupted protein biosynthesis, accelerated mutagenic effects, and promoted oxidative stress. Remarkable changes in enzymatic activity reflect that cell exposure to nitrofurans decreases their ability to cope with environmental stress.

To conclude, environmental bacteria are able to use NFT as a source of carbon and energy, however, this degradation leads to formation of stable transformation products, that affect the properties of cells. The possible NFT contamination would affect the composition of aqueous microbial communities. Prolonged exposure of strains to nitrofurans leads to modifications of cell structure and cell metabolism. These effects are strain specific. This dissertation has contributed to a better understanding of the environmental impact of nitrofurans and its intermediates. Results could be helpful during designing the technologies of bioremediation of sites contaminated with antibiotics.

Streszczenie

Pochodne nitrofuranu to syntetyczne antybiotyki o szerokim spektrum działania. Znaczne wykorzystanie nitrofuranów powoduje, że związki te przedostają się do środowiska naturalnego, co może mieć negatywny wpływ na (mikro)organizmy tam bytujące. W związku z tym, niezbędne jest poznanie wpływu nitrofuranów na środowisko i opracowanie skutecznych strategii ich usuwania. Celem podjętych badań było zbadanie biodegradacji wybranych nitrofuranów przez bakterie środowiskowe i zrozumienie, w jaki sposób wpływają one na szczepy bakterii środowiskowych. Wyniki przedstawione w dysertacji zostały opublikowane w pięciu artykułach badawczych w czasopismach indeksowanych przez Journal Citation Reports. Dotyczą one badań z pojedynczymi, nowo wyizolowanymi, szczepami bakteryjnymi oraz konsorcjami bakteryjnymi pod kątem ich krótkotrwałej ekspozycji na nitrofurantoinę (NFT) (P1, P3, P5) oraz pojedynczymi szczepami poddanymi długotrwałej ekspozycji na NFT i furaltadon (FTD) (P2, P4).

Publikacja P1 opisuje (i) izolację pojedynczych szczepów bakteryjnych z miejskiego i wiejskiego osadu czynnego, (ii) zdolność nowych szczepów do degradacji NFT oraz (iii) wpływ NFT na komórki bakteryjne. Wyniki wskazują, że oba źródła drobnoustrojów zawierają szczepy zdolne do wykorzystania NFT jako źródła węgla i energii. Ponadto, NFT znacząco wpływa na przepuszczalność błony komórkowej, hydrofobowość powierzchni komórki czy aktywność metaboliczną komórek; jednak zmiany te są niejednoznaczne. Publikacja P3 obejmuje wyniki poświęcone (i) biodegradacji NFT przez konsorcja mikroorganizmów pobrane z dwóch środowisk wodnych, (ii) oznaczeniu produktów biotransformacji NFT oraz (iii) analizie zmian w strukturze i bioróżnorodności konsorcjów bakteryjnych podczas biodegradacji. Wyniki badań wykazały, że obecność NFT w hodowli bakteryjnej przyczynia się do istotnych zmian w strukturze konsorcjów bakteryjnych. Ponadto, wyższa bioróżnorodność konsorcjów bakteryjnych nie wskazuje na większą zdolność do biodegradacji. Pierwotna biodegradacja NFT doprowadziła do powstania stabilnych produktów degradacji, takich jak 1-aminohydantoina, semikarbazyd i hydrazyna. W publikacji P5 zanalizowano (i) biodegradację NFT przez trzy nowo wyizolowane szczepy bakterii, (ii) zmiany w komórkach podczas biodegradacji NFT oraz (iii) wpływ produktów degradacji na wykorzystywane szczepy. Wyniki wskazują, między innymi, że wysokim zdolnościom do biodegradacji NFT towarzyszą najmniejsze zmiany we właściwościach komórek testowanych szczepów. Publikacje P2 i P4 dotyczą odpowiedzi pojedynczych szczepów bakteryjnych na długotrwały kontakt z NFT i FTD. Wykazano, że długotrwała ekspozycja szczepów na nitrofurany przyczyniła się do zmian zachodzących w komórkach na poziomie ich właściwości morfologicznych, biosyntezy białek, efektów mutagennych czy zwiększonego stresu oksydacyjnego.

Podsumowując, bakterie środowiskowe wykazują zdolność do wykorzystywania NFT jako źródła węgla i energii, jednakże biodegradacja prowadzi do powstania stabilnych produktów pośrednich, które istotnie wpływają na właściwości komórek. Zatem, zanieczyszczenie środowiska naturalnego pochodnymi nitrofuranu może przyczyniać się do zmian w mikrobiomie środowisk wodnych. Ponadto długotrwała ekspozycja szczepów bakteryjnych na antybiotyki nitrofuranowe prowadzi do istotnych modyfikacji struktury komórek i ich metabolizmu. Wyniki opisane w niniejszej rozprawie przyczyniają się do lepszego zrozumienia wpływu nitrofuranów na środowisko naturalne, jak również mogą być pomocne przy projektowaniu technologii bioremediacji miejsc skażonych antybiotykami.

List of abbreviations

5-NFs	(5-)nitrofurans
8-oxodD	8-Oxo-2'-deoxyguanosine
aa-tRNA	Aminoacyl-tRNA
Acb	*Achromobacter pulmonis (xylosoxidans)* NFZ2
AFM	Atomic force microscopy
AHD	1-aminohydantoin
AMOZ	3-amino-5-morpholino-methyl-1,3-oxazolidinone
AOZ	3-amino-2-ozaxolidinone
CAT	Catalase
CSH	Cell surface hydrophobicity
DAMs	Differentially accumulated metabolites
EU	the European Union
FC	Flow cytometry
FDA	U.S. Food and Drug Administration
FTD	Furaltadone
FZD	Furazolidone
GSH	Glutathione
GSTs	Glutathione-S-transferases
HYD	Hydrazine
IMP	Inner membrane permeability
K3a	*Sphingomonas paucimobilis* K3a
K3b	*Ochrobactrum antrophi* K3b
LC-MS/MS	Liquid chromatography coupled with mass spectrometry
LPX	Lipid peroxidation
MBT	Mechanical biological treatment
MetAct	Metabolic activity
mNGS	Metagenomic next generation sequencing
MHA	Mueller Hinton Agar
MRPL	Minimum required performance limit
NBA	2-nitrobenzaldehyde
NFT	Nitrofurantoin

NFZ	Nitrofurazone
NW	Mountain stream water sample
OECD	Organisation for Economic Co-operation and Development
P3d	*Sphingobacterium thalpophilum* P3d
P4a	*Pseudomonas aeruginosa* P4a
P4c	*Rhizobium radiobacter* P4c
PCA	Principal component analysis
PdI	Polydispersity index
PS	Particle size distribution
Psd	*Pseudomonas hibiscicola* FZD2
Psi	*Pseudomonas indoloxydans* WB
R3z	Average roughness depth
Ra	Average roughness
RAPD-PCR	Random amplification of polymorphic DNA
RASFF	Rapid Alert System for Food and Feed
RMA	Relative metabolic activity
RMS	Root mean square roughness
SEM	Semicarbazide
SOD	Superoxide dismutase
Sph	*Sphingobacterium siyangense (caeni)* FTD2
Srm	*Serratia marcescens* ODW152
SS	Seaport water sample
Sta	*Stenotrophomonas acidaminiphila* N0B
Stm	*Stenotrophomonas maltophilia* FZD2
TEM	Transmission electron microscopy
TMP	Outer membrane permeability
TOC	Total organic carbon
TPs	Transformation products
WGS	Whole genome sequencing
WWTP	Wastewater treatment plant
ZP	Zeta potential
λq	Wavelength of the profile

Chapter 1

Literature review

Brief introduction to antibiotics

It has been almost a hundred years since Alexander Fleming accidentally noticed that a large colony of a mold contaminating an agar plate prevents the bacteria around it from growing (Fleming, 1929). This event most likely happened on September 3, 1928 and definitely changed the course of medicine. It was one of the most important achievements of the 20th century (Felis et al., 2020). A decade later, the golden era of antibiotics has begun (Balouiri et al., 2016). Nowadays, these powerful compounds are the most produced drugs worldwide as they have contributed to economic development and living standards of the modern world (Grenni et al., 2018; Kumar et al., 2019).

Antibiotics are biologically active molecules that kill or inhibit the growth of microorganisms, such as bacteria, fungi, or protozoa. They have bactericidal (causing cells to die) or bacteriostatic (inhibiting growth) effect on cells. Antibiotics can be natural, synthetic, or semi-synthetic. They are also referred to as chemotherapeutic or antimicrobial agents, however, these terms do not mean exactly the same. Chemotherapeutics are chemicals that destroy all types of cells (both microbial and cancer cells) while antibiotics specifically kill microorganisms (that is why antibiotic therapy is also called antimicrobial chemotherapy). In addition, the term *antibiotic* is referred to substances of biological origin whereas the term chemotherapeutic agent refers to synthetic chemicals. Currently all drugs are produced by either chemical synthesis or chemical modification of natural compounds. Therefore, distinction between antibiotics and chemotherapeutics is not clear and the term *antibiotic* is often used to refer to all types of antimicrobial agents (Kümmerer, 2009; Madigan et al., 2018).

Antibiotics constitute a broad group of chemicals that play a vital role in curing infectious diseases and promoting animal growth. The mass production and excessive consumption of antibiotics has contributed to a heightened risk of environmental pollution (Danner et al., 2019). Fourteen years ago, more than 250 various chemical compounds were registered as antibiotics for human and animal use (Kümmerer, 2009). As of today, this value probably is not much higher. Even though many researchers are interested in development of plant extracts, essential oils, and pure secondary metabolites as potential antimicrobial agents, only two new antibiotic classes (lipopeptides and oxazolidinones) have been designed and approved by international drug agencies between 1997 and 2017 (Álvarez-Martínez et al., 2021; Barzegar et al., 2021; Chassagne et al., 2021; Dawood et al., 2021; Tacconelli et al., 2018). Lack of interest in development of new antibiotics by pharmaceutical companies is likely to be related with difficulties in clinical development as well as regulatory, scientific, and economic issues (Tacconelli et al., 2018). In addition, determining the specific and accurate effect of the novel natural products is difficult because of the insufficient guidelines and the use of different non-standardized approaches by researchers (Balouiri et al., 2016). Considering all these facts, a renewed interest in old antibiotics groups, the use of which has been reduced in the recent past is currently being observed.

There are several groups of antibiotics which can be classified based on their mechanisms of action or chemical structure. The most well-known classes of antibiotic compounds include β-lactams, tetracyclines, aminoglycosides, macrolides, glycopeptides, sulfonamides, trimethoprim and (fluoro)quinolones (**Tab. 1**) (Felis et al., 2020; Kümmerer, 2009). Within this group, β-lactams, macrolides, and fluoro-quinolones were the most frequently used globally in the last decades (Van Boeckel et al., 2014). Their environmental impact is well documented (Ajibola et al., 2021; Han et al., 2022; Monahan et al., 2023; Nesse et al., 2022; Szekeres et al., 2018; Tan et al., 2018; Tran et al., 2019). Other antibiotics groups include, among others, actinomycines, amino acid and peptide derivates, anthracyclines, anthracenones, diaminopyrimidines, enediynes, epothilones, glycopeptides, lincosamides, macrolides, mitosanes, nitrofurans (5-NFs), nitroimidazoles, phenicols and amphenicols, phosphonates, polyether ionophores, rifamycins (Grenni et al., 2018).

Tab. 1 Common classes of antimicrobials and their representative substances.

Class	Representative compounds
β-lactams	Amoxicillin, ampicillin, benzylpenicillin, cefuroxime, cefotaxime, penicillin G, piperacillin, meropenem
Aminoglycosides	Amikacin, gentamycin, kanamycin, neomycin, streptomycin
Glycopeptides	Polymyxins, vancomycin
Macrolides	Azithromycin, clarithromycin, erythromycin, natamycin, tylosin
Fluoroquinolones and quinolones	Ciprofloxacin, enrofloxacin, oxolinic acid
Sulfonamides and trimethoprim	Sulfachloropyridazine, sulfamethoxazole, sulfapyridine
Tetracyclines	Chlortetracycline, doxycycline, oxytetracycline, tetracycline

Characterization of nitrofurans

Nitrofurans are synthetic, bactericidal, broad-spectrum antimicrobials. These crystalline and yellow aromatic compounds contain a common 5-nitrofuran core connected through a methylenamine bridge with various substituent groups at the 2-position of the furan ring (**Fig. 1**, **Tab. 2**) (Manzetti and Ghisi, 2014). Nitrofuran molecules contain two pharmacophores: a nitro group attached to a furan ring (pale brown in **Fig. 1**) and a hydrazone moiety (violet in **Fig. 1**). The nitro group is the primary pharmacophore in the nitrofuran molecules, while hydrazone moiety contain carbon atom that has zwitterionic properties and supports the overall chemical stability of the nitrofuran ring (Zuma et al., 2019).

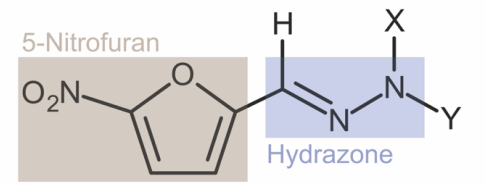

Fig. 1 Schematic representation of the chemical structure and pharmacophores present in the nitrofuran molecules. X, Y = hydrogen atom or R-group. Adapted from Zuma et al. (2019).

Despite nitrofurans are old drugs, their mechanism of action against bacteria is not fully understood. Most information about nitrofurans action is based on decades-old studies which used outdated laboratory equipment and analytical techniques. Nitrofurans probably present multiple mechanisms of action such as inhibition of enzymes involved in DNA and RNA synthesis. Thus, nitrofurans attack multiple key metabolic pathways in microorganisms, such as replication, translation, transcription, and the Krebs cycle. Due to the multiple biological targets, no significant resistance against these antibiotics has developed in bacteria (Huttner et al., 2015; McOsker and Fitzpatrick, 1994).

The most common representatives of the nitrofuran family include nitrofurantoin (NFT), furaltadone (FTD), nitrofurazone (NFZ), and furazolidone (FZD). Their molecular formulas and chemical structures are summarized in **Tab. 2**. Other examples of nitrofurans include furazidin, nifurtoinol, nitrofural, nifurzide, nifuratel, nifurtimox, nifuroxazide, nifursol (Cooper et al., 2018; Olender et al., 2018; Zuma et al., 2019).

Tab. 2 Molecular formulas and structures of most common nitrofuran derivatives.

Compound	Molecular formula	Molecular weight [g/mol]	Structure
Nitrofurantoin (NFT)	C8H6N4O5	238.16	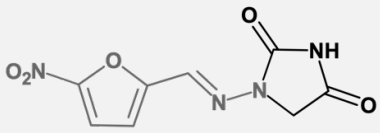
Nitrofurazone (NFZ)	C6H6N4O4	198.14	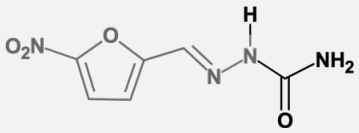
Furazolidone (FZD)	C8H7N3O5	225.16	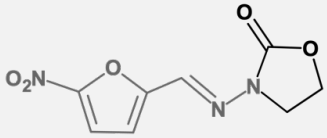
Furaltadone (FTD)	C13H16N4O6	324.29	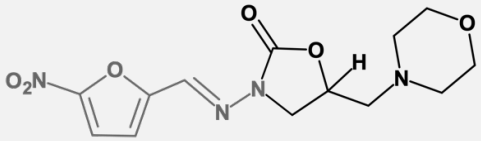

Nitrofuran antibiotics have been employed as pharmaceuticals, food additives, conservatives, and growth promoters in food animals since 1940s. They were once commonly used in growth promotion of animals (poultry, swine, cattle), aquaculture (fish, shrimp), and bee colonies. In veterinary medicine, they had been commonly used in the therapeutic and prophylactic treatment of bacterial and protozoan infections of swine, cattle, poultry, and rabbits (Vass et al., 2008). Currently, they are no longer permitted for use in food-producing animals in the European Union (EU). In some third countries, nitrofurans can be legally used in aquaculture to prevent or control bacterial diseases of fish and crustaceans, however, specific information on the actual usage is not available. In human medicine, NFT, NFZ, and FZD are still commonly used (**Fig. 2**) (European Food Safety Authority, 2015).

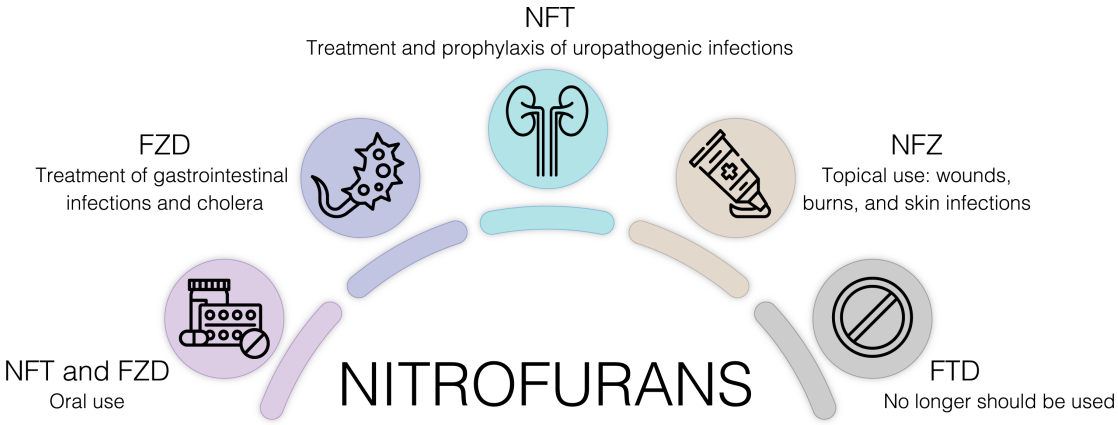

Fig. 2 Common areas of application of four main nitrofuran compounds. NFT– nitrofurantoin, FZD – furazolidone, NFZ – nitrofurazone, FTD – furaltadone, UTI – urinary tract infections.

Nitrofurantoin, N-(5-nitro-2-furfurylidene)-1-aminohydantoin, is a cyclic amide containing the 5-nitrofuran ring (Zuma et al., 2019). It has been introduced and approved by the U.S. Food and Drug Administration (FDA) as the first-line therapy for acute and chronic lower urinary tract infections in 1953 (Horton, 2015; Huttner et al., 2015). Nitrofurantoin is currently available as an oral capsule and an oral suspension. It has a bactericidal effect against Gram-negative uropathogens such as *Escherichia coli* or *Enterococcus faecalis* (Huttner et al., 2015; Novelli and Rosi, 2017). Its activity against *Mycobacterium tuberculosis* has been also reported (Zuma et al., 2020). Bioavailability is reported to be 80-90%, elimination half-live is smaller than one hour and the drug is predominantly excreted unchanged non-metabolized in the urine (Huttner et al., 2015; Novelli and Rosi, 2017). Some authors declare that <50% is excreted unchanged in the urine (Gardiner et al., 2019; Hammam, 2002).

Furaltadone, 5-morpholinomethyl-3-(5-nitrofurfurylideneamino)-2-oxazolidinone, was introduced in 1958. It is the least known antibiotic in the nitrofurans family. Furaltadone is active against many Gram-negative and Gram-positive bacteria, especially *E. coli* and *Salmonella* spp. It was formerly used to promote growth, treat, and prevent bacterial infections in aquatic organisms (Barbosa et al., 2011). In human

therapy, FTD was also given orally as an antibacterial agent. It was later withdrawn due to its toxicity, however, recent studies show the ability of FTD to inhibit allergic responses (Nam et al., 2018).

Nitrofurazone, [(E)-(5-nitrofuran-2-yl)methylideneamino]urea, is a hydrazine derivative of carboxamide containing the 5-nitrofuran ring. It is the only compound in the nitrofurans family that lacks the second cyclic moiety (Zuma et al., 2019). Nitrofurazone was the first nitrofuran antibiotic whose antimicrobial activity has been confirmed in 1944 (Zhang et al., 2016). It is used in topical formulations on infected burns, ulcers, wounds, and skin infections (Vass et al., 2008; Zuma et al., 2019). Due to wound healing activity, nitrofurazone can be used as topical antimicrobial agent in novel wound dressing systems based on polyvinyl alcohol and sodium alginate hydrogels (Kim et al., 2008). Its activity against parasites of the species *Trypanosoma brucei* has also been reported, however due to high toxicity its use in oral applications is currently not allowed (La-Scalea et al., 2005).

Furazolidone, 3-[(5-nitrofuran-2-yl)methylideneamino]-1,3-oxazolidin-2-one, is a 2-oxazolidone derivative of 5-nitrofuran. It is active against Gram-positive and Gram-negative bacteria, particularly the gastrointestinal pathogens, such as *E. coli* and *Salmonella* spp. Use in treating *Helicobacter pylori* infections has been proposed (De Francesco et al., 2012). Furazolidone has also antiprotozoal activity against *Giardia lambia*, *Eimeria* spp., *Leishmania*, *Trichomonas* and *Trypanosoma* (Zuma et al., 2019). This antibiotic is used for the oral treatment of cholera, typhoid fever, *Salmonella* infections, bacterial diarrhea and parasitic diseases (Vass et al., 2008).

All nitrofuran compounds are believed to be unstable and rapidly metabolized to residues that covalently bind to tissue proteins and are detectable for several weeks after exposure. The tissue-bound residues of nitrofurans are stable and not degradable upon common food preparation techniques like baking, cooking, microwaving, or grilling (Shakila et al., 2008). Consequently, these substances act as marker residues for the detection of nitrofurans abuse (Leston et al., 2011; Vass et al., 2008; Zuma et al., 2019). The most well-known metabolites of nitrofurans include:

- 1-aminohydantoin (AHD) – the marker residue for NFT.
- 3-amino-5-morpholino-methyl-1,3-oxazolidinone (AMOZ) – the marker residue for FTD.
- Semicarbazide (SEM) – the marker residue for NFZ.
- 3-amino-2-ozaxolidinone (AOZ) – the marker residue for FZD.

Why nitrofurans are prohibited from use in food-producing animals?

At present, the use of 5-NFs in food-producing animals has been forbidden in many countries including the EU and the US (Kokulnathan and Chen, 2020). The reason for this is the possible genotoxic, carcinogenic, and non-neoplastic effects of nitrofurans and their marker metabolites in animals (European Food Safety Authority, 2015; Takahashi et al., 2000). In addition to genotoxic and carcinogenic impact, nitrofurans effect toward humans include, among others, acute and chronic pulmonary toxicity (Claussen et al., 2017; Goemaere et al., 2008; Livanios et al., 2016; Williams and Triller, 2006), hepatotoxicity (Bessone et al., 2023; Claussen et al., 2017; Kapral et al., 2018; Li et al., 2019), and neurotoxicity (Dempsey et al., 2019; Tian et al., 2021).

These compounds accumulate in organisms of animals which enhances this adverse effect. To investigate how nitrofuran residues accumulate in animal tissues Mccracken et al. (2005) exposed chickens to both a dietary and an environmental source of nitrofurans. During dietary exposure, chickens were fed a diet supplemented with one of the nitrofurans (FZD, NFZ, NFT, or FTD) at five different concentrations ranging from 30 to 3,000 mg/kg. At the lowest concentration of nitrofurans contamination, nitrofuran residues, namely AOZ, AMOZ, and SEM, were detected in the liver and muscle of the birds. To investigate environmental source of contamination, animals were placed in a pen that was previously occupied by chickens fed a diet containing nitrofurans. A 24-hour exposure of animals to the litter of chickens fed with FZD resulted in elevated level of FZD residues in liver and muscle.

Due to the adverse effect of nitrofurans to humans and animals, FTD, NFT, and NFZ were prohibited from use in food-producing animals in the EU in 1990 by their inclusion in Annex IV of Council Regulation 2377/90. Furazolidone was included in Annex IV five years later in 1995. Consequently, the legal application of nitrofurans in food-producing animals is not allowed in all EU countries, starting from 1 January 1997 (Barbosa et al., 2011; Commission Regulation, 1995; Leitner et al., 2001). Theoretically, there is a zero-tolerance policy for any nitrofuran residue and food producing animals must be completely free of these compounds. This means that no maximum concentration of nitrofurans residues is permitted in food of animal origin.

The minimum required performance limit (MRPL)[1] of 1 μg/kg was assigned for nitrofuran metabolites in poultry meat and aquaculture products in the EU in 2003 (Commission Decision, 2003). More recently, the MRPL level was reduced to 0.5 μg/kg for all nitrofurans and their metabolites (Commission Regulation, 2019). This regulation has been effective since November 2022. In the US the tolerance level for AHD, AMOZ, SEM, and AOZ is set up to 0.5 μg/kg (U.S. Food and Drug

[1] The minimum required performance limit (MRPL) is the concentration of a Prohibited Substance or Metabolite of a Prohibited Substance or Marker of a Prohibited Substance or Method that Laboratories shall be able to routinely detect and identify.

Administration, 2020). This, however, indicates that levels below 0.5 μg/kg are still acceptable in both the US and the EU.

Nitrofurans are detected in animal food products

Even though their use in food animal production is prohibited in many countries, nitrofurans are often found in animal food products. Between 2000 and 2015, more than 700 notifications of nitrofuran contamination in the EU have been reported in the online database of the Rapid Alert System for Food and Feed (RASFF). The ranges of the reported concentrations are the following:

- From 0.3 to 40 μg/kg for AHD (indicator of NFT contamination)
- From 0.3 to 140 μg/kg for AMOZ (indicator of FTD contamination)
- From 0.37 to 7 500 μg/kg for SEM (indicator of NFZ contamination)
- From 0.1 to 200 μg/kg for AOZ (indicator of FZD contamination)

Importantly, AOZ and SEM were reported the most often. The residues were detected in such imported products as crustaceans, poultry, fish, meat other than poultry, honey, eggs, food additives and flavorings, prepared dishes, and snacks (European Food Safety Authority, 2015).

Unfortunately, notifications of nitrofuran contamination in the EU are still reported in the RASFF. Some of them are summarized in **Tab. 3**. In the last three years, nitrofuran residues were mostly detected in meat and seafood products imported from the East (e.g., China, Sri Lanka, India, Pakistan, Vietnam). Most notifications on nitrofurans presence are marked as the ones presenting a serious health risk for humans. The countries in question are also among the top exporters of seafood in the US, however, only about 2% of imported products are tested by the FDA to detect any trace level of antimicrobials. Considering a very small amount of food inspected, antibiotic residues are still a major problem in imported seafood (Khan and Lively, 2020).

Many recent research studies were recently devoted to detection of nitrofurans presence in food products of animal origin. Gong et al. (2020) detected nitrofuran metabolites in Gelatin Chinese medicine: SEM (1.27 μg/kg and 2.52 μg/kg), AOZ (6.27 μg/kg) and AMOZ (9.53 μg/kg). Yuan et al. (2020) investigated occurrence of eight nitrofurans in freshwater and marine fish samples collected from South China. The residues of SEM, AOZ, AMOZ, and AHD were detected in the animal tissue. The detected content of these compounds reached 8 μg/kg. A recent study by Khan and Lively (2020) aimed to determine if imported shrimps available in the US markets contain, among others, nitrofuran residues. Almost all samples tested positive for nitrofurantoin residue (this was the most often detected antibiotic among all samples tested). Shrimp containing NFT residue were imported from Bangladesh (100% of samples), Ecuador (100%), Vietnam (86%), Thailand (77%), India (67%), Indonesia (60%), and China (33%). In aquaculture-commercial fish (trout, shad, pacú and

salmon) purchased in Argentina, FZD was detected in 22% of the tested samples with the maximum concentration of 11,558 μg/kg d.w. Nitrofurantoin was detected in 4% of samples at a maximum concentration of 8.61 μg/kg d.w. Residues of other nitrofurans were not analyzed (Griboff et al., 2020). Elevated level of two nitrofurans was also detected in muscles of Nile tilapia in Egypt. Nitrofurazone was the most frequently detected antibiotic (12% of all tested samples, concentration ranging from 9 to 52 μg/kg), followed by NFT (5% of samples tested, concentration ranging from 1 to 2 μg/kg) (Eissa et al., 2020).

Tab. 3 Notifications in RASFF on the presence of nitrofurans and their metabolites in animal food products imported into the EU.

Compound	Product	Date	Notifying country
SEM	Pork casings from China	Jan 2023	Germany
SEM	Shrimps (*Macrobrachium rosenbergii*) from Sri Lanka	Dec 2022	Germany
AOZ	Shrimps from India	Oct 2022	Belgium
SEM	Pork casings from China	Jul 2022	Poland
SEM	Gelatin from Pakistan	Jun 2022	Italy
AOZ	Feed for bees	Mar 2022	Ireland
FZD	Iridescent shark (*Pangasianodon hypophthalmus*)	Feb 2022	Netherlands
AOZ	Frog legs from Vietnam	Jan 2022	Denmark
SEM	Live crayfish (*Astacus leptodactylus*) from Turkey	Nov 2021	Germany
FZD	Frozen frog legs from Vietnam	Sep 2021	France
AOZ	Frozen shrimps from India	Sep 2021	Germany
FZD	Frozen frog legs from Vietnam	May 2021	France
FZD	Shrimps from India	Mar 2021	France
AOZ	Frozen shrimps from India	Aug 2020	Netherlands
5-NF n/s	Honey	May 2020	Belgium
5-NF n/s	Aquaculture shrimps from India	Apr 2020	France

Note. AOZ (3-amino-2-ozaxolidinone - the marker residue for furazolidone); FZD (furazolidone); SEM (semicarbazide – the marker residue for nitrofurazone), 5-NF n/s – nitrofuran not specified.

Ubiquitous presence of nitrofuran residues in animal food products suggests that nitrofurans are illegally used in aquaculture. Because nitrofuran residues are found in numerous samples around the world, many researchers work on development of novel tools and methods for screening tests and detection in various samples (from food to environmental matrixes) (Cheng et al., 2023; Krishnan et al., 2023; Li et al., 2017; Yuan et al., 2020). The analytical strategy for nitrofurans quantification is based on the determination of parent compounds and/or their persistent metabolites. Detection of nitrofurans in food products is typically based on instrumental methods, such as gas chromatography, liquid chromatography, electrochemical sensors, immunoassays, or fluorescence quenching (An et al., 2020; Chen et al., 2020; Cheng et al., 2023; Douny et al., 2013; Krishnan et al., 2023; Li et al., 2017; Liu et al., 2023; Ouyang et al., 2022; Roushani and Rahmati, 2019; Wang et al., 2022, 2020; Yang et al., 2022). New methods for nitrofuran quantification allow for their detection at a concentration as low as 0.1 μg/kg (Ouyang et al., 2022) or below 1 ng/mL (Cheng et al., 2023; Liu et al., 2023; Wang et al., 2022).

Consumption of antimicrobials

Over the last few decades, the global antibiotic consumption has been largely increasing in both human and animal use, as is evidenced by many studies (Browne et al., 2021; Klein et al., 2021, 2018, 2018; Van Boeckel et al., 2015, 2014). Below are some of the main reasons for the increasing global antibiotics consumption:

- Increase in human population that intensified the consumption of pharmaceuticals (according to the United Nations, the World population has reached eight billion in 2022 and is expected to reach about ten billion until 2060).
- Easy access to medicines in high income countries and increased global wealth.
- Increased demand for food of animal origin which requires a larger use of growth promoting substances (Food and Agriculture Organization, 2018; United Nations, 2022; Van Boeckel et al., 2015; Zhao et al., 2019).

Based on a recent spatial modelling study that covered the period of 19 years and 204 countries, a global antibiotic consumption rate by humans increased by 46% in 2018 relative to 2000. A large increase in the consumption of fluoroquinolones and third generation cephalosporins in North Africa and Middle East, and south Asia was identified (Browne et al., 2021). Another study, based on pharmaceutical sales data in 76 countries has shown that between 2000, and 2015 global per-capita consumption of *Watch*[2] antibiotics increased by more than 90%. Consumption of *Access* antibiotics increased by over 26% (Klein et al., 2021).

[2] In 2017, WHO developed the AWaRe Classification of antibiotics (Access, Watch, Reserve). *Access* antibiotics are typically used as first-line therapy. *Watch* group is recommended only for specific indications due to higher antimicrobial resistance potential. *Reserve* group is the last resort option and should be reserved for treatment of confirmed or suspected infections due to multi-drug-resistant organisms.

Antibiotic use per capita is generally the highest in high-income countries, but the greatest increase in antibiotic use is observed in low- and middle-income countries (Klein et al., 2021; Van Boeckel et al., 2014). India, China, and the US were the largest consumers of antibiotics in 2010. The use of antibiotics for both humans and animals in China was 162,000 tons in 2013 (**Tab. 4**). Human consumption accounted for 48% and veterinary use for 52% (Zhang et al., 2015). In the EU, 3,821 tons of active substance of antimicrobials were sold for use in humans and 8,927 tons for food-producing animals in 2014. Within the EU, the use of antimicrobials in Poland accounted for 841 tons (European Centre for Disease Prevention and Control et al., 2017).

Tab. 4 Antibiotic consumption in the EU and China.

	The EU (2014)	Poland (2014)	China (2013)
Total antibiotic consumption (tons/year)	12,748	841	162,000
Human consumption	30%	31%	48%
Animal consumption	70%	69%	52%

Note. The above information is based on (ECDC, 2017) and (Zhang et al., 2015).

There are two main reasons for use of antimicrobial agents in animal farming. Firstly, antibiotics act as growth promoters to improve productivity of domesticated animals. Secondly, antibiotics are improper low-cost substitutes for hygiene measures that could prevent infections in animals (Van Boeckel et al., 2017).

Antibiotics use for growth promotion has been restricted in the EU since 2006 and the US since 2017. They are, however, still used in other countries such as China or India (Kokulnathan and Chen, 2020; Kumar et al., 2019; Robinson et al., 2018). The worldwide use of antimicrobials in food animals was estimated at 131,109 tons in 2013 and, unfortunately, is projected to reach 200,235 tons by 2030. The largest producer and consumer of veterinary antimicrobials in the world is China. In 2018, almost 29,800 tons of antimicrobials were used in food animals of which 53% was used to promote animal growth (Ma et al., 2021). The use of antibiotics in food animals exceeded 14,600 tons in 2012 in the US (Food and Drug Administration, 2014) and 8,9 tons in the EU (European Centre for Disease Prevention and Control et al., 2017).

Overall, the most frequently consumed antibiotics in the EU in human medicine were penicillins, macrolides and fluoroquinolones, whereas tetracyclines, penicillins and sulfonamides were the most used antimicrobial classes in veterinary medicine (European Centre for Disease Prevention and Control et al., 2017). In the report provided by the European Centre for Disease Prevention and Control (2017), nitrofurans were among antibiotics not included in the evaluation despite an increase in the use of nitrofurantoin was observed between 2013 and 2015 (Dolk et al., 2018).

Occurrence of antibiotics in the environment

The mass production and excessive consumption of antibiotics and other pharmaceuticals have contributed to a heightened risk of environmental pollution. Several thousand tons of antimicrobials and their transformation products are introduced to the environment annually (Felis et al., 2020). A study conducted in 2015 revealed that more than 600 various pharmaceuticals have been detected in the natural environments in more than seventy countries on each continent (aus der Beek et al., 2016).

Not surprisingly, numerous antibiotics residues are ubiquitous in wastewater and wastewater-impacted water bodies, at a trace level of up to a few μg/L (Felis et al., 2020; Luo et al., 2014; Tran et al., 2019). Many research studies about the occurrence of antibiotics in the wastewater treatment plants (WWTPs) and other water bodies have been conducted in the last decades. Most of these reports, however, have focused on a limited amount of target antibiotics. Because of the lack of standardized methods, data reported in distinct studies are poorly comparable. Rodriguez-Mozaz et al. (2020) suggest that global monitoring programs would allow acquire reliable and comparable analytical data concerning antibiotics occurrence at an international level. Such regulations would provide the basis for international action and allow assess the progress achieved related to any potential environmental protection action.

Adeleye et al. (2022) extensively reviewed the occurrence of antibiotics in raw municipal wastewater on different continents. They reported that the concentration of antibiotics in raw municipal wastewater around the world ranges between 1 and 303,500 ng/L (**Fig. 3**). The calculations were based on 1235 datapoints. The most detected antibiotics in raw municipal wastewater are ciprofloxacin, sulfamethoxazole, erythromycin, trimethoprim, and tetracycline. 75% of municipal WWTPs with the highest content of antibiotics in their influents were in India. This was due to loosen regulations, which allow discharge of inadequately treated wastewater from industries and hospitals. The median concentration of antibiotics in African wastewaters (1530 ng/L) is orders of magnitude higher than the rest of the world. This is because in Africa some antibiotics are available without prescription. They are also broadly used to treat infections occurring in people living with HIV/AIDS (Frank et al., 2019; K'oreje et al., 2018). It should be highlighted that the number of datapoints used to calculate mean and median concentrations of antibiotics in WWTPs effluents was much lower for Africa than for Europe, North America, and Asia. The concentrations of antibiotics in WWTPs influents usually exhibits a seasonal pattern, with the lowest concentrations observed in the summer and highest concentrations in the winter. High concentrations of antibiotics in winter are linked to increased incidences infections in colder seasons and to lower biodegradation rates of some antibiotics (Adeleye et al., 2022). Therefore, the monitoring studies should evaluate the temporal and geographical trends in antibiotic occurrence (Rodriguez-Mozaz et al., 2020).

Fig. 3 Median concentration of antibiotics reported in municipal wastewater treatment plant influents on different continents. Adapted from Adeleye et al. (2022).

Nitrofurans are among the few antibiotic groups whose environmental impact is not sufficiently understood, and data on their concentration in the environment is very limited. So far, the quantitative occurrence of nitrofurans in environmental water bodies and sediment has been reported in China only. Hou et al. (2015) have found FZD in amended soil and animal manure at a concentration of 15 and 10 μg/kg, respectively. Yu et al. (2013) confirmed the presence of the residues of four nitrofurans and their metabolites in pond water and the sediment slurries. They were detected in water at concentrations ranging from 0.2 to 0.4 μg/L and the sediment within the range of 0.2 – 0.6 μg/L.

Sources and fate of antibiotics in the environment

The major sources of antibiotic residues in the environment include effluents from WWTPs, chemical manufacturing plants, and animal husbandry and aquaculture.

Antibiotics after being used by humans and animals are eliminated from the organism in urine and feces. They can also be directly released from transdermal use. Antibiotics can be excreted from the body as unchanged parent compound, metabolized derivative, and conjugate with glucuronic or sulfuric acid (Kovalakova et al., 2020). Most antibiotics, however, are not well absorbed into human and animal body. Consumed antibiotics are mainly excreted unmetabolized reaching the values up to 75% (Evgenidou et al., 2015) or even 90% (Mompelat et al., 2009).

There are many routes, pharmaceuticals designated for human use are introduced into the environment (**Fig. 4**). Hospital, household, and industrial effluents as well as household waste are among the major sources. Usually, hospitals are associated as the

greatest reservoir of pharmaceutical pollutants, however, data from twenty seven European countries indicate that 90% of antimicrobials use by humans is related to consumption outside hospitals (Felis et al., 2020). This means that controlling of their release into the environment is practically impossible. Emissions from manufacturing sites and incorrect disposal are among minor sources of antibiotics in the environment. The effluents are introduced into the WWTPs where antibiotics (and other pollutants) undergo biodegradation, transformation, and sorption onto the activated sludge. Due to heightened level of pollution, the WWTPs are not always capable to completely remove all antibiotic residues. These residues remain in the WWTPs effluents and biosolids/sewage sludge and then reach surface water, sediments, and soil. Therefore, the WWTPs are indicated to be the main source of environmental pollution with human antibiotic residues. Minor sources of antibiotics include leaching from landfills, and reuse of water for irrigation. Consequently, antibiotic residues can potentially accumulate in soil, be absorbed by crops or leach into groundwater (Chaturvedi et al., 2021; Felis et al., 2020; Kovalakova et al., 2020; Zuccato et al., 2010).

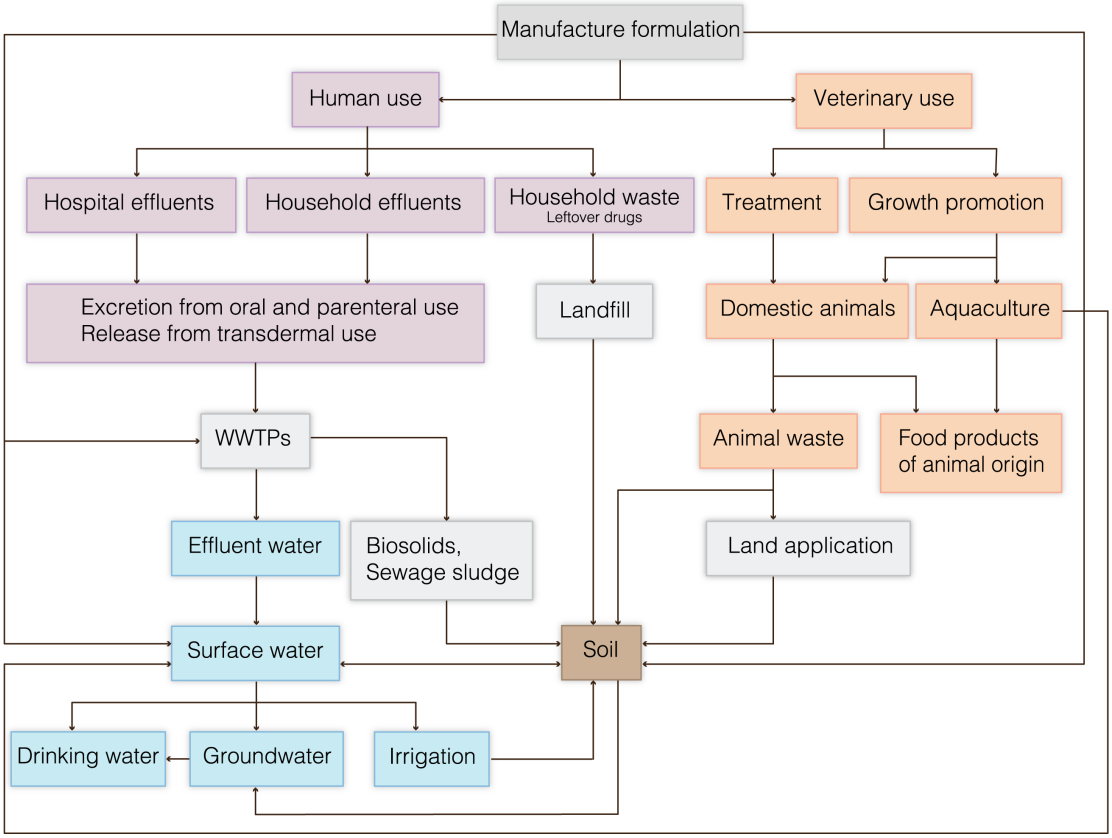

Fig. 4 Fate of antimicrobials in the environment. Pathways of antibiotics for human consumption are marked with pink color; animal food industry and aquaculture – orange color; transport inside the aquatic environment – blue color. Adapted from Kovalakova et al. (2020).

The chemical and physical properties of antibiotics molecules modify their persistence and mobility in the environment. For example, a recent study reported that NFT exhibits small affinity to accumulate in sediments, therefore, it shows high mobility in the environment (Tolić et al., 2019). In addition, antibiotics can adsorb on microplastic particles which serve as their carrier in the aquatic environment. This indicates that both could have higher toxic effects on aquatic life due to the combined pollution (Li et al., 2018).

Veterinary antibiotics spread in the natural environment in different pathways than the human antibiotics (**Fig. 4**). The most significant sources of veterinary drugs used for treatment of growth promotion are farms and aquaculture. Antimicrobials given to animals are spread in fields through manure and then reach soil and groundwater. Antibiotics used in crops and aquaculture contribute to contamination through their accumulation in soil or sediment. Inappropriate disposal of unused drugs and livestock feed are also among the sources of veterinary antibiotics in the environment. Application of high amount of veterinary pharmaceuticals in animal husbandry is one of the main sources of pharmaceuticals into terrestrial environment (Felis et al., 2020; Knäbel et al., 2016; Zuccato et al., 2010).

Do nitrofurans affect (micro)organisms?

The occurrence of antibiotic residues in the environment poses a risk for organisms at various trophic levels – from microorganisms, through plants and animals to humans. Antibiotics can pose acute or chronic toxicity on non-target organisms. This is a result of the immediate exposure to therapeutic levels or the long-term exposure to subtherapeutic concentrations of pollutants (Bengtsson-Palme and Larsson, 2016; Danner et al., 2019; Kümmerer, 2009).

One of the most important threats related with occurrence of antibiotics in the natural environment is development of antibiotic resistance worldwide (Berendonk et al., 2015). Antibiotics residues can have also other adverse effects, as follows:

- Disturbance of the bacterial cell cycles, mechanisms and processes, essential to maintaining the aquatic balance, soil fertility, agricultural balance and animal production (Kumar et al., 2019).
- Modifications of the structure of human intestinal microflora[3] (Ben et al., 2020, 2019).
- Ecotoxicity towards algae, cyanobacteria, plants, crustaceans, fish, and bacteria (Kovalakova et al., 2020).
- Generation of excessive reactive oxygen species and inhibition of defensive mechanisms in cells (Chen et al., 2019; Liu et al., 2015).

3 Changes in the intestinal microflora can lead to excessive proliferation of pathogenic and opportunistic bacteria which can further contribute to numerous diseases, such as intestinal disorders, pseudomembranous colitis, colorectal cancer.

- Reduced germination, growth and development of crops (Pan and Chu, 2017).
- Changes in behavior, growth, and reproduction of animals (Janecko et al., 2016).

Antimicrobials affect microbial cells by various mechanisms, including inhibition of nucleic acids synthesis, protein synthesis, or cell envelope synthesis. These compounds are designed to treat bacterial infections in humans and animals. They are not designed to affect mammalian cells, therefore, their negative impact on humans and animals should be rather negligible. Therefore, subtherapeutic exposure to antibiotic residues can exert more toxic effects on environmental microorganisms than the vertebrates (Patel et al., 2019).

Just as typical antibiotics, nitrofurans also present notable human health and ecological concerns. Both parent compounds and their metabolites have been reported to show mutagenic, teratogenic, and carcinogenic properties for humans and animals (Leston et al., 2011; Zuma et al., 2019). The impact of nitrofurans on the microbial communities can be significant, although, to date, it has only been examined in a very few studies. Available information about impact of nitrofurans on organisms (microorganisms, protists, plants, and aquatic animals) is summarized in **Tab. 5**. The results published by the author are not included in the list.

Tab. 5 Impact of nitrofurans on microorganisms, plants, and aquatic animals. The results published by the author are not included in the list.

Group of organisms	Specific organism	Compound studied	Impact	References
Microorganisms	*Vibrio fischeri*	NFT	Toxic effect (EC50= 4.0 mg/L)	(Biošić et al., 2021)
	Allivibrio fischeri	NFT	Toxic effect (EC50=2.066 mg/L)	(Lewkowski et al., 2019)
	Allivibrio fischeri	FZD	Toxic effect (EC50=2.051 mg/L)	(Lewkowski et al., 2019)
	Salmonella typhimurium	NFT	Mutagenic effect	(Klobučar et al., 2013)
Protists	Ciliate (*Paramecium jenningsi)*	NFZ	Reduced relative population growth rate, increased activity of catalase, superoxide dismutase, glutathione peroxidase	(Li et al., 2023)
	Periphytic ciliates communities	NFZ	Affected community structure	(Kazmi et al., 2022)
	Protozoan periphyton communities	NFZ	Variation in the functional patterns, reduced functional diversity indices	(Uroosa et al., 2021)
	Algae (*Desmodesmus subspicatus*)	NFT	Inhibited growth, harmful effect (EC50=12.4 - 17.4 mg/L)	(Klobučar et al., 2013)
	Macroalage (*Ulva lactuca*)	FTD	Decreased growth rate	(Leston et al., 2011)
	Euplotes vannus	NFZ	Reduced viability, observed DNA damage	(Zhou et al., 2011)
Plants	Mung bean seeds (*Vigna radiata*)	FZD	Inhibited growth, morphological changes in sprouts	(Cao et al., 2022)
	Common radish (*Raphanus sativus*)	NFT, FZD	Totally inhibited growth at 1000 mg/kg; Inhibited growth of shoots and roots 100 mg/kg; increased the plant dry weight; adverse effect of germination; decreased total chlorophyll and carotenoid level	(Lewkowski et al., 2019)

Tab.5 *(continued)*

Group of organisms	Specific organism	Compound studied	Impact	References
Plants	Oat (*Avena sativa*)	NFT, FZD	Inhibited growth of shoots and roots 100 mg/kg; increased the plant dry weight; adverse effect of germination; decreased total chlorophyll and carotenoid level	(Lewkowski et al., 2019)
Aquatic animals	Fish embryos (*Danio rerio*)	NFT	Short-term exposure: Induced mortality, detected alterations in normal development > 10 mg/L. Acute effects not expected to occur in natural ecosystems. Biochemical changes > 10 mg/L. Expected negative long-term effects.	(de Oliveira et al., 2020)
	Crustaceans (*Heterocypris incongruens*)	FZD, NFT	Increased mortality: 91% (FZD), 96% (NFT) mortality rate at 50 mg/kg s.d.w., total mortality (FZD, NFT) at 100 mg/kg s.d.w.	(Lewkowski et al., 2019)
	Fish cell lines (*Danio rerio* and *Poeciliopsis lucida)*	NFT	Reduced viability of cells (EC50=11.9 mg/L)	(Klobučar et al., 2013)
	Fish cell lines (*Oncorhychus mykiss)*	NFT	Reduced viability of cells (EC50=3.57 mg/L)	(Klobučar et al., 2013)
	Fish embryos (*Danio rerio*)	NFT	Induced genotoxicity at 1.2 mg/mL.	(Kosmehl et al., 2006)
	Fish (*Poecilia formosa*)	FZD	Liver steatosis, increased internal organs, developed renal and hepatic melanohistocytomes	(Auro et al., 2004)
	Fish (*Oreochromis niloticus*)	FZD	Liver steatosis	(Auro et al., 2004)

Note. NFT – nitrofurantoin, FTD – furaltadone, FZD – furazolidone, NFZ – nitrofurazone, EC50 – half maximal effective concentration.

Strategies for the removal of antibiotics residues

To minimize the adverse effects of antibiotic residues on (micro)organisms in the natural environment, development of cost-effective and efficient strategies of their removal is essential. Common decontamination methods for antibiotics polluted sites include physical remediation, chemical remediation, and bioremediation.

Physical remediation techniques include adsorption, dialysis, electrodialysis, evaporation, flocculation, filtration, reverse osmosis, sedimentation, stream stripping. Chemical treatment methods include ion-exchange, calcination, neutralization, precipitation, and reduction. Biological treatment include aerobic and anaerobic microbial degradation in WWTPs, aerated lagoons, tricking filters, or waste stabilization ponds (Patel et al., 2019).

Generally, bioremediation refers to phytoremediation or microbial remediation. Compared to physical and chemical remediation technologies, biological treatment is more promising due to robustness, eco-friendly approach, and cost-effectiveness (Azubuike et al., 2016; Ye et al., 2017). Phytoremediation uses living plants to decontaminate polluted environments while microbial bioremediation[4] is based on natural abilities of microorganisms to transform hazardous pollutants into simpler, less toxic, or non-toxic substances (Azubuike et al., 2016; Kafle et al., 2022). The Organisation for Economic Co-operation and Development (OECD) in their guidelines distinguishes two main types of biodegradations (**Fig. 5**). The total mineralization (ultimate biodegradation) occurs when the test compound is completely utilized by microorganisms. As a result, carbon dioxide, water, mineral salts, and biomass are produced. During primary biodegradation (biotransformation) the structural change of a parent compound occurs resulting in the loss of specific properties of that substance (Organisation for Economic Co-operation and Development, 1992).

Each bioremediation technology tends to decompose the pollutant of interest into a harmless product. However, a major drawback of these processes is formation of transformation products (TPs) which can show similar or even higher toxicity then the parent compounds (Vasquez et al., 2013). These products usually are characterized by increased stability and can remain pharmacologically active in the environment for a long time (López-Serna et al., 2013).

The global market size of bioremediation was worth $106 Billion in 2019 and is expected to reach $335 Billion by 2027 (Tran et al., 2021). This indicates that new, and effective remediation technologies develop successively.

---

[4] The term *bioremediation* is often used interchangeably with *biodegradation*. However, biodegradation is defined as process of decomposition of complex compounds into simpler molecules with the help of living organisms that occur naturally while bioremediation is an engineered technique of degradation of environmental contaminants by microorganisms occurring naturally or deliberately introduced to the polluted site.

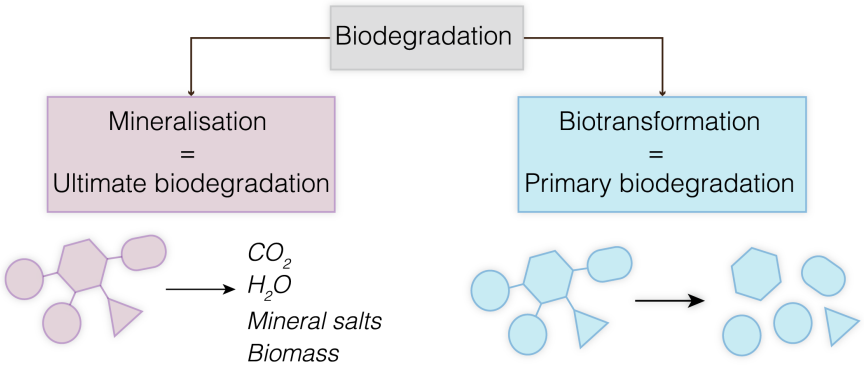

Fig. 5 Two types of biodegradation according to the OECD.

The microbial species used in bioremediation processes are usually isolated from natural microbial communities chronically inhabiting contaminated areas. The overall scheme to isolate single bacterial strains includes several major steps (Pacholak et al., 2019, 2023b; Tran et al., 2021):

1. Environmental sample collection using aseptic technique.
2. Screening of pure strains by their cultivation in a medium containing the target compound.
3. Identification of single species by sequencing.
4. Characterization of the single species, discarding the pathogenic strains.
5. Evaluation of biodegradation potential.

It is commonly believed that mixed microbial communities are more powerful in degradation of organic compounds than the single species (Nnabuife et al., 2022). However, bioaugmentation with efficient species of high ability to degrade the pollutants is a promising strategy for bioremediation of contaminated environments (Li et al., 2020). Some examples of the bacterial species recently used for bioremediation of antimicrobials include *Burkholderia cepacia* (remediation of tetracycline) (Hong et al., 2020), *Bacillus paramycoides* SDB4 (remediation of sulfamethoxazole) (Chen et al., 2022), *Ochrobactrum* sp. TCC-2 (triclocarban) (Bai et al., 2021).

There are three crucial factor that limit bioremediation and biodegradation efficiency (Ossai et al., 2020). These factors include (i) physicochemical parameters of the surrounding environment, (ii) characteristics of the pollutants, (iii) properties of the microbial cells. Important properties of the microbial cells include not only the ability to biodegrade xenobiotics, but also tolerance of cells to grow and survive in toxic environment, metabolic activity, cells viability, structure of microbial communities, and surface properties of the cells (Ma et al., 2018). Cell surface properties determine uptake and bioavailability of the contaminants, hence, evaluation of changes in these cells features is crucial in monitoring of biodegradation of antibiotics and other xenobiotics. Important cell surface properties include, among others, cell surface zeta potential, cell size, ultrastructure, morphology, membrane permeability, and surface hydrophobicity (Kaczorek et al., 2018).

Removal of nitrofurans

To date, research about removal of 5-NFs from the environment has focused on physicochemical methods (**Tab. 6**). Several studies reported the removal of nitrofuran antibiotics from the environment using different techniques such as electrochemical degradation (Kong et al., 2015), adsorption using synthetic and natural adsorbents like carbon nanotubes (Zhen-Yuan and Zhen-Hu, 2015) or waste banana pseudostem biomass (Gurav et al., 2020). Photocatalysis was another strategy used for removal of nitrofurans (Durán et al., 2022; Lai et al., 2022; Szabó-Bárdos et al., 2020; Yashas et al., 2022). Edhlund et al. (2006) investigated for the first time photodegradation of FTD, FZD, and NFT. Efficient removal of 5-NFs was obtained, and some degradation products were proposed (nitrofuraldehyde as was found to be the primary degradation product of all nitrofurans tested).

Because nitrofurans are defined as unstable compounds, Biošić et al. (2017) investigated hydrolytic degradation of NFT in various pH values and temperatures. Hydrolytic degradation was much slower in acidic environment compared to neutral and alkaline environment at all investigated temperatures (20, 40, and 60 °C). In addition, degree of NFT hydrolysis increased with temperature at all investigated pH-values. An in-depth examination of results obtained for experiments performed at 20 °C (temperature the closest to temperature of the surrounding environment) show that NFT degradation reached 1.6% at pH 4, 6.5% at pH 7, and 27% at pH 9 after 30 days. These results, together with selected results of 5-NFs biodegradation published by author of this thesis (Pacholak et al., 2023b, 2023a, 2020, 2019), indicate that nitrofuran antibiotics are more stable than commonly believed.

Despite good efficiency of nitrofurans removal by the above-mentioned methods, their use is limited due to economic reasons and high energy requirements (Gurav et al., 2020). Limitations of heterogenous photocatalysis also include difficulty in recovery and uniform distribution of nanoparticles, low adsorption of organic pollutants, and aggregation of nanoparticles (Dong et al., 2015). As for the adsorption process, regeneration of adsorbents may be not feasible and problems with posttreatment disposal may occur (Jadhav and Jadhav, 2021). Nanomaterials used for photocatalysis as well as adsorbents also may cause secondary pollution and their migration in organisms and the environment is not sufficiently understood. In addition, nanomaterials are often toxic to living organisms (Peng et al., 2020).

Very limited information is available about removal of nitrofurans from the environment by biological methods (excluding articles co-authored by the author of this dissertation). The most advanced study related with biological treatment of 5-NFs analyzed biodegradation of FZD by three bacterial strains (**Tab. 6**) (Zhang et al. (2013).

Tab. 6 Summary of the removal of nitrofurans reported in the literature. The results published by the author are not included in the list.

Method	Antibiotic	Treatment type	Influent concentration	Removal rate	Time	TPs identified?	References
Biodegradation	FZD	Bacterial degradation by *Acinetobacter calcoaceticus* T32	5 mg/L	95%	24 h	No	(Zhang et al., 2013)
Biodegradation	FZD	Bacterial degradation by *Pseudomonas putida* SP1	5 mg/L	89%	3 days	No	(Zhang et al., 2013)
Biodegradation	FZD	Bacterial degradation by *Proteus mirabilis* V7	5 mg/L	82%	3 days	No	(Zhang et al., 2013)
Electrochemical	NFZ	Cyclic voltammetry	50 mg/L	85 – 99%	9 h	Yes	(Kong et al., 2015)
Physical	FTD	UV light-driven photocatalysis intensified by persulfate	10 mg/L	80%	30 min	Yes	(Durán et al., 2022)
Physical	NFT	Visible light-driven photocatalysis using ruthenium nanoparticles-incorporated hafnium oxide	24 mg/L	100%	15 min	No	(Lai et al., 2022)
Physical	NFT	Visible light-driven photocatalysis using molybdate tethered polypyrrole nanocomposite	15 mg/L	93%	80 min	No	(Yashas et al., 2022)
Physical	FZD	Adsorption on magnetic biochar derived from waste banana pseudostem biomass	100 mg/L	44 - 55%	60 min	No	(Gurav et al., 2020)
Physical	NFT	Visible light-driven photocatalysis using TiO_2	10 mg/L	100%	90 min	Yes	(Szabó-Bárdos et al., 2020)

Tab. 6 *(continued)*

Method	Antibiotic	Treatment type	Influent concentration	Removal rate	Time	TPs identified?	References
Physical	FZD	Adsorption on magnetic multi-wall carbon nanotubes	10 mg/L	97.8%	200 min	No	(Zhen-Yuan and Zhen-Hu, 2015)
Physical	NFZ	Adsorption on magnetic multi-wall carbon nanotubes	10 mg/L	93%	200 min	No	(Zhen-Yuan and Zhen-Hu, 2015)
Physical	NFT	Adsorption on magnetic multi-wall carbon nanotubes	10 mg/L	96.5%	200 min	No	(Zhen-Yuan and Zhen-Hu, 2015)
Physical	FTD	Adsorption on magnetic multi-wall carbon nanotubes	10 mg/L	94.2%	200 min	No	(Zhen-Yuan and Zhen-Hu, 2015)
Combined	NFZ	Bio-photoelectrochemical system with bioanode and the g-C3N4/CdS heterojunction photocathode inoculated with municipal activated sludge	50 mg/L	80%	10 h	Yes	(Hou et al., 2020b)
Combined	NFZ	Bio-photoelectrochemical system with g-C3N4/CdS heterojunction photocatalyst inoculated with municipal activated sludge	10 mg/L	83%	4 h	No	(Hou et al., 2020a)
Combined	NFZ	Bioelectrodegradation – bioelectrochemical system inoculated with municipal activated sludge	50 mg/L	42 – 71%	60 min	Yes	(Kong et al., 2017)

Note. TPs – transformation products, FZD – furazolidone, NFZ – nitrofurazone, FTD – furaltadone, NFT – nitrofurantoin.

Chapter 2

Dissertation aims and outline

Research gap and hypothesis

Nitrofuran derivatives are bactericidal, broad-spectrum antibiotics. The representatives of the nitrofuran family include, among others, NFT, NFZ, FZD and FTD. They have been employed as pharmaceuticals, food additives, conservatives, and growth promoters for a long time. Currently, nitrofurans are no longer permitted for use in food-producing animals in many countries, including the EU member states and the US, due to the possible genotoxic, carcinogenic, and non-neoplastic effects. Even though their use in food animal production is prohibited in many countries, nitrofurans are often found in animal food products. In addition, in some third countries, nitrofurans can be legally used in food producing animals, however, specific information on the actual usage is not available. In human medicine, NFT, NFZ, and FZD are still commonly used. The mass production and excessive consumption of nitrofurans has contributed to a heightened risk of environmental pollution, which may negatively affect living organisms. Nitrofurans are among the few antibiotic groups whose environmental impact is not sufficiently understood, and data on their concentration in the environment is very limited. Nitrofurans lack enough attention of the scientific community as most of reports about antibiotics occurrence and environmental impact do not consider nitrofurans at all (Danner et al., 2019; Felis et al., 2020; Kovalakova et al., 2020; Zuccato et al., 2010). Therefore, information on nitrofurans environmental fate is scarce compared to other commonly used antibiotics (**Fig. 6**). Previous studies mostly focused on nitrofurans clinical aspects (e.g. metabolism, efficacy and toxicity, pharmacokinetics, application) rather than their environmental aspects (Bessone et al., 2023; Gallardo-Garrido et al., 2020; Nakagawa et al., 2021; O'Connor et al., 2022). Despite this, nitrofurans mechanism of action against bacteria is not fully understood.

To address the above identified research gap, selected nitrofurans were investigated in terms of their biodegradability as well as short- and long-term influence on the bacterial strains. Specifically, the following hypotheses will be verified:

H-1: Natural microbial communities contain bacterial strains capable of degrading nitrofurans efficiently (P1, P3, P5).

H-2: Nitrofurantoin biodegradation leads to formation of transformation products that strongly affect bacterial cells (P3, P5).

H-3: Bacterial cell properties and metabolic activity change dynamically during biodegradation of nitrofurantoin (P5).

H-4: Nitrofuran antibiotics significantly affect the properties of environmental bacterial strains (P1, P2, P4, P5).

H-5: Nitrofurantoin affect the structure of natural microbial communities (P3).

H-6: Prolonged exposure of bacterial strains to nitrofuran antibiotics leads to significant modifications of cell structure and cell metabolism. These effects are compound specific (P2, P4).

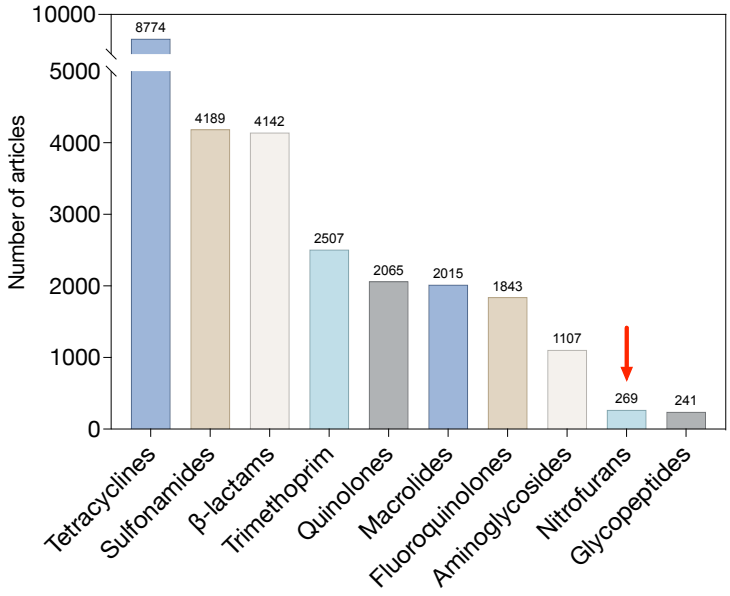

Fig. 6 Number of journal articles published in the last ten years (2013 – 2023) on environmental aspects of nitrofurans compared with other common antibiotics (as defined in Tab. 1). Data was collected from the Scopus database using "environmental science" as the subject area and antibiotic class names as the keyword. β-lactams include penicillins, cephalosporins, monobactams, and carbapenems, therefore the individual subclasses names were used as the keywords for β-lactams class.

Aims and objectives

The overall purpose of this dissertation is to explore the biodegradation of selected nitrofurans by environmental bacteria and to understand how nitrofurans affect the cell properties. The above issues were investigated with a multi-faceted approach using newly isolated pure bacterial strains as well as microbial consortia. Conventional culture methods (e.g. various colorimetric assays) were complemented with modern powerful techniques, such as atomic force microscopy (AFM), flow cytometry (FC), metabolomics, and metagenomics. The specific objectives of this dissertation are, as follows:

- To isolate and identify the pure bacterial strains from various environmental niches (urban and municipal wastewater, soil, water reservoirs) (P1, P2, P4, P5).
- To explore the biodegradation of nitrofurans by the single strains and the microbial consortia collected from various environments (P1, P3, P5).
- To identify NFT biotransformation products and determine their effect on the bacterial strains (P3, P5).
- To understand the effect of nitrofurans on cell metabolic activity and cell properties, such as membrane permeability and surface hydrophobicity (P1).

- To critically assess the dynamic changes in the composition and diversity of the microbial communities during biodegradation of NFT (P3).
- To expose the isolated strains to NFT and FTD for 12 months (P2, P4).
- To study modifications of cells shape and structure triggered by prolonged exposure to nitrofurans (P2).
- To assess the biochemical response of cells exposed to nitrofurans for 12 months by analysis of changes in cell membrane permeability, surface hydrophobicity and fatty acids profile (P2).
- To understand the effect of a 12-month continuous exposure of strains to nitrofurans on metabolomic profile, damage of the genetic material, metabolic activity, and stress response within the cells (P4).

Dissertation structure

This dissertation comprises five research chapters, list of references and author's scientific activity and three appendices. **Chapter 1** provides the current state of knowledge about antibiotics pollution with emphasis put on nitrofuran derivatives. Research gap, questions, aims, and objectives are provided in **Chapter 2.** Dissertation is based on five original research articles which are listed in **Chapter 3.** A summary of results presented in these articles is described in **Chapter 4**. **Chapter 4** begins with short introduction. Next, the main results, divided into two sections, are described. The first section is based on three publications (P1, P3, and P5) in which degradation of NFT as well as the effect of short-term exposure of bacteria to nitrofurantoin is discussed. The second section is based on two articles (P2, P4) and describes the effect of prolonged exposure of strains to NFT and FTD. In the last section of **Chapter 4**, additional achievements are briefly described. These achievements include three publications related to nitrofurans biodegradation and/or impact on cell properties. They are not, however, directly included in this dissertation. Dissertation is concluded in **Chapter 5** where the main findings are summarized, and their significance is discussed. Limitations and potential extensions of this work are also outlined. Additional sections of this dissertation include a **list of publications cited**, author's **scientific activity**, and three appendices (A-C). **Appendix A** contains full texts of papers P1 – P5. Author's contribution is presented in **Appendix B**, and co-authors statements, describing the individual contribution of each co-author, in **Appendix C**.

Chapter 3

Publications included in dissertation

List of publications

This dissertation is based on results published in the journals indexed by the Journal Citation Reports as below. Publications are arranged in chronological order.

P1. **A. Pacholak**, W. Smułek, A. Zgoła-Grześkowiak, E. Kaczorek*, *Nitrofurantoin – microbial degradation and interactions with environmental bacterial strains*, International Journal of Environmental Research and Public Health 16 (2019) 1526, doi:10.3390/ijerph16091526

P2. **A. Pacholak*,** N. Burlaga, U. Guzik, E. Kaczorek*, *Investigation of the bacterial cell envelope nanomechanical properties after long-term exposure to nitrofurans*, Journal of Hazardous Materials 407 (2021) 124352, doi: doi:10.1016/j.jhazmat.2020.124352

P3. **A. Pacholak***, A. Zgoła-Grześkowiak, E. Kaczorek, *Dynamics of microbial communities during biotransformation of nitrofurantoin*, Environmental Research 2016 (2023) 114531, doi:10.1016/j.envres.2022.114531

P4. **A. Pacholak*,** J. Żur-Pińska, A. Piński, Q. A. Nguyen, M. Ligaj, M. Łuczak, L. D. Nghiem, E. Kaczorek, *Potential negative effect of long-term exposure to nitrofurans on bacteria isolated from wastewater,* Science of the Total Environment 872 (2023a) 162199, doi:10.1016/j.scitotenv.2023.162199

P5. **A. Pacholak***, W. Juzwa, A. Zgoła-Grześkowiak, E. Kaczorek, *Multi-faceted analysis of bacterial transformation of nitrofurantoin,* Science of the Total Environment 874 (2023b) 162422, doi:10.1016/j.scitotenv.2023.162422

* Denotes the corresponding author

Full texts of papers P1 – P5 are provided in Appendix A, author's contribution in Appendix B, and the co-authors statements, describing the individual contribution of each co-author, in Appendix C.

Bibliometric indicators

The bibliometric indicators presented in **Tab. 7** include Impact Factor (IF), 5-year Impact Factor (5-y IF), and Ministry of Education and Science Points (MEiN). IF reflects the Impact Factor for the journal for the year of publication. 5-y IF reflects the 5-year journal Impact Factor for the years 2017-2022. MEiN reflects the points awarded by a journal included in the list of ranked journals published in 2021 by Ministry of Education and Science in Poland (*Ministerstwo Edukacji i Nauki*, MEiN).

Tab. 7 Bibliometric indicators of papers included in dissertation.

Lp.	Paper	IF	5-y IF	MEiN	Rank
P1.	A. Pacholak et al. Int. J. Environ. Health Res. (2019)	2.849	4.799	70	Q2
P2.	A. Pacholak et al. J. Hazard. Mater. (2021)	14.224	12.984	200	Q1
P3.	A. Pacholak et al. Environ. Res. (2022)	8.431	8.399	100	Q1
P4.	A. Pacholak et al. Sci. Total Environ. (2023a)	10.753	10.237	200	Q1
P5.	A. Pacholak et al. Sci. Total Environ. (2023b)	10.753	10.237	200	Q1
	Sum	**47.010**	**46.656**	**770**	-
	Average	**9.402**	**9.331**	-	-

Chapter 4

Summary of results

Introduction

Results conducted within this dissertation are divided into two parts. The first part includes evaluation of impact of short-term exposure of newly isolated bacterial strains and bacterial consortia to nitrofurantoin. The following publications are included in this section:

P1. A. Pacholak, W. Smułek, A. Zgoła-Grześkowiak, E. Kaczorek, *Nitrofurantoin – microbial degradation and interactions with environmental bacterial strains*, International Journal of Environmental Research and Public Health 16 (2019) 1526, doi:10.3390/ijerph16091526

P3. A. Pacholak, A. Zgoła-Grześkowiak, E. Kaczorek, *Dynamics of microbial communities during biotransformation of nitrofurantoin*, Environmental Research 2016 (2023) 114531, doi:10.1016/j.envres.2022.114531

P5. A. Pacholak, W. Juzwa, A. Zgoła-Grześkowiak, E. Kaczorek, *Multi-faceted analysis of bacterial transformation of nitrofurantoin,* Science of the Total Environment 874 (2023b) 162422, doi:10.1016/j.scitotenv.2023.162422

The second part refers to studies about bacterial strains subjected to prolonged (12-month) exposure to nitrofurantoin and furaltadone. The following publications are included in this section:

P2. A. Pacholak, N. Burlaga, U. Guzik, E. Kaczorek, *Investigation of the bacterial cell envelope nanomechanical properties after long-term exposure to nitrofurans*, Journal of Hazardous Materials 407 (2021), doi:124352, doi:10.1016/j.jhazmat.2020.124352

P4. A. Pacholak, J. Żur-Pińska, A. Piński, Q. A. Nguyen, M. Ligaj, M. Łuczak, L. D. Nghiem, E. Kaczorek, *Potential negative effect of long-term exposure to nitrofurans on bacteria isolated from wastewater,* Science of the Total Environment 872 (2023a) 162199, doi:10.1016/j.scitotenv.2023.162199

Short-term exposure of microorganisms to nitrofurantoin

Publication P1

Nitrofurantoin – microbial degradation and interactions with environmental bacterial strains

Publication P1 presents the results of biodegradation of NFT and its influence on the properties of bacterial cells. The specific objectives of experiments performed within P1 are, as follows:

- To identify and characterize the pure bacterial strains isolated from the municipal and rural activated sludge.
- To determine the ability of the novel strains to degrade NFT.
- To assess the modifications of the cell properties of the novel strains cultivated with NTF.

The first part of the experiments aimed to isolate the pure bacterial strains from the activated sludge collected from the rural and municipal WWTPs. Both sewage facilities are located in Poznań County in Poland and use a mechanical biological treatment (MBT) technology, however, they differ in the maximum capacity and the operational area (**Tab. 8**).

Tab. 8 Characteristics of the wastewater treatment facilities from which the bacterial strains were isolated.

	Geographical location	Operational area	Capacity	Treatment type
Rural WWTP	52°29′41.6″ N, 16°35′08.8″ E	Rural area with over eight thousand citizens	1150 m^3/24 h	MBT
Municipal WWTP	52°25′53.1″ N, 16°57′31.8″ E	Urban area with a population of at least 500,000	50000 m^3/24 h	MBT with increased nutrient removal and full treatment of generated sewage sludge

Note. MBT – Mechanical Biological Treatment, WWTP – wastewater treatment plant.

The selective enrichment method was used to isolate the single strains. As a result, eighteen bacterial strains were isolated from the rural wastewater and thirteen strains from the municipal wastewater. Based on the ability to grow in the presence of NFT,

five strains were chosen for further research (two from the rural wastewater, and three from the urban wastewater):

- *Sphingomonas paucimobilis* K3a
- *Ochrobactrum antrophi* K3b
- *Rhizobium radiobacter* P4c
- *Pseudomonas aeruginosa* P4a
- *Sphingobacterium thalpophilum* P3d

The biochemical profile and ability to produce hemolysins were evaluated for these strains. Furthermore, the bacterial cultures were established to investigate the impact of NFT of the cell properties. The tested cell features include inner membrane permeability (IMP), total membrane permeability (TMP), cell surface hydrophobicity (CSH), and the metabolic activity (MetAct). To understand the general effect of xenobiotics on the cells, evaluation of these parameters is important. For example, increased inner and total cell membrane permeability can indicate the cell's rupture due to toxic effect of a substance, but on the other hand, it can facilitate the uptake of the compound by the cell for its biodegradation. Decreased membrane permeability, however, may indicate on sealing the outer layers of the cell to prevent the xenobiotics from entering the cell. Cell surface hydrophobicity, however, point out the bioavailability of microbial cell to chemical compounds. Its modifications can indicate remodeling of the outer layers of bacterial cells. Taken together, all these parameters may suggest the initiated defensive mechanisms against the exogenous substance or its toxic effect.

The modifications of IMP, TMP, CSH, and MetAct were tested after 24 h exposure of cell to NFT at the initial concentration of 5 mg/L. Results of experiments are summarized in **Tab. 9**. NFT induced a statistically significant modifications of inner membrane permeability in four strains (K3b, P4c, P3d, P4a), total membrane permeability in three strains (K3a, P4c, P3d), and cell surface hydrophobicity in three strains (K3a, P4c, P3d). Exposure of cells to NFT promoted significant reduction of cell metabolic activity in the K3a, K3b, P4c, and P4a strains.

The next part of research was devoted to analysis of primary biodegradation of NFT. For this purpose, NFT removal from the bacterial cultures was evaluated as well as the kinetic parameters according to the Monod equation were calculated. The highest removal rate was measured within the first two days of cultivation for all strains. The strains isolated from the rural wastewater exhibited higher removal efficiency than the strains from the municipal wastewater. In two days, >90% of the initial concentration of NFT was removed from the cultures containing the strains isolated from the rural wastewater. The average primary biodegradation reached 96% for the K3a strain and 93% for the K3b strain. Among the strains isolated from the municipal wastewater, the most effective primary biodegradation was observed for the P4c strain, and the least effective degradation for the P4a strain.

The obtained results of primary biodegradation efficiency and modifications of cell properties indicate that the response of cells to NFT was not unequivocal. In the K3a strain, a high degradation was accompanied by the modification of cell surface towards hydrophilic properties and TMP towards lower values with unchanged IMP. The opposite situation was observed in the K3b strain for which a high degradation was accompanied by lowered inner membrane permeability with unchanged values of CSH and TMP. The P4c strain was the most susceptible to modifications as TMP, CSH, MetAct significantly increased, and IMP significantly decreased in the presence of NFT. The P3d strain had specific characteristics as it was the only strain for which no significant modifications of MetAct were observed and its outer surface was modified towards hydrophobic properties after exposure to NFT. In addition, both IMP and TMP decreased in cultures containing NFT. The lowest NFT removal was observed for the P4a strain. This strain was initially characterized by the lowest MetAct which was additionally reduced in cells exposed to NFT.

Tab. 9 Summary of most important results presented in P1. The direction of arrows indicates up- or downregulation (control vs. treated sample). Not significant comparisons are labelled as "ns". Results of primary biodegradation refer to 28-day cultures.

Strain	K3a	K3b	P4c	P3d	P4a
TMP	↓	ns	↓	↓	ns
IMP	ns	↓	↑	↓	↑
CSH	↓	ns	↓	↑	ns
MetAct	↓	↓	↓	ns	↓
Average primary biodegradation (%)	96	93	84	70	50

Note. TMP – total membrane permeability, IMP – inner membrane permeability, CSH – cell surface hydrophobicity, MetAct – metabolic activity.

Conclusions:

To conclude, both microbial consortia contained the strains that were able to biodegrade NFT. The removal rate ranged from 50 to 96% in 28 days. Although the strains were able to degrade NFT, exposure to this antibiotic significantly affected cell properties. P1 is the first general but comprehensive report about the impact of NFT on single bacterial strains.

Publication P3

Dynamics of microbial communities during biotransformation of nitrofurantoin

Results presented in publication P3 describe efficiency of biodegradation of NFT by microbial consortia collected from two aqueous environmental niches (mountain stream and seaport seawater); detection of transformation products formed, and broad analysis of shifts in microbial communities during biodegradation.

Protected areas, such as national parks, wilderness areas and nature reserves, due to their long-term protection are expected to be a mainstay of biodiversity conservation. Therefore, they should be characterized by negligible concentration of anthropogenic pollutants. Supposedly, microorganisms present in the water bodies of such pristine areas have not been exposed to anthropogenic contaminants, therefore, they might not have the adaptative mechanisms developed. Hence, the bacteria can be very sensitive to chemical pollution and exhibit low biodegradation potential. On the other hand, the aqueous environmental compartments, such as seaport seawater, may contain microorganisms with greater biodegradation potential. The microorganisms were expected to have adaptive responses greatly developed to survive in adverse environments due to the numerous contaminants they receive.

The following are the specific objectives of experiments performed within P3:

- To understand the biodegradation of NFT by bacterial consortia collected from two distinct environmental niches: the reserve of the protected area (mountain stream) and the contaminated area (seaport water).
- To critically assess the dynamic changes in the composition and diversity of the microbial communities during biodegradation of NFT.

The samples of water were aseptically collected from the environmental niches, as follows:

- The mountain stream (NW) which represents the reserve of the protected area with no human intervention. The sample was collected from the area nearby Siklawica Waterfall in Tatra National Park in Poland (geographical location: 49◦ 15′ 34″ N 19◦ 55′ 44″ E).
- The seaport seawater (SS) which represents the area that concentrates diverse human activities and receives numerous contaminants including petroleum hydrocarbons, pesticides, microplastic, and metals. The sample was collected from the area of the Port of Gdańsk, one of the largest seaports on the Baltic Sea located on the southern coast of Gdańsk Bay in Poland (geographical location 54◦ 23′ 36″ N 18◦ 40′ 12″ E).

Once the water samples were collected, they were transported to the laboratory and aerated for 24 h. Next, the enrichment cultures were established and used for

inoculation to start liquid cultures for further experiments. Four initial concentrations of NFT were chosen for testing: 5, 10, 15, and 20 mg/L. The cultures were incubated for 28 days at room temperature on a horizontal shaker in the dark. To analyze the biodegradation rate, detect degradation products and investigate shifts in the microbial communities, small volumes of samples were collected in a few days intervals. To investigate biodegradation rate, the samples were filtered, diluted with methanol, and analyzed qualitatively and quantitatively for the residual NFT using liquid chromatography coupled with mass spectrometry (LC-MS/MS). In addition, the total organic matter removal was determined based on measurements of ultraviolet absorption at 254 nm wavelength. To detect degradation products, the samples were derivatized with 2-nitrobenzaldehyde and then analyzed using LC-MS/MS. To investigate shifts in the microbial communities, DNA from bacterial cells was isolated and iTag sequencing of 16S rRNA genes was performed. A scheme of procedures during experiments performed within P3 is presented in **Fig. 7**.

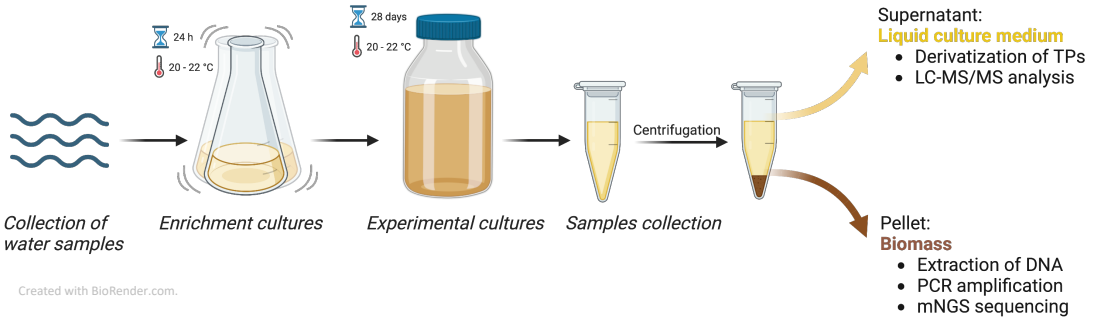

Fig. 7 A scheme of the experiments performed within publication P3.

Results of primary biodegradation were unexpected because NFT removal by microorganisms in the NW sample was much more efficient than its elimination by microbes in the SS sample. A complete NFT primary biodegradation by the NW consortium has been achieved in samples with the two lowest initial concentrations of NFT (5 and 10 mg/L) as opposed to the analogic samples containing the SS consortium (**Tab. 10**). Moreover, in the cultures with the highest initial NFT concentration (20 mg/L), the final degradation efficiency by the NW consortium (88 ± 1%) was more efficient than the SS consortium (64 ± 2%).

An important part of degradation studies was analysis of the total organic carbon (TOC) content during biodegradation in the bacterial cultures. The calculated TOC decreased with time. The higher concentration of NFT, the higher TOC was calculated. In addition, a considerable difference between the two bacterial communities was observed.

Tab. 10 Primary biodegradation (%) of NFT measured in the 28-day cultures.

NFT initial concentration	5 mg/L	10 mg/L	15 mg/L	20 mg/L
NW	99.9 ± 0.1	100.0 ± 0.8	94.0 ± 0.5	88.1 ± 1.0
SS	91.3 ± 1.7	76.3 ± 1.6	70.3 ± 5.0	63.5 ± 2.2

Note. NW - consortium from the mountain stream water sample, SS – consortium from the seaport seawater sample.

The primary biodegradation of many anthropogenic substances can lead to the generation of TPs that can remain unchanged in the ecosystems for a long time. The proposed TPs of NFT biodegradation include AHD, SEM and hydrazine (HYD). They were formed as a result of cleavage at the carbon-carbon bond linking the aromatic 5-nitrofuran ring and the tail group of the NFT molecule. A modification of the side ring moiety has also occurred. AHD was assumed to be a primary TP, which was later transformed into two secondary TPs: SEM and HYD (**Fig. 8**). Biodegradation of NFT followed the same pathways for both consortia and led to formation of similar TPs.

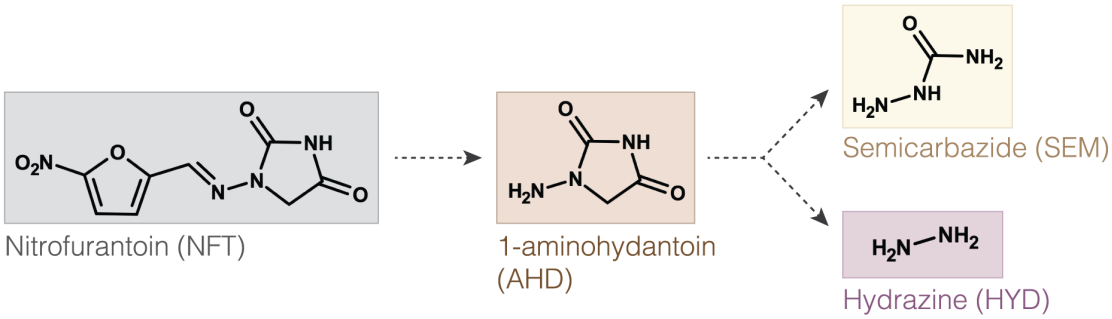

Fig. 8 Transformation products formed during NFT biodegradation.

Analysis of changes in AHD and SEM content during NFT biotransformation shows that the content of primary biodegradation product (AHD) decreased with time and secondary biodegradation product (SEM) slightly increased with time. Both AHD and SEM were still detected in 20-day cultures. This indicates that the complete mineralization of NFT did not occur, and TPs formed would remain unchanged in water for a long time.

Together with biodegradation analysis, results presented in P3 show the bacterial biodiversity and composition of the two bacterial communities. The identification of the microbial communities and assessment of their diversity were achieved by amplifying and sequencing the hypervariable regions of the 16S rRNA gene. Shifts in microbial communities were analyzed by metagenomic next generation sequencing (mNGS) which enabled detection and construction of the bacterial profiles of each bacterial community at various taxonomic levels from phylum to genus. The extracted DNA was analyzed at three different timepoints, chosen based on level of NFT primary biodegradation:

- The initial samples were analyzed at the start of experiments for both NW and SS consortium.
- Additional analysis was performed when a complete removal of NFT was measured (day four in NW cultures treated with 5 and 10 mg/L NFT) or flattening the curve was observed (day four in SS cultures treated with 5 mg/L NFT).
- All samples (both consortia treated with 5, 10, 15, and 20 mg/L NFT) were analyzed at the end of experiment, in 28-day cultures.

The results obtained by the mNGS and bioinformatic analysis include:

- Analysis of composition of two bacterial communities treated with NFT (5, 10, 15, and 20 mg/L).
- Determination of genera domination patterns.
- Analysis of richness and diversity of each bacterial consortium treated with NFT (α diversity).
- Analysis of differences in bacterial composition between the samples (β diversity).

The composition of the bacterial consortia was determined from the phylum to the species level. In total, six phyla, thirteen classes, thirty-one orders, sixty-five families, 119 genera, and 134 species were found in the tested samples. *Proteobacteria* was the most dominant phylum in both communities followed by *Bacteroidetes. Gammaproteobacteria* and *Betaproteobacteria* were the most abundant classes in the *Proteobacteria* phylum in the NW cultures, however, only *Gammaproteobacteria* dominated the communities in the SS cultures. *Flavobacteriia* was the most abundant class in the *Bacteroidetes* phylum in both communities. The top five families in the initial NW culture include: *Comamonadaceae*, *Pseudomonadaceae*, [*Weeksellaceae*], *Enterobacteriaceae*, and *Xanthomonadaceae*. The top five families in the initial SS culture were *Aeromonadaceae*, *Vibrionaceae*, *Pseudoalteromonadaceae*, [*Acidaminobacteraceae*], and *Shewanellaceae*.

Apart from detecting the composition of initial control cultures, the obtained results show the influence of NFT on the microbial communities. Changes in the composition of two consortia studied indicate that the *Xanthomonadaceae* family was remarkably enriched in all samples treated with NFT in comparison with the initial consortia. Moreover, the proportion of *Xanthomonadaceae* was higher in the NW culture, for which the complete primary biodegradation was measured. In addition, the unclassified *Xanthomonadaceae* species showed domination in these cultures. This suggests that *Xanthomonadaceae* sp. could be one of the main drivers of NFT biodegradation in the NW consortium. On the other hand, the proportion of *Comamonadaceae* and *Pseudomonadaceae* significantly decreased in the NFT-treated samples of the NW consortium suggesting that these species did not contribute to biodegradation. The [*Weeksellaceae]* family remarkably increased in the 4-day cultures which was followed by a strong reduction in the abundance of these microbes. This suggests that the

[*Weeksellaceae]* family could have been responsible for the primary biodegradation of NFT. *Chryseobacterium*, a genus from the [*Weeksellaceae]* family, has been detected as one of the dominating genera in bacterial cultures. Description of specific relationships regarding NFT effect on bacterial consortia is thoroughly presented in section 3.3.2 and 3.3.3 of publication P3.

In addition to analysis of changes in the bacterial community, domination and co-domination patterns between bacterial genera in each culture were assessed. Domination was defined as the presence of bacterial genera at 10% relative abundance of higher. The results indicate that the dominating genera in the initial NW sample include *Delftia* sp. (42.6%), *Pseudomonas* sp. (13.5%) and *Chryseobacterium* sp. (12.1%). The most abundant group (29.6%) in the initial SS sample included bacterial genera with no domination. Dominating bacterial genus was affected by NFT treatment in both communities. In the NW communities, the proportion of the genera that did not show any domination increased with the concentration of NFT suggesting that NFT promotes greater biodiversity within bacterial cultures. In the SS communities, the relative abundance of the unclassified genus within the *Xanthomonadaceae* family increased with the increasing content of NFT.

The variations of microbial communities are typically determined by α and β diversity. α diversity refers to the diversity within individual samples and is usually expressed by the species richness (number of species in the sample) while β diversity quantifies diversity between the samples and is measured as the number of species change between the ecosystems. The most common α diversity estimators include the richness (Observed OTUs, Chao1, ACE) and diversity (Shannon and Simpson) indices. Ordination techniques, such as principal coordinates analysis, principal component analysis (PCA), or Bray–Curtis ordination are commonly used for visualizing β diversity data.

Based on α and β diversity measures, the increasing concentration of NFT resulted in differences in the overall bacterial community diversities. All α diversity indices indicate that NFT-treated SS consortia were more diverse than the NW consortia. The biodiversity significantly increased in both consortia treated with NFT compared to the initial samples.

Conclusions:

To conclude, the results presented in P3 demonstrate that NFT biodegradation and shifts in the microbial communities' compositions revealed that aqueous bacterial communities are likely influenced by NFT concentration in the surrounding environment. Clear deviations between the two communities were observed. The initial microbial consortium from the contaminated aquatic systems (SS) was more diverse than the consortium isolated from the natural area (NW). The results also show that increase in biodiversity of microbial community does not have to be correlated with an

increase in functional capacity, such as the ability to biodegradation. In this study, higher biodiversity corresponded to lower biodegradation. An alleged bacterial exposure to environmental pollutants was not related with increased NFT biodegradation. The highest removal efficiency was observed for microbial communities at the lowest NFT concentration. Higher primary degradation of NFT was followed by a higher concentration of primary TPs and lower concentration of secondary TPs, however, lower primary degradation of NFT was followed by low concentration of primary TPs and high concentration of secondary TPs.

Taken together, presented results demonstrate that possible NFT contamination may affect the composition of aqueous microbial communities and microbial community structure can be directly correlated with the presence of NFT.

Publication P5

Multi-faceted analysis of bacterial transformation of nitrofurantoin

Publication P5 presents the results of efficiency of biodegradation of NFT by three novel bacterial species isolated from areas contaminated with organic compounds. Results present also dynamic changes within the cells during NFT biodegradation. For this purpose, single cell analyses (AFM, FC) and bulk analyses (zeta potential, particle size distribution measurements) were applied. In addition, transformation products formed during NFT biodegradation were detected and their effect on the cells was evaluated. The specific objectives of publication P5 include:

- To isolate the pure bacterial strains from contaminated environments.
- To investigate biodegradation of nitrofurantoin by these novel species.
- To identify biotransformation products and evaluate their impact on the strains.
- To analyze dynamic changes in the cell surface properties and metabolic activity during biodegradation of NFT.

The bacterial strains were isolated from three contaminated sites using the selective culture method as described in publication P1. The strains isolated and identified are listed in **Tab. 11**.

Tab. 11 Strains used in experiments in P5.

Strain	Abbreviation	GenBank	Isolation site
Stenotrophomonas acidaminiphila N0B	*Sta*	KY561351	Contaminated soil
Pseudomonas indoloxydans WB	*Psi*	MK503999	Water reservoir
Serratia marcescens ODW152	*Srm*	MN960427	Contaminated soil

The strains were used for inoculation to start liquid cultures to investigate the biodegradation of NFT and its effect on the cell properties. To analyze the biodegradation rate, detect degradation products and investigate dynamic changes in cell properties during NFT degradation, small volumes of samples were collected in a few days intervals. To investigate biodegradation rate, the samples were filtered, diluted with methanol, and analyzed qualitatively and quantitatively for the residual NFT using LC-MS/MS. To detect degradation products, the samples were derivatized with 2-nitrobenzaldehyde and then analyzed using LC-MS/MS. To investigate changes in the cell shape and topography, AFM was used. Stability of the microbial suspensions during biodegradation was determined by analysis of zeta potential and particle size distribution. Variations in the metabolic activity and viability of the bacterial cells during biodegradation of NFT were determined by FC. To investigate

effect of NFT and two TPs on the strains, the bacterial growth in the presence of these compounds as well as modifications of total membrane permeability (TMP), relative cytotoxicity (measured by colorimetric test), and metabolic activity (measured by FC) were monitored. At the end of the process of degradation, cells were sorted into subpopulations representing two physiological states (active and non-active) using flow cytometry assisted cell sorting. The sorted cells were analyzed by AFM. A scheme of procedures during experiments performed within P5 is presented in **Fig. 9**.

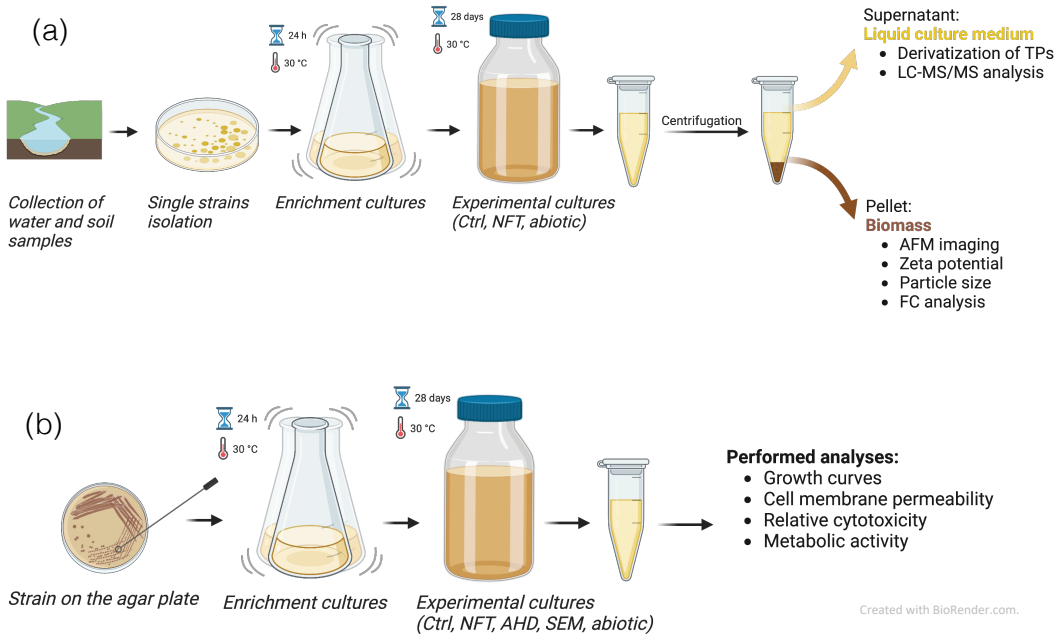

Fig. 9 A scheme of experiments performed within P5. Biodegradation of NFT and dynamic changes in cell properties (a). Effect of TPs on bacterial cells (b).
Note. Ctrl – control culture, NFT – nitrofurantoin, TPs – transformation products, AFM – atomic force microscopy, FC – flow cytometry, AHD – 1-aminohydantoin, SEM – semicarbazide.

Dynamic modifications of cell properties during biodegradation of NFT

Results of the primary biodegradation indicate that the highest NFT removal (97 ± 1%) was observed for the *Srm* strain. The two other strains, namely *Psi* and *Sta*, exhibited the final degradation rate as high as 84 ± 4% and 76 ± 3%. Along with the studies focused on NFT removal efficiency, changes in the bacterial strains during biodegradation were evaluated.

The AFM imaging was performed in 1-, 3-, 7-, and 28-day cultures to investigate morphological changes in cell shape and surface topography due to potential cell damage. The strains exposed to NFT showed significant modifications of cell shape and texture in contrast to control samples. Images of the control cells of each strain revealed a homogenous, smooth surface topography, especially during the first three

sampling days. Exposure to NFT significantly affected cell surface of each strain. Cells in NFT-treated samples were completely different than these in control samples. NFT promoted a significant cells deformation and corrugation of their surface. Specifically, the NFT-exposed *Sta* and *Psi* strains showed a loss of their original structure. A similar but less severe phenomenon was observed in the *Srm* strain in 7- and 28-day cultures.

Zeta potential (ZP), particle size (PS) and polydispersity index (PdI), were measured in the initial cultures (day 0), and 1-, 3-, 7-, and 28-day cultures to investigate the dispersive properties of the bacterial suspensions. Each strain exhibited a negative ZP due to negatively charged functional groups such as phospholipids, lipopolysaccharide, and proteins. Each strain was characterized by different dynamic of change. Most significant modifications in the ZP were observed for the *Sta* and *Psi* strains. Greater differences were observed over time (between the measurements on specific days) then between treated/control samples. The fewest differences in the ZP between the treated and control cells over time were measured for the *Srm* strain. Among all strains tested, the *Srm* strain was also characterized by the lowest absolute value of ZP.

The average size distribution in each culture over time presented a unimodal pattern. In the *Sta* strain, monodispersity of the suspension increased with the incubation time increasing. Suspensions exposed to NFT had always a broader size distribution than the control cultures due to increased cells agglomeration or aggregation. In the *Psi* strain, a wider size range accompanied by greater PdI was observed for treated cells than for the control cells. In the *Srm* strain, the size distribution was very similar to that of the other strains, however, the differences between treated and control cells were much smaller.

Flow cytometry enabled the characterization of physiological states of bacterial cells during NFT biodegradation. To assess the distribution of the defined subpopulations (non-active and active), the relative cellular activity index was calculated based on the percentages of non-active and active cells within the control and treated samples. The cellular metabolic activity of was stimulated by NFT in the *Sta* strain (only during the first day) and *Psi* strain (day 1, 3, and 7). Interestingly, the strain *Srm* occurred the most sensitive to NFT treatment as significant decrease in active bacterial cells was observed for each timepoint tested.

On the last incubation day, bacterial samples were collected and sorted into two subpopulations using flow cytometry assisted cell sorting. The sorted subpopulations were analyzed by AFM to calculate changes in the average roughness of cell surface (Ra). Active cells in each culture were characterized by lower Ra than the non-active cells suggesting severe membrane damage of the non-active subpopulation. Significant differences between the non-active and active subpopulations were observed for both Ctrl and NFT-treated cells of the *Sta* strain. In addition, differences between Ra of non-active cells collected from the control and treated cultures were statistically significant for each strain.

Transformation products detection and their effect on the cells

Two NFT biotransformation products were identified in this study: AHD was accepted as the primary transformation product, which was next transformed into SEM (secondary TP). Both TPs were detected in NFT-treated cultures of each strain (*Sta*, *Psi*, and *Srm*) which indicates that NFT biotransformation pathways were similar. The AHD signal decreased over time in each culture and the SEM signal increased over time for the *Sta* and *Srm* strains. The SEM signal was significantly lower in the *Srm* strain than that in the *Sta* strain. The *Srm* strain exhibited almost complete primary NFT biodegradation while the final NFT removal measured for the *Sta* strain was the lowest among all strains tested. Both AHD and SEM have been detected in all NFT-treated cultures even at the last degradation day. This raises considerable toxicological concerns. Results in this study are consistent with results of NFT biotransformation carried out by mixed microbial consortia in publication P3, therefore, it can be concluded that biodegradation of NFT leads to formation of stable products and follows similar pathways regardless of the source of microorganisms used for biodegradation study.

Growth of the *Sta*, *Psi*, and *Srm* strains in the presence and absence NFT, AHD, or SEM was monitored. Shape of a bacterial growth curve was different for each strain. None of the strains exhibited the conventional growth curve with four discernible stages. The best growth of the *Psi* strain was observed for the control cultures and the cultures treated with AHD. The exponential phase of growth was observed about four hours after starting the incubation. In the presence of NFT, bacterial growth was delayed as cells entered the log phase after about five hours, however, the cultures reached the same optical density as the control and ATH-treated cultures. Growth of the *Psi* strain in the presence of SEM was significantly inhibited. Substantial differences in bacterial growth were observed also in the *Srm* strain. The best growth in the control cultures and the cultures containing AHD. The greatest reduction in cell density was measured in the presence of NFT and SEM.

Modifications of TMP indicate that exposure of the *Sta* strain to AHD and SEM significantly reduced permeability of bacterial membrane. In addition, exposure of *Psi* strain resulted in a reduction of TMP by around 25% in cells exposed to NFT, AHD, and SEM. On the other hand, the *Srm* strain showed significantly increased membrane permeability in the presence of SEM. The *Srm* strain also demonstrated the lowest permeability among all strains tested.

The relative cytotoxicity of NFT, AHD, and SEM, evaluated by the colorimetric alamarBlue® Assay indicate that the greatest modifications of the reduction of alamarBlue were observed for the *Psi* strain. The lowest cytotoxicity was measured in the AHD-exposed cells and the highest toxicity in cells exposed to SEM. Significant changes between NFT/AHD samples and AHD/SEM samples were also observed for

the *Srm* strain. The lowest cytotoxicity was also measured in the AHD-exposed cells; however, the specific value was much lower than that of the *Psi* strain.

Flow cytometry analysis allowed determine the cellular metabolic activity and viability of the strains exposed to NFT, AHD, or SEM. The highest proportion of active cells was observed for the *Sta* strain non-exposed and exposed to NFT and AHD. The proportion of active cells in cultures of the *Sta* and *Psi* strains exposed to SEM decreased significantly. These strains also showed decreased membrane permeability in SEM-exposed cultures compared to non-treated cultures. In addition, growth of the *Psi* strain was significantly inhibited in the presence of SEM. The lowest proportion of active subpopulation and the fewest modifications in fractional composition of cell populations among all strains tested were observed in the *Srm* strain. It is worthwhile to notice that the *Srm* strain showed the best degradation efficiency, and the fewest modification within other cells features during biodegradation were observed for this strain.

Conclusions:

Results from this study provide new information about potential ability of autochthonous bacterial strains isolated from contaminated sites to decompose NFT. The possible effect of transformation products generated during NFT biodegradation on the isolated bacteria was evaluated. The *Srm* strain eliminated nitrofurantoin completely, however, stable transformation products were detected at the end of 28-day biodegradation process. In addition, the fewest variations in cell properties were observed for the *Srm* strain during biodegradation. Cell sorting and surface roughness analysis revealed that non-active cells present higher Ra than the active cells, however, the analogous subpopulations collected from different cultures were characterized by significant differences in Ra. AHD was identified as a primary biotransformation product and SEM as a secondary product. SEM revealed higher toxicity than NFT and AHD in strains with lower degradation potential.

Prolonged exposure of strains to nitrofurantoin and furaltadone

Publication P2

Investigation of the bacterial cell envelope nanomechanical properties after long-term exposure to nitrofurans

Publication P2 describes the effect of a 12-month exposure to nitrofurantoin and furaltadone on cell envelopes [5] of three novel bacterial strains isolated from wastewater. Results present modifications of the cell morphology and topography, cell nanomechanical properties as well as some cell biochemical features measured by classic microbiological methods, such as surface hydrophobicity, permeability of bacterial membrane, and fatty acids composition. The specific objectives of publication P2 are:

- To isolate and identify the pure bacterial strains (based on the 16S rRNA sequences) from municipal wastewater.
- To expose the isolated strains to NFT and FTD for 12 months.
- To study the modifications in microbial shape and surface triggered by long-term exposure of strains to nitrofurans.
- To investigate modifications in cell nanomechanical properties triggered by long-term exposure of strains to nitrofurans.
- To analyze biochemical response of cells exposed to nitrofurans by measuring bacterial membrane permeability, surface hydrophobicity and fatty acids profile.

The bacterial strains were isolated from the urban WWTP in Poznań, Poland (geographical location: 52◦25′53.1″N, 16◦57′31.8″E) using the selective culture method as described in publication P1. The strains isolated were identified based on the 16S rRNA sequences as *Sphingobacterium caeni* FTD2, *Achromobacter xylosoxidans* NFZ2 and *Pseudomonas hibiscicola* FZD2 (**Tab. 12**).

Tab. 12 Strains used in experiments described in P2 (identification based on 16S rRNA sequencing).

Strain	Abbreviation	GenBank
Sphingobacterium caeni FTD2	*Sph*	MK493331
Achromobacter xylosoxidans NFZ2	*Acb*	MK493330
Pseudomonas hibiscicola FZD2	*Psd*	MK493329

5 Cell envelope is a multilayered structure that separates the interior of the bacterial cell from the outside environment. The cell envelope of Gram-negative bacteria is composed of the inner cell membrane, the periplasmic space containing cell wall composed of peptidoglycan and the outer cell membrane containing lipopolysaccharide.

To induce a bacterial stress response to prolonged presence of 5-NFs, the isolated strains were cultivated for 12 months on the Mueller Hinton Agar (MHA) plates supplemented with NFT (20 mg/L) or FTD (20 mg/L). Simultaneously, the control cells were maintained on the MHA without any addition of 5-NFs. Both treated and the control cell lines were sub-cultivated every 2 weeks to provide fresh nutrients (control cells) or nutrients with NFT or FTD (treated cells). After 12 months of the continuous cultivation of the strains, the cell suspensions were stored at -80°C with the addition of glycerol to preserve them for long term storage and ensure that pure cultures are kept in as similar condition as when collected after 12 months of exposure to NFT and FTD. To recover the cryoprotected cells, the bacterial samples were picked from the frozen cryogenic vials and streaked onto the MHA or MHA supplemented with NFT or FTD. A schematic representation of procedures during exposure of cells to nitrofurans is presented in **Fig. 10**.

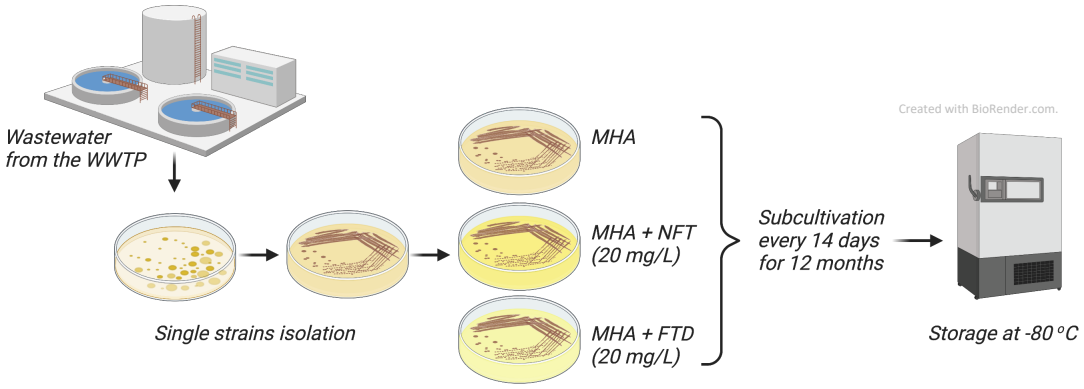

Fig. 10 Schematic representation of activities during long-term exposure of strains to NFT and FTD.

Note. WWTP – wastewater treatment plant, MHA – Mueller Hinton Agar, NFT – nitrofurantoin, FTD – furaltadone.

To investigate the effect of prolonged exposure to NFT and FTD on cell envelopes of the strains, the following analyses were made:

- Characterization of bacterial cell morphology and topography by AFM and TEM.
- Determination of surface roughness by AFM.
- Determination of cell surface nanomechanical properties, such as adhesion energy, adhesion force, deformation, energy dissipation, elastic modulus, stiffness, and elastic modulus.
- Analysis of cell biochemical properties: IMP, TMP, CSH, and fatty acids composition.

First, variations in the bacterial cell morphology and topography of cells subjected to 12-month exposure to NFT and FTD were investigated using AFM and transmission electron microscopy (TEM). Prolonged exposure to NFT and FTD induced significant changes in bacterial shape as evidenced with AFM imaging. Significant increase in the

length of the cells was observed for the *Sph*, *Acb*, and *Psd* strains treated with FTD as well as the *Acb* and *Psd* strains treated with NFT. The greatest differences in cells dimensions between the control and treated samples were observed for the *Psd* strain (cells became more spherical after treatment with NFT and FTD) and the smallest differences were noted for the *Sph* strain (**Tab. 13**). In addition, cell imaging by TEM revealed considerable changes in cells surface structure due to prolonged exposure to NFT and FTD. A total loss of wide, dark boundary around the cell (attributed to extracellular substances secreted by the cell) was observed in the FTD-treated *Sph* strain. Heterogeneous appearance of the cytoplasm, disintegration and thickening of the cell wall as well as presence of condensed spots and septal rings was observed in the *Acb* treated with both antibiotics.

Another significant point for consideration in cell surface characterization is the cell texture. Surface texture is referred to as surface roughness, described by different quantitative parameters, including the average roughness (Ra), the root mean square roughness (RMS), average roughness depth (R3z), and wavelength of the profile (λq) (**Tab. 13**). The long-term exposure of cells to 5-NFs contributed to the substantial increase of Ra in all strains tested. Different observations were made for RMS, which did not exhibit such significant modifications as Ra. The statistical increase in RMS between control and treated samples were calculated only for the *Psd* strain. Modifications of R3z of all strains resemble these of Ra. Exposure to nitrofurans induced significant alterations in λq of the NFT-treated *Acb* strain only, for which a substantial increase was calculated in comparison to control sample. Increased parameters of the cell surface roughness can indicate cell membrane destruction; however, TEM and AFM images do not clearly indicate leakage of cell content or extensive membrane damage. Increased cell surface roughness can also be due to increased synthesis of biopolymers on the cell surface.

The initial adhesion energy calculated for control samples was different for each strain tested. The *Sph* strain was characterized by the lowest value and the *Psd* strain by the highest value. Bacteria exposed to NFT significantly increased adhesion energy in comparison to control samples. Bacteria exposed to FTD had always lower adhesion energy than the ones exposed to NFT. The average adhesion force was also the lowest in the *Sph* strain and the highest in the *Psd* strain, however, the greatest modifications between control and treated samples were observed for the *Acb* strain. An increase in adhesive properties of cells shall be assigned to the leakage of cytoplasm; however, this can be caused by the presence of antimicrobial agents but also AFM tip penetrating inside the cytoplasm.

Deformation of the cell envelope, elastic modulus and cell stiffness measured by AFM has provided some information about elastic properties of cells. A significant increase in deformation was noted for NFT-exposed cells of all strains in comparison to control samples. Modification of elastic modulus and stiffness of cells revealed that prolonged contact of the strains with NFT or FTD has undoubtedly increased their

elastic properties. The cells which showed significant alterations of Young modulus, exhibited also considerable heterogenicity. Importantly, high homogeneity of cell populations is positively correlated with bacterial adaptation to external stimuli. Summary of cell nanomechanical properties is presented in **Tab. 13**.

Tab. 13 Summary of selected results presented in P2. The direction of arrows indicates up- or downregulation (control vs. long-term treated sample). Not significant comparisons are labelled as "ns".

Analysis	Specific property	*Sph*		*Acb*		*Psd*	
		NFTs	*FTDs*	*NFTs*	*FTDs*	*NFTs*	*FTDs*
Dimensions	Length	ns	↓	↑	↑	↓	↓
	Width	ns	ns	ns	↑	ns	ns
	Height	ns	ns	ns	ns	↑	ns
Surface roughness	Ra	↑	↑	↑	ns	↑	↑
	RMS	ns	ns	ns	ns	↑	↑
	R3z	↑	↑	↑	ns	↑	↑
	λq	ns	ns	↑	ns	ns	ns
Nanomechanical properties	Adhesion energy	↑	ns	↑	↓	↑	↑
	Adhesion force	ns	↓	↑	↑	↑	ns
	Deformation	↑	ns	↑	↑	↑	↑
	Elastic modulus	↑	↑	↑	↑	↑	↑
	Stiffness	↑	↑	↑	↑	↑	↑
Biochemical properties	TMP	↑	↑	ns	↓	↑	ns
	IMP	↑	↑	↑	↓	↑	↑
	CSH	ns	ns	ns	ns	ns	↓

Note. Ra - the average roughness, RMS - the root mean square roughness, R3z - average roughness depth, λq - wavelength of the profile, TMP – total membrane permeability, IMP – inner membrane permeability, CSH – cell surface hydrophobicity.

The next part of experiments was devoted to analysis of changes in the biochemical properties of the cells. Summary of the results obtained is presented in **Tab. 13**. In the case of IMP, TMP, and CHS, analyses were made for control cells, cells exposed to 5-NFs for 24 hours (short-term exposure), and cells exposed to 5-NFs for 12 months

(long-term exposure). In the *Sph* strain, the lowest TMP was measured for the control sample and an increase by around 10% in every other sample was measured, however, no significant differences between these samples in TMP was measured. Different observations were made for the *Acb* and *Psi* strains. In these strains, the highest modifications of TMP were mostly observed between control samples and bacteria after short-term contact with 5-NFs. Most often than not, TMP increased in the treated samples. The directions of the modifications of IMP measurements were similar to these of the TMP except for the *Acb* strain exposed to NFT for 12 months and the *Psd* strain after long-term exposure to FTD. The greatest variations of IMP were measured for the *Psd* strain. The highest values of IMP were noted for samples after short-term contact with 5-NFs. Probably, this was due to lack of efficient adaptation of strains to the presence of nitrofurans in their surrounding environment. Thus, antibiotics might have promoted a disintegration of bacterial membrane. Cell adhesion properties did not show significant variations in cells after prolonged exposure to 5-NFs except for the *Psd* strain exposed to FTD. Short-term exposure to FTD promoted statistically significant modification of CHS in the *Acb* strain and to NFT in the *Psd* strain.

Analysis of fatty acid profiles indicate that the greatest differences between the control and treated samples were observed in the *Psd* strain, and the smallest differences were observed for in the *Sph* strain. Among five groups of fatty acids tested (unsaturated, hydroxy, cyclopropane, branched, straight chain), only the hydroxy fatty acids were not affected by nitrofurans.

Conclusions:

Results from this study demonstrated that prolonged exposure of bacteria to 5-NFs induces changes in the cell envelope, as evaluated with microscopic and biochemical methods. AFM and TEM imaging have shown than both NFT and FTD contribute to morphological changes in the cell. Surface texture has also significantly increased in treated cells. Nanomechanical properties of the strains have been altered after 12-month bacterial exposure to nitrofurans. Most often than not, in increase in these parameters was observed. Modifications of the bacterial cell structure were strongly modulated by the nature of the pharmaceutical's molecule and the bacterial cell type. Mostly, NFT promoted greater remodeling of the cells structure than FTD (this was particularly visible in the *Acb* strain). Studies of bacterial cells mechanics taken together with classic biochemical methods provided complex information about bacterial cell response to 5-NFs. In general, the *Psd* strain exhibited the greatest modifications of cell envelope, and the *Sph* strain showed the fewest variations due to prolonged exposure to 5-NFs. The knowledge obtained within this study may help improve our understanding of nitrofurans that receive attract little scientific attention but pose a risk to the environment and human health.

Publication P4

Potential negative effect of long-term exposure to nitrofurans on bacteria isolated from wastewater

Results presented in P2 served as a basis for deeper investigation of long-term impact of 5-NFs towards bacteria isolated from wastewater. Consequently, whole-genome sequencing performed to further investigate the underlying genetic aspects of response of the previously isolated strains to NFT and FTD. In addition, this study used a combination of molecular biology, electrochemical, and classic culture methods to functionally analyze the isolated strains exposed to 5-NFs. The objectives of results presented in P4 are to investigate the effects of a 12-month continuous exposure of three strains to NFT and FTD on:

- Metabolomic profile.
- Detection of DNA damage.
- Metabolic activity, and stress response within the bacterial cells.

The bacterial strains used in this study were isolated from the WWTP in Poznań, Poland as described in P2 (**Tab. 14**). Bacterial whole-genome sequencing, phylogenetic analysis and secondary metabolite gene clusters prediction were performed. As a result, the strains were identified as *Sphingobacterium siyangense* FTD2 (previous identification based on 16S rRNA: *Sphingobacterium caeni* FTD2), *Achromobacter pulmonis* NFZ2 (previous identification based on 16S rRNA: *Achromobacter xylosoxidans* NFZ2), and *Stenotrophomonas maltophilia* FZD2 (previous identification based on 16S rRNA: *Pseudomonas hibiscicola* FZD2).

Tab. 14 Strains used in experiments described in P4 (identification based on whole-genome sequencing).

Strain	Abbreviation	GenBank
Sphingobacterium siyangense FTD2	*Sph*	CP080574
Achromobacter pulmonis NFZ2	*Acb*	JAIFOT010000000
Stenotrophomonas maltophilia FZD2	*Stm*	CP080573

To induce a long-term stress response, the strains were continuously cultivated in the presence of either NFT or FTD for 12 months as described in P2.

Metabolomics analysis

Metabolomics analysis was used to screen potential biologically relevant markers to explore the metabolic processes involved bacterial adaptation to NFT and FTD.

To understand the general metabolomic profile of each group, the PCA analysis was performed. Results indicate that the control samples clustered separately from both the FTDs and NFTs, indicating differences in the metabolomic characteristics. The smallest separation of clusters between control and treated samples was found in the *Acb* strain. The greatest differences were observed for the *Stm* strain. Differences between NFT- and FTD-exposed samples of each strain were negligible, eliciting a similar but not identical response of strains to 5-NFs tested. Out of 1371 metabolites identified, 184 compounds differed significantly among the treatments and the strains – they are referred to as differentially accumulated metabolites (DAMs).

Identified DAMs were functionally analyzed to investigate if certain pathways or processes are significantly different between the control and treated samples. Results indicate that the most significantly altered pathways were observed in:

- Amino acid metabolism
    - Ala, Asp and Glu metabolism
    - Phe, Tyr and Trp metabolism
    - Arg and Pro metabolism
    - Ala metabolism
- Sugar metabolism
    - Glucose metabolism
    - Galactose metabolism
- Aminoacyl-tRNA (aa-tRNA) biosynthesis
- Novobiocin biosynthesis

All the above-mentioned metabolic pathways were related to long-term exposure to NFT. Seven pathways were detected in the *Stm* strain, five pathways in *Sph* and three in the *Acb* strain. A total of seven metabolic pathways were associated with FTD prolonged exposure. Every one of them was identified in the *Sph* strain, two pathways in *Acb* and three in *Stm.*

The most affected metabolites are components of biological pathways involved in amino acid and sugar metabolism as well as aa-tRNA biosynthesis. Therefore, differences in concentration of differentially accumulated amino acids among three sample groups were thoroughly examined. Accumulation of most amino acids and derivatives decreased significantly in cells of all strains exposed to FTD and NFT. Some individual examples of increased amino acids were observed in the *Sph* and *Stm* strains (e.g. Isoleucine increased after treatment with NFT in both strains). Cells of the *Acb* strain exhibited lower accumulation of all protein-building amino acids in response to both antibiotics. A significant decrease in the abundancy of protein-building amino acids in response to NFT and FTD treatment is in agreements with the proposed mode of action of these antibiotics[6].

---

6 Suggested mechanism of action of NFT involves the binding of NFT molecule to ribosomes, inhibiting the total protein synthesis as well as the activity of enzymes responsible for the synthesis of DNA and RNA. To date, the exact mechanism of action of 5-NFs is not understood (Blass, 2015; Hutttner et al. 2015; McOsker and Fitzpatrick, 1994).

Glutathione (GSH) is a tripeptide commonly found in prokaryotic and eukaryotic cells. GSH plays a key role in intracellular redox homeostasis and adaptation to stress in bacterial cells (Smirnova and Oktyabrsky, 2005). GSH also promotes metabolism of many xenobiotics. Its conjugation to these chemicals facilitates their further metabolism and is catalyzed by glutathione S-transferase enzymes. In this study, eight compounds involved in the metabolism of GSH (glycine, glutamic acid, cysteine, 5-oxoproline, spermidine, ornithine, putrescine, and cadaverine) were detected during metabolomic analysis. In most of the cases, treatment of strains with NFT and FTD contributed to decreased level of metabolites. The greatest modifications were noted for glycine and glutamic acid in the *Sph* and *Acb* strains. The slightest modifications were observed in the *Stm* strain. Together with analysis of specific compounds involved in GSH metabolism, activity of glutathione-S-transferases (GSTs) enzymes (as well as three other biochemical parameters) was analyzed. The greatest increase in GSTs activity was observed in the *Stm* strain and a slight decrease was measured in the *Sph* strain. Description of these results is presented in the following paragraphs.

To correlate information from the metabolomic studies with the genetic information provided by the whole genome sequencing, the KEGG analysis of the identified DAMs was performed. The pathways of GSH metabolism and aa-tRNA biosynthesis with the genes present in each strain and detected DAMs were analyzed. Five downregulated metabolites involved in the GSH metabolic pathway were revealed in the *Sph* strain. Six downregulated metabolites were detected in the *Acb* strain. In the *Stm* strain, no metabolites were detected in response to NFT, and two metabolites were detected in response to FTD. Upregulated metabolites were not detected.

The largest number of downregulated metabolites involved in the aa-tRNA pathway was detected in the *Sph* strain exposed to NFT, however, the smallest number was observed in the NFT-exposed *Stm* strain. Upregulated metabolites were not detected. Aa-tRNAs are responsible for delivering amino acids for protein synthesis at the ribosome. They also participate in several other processes such cell wall formation or cell envelope remodeling (Moutiez et al., 2017). These results are consistent with results presented in P4, which demonstrated that the *Sph* strain showed the fewest variations due to prolonged exposure to 5-NFs.

Effect of long-term exposure to NFT and FTD on DNA damage

Damage of genetic material of strains exposed to NFT and FTD was analyzed by electrochemical DNA sensors and random amplification of polymorphic DNA (RAPD-PCR).

Electrochemical method was based on detection of the voltametric signals of the following nucleobases: 8-Oxo-2'-deoxyguanosine - an oxidized derivative of deoxyguanosine (8-oxodD), guanine, and adenine. Strength of guanine oxidation and the formation of 8-oxodG represented 5-NFs long-term mutagenic effect on the

bacterial DNA. In the *Sph* strain, a significant reduction in the electric current of guanine was observed in NFT- and FTD-treated cells. In addition, an appearance of 8-oxodG signal in FTD-treated cells was observed. In the *Acb* strain, the long-term exposure with NFT and FTD generated a formation of 8-oxodD signals. The signal was much more intense after treatment with FTD. In the *Stm* strain, a significant reduction in the electric current of guanine was observed in all treated samples. Two strong, distinct oxidation signals at potential maxima of approximately 0.65 V and 0.75 V were additionally observed in FTD-treated cells. The adenine signal was shifted towards the lower potential, indicating breaking the hydrogen bonds between the nucleotide base pairs in double-stranded DNA. For all analyzed DNA samples, an increased width of guanine signals was observed, indicating the breaking of some hydrogen bonds that stabilize the double-stranded structure of DNA. 8-oxodG signal was particularly evident in samples treated with FTD, indicating its considerable mutagenic effect. The changes in the DNA of the strains exposed to NFT or FTD were confirmed by RAPD-PCR. The greatest differences between control and FTD-treated samples were observed in the *Stm* strain.

Stress response to long-term NFT and FTD exposure

Several biochemical cell properties were measured to determine the bacterial stress response to prolonged exposure to 5-NFs. These properties include relative metabolic activity (RMA), lipid peroxidation (LPX), the activity of superoxide dismutase (SOD), catalase (CAT), and GSTs. RMA determine the overall cell metabolism, LPX refers to the oxidative degradation of lipids. SOD and CAT protect cells from oxidative damage by reactive oxygen species while GSTs play a key role in cell detoxification.

RMA was investigated at four different concentrations of 5-NFs: 5, 10, 15, and 20 mg/L. Each strain exposed to NFT or FTD responded differently to the increasing concentration of each antibiotic. For example, the RMA of the *Sph* strain increased when cultivated at concentrations of NFT ranging from 5 to 15 mg/L. On the other hand, no significant modifications in the analogical samples containing FTD. In addition, the RMA of the *Acb* strain cultivated with NFT was strikingly lower than that in the control cells regardless of the NFT concentration. No statistically significant differences were observed in the RMA of the *Stm* strain treated with NFT, however, the increased concentration of FTD resulted in increased RMA.

LPX, SOD, CAT, and GSTs were measured in cells cultivated with 5 mg/L of 5-NFs. LPX was determined by the detection of malondialdehyde (MDA), which was synthesized as a result of oxidative degradation of lipids. The results revealed different patterns of MDA synthesis for each treatment. The greatest LPX was detected in the NFT-treated *Acb* strain. The highest values of SOD, reaching up to 90%, were measured for *Sph* strain, however, no difference between control and treated cells was observed. A statistically significant increase in SOD was noted in the FTD-treated *Acb*

strain. The opposite situation was for the *Stm* strain, for which a decrease in SOD was measured. NFT did not affect SOD by any of the strains used in this study. Exposure of the *Sph* and *Acb* strains to NFT and FTD decreased activity of CAT, and exposure of the *Stm* strain increased activity of CAT.

Long-term exposure of the *Sph* to FTD resulted in a decreased activity of GSTs; and no difference between the treatments was observed. Different observations were made for two other strains, which significantly increased the GSTs activity when cultivated under stress conditions. Exposure to NFT resulted in more potent induction of the GSTs enzymatic pathways than exposure to FTD in both strains.

Conclusions:

Results from publication P4 shed light into the potential risks of the prolonged presence of 5-NFs in the environment and provide additional information on the possible impact of NFT and FTD on the bacterial cells isolated from wastewater. Long-term exposure of strains to NFT and FTD altered metabolomic characteristics, disrupted protein biosynthesis, accelerated mutagenic effects, and promoted oxidative stress within the cells. Significant changes in LPX, SOD, CAT, and GSTs reflect that cell exposure to 5-NFs decreases cell ability to cope with environmental stress. This was specifically visible in the *Sph* strain for which the strongest decline in the parameters in question were visible. NFT and FTD showed similar, but not identical, mechanisms of action towards environmental bacteria. Interactions of these antibiotics with cells depend more on characteristics of the strain than properties of the individual nitrofurans.

Supplementary studies

Author was involved in publication of three more papers (S1 – S3) related to nitrofurans biodegradation and/or impact on bacterial strains. These publications should be considered as the additional achievements, they are not directly included in dissertation.

Publication S1

A. Pacholak, A. Zdarta, R. Frankowski, Z. Cybulski, E. Kaczorek, *Exploring elimination kinetics of four 5-nitrofuran derivatives by microbes present in rural and municipal activeted sludge*, Water, Air, & Soil Pollution 231 (2020) 252, doi:10.1007/s11270-020-04634-7

Short description and the main findings:

The aim of this study was to characterize wastewater collected from rural and municipal WWTP in Poland using metagenomic analysis and to analyze the ability of microbial communities to biodegrade four nitrofuran antibiotics: NFT, NFZ, FTD, and FZD. Metagenomic analysis provided information about the bacterial biodiversity in the WWTPs. In both samples, the most abundant phylum was *Proteobacteria* followed by *Bacteroidetes*. Bacterial community in the municipal wastewater exhibited greater biodiversity than the community in rural wastewater. The results of LC-MS/MS analysis and kinetic calculations allowed determine FZD, FTD, NFT, and NFZ elimination half-time varying from 104 to 327 h. A comparison of the effectiveness of the two communities in biodegradation of nitrofurans, revealed that both consortia contained bacterial strains capable of using all nitrofurans as a source of carbon and energy, however, the poorer performance of the strains from the smaller, rural WWTP was observed. In 72 hours, 87% removal of FTD, 63% FZD, 61% NFT, and 55% NFZ was measured in municipal wastewater. Simultaneously, 33% removal of FTD, 23% FZD, 23% NFT, and 19% NFZ was measured in rural wastewater. Due to incomplete elimination of all nitrofurans, additional analysis of nitrofurans content was performed in 24-day cultures. The municipal wastewater was able to a total elimination of FTD and NFT. In addition, 86% removal of NFT and 90% removal of FZD was measured. The final elimination rate, measured on the 24th day was 63% for NFT, 45% for FZD, and 49% for FTD.

Publication S2

W. Smułek, Z. Bielan, **A. Pacholak**, A. Zdarta, A. Zgoła-Grześkowiak, A. Zielińska-Jurek, E. Kaczorek, *Nitrofurazone Removal from Water Enhanced by Coupling Photocatalysis and Biodegradation*, International Journal of Molecular Sciences, 22 (2021) 2186, doi:10.3390/ijms22042186

Short description and the main findings:

Conventional methods of wastewater treatment are mostly ineffective towards pharmaceuticals, therefore development of new and effective strategies for their degradation is essential. Given the low efficiency of biodegradation, the aim of this study was to assess the possibilities of supporting biodegradation with photocatalytic processes in NFZ removal. This publication explored efficiency of different methods of NFZ degradation: photolysis and photodegradation in the presence of two photocatalysts. Additionally, the effects of the photodegradation products on bacterial cell surface properties and cell membranes were studied. Results indicate that photocatalysis with TiO2-P25 allowed almost complete elimination of NFZ (>90%), demonstrating that this method is twice as effective as photolysis alone. Photocatalysis alone or coupled with biodegradation with the environmental bacterial strain leads to efficient degradation and almost complete mineralization of NFZ. Furthermore, the experiments showed that the products of NFZ degradation can be toxic to bacterial cells and affect their membranes. Therefore, it seems beneficial to combine photocatalytic degradation with biodegradation. The photocatalytic system combined with biodegradation by *Achromobacter xylosoxidans* allows effective mineralization (over 95%) of NFZ in contaminated water. This observation opens new and promising perspectives to reduce the threat of pharmaceutical pollution in water ecosystems.

Publication S3

W. Smułek, M. Rojewska, **A. Pacholak**, O. Machrowicz, K. Prochaska, E. Kaczorek, *Co-interaction of nitrofurantoin and saponins surfactants with biomembrane leads to an increase in antibiotic's antibacterial activity*, Journal of Molecular Liquids 364 (2022) 120070, doi: 10.1016/j.molliq.2022.120070

Short description and the main findings:

Limited bioavailability of antibiotics is a major challenge in the treatment of bacterial infections. To increase transport of NFT into the bacterial cells the proposed strategy is to use saponins, the natural surface-active agents extracted from *Sapindus mukorossi* L. The aim of this study was to investigate the ability of saponins to increase the antibacterial action of NFT against Gram-negative bacterium *Pseudomonas aeruginosa* NFT3. The results indicate that the activity of cells treated with NFT was almost 35% lower after 8 h compared to control, however, in the presence of *S. mukorossi* L. saponins over 75% reduction in the activity of the cells was observed. The Langmuir monolayer technique proved the incorporation of plant surfactant molecules into the phospholipid membrane. The analysis with living bacterial cells showed a significant decrease of TMP in the presence of NFT with a negligible effect of saponins on this parameter. TEM and AFM imaging confirmed the deformation of the bacterial cell wall in the presence of saponins. As a conclusion, the synergistic co-action of the saponins and NFT was proved, which facilitates the bioavailability of NFT towards the bacterial cells and increases its effectiveness as a biocidal agent. The research results indicate the possibility of using new, biodegradable surfactants in antimicrobial therapies.

Chapter 5

Concluding remarks

Overall conclusions

This chapter will conclude the dissertation by summarising the key findings in relation to the research objectives and hypotheses (H1 to H6). It will also review the limitations of the study and propose opportunities for future research.

The aim of this dissertation is to explore the biodegradation of selected nitrofurans by environmental bacteria and to understand how nitrofurans affect the cell properties. Experimental work was carried out to investigate selected nitrofuran antibiotics in terms of their biodegradability as well as short- and long-term influence on the bacterial strains. Results of this dissertation comprise five full length research articles (P1 – P5) published in the journals indexed by the Journal Citation Reports.

The first step of the research was isolation of single bacterial strains from various environmental compartments and their identification. Overall, **eleven pure Gram-negative strains were isolated and identified** as presented in **Tab. 15**.

Tab. 15 Bacterial strains used in experiments performed within the presented dissertation.

Strain	Isolated from	Used in publication
Sphingomonas paucimobilis K3a	Rural wastewater	P1
Ochrobactrum antrophi K3b	Rural wastewater	P1
Rhizobium radiobacter P4c	Urban wastewater	P1
Pseudomonas aeruginosa P4a	Urban wastewater	P1
Sphingobacterium thalpophilum P3d	Urban wastewater	P1
Sphingobacterium siyangense FTD2*	Urban wastewater	P2, P4
Achromobacter pulmonis NFZ2*	Urban wastewater	P2, P4
Stenotrophomonas maltophilia FZD2*	Urban wastewater	P2, P4
Stenotrophomonas acidaminiphila N0B	Contaminated soil	P5
Pseudomonas indoloxydans WB	Water reservoir	P5
Serratia marcescens ODW152	Contaminated soil	P5

Note. * denotes strains identified based on whole genome sequencing. The remaining strains were identified based on 16S rRNA sequencing.

One of the major objectives of this dissertation was to explore biodegradation of nitrofurans by the single strains and the microbial consortia collected from various

environments. The experiments focused on nitrofurantoin removal efficiency as well as identification of transformation products and determination of their impact on the cells.

Biodegradation by single strains is presented in publications P1 and P5. Out of eight pure strains tested, **three strains were able to degrade >90% of NFT** in 28 days (*Sphingomonas paucimobilis* K3a, *Ochrobactrum antrophi* K3b, *Serratia marcescens* ODW152) **(H1)**. The remaining strains showed biodegradation of NFT between 50 and 84%.

Biodegradation of NFT by mixed bacterial consortia was investigated in publication P3. The consortia used in the study were collected from the mountain stream (NW), representing the reserve of the protected area with no human intervention, and the seaport seawater (SS) representing the area that concentrates diverse human activities and receives numerous contaminants. Results indicate that **NFT removal by microorganisms in the NW cultures was much more efficient than in the SS cultures** (**Tab. 10**), suggesting that autochthonous microorganisms in the contaminated areas that concentrate various human activities have lower degradation abilities than microorganisms in the protected areas with no human intervention. **Total NFT primary biodegradation has been achieved** by the NW consortium in samples with the two lowest initial concentrations of NFT **(H1).** A complete degradation has not been measured in the SS cultures, however, the highest degradation efficiency reached 91% in the sample with the lowest NFT initial concentration. **The highest removal efficiency was observed for microbial communities at the lowest NFT concentration**.

The primary biodegradation of xenobiotics often leads to the generation of TPs that remain unchanged in the ecosystems for a long time. Products of NFT primary degradation by mixed consortia were proposed in publication P3 and by single strains in publication P5. **The proposed products of NFT biodegradation include AHD, SEM and HYD** (the latter was only detected in cultures containing bacterial communities in P3). 1-aminohydantoin was assumed to be a primary product of NFT biotransformation, and it was later transformed into two secondary products: SEM and HYD (**Fig. 8**). **Biodegradation of NFT followed the same pathways for two mixed consortia and single strains** and led to generation of similar TPs. In addition, the **AHD signal decreased over time and the SEM signal increased over time.** Both compounds were still detected at the end of the process, indicating that the **complete mineralization of NFT did not occur**, which raises considerable toxicological concerns **(H2).**

Effect of transformation products formed (AHD and SEM) on three bacterial strains was evaluated in publication P5. Specifically, the following properties of the *Sta*, *Psi*, and *Srm* strains in the presence and absence NFT, AHD, or SEM were monitored: growth curves, modifications of TMP, the relative cytotoxicity, and metabolic activity. The results indicate that **the greatest reduction in cell density (growth inhibition) was measured in the presence of NFT and SEM** in the *Psi* and *Srm* strains. In addition, the most significant impact on the bacterial membrane permeability was observed for SEM.

Semicarbazide revealed higher toxicity than NFT and AHD in strains with lower degradation potential (H2).

Another objective of this dissertation was to explore the impact of nitrofurans on cell metabolic activity and cell properties, such as membrane permeability and surface hydrophobicity. Such experiments, focused on short-term impact of NFT on the single strains, were performed within publication P1. To understand the general effect of pharmaceutical residues on the cells, evaluation of these parameters is essential as they provide information about remodeling of the outer layers of bacterial cells, and defensive mechanisms implemented in response to the presence of the pollutant. The obtained results indicate that **NFT affects the properties of single bacterial strains significantly, however, the cells response is not unequivocal (H4)**. Nonetheless, in strains with the highest degradation efficiency, the cell properties are modified towards towards lower values, suggesting on sealing of the outer layers of the cell to prevent the xenobiotics from entering the cell. In addition, dynamic modifications of cell properties during nitrofurantoin biodegradation were determined (P5). The dispersive properties of the bacterial cultures and metabolic activity changed dynamically during biodegradation of nitrofurantoin. The fewest variations of stability of microbial suspension and metabolic activity during biodegradation were observed for the strain that showed the best degradation efficiency **(H3).**

Critical assessment of the dynamic changes in the composition and diversity of the microbial communities during biodegradation of NFT was important element of the research. Results of these experiments are presented in publication P3. Nitrofurantoin biodegradation and shifts in the microbial communities' compositions revealed that **aqueous bacterial communities are likely influenced by NFT** concentration in the surrounding environment **(H5).** Clear deviations between the two communities were observed. **The initial microbial consortium from the contaminated aquatic systems (SS) exhibited greater biodiversity than the consortium isolated from the natural area (NW).** The results also show that **increase in biodiversity of microbial community does not have to be correlated with an increase in functional capacity**, such as the ability to biodegradation - **greater biodiversity corresponded to lower biodegradation**. The main drivers of NFT biodegradation in the NW consortium are the members of *Xanthomonadaceae* and [*Weeksellaceae]* families because their abundance was enriched in all samples treated with NFT in comparison with the initial consortia. In addition to analysis of changes in the bacterial community, **domination and co-domination patterns between bacterial genera were assessed**. Results indicate that the **dominating bacterial genus was affected by NFT treatment in both communities**. Based on α and β diversity measures, the increasing concentration of NFT resulted in differences in the overall bacterial community diversities. All α diversity indices indicate that the NFT-treated SS consortia were more diverse than the NW consortia. The biodiversity significantly increased in both consortia treated with NFT compared to the initial samples **(H5).**

The following part of this section will focus on studies related to **prolonged exposure of bacterial strains to NFT and FTD** (P2, P4). To induce a bacterial stress response to prolonged presence of selected nitrofurans, the strains were cultivated for 12 months on the MHA plates supplemented with NFT or FTD. As presented in publication P2, **12-month exposure of strains to nitrofurans induces changes in the bacterial cell envelope (H6)**. AFM and TEM imaging have shown than both NFT and FTD contribute to morphological modifications of the cell. Another significant point for consideration in cell surface characterization is the cell texture, which is referred to as surface roughness, described by different quantitative parameters. Results of the study clearly show that **cell surface texture has significantly increased in NFT- and FTD-treated cells**. This was particularly visible in measurements of the average cell roughness. Increased parameters of the cell surface roughness suggest on destruction of cell membrane; however, TEM and AFM images did not clearly indicate leakage of cell content or extensive membrane damage. Increased cell surface roughness could also be due to increased synthesis of biopolymers on the cell surface. **Nanomechanical properties of the cells have altered significantly after 12-month bacterial exposure to nitrofurans**. Most often than now, in increase in these parameters was observed. **Modifications of the bacterial cell structure were strongly modulated by the nature of the pharmaceutical's molecule and the bacterial species. Mostly, NFT promoted greater remodeling of the cells structure than FTD (H6).**

Analysis of biochemical properties of the cells exposed for 12-months to nitrofurans indicate that **the variations in cell membrane permeability, surface hydrophobicity and fatty acids profile are different for each strain (H6)**. However, most often than not, membrane permeability increased and CSH did not show significant variations in cells exposed to nitrofurans. Significant variations were also noted for fatty acid profiles. Among five groups of fatty acids tested (unsaturated, hydroxy, cyclopropane, branched, straight chain), only the hydroxy fatty acids were not affected by nitrofurans.

Results presented in P2 served as a basis for deeper investigation of long-term impact of nitrofurans towards bacteria isolated from wastewater. Consequently, the effects of a 12-month continuous exposure of three strains to NFT and FTD on the metabolomic profile, DNA damage and stress response within the bacterial cells were evaluated within publication P4. Metabolomics analysis revealed **differences in the metabolomic characteristics between control and treated samples of each strain** tested. Variations between NFT- and FTD-exposed samples of each strain were negligible, eliciting **a similar but not identical response of strains to nitrofurans** tested **(H6)**. Based on the functional analysis of differentially accumulated metabolites, the most significantly altered metabolic pathways were observed in amino acid metabolism, sugar metabolism, aa-tRNA biosynthesis, and novobiocin biosynthesis. Specifically, **accumulation of most protein building amino acids decreased significantly in strains exposed to FTD and NFT** which is in agreements with the proposed mode of action of these antibiotics. In addition, a decreased level of several compounds involved in the

metabolism of GSH was detected. To correlate information from the metabolomic studies with the genetic information provided by the WGS, the KEGG analysis of the identified DAMs was performed. The pathways of GSH metabolism and aa-tRNA biosynthesis with the genes present in each strain and detected DAMs were analyzed. In each pathway, several downregulated metabolites were identified. No upregulated metabolites were detected.

The 12-month continuous exposure of strains to nitrofurans contributed to **damage of their genetic material as evidenced by electrochemical DNA sensors** and RAPD-PCR. Remarkable changes in LPX, SOD, CAT, and GSTs reflect that **cell exposure to nitrofurans decreases cell ability to cope with environmental stress**. This was specifically visible in the *Sph* strain. Overall, **NFT and FTD showed similar, but not identical, mechanisms of action towards environmental bacteria. Interactions of these antibiotics with cells depend more on characteristics of the strain than properties of the individual nitrofurans (H4, H6).**

Limitations and future directions

There are several possibilities to extend the work presented in this dissertation. As a starting point, it should be highlighted that the use of nitrofurans has increased recently. Nonetheless, little information is available about occurrence of nitrofurans and their marker residues in wastewater and other water bodies. Research focused on detecting nitrofurans and their marker residues around the world should be conducted to learn about the actual contamination of the natural environment with these antibiotics. Additional work is required to understand the levels of nitrofurans entering the natural environmental compartments and efforts should be directed at determining where this contamination occurs.

Efforts should be also made to improve awareness of the society about dangers related with antibiotic pollution. In particular, trainings for agronomists and farmers should be provided to encourage them to use alternatives instead of antibiotics to promote growth of animals.

This dissertation focused on nitrofurantoin, which is the major representative of the nitrofuran antibiotics. Therefore, another natural extension of this work is in-depth investigation of biodegradation and environmental impact of other nitrofurans, such as furazolidone or nitrofurazone. While primary biodegradation of nitrofurantoin has led to formation of stable transformation products, it would be interesting to investigate their biodegradability by the bacterial strains. In addition, experiments on mineralization of nitrofurantoin and products of its transformation could complement the existing results. To this end, it would be interesting to thoroughly investigate mechanisms of nitrofurans biodegradation by bacteria.

While modifications occurring at the molecular level in the cells of strains biodegrading nitrofurans remain unknown, it would be interesting to include (and combine) additional omics techniques, such as transcriptomics or proteomics.

The further work outlined above would help clarify some of the results obtained in this dissertation and help understand the environmental impact of nitrofurans.

Concluding statement

What emerges out of this dissertation is the fact that environmental bacterial consortia contain strains capable of biodegrading nitrofurantoin. Nonetheless, biodegradation of nitrofurantoin leads to formation of stable products (such as 1-aminohydantoin, semicarbazide and hydrazine) and follows similar pathways regardless of the source of microorganisms used for biodegradation study. The possible nitrofurantoin contamination may affect the composition of aqueous microbial communities and microbial community structure can be directly correlated with the presence of nitrofurantoin. Long-term exposure of bacterial strains to nitrofurans can induce morphological changes within the cells, alter metabolomic characteristics, disrupt protein biosynthesis, accelerate mutagenic effects, and promote oxidative stress. Studies of bacterial cells mechanics taken together with classic biochemical methods provided complex information about bacterial cell response to nitrofurans. The knowledge obtained within this dissertation may help improve our understanding of nitrofurans that receive attract little scientific attention but pose a risk to the environment and human health. This dissertation has also contributed to a better understanding of the environmental impact of nitrofurantoin and its intermediates. Results could be helpful during designing the technologies of bioremediation of sites contaminated with antibiotics.

References

Adeleye, A.S., Xue, J., Zhao, Y., Taylor, A.A., Zenobio, J.E., Sun, Y., Han, Z., Salawu, O.A., Zhu, Y., 2022. Abundance, fate, and effects of pharmaceuticals and personal care products in aquatic environments. Journal of Hazardous Materials 424, 127284. https://doi.org/10.1016/j.jhazmat.2021.127284

Ajibola, A.S., Amoniyan, O.A., Ekoja, F.O., Ajibola, F.O., 2021. QuEChERS Approach for the Analysis of Three Fluoroquinolone Antibiotics in Wastewater: Concentration Profiles and Ecological Risk in Two Nigerian Hospital Wastewater Treatment Plants. Arch Environ Contam Toxicol 80, 389–401. https://doi.org/10.1007/s00244-020-00789-w

Álvarez-Martínez, F.J., Barrajón-Catalán, E., Herranz-López, M., Micol, V., 2021. Antibacterial plant compounds, extracts and essential oils: An updated review on their effects and putative mechanisms of action. Phytomedicine 90, 153626. https://doi.org/10.1016/j.phymed.2021.153626

An, J.D., Wang, T.T., Shi, Y.F., Wu, X.X., Liu, Y.Y., Huo, J.Z., Ding, B., 2020. A multi-responsive regenerable water-stable two-dimensional cadmium (II) fluorescent probe for highly selective, sensitive and real-time sensing of nitrofurazone and cupric ion. Journal of Molecular Structure 1216, 128328. https://doi.org/10.1016/j.molstruc.2020.128328

Auro, A., Sumano, H., Ocampo, L., Barragán, A., 2004. Evaluation of the carcinogenic effects of furazolidone and its metabolites in two fish species. Pharmacogenomics J 4, 24–28. https://doi.org/10.1038/sj.tpj.6500216

aus der Beek, T., Weber, F.-A., Bergmann, A., Hickmann, S., Ebert, I., Hein, A., Küster, A., 2016. Pharmaceuticals in the environment-Global occurrences and perspectives: Pharmaceuticals in the global environment. Environ Toxicol Chem 35, 823–835. https://doi.org/10.1002/etc.3339

Azubuike, C.C., Chikere, C.B., Okpokwasili, G.C., 2016. Bioremediation techniques–classification based on site of application: principles, advantages, limitations and prospects. World J Microbiol Biotechnol 32, 180. https://doi.org/10.1007/s11274-016-2137-x

Bai, Y., Liang, B., Yun, H., Zhao, Y., Li, Z., Qi, M., Ma, X., Huang, C., Wang, A., 2021. Combined bioaugmentation with electro-biostimulation for improved bioremediation of antimicrobial triclocarban and PAHs complexly contaminated sediments. Journal of Hazardous Materials 403, 123937. https://doi.org/10.1016/j.jhazmat.2020.123937

Balouiri, M., Sadiki, M., Ibnsouda, S.K., 2016. Methods for in vitro evaluating antimicrobial activity: A review. Journal of Pharmaceutical Analysis 6, 71–79. https://doi.org/10.1016/j.jpha.2015.11.005

Barbosa, J., Freitas, A., Moura, S., Mourão, J.L., Noronha da Silveira, M.I., Ramos, F., 2011. Detection, Accumulation, Distribution, and Depletion of Furaltadone and Nifursol Residues in Poultry Muscle, Liver, and Gizzard. J. Agric. Food Chem. 59, 11927–11934. https://doi.org/10.1021/jf2029384

Barzegar, S., Zare, M.R., Shojaei, F., Zareshahrabadi, Z., Koohi-Hosseinabadi, O., Saharkhiz, M.J., Iraji, A., Zomorodian, K., Khorram, M., 2021. Core-shell chitosan/PVA-based nanofibrous scaffolds loaded with Satureja mutica or Oliveria decumbens essential oils as enhanced antimicrobial wound dressing. International Journal of Pharmaceutics 597, 120288. https://doi.org/10.1016/j.ijpharm.2021.120288

Ben, Y., Fu, C., Hu, M., Liu, L., Wong, M.H., Zheng, C., 2019. Human health risk assessment of antibiotic resistance associated with antibiotic residues in the environment: A review. Environmental Research 169, 483–493. https://doi.org/10.1016/j.envres.2018.11.040

Ben, Y., Hu, M., Zhang, X., Wu, S., Wong, M.H., Wang, M., Andrews, C.B., Zheng, C., 2020. Efficient detection and assessment of human exposure to trace antibiotic residues in drinking water. Water Research 175, 115699. https://doi.org/10.1016/j.watres.2020.115699

Bengtsson-Palme, J., Larsson, D.G.J., 2016. Concentrations of antibiotics predicted to select for resistant bacteria: Proposed limits for environmental regulation. Environment International 86, 140–149. https://doi.org/10.1016/j.envint.2015.10.015

Berendonk, T.U., Manaia, C.M., Merlin, C., Fatta-Kassinos, D., Cytryn, E., Walsh, F., Bürgmann, H., Sørum, H., Norström, M., Pons, M.-N., Kreuzinger, N., Huovinen, P., Stefani, S., Schwartz, T., Kisand, V., Baquero, F., Martinez, J.L., 2015. Tackling antibiotic resistance: the environmental framework. Nat Rev Microbiol 13, 310–317. https://doi.org/10.1038/nrmicro3439

Bessone, F., Ferrari, A., Hernandez, N., Mendizabal, M., Ridruejo, E., Zerega, A., Tanno, F., Reggiardo, M.V., Vorobioff, J., Tanno, H., Arrese, M., Nunes, V., Tagle, M., Medina-Caliz, I., Robles-Diaz, M., Niu, H., Alvarez-Alvarez, I., Stephens, C., Lucena, M.I., Andrade, R.J., 2023. Nitrofurantoin-induced liver injury: long-term follow-up in two prospective DILI registries. Arch Toxicol 97, 593–602. https://doi.org/10.1007/s00204-022-03419-7

Biošić, M., Dabić, D., Škorić, I., Babić, S., 2021. Effects of environmental factors on nitrofurantoin photolysis in water and its acute toxicity assessment. Environ. Sci.: Processes Impacts 23, 1385–1393. https://doi.org/10.1039/D1EM00133G

Biošić, M., Škorić, I., Beganović, J., Babić, S., 2017. Nitrofurantoin hydrolytic degradation in the environment. Chemosphere 186, 660–668. https://doi.org/10.1016/j.chemosphere.2017.08.011

Browne, A.J., Chipeta, M.G., Haines-Woodhouse, G., Kumaran, E.P.A., Hamadani, B.H.K., Zaraa, S., Henry, N.J., Deshpande, A., Reiner, R.C., Day, N.P.J., Lopez, A.D., Dunachie, S., Moore, C.E., Stergachis, A., Hay, S.I., Dolecek, C., 2021. Global antibiotic consumption and usage in humans, 2000–18: a spatial modelling study. The Lancet Planetary Health 5, e893–e904. https://doi.org/10.1016/S2542-5196(21)00280-1

Cao, J., Wang, Y., Wang, G., Ren, P., Wu, Y., He, Q., 2022. Effects of Typical Antimicrobials on Growth Performance, Morphology and Antimicrobial Residues of Mung Bean Sprouts. Antibiotics 11, 807. https://doi.org/10.3390/antibiotics11060807

Chassagne, F., Samarakoon, T., Porras, G., Lyles, J.T., Dettweiler, M., Marquez, L., Salam, A.M., Shabih, S., Farrokhi, D.R., Quave, C.L., 2021. A Systematic Review of Plants With Antibacterial Activities: A Taxonomic and Phylogenetic Perspective. Front. Pharmacol. 11, 586548. https://doi.org/10.3389/fphar.2020.586548

Chaturvedi, P., Shukla, P., Giri, B.S., Chowdhary, P., Chandra, R., Gupta, P., Pandey, A., 2021. Prevalence and hazardous impact of pharmaceutical and personal care products and antibiotics in environment: A review on emerging contaminants. Environmental Research 194, 110664. https://doi.org/10.1016/j.envres.2020.110664

Chen, D., Delmas, J.-M., Hurtaud-Pessel, D., Verdon, E., 2020. Development of a multi-class method to determine nitroimidazoles, nitrofurans, pharmacologically active dyes and chloramphenicol in aquaculture products by liquid chromatography-tandem mass spectrometry. Food Chemistry 311, 125924. https://doi.org/10.1016/j.foodchem.2019.125924

Chen, X., Lin, H., Dong, Y., Li, B., Liu, C., Yin, T., 2022. Mechanisms underlying enhanced bioremediation of sulfamethoxazole and zinc(II) by Bacillus sp. SDB4 immobilized on biochar. Journal of Cleaner Production 370, 133483. https://doi.org/10.1016/j.jclepro.2022.133483

Chen, X., Yin, H., Li, G., Wang, W., Wong, P.K., Zhao, H., An, T., 2019. Antibiotic-resistance gene transfer in antibiotic-resistance bacteria under different light irradiation: Implications from oxidative stress and gene expression. Water Research 149, 282–291. https://doi.org/10.1016/j.watres.2018.11.019

Cheng, Y., Liu, X., Yang, M., Xia, F., Fan, L., Gao, X., Sun, X., Zhu, L., 2023. Ratiometric fluorescent immunochromatography for simultaneously detection of two nitrofuran metabolites in seafoods. Food Chemistry 404, 134698. https://doi.org/10.1016/j.foodchem.2022.134698

Claussen, K., Stocks, E., Bhat, D., Fish, J., Rubin, C.D., 2017. How Common Are Pulmonary and Hepatic Adverse Effects in Older Adults Prescribed Nitrofurantoin? J Am Geriatr Soc 65, 1316–1320. https://doi.org/10.1111/jgs.14796

Commission Decision, 2003. 2003/181/EC: Commission Decision of 13 March 2003 amending Decision 2002/657/EC as regards the setting of minimum required performance limits (MRPLs) for certain residues in food of animal origin (Text with EEA relevance) (notified under document number C(2003) 764).

Commission Regulation, 2019. Commission Regulation (EU) 2019/1871 of 7 November 2019 on reference points for action for non-allowed pharmacologically active subst ances present in food of animal origin and repealing Decision 2005/34/EC.

Commission Regulation, 1995. Commission Regulation (EC) 1995/1442/EC (1995). Amending Annexes I, II, III and IV of Regulation (ECC) No 2377/90 laying down a Community Procedure for the establishment of maximum residue limits of veterinary medicinal products in foodstuffs of animal origin. OJ, 143, 26–30.

Cooper, K.M., Fodey, T.L., Campbell, K., Elliott, C.T., 2018. Development of Antibodies and Immunoassays for Monitoring of Nitrofuran Antibiotics in the Food Chain. COC 21. https://doi.org/10.2174/1385272821666170427160210

Danner, M.-C., Robertson, A., Behrends, V., Reiss, J., 2019. Antibiotic pollution in surface fresh waters: Occurrence and effects. Science of The Total Environment 664, 793–804. https://doi.org/10.1016/j.scitotenv.2019.01.406

Dawood, M.A.O., El Basuini, M.F., Zaineldin, A.I., Yilmaz, S., Hasan, Md.T., Ahmadifar, E., El Asely, A.M., Abdel-Latif, H.M.R., Alagawany, M., Abu-Elala, N.M., Van Doan, H., Sewilam, H., 2021. Antiparasitic and Antibacterial Functionality of Essential Oils: An Alternative Approach for Sustainable Aquaculture. Pathogens 10, 185. https://doi.org/10.3390/pathogens10020185

De Francesco, V., Ierardi, E., Zullo, A., Hassan, C., 2012. Furazolidone-based therapies for Helicobacter pylori infection: A pooled-data analysis. Saudi J Gastroenterol 18, 11. https://doi.org/10.4103/1319-3767.91729

de Oliveira, R.C.S., Oliveira, R., Rodrigues, M.A.C., de Farias, N.O., Sousa-Moura, D., Nunes, N.A., Andrade, T.S., Grisolia, C.K., 2020. Lethal and Sub-lethal Effects of Nitrofurantoin on Zebrafish Early-Life Stages. Water Air Soil Pollut 231, 54. https://doi.org/10.1007/s11270-020-4414-4

Dempsey, J.L., Little, M., Cui, J.Y., 2019. Gut microbiome: An intermediary to neurotoxicity. NeuroToxicology 75, 41–69. https://doi.org/10.1016/j.neuro.2019.08.005

Dolk, F.C.K., Pouwels, K.B., Smith, D.R.M., Robotham, J.V., Smieszek, T., 2018. Antibiotics in primary care in England: which antibiotics are prescribed and for which conditions? Journal of Antimicrobial Chemotherapy 73, ii2–ii10. https://doi.org/10.1093/jac/dkx504

Dong, H., Zeng, G., Tang, L., Fan, C., Zhang, C., He, X., He, Y., 2015. An overview on limitations of TiO2-based particles for photocatalytic degradation of organic pollutants and the corresponding countermeasures. Water Research 79, 128–146. https://doi.org/10.1016/j.watres.2015.04.038

Douny, C., Widart, J., De Pauw, E., Silvestre, F., Kestemont, P., Tu, H.T., Phuong, N.T., Maghuin-Rogister, G., Scippo, M.-L., 2013. Development of an analytical method to detect metabolites of nitrofurans. Aquaculture 376–379, 54–58. https://doi.org/10.1016/j.aquaculture.2012.11.001

Durán, A., Monteagudo, J.M., Castillo, D., Expósito, A.J., 2022. UV/solar photo-degradation of furaltadone in homogeneous and heterogeneous phases: Intensification with persulfate. Journal of Environmental Management 319, 115712. https://doi.org/10.1016/j.jenvman.2022.115712

Edhlund, B.L., Arnold, W.A., McNeill, K., 2006. Aquatic Photochemistry of Nitrofuran Antibiotics. Environ. Sci. Technol. 40, 5422–5427. https://doi.org/10.1021/es0606778

Eissa, F., Ghanem, K., Al-Sisi, M., 2020. Occurrence and human health risks of pesticides and antibiotics in Nile tilapia along the Rosetta Nile branch, Egypt. Toxicology Reports 7, 1640–1646. https://doi.org/10.1016/j.toxrep.2020.03.004

European Centre for Disease Prevention and Control, European Food Safety Authority, European Medicines Agency, 2017. ECDC/EFSA/EMA second joint report on the integrated analysis of the consumption of antimicrobial agents and occurrence of antimicrobial resistance in bacteria from humans and food-producing animals. EFS2 15. https://doi.org/10.2903/j.efsa.2017.4872

European Food Safety Authority, 2015. Scientific Opinion on nitrofurans and their metabolites in food. EFS2 13. https://doi.org/10.2903/j.efsa.2015.4140

Evgenidou, E.N., Konstantinou, I.K., Lambropoulou, D.A., 2015. Occurrence and removal of transformation products of PPCPs and illicit drugs in wastewaters: A review. Science of The Total Environment 505, 905–926. https://doi.org/10.1016/j.scitotenv.2014.10.021

Felis, E., Kalka, J., Sochacki, A., Kowalska, K., Bajkacz, S., Harnisz, M., Korzeniewska, E., 2020. Antimicrobial pharmaceuticals in the aquatic environment - occurrence and environmental implications. European Journal of Pharmacology 866, 172813. https://doi.org/10.1016/j.ejphar.2019.172813

Fleming, A., 1929. On the antibacterial action of cultures of a Penicillium with special reference to their use in the isolation of B. influenza. British Journal of Experimental Pathology 10, 226–236.

Food and Agriculture Organization, 2018. The future of food and agriculture – Alternative pathways to 2050. Supplementary material.

Food and Drug Administration, 2014. Antimicrobials Sold or Distributed for Use in Food-Producing Animals.

Frank, T.D., Carter, A., Jahagirdar, D., et al. 2019. Global, regional, and national incidence, prevalence, and mortality of HIV, 1980–2017, and forecasts to 2030, for 195 countries and territories: a systematic analysis for the Global Burden of Diseases, Injuries, and Risk Factors Study 2017. The Lancet HIV 6, e831–e859. https://doi.org/10.1016/S2352-3018(19)30196-1

Gallardo-Garrido, C., Cho, Y., Cortés-Rios, J., Vasquez, D., Pessoa-Mahana, C.D., Araya-Maturana, R., Pessoa-Mahana, H., Faundez, M., 2020. Nitrofuran drugs beyond redox cycling: Evidence of Nitroreduction-independent cytotoxicity mechanism. Toxicology and Applied Pharmacology 401, 115104. https://doi.org/10.1016/j.taap.2020.115104

Gardiner, B.J., Stewardson, A.J., Abbott, I.J., Peleg, A.Y., 2019. Nitrofurantoin and fosfomycin for resistant urinary tract infections: old drugs for emerging problems. Aust Prescr 42, 14. https://doi.org/10.18773/austprescr.2019.002

Goemaere, N.N.T., Grijm, K., van Hal, P.T.W., den Bakker, M.A., 2008. Nitrofurantoin-induced pulmonary fibrosis: a case report. J Med Case Reports 2, 169. https://doi.org/10.1186/1752-1947-2-169

Gong, J., Li, J., Yuan, H., Chu, B., Lin, W., Cao, Q., Zhao, Q., Fang, R., Li, L., Xiao, G., 2020. Determination of four nitrofuran metabolites in gelatin Chinese medicine using dispersive solid phase extraction and pass-through solid phase extraction coupled to ultra high performance liquid

chromatography-tandem mass spectrometry. Journal of Chromatography B 1146, 122018. https://doi.org/10.1016/j.jchromb.2020.122018

Grenni, P., Ancona, V., Barra Caracciolo, A., 2018. Ecological effects of antibiotics on natural ecosystems: A review. Microchemical Journal 136, 25–39. https://doi.org/10.1016/j.microc.2017.02.006

Griboff, J., Carrizo, J.C., Bonansea, R.I., Valdés, M.E., Wunderlin, D.A., Amé, M.V., 2020. Multiantibiotic residues in commercial fish from Argentina. The presence of mixtures of antibiotics in edible fish, a challenge to health risk assessment. Food Chemistry 332, 127380. https://doi.org/10.1016/j.foodchem.2020.127380

Gurav, R., Bhatia, S.K., Choi, T.-R., Park, Y.-L., Park, J.Y., Han, Y.-H., Vyavahare, G., Jadhav, J., Song, H.-S., Yang, P., Yoon, J.-J., Bhatnagar, A., Choi, Y.-K., Yang, Y.-H., 2020. Treatment of furazolidone contaminated water using banana pseudostem biochar engineered with facile synthesized magnetic nanocomposites. Bioresource Technology 297, 122472. https://doi.org/10.1016/j.biortech.2019.122472

Hammam, E., 2002. Determination of nitrofurantoin drug in pharmaceutical formulation and biological fluids by square-wave cathodic adsorptive stripping voltammetry. Journal of Pharmaceutical and Biomedical Analysis 30, 651–659. https://doi.org/10.1016/S0731-7085(02)00344-8

Han, Y., Ma, Y., Chen, B., Zhang, J., Hu, C., 2022. Hazard assessment of beta-lactams: Integrating in silico and QSTR approaches with in vivo zebrafish embryo toxicity testing. Ecotoxicology and Environmental Safety 229, 113106. https://doi.org/10.1016/j.ecoenv.2021.113106

Hong, X., Zhao, Y., Zhuang, R., Liu, J., Guo, G., Chen, J., Yao, Y., 2020. Bioremediation of tetracycline antibiotics-contaminated soil by bioaugmentation. RSC Adv. 10, 33086–33102. https://doi.org/10.1039/D0RA04705H

Horton, J.M., 2015. Urinary tract agents: nitrofurantoin, fosfomycin, and methenamine, in: Mandell, Douglas, and Bennett's Principles and Practice of Infectious Diseases. Elsevier, pp. 447–451.

Hou, J., Wan, W., Mao, D., Wang, C., Mu, Q., Qin, S., Luo, Y., 2015. Occurrence and distribution of sulfonamides, tetracyclines, quinolones, macrolides, and nitrofurans in livestock manure and amended soils of Northern China. Environ Sci Pollut Res 22, 4545–4554. https://doi.org/10.1007/s11356-014-3632-y

Hou, Y., Yuan, G., Qin, S., Tu, L., Yan, Y., Yu, Z., Lin, H., Chen, Y., Zhu, H., Song, H., Wang, S., 2020a. Photocathode optimization and microbial community in the solar-illuminated bio-photoelectrochemical system for nitrofurazone degradation. Bioresource Technology 302, 122761. https://doi.org/10.1016/j.biortech.2020.122761

Hou, Y., Yuan, G., Wang, S., Yu, Z., Qin, S., Tu, L., Yan, Y., Chen, X., Zhu, H., Tang, Y., 2020b. Nitrofurazone degradation in the self-biased bio-photoelectrochemical system: g-C3N4/CdS photocathode characterization, degradation performance, mechanism and pathways. Journal of Hazardous Materials 384, 121438. https://doi.org/10.1016/j.jhazmat.2019.121438

Huttner, A., Verhaegh, E.M., Harbarth, S., Muller, A.E., Theuretzbacher, U., Mouton, J.W., 2015. Nitrofurantoin revisited: a systematic review and meta-analysis of controlled trials. J. Antimicrob. Chemother. 70, 2456–2464. https://doi.org/10.1093/jac/dkv147

Jadhav, A.C., Jadhav, N.C., 2021. Treatment of textile wastewater using adsorption and adsorbents, in: Sustainable Technologies for Textile Wastewater Treatments. Elsevier, pp. 235–273. https://doi.org/10.1016/B978-0-323-85829-8.00008-0

Janecko, N., Pokludova, L., Blahova, J., Svobodova, Z., Literak, I., 2016. Implications of fluoroquinolone contamination for the aquatic environment-A review: Fluoroquinolone in the aquatic ecosystem-A review. Environ Toxicol Chem 35, 2647–2656. https://doi.org/10.1002/etc.3552

Kaczorek, E., Pacholak, A., Zdarta, A., Smułek, W., 2018. The Impact of Biosurfactants on Microbial Cell Properties Leading to Hydrocarbon Bioavailability Increase. Colloids and Interfaces 2, 35. https://doi.org/10.3390/colloids2030035

Kafle, A., Timilsina, A., Gautam, A., Adhikari, K., Bhattarai, A., Aryal, N., 2022. Phytoremediation: Mechanisms, plant selection and enhancement by natural and synthetic agents. Environmental Advances 8, 100203. https://doi.org/10.1016/j.envadv.2022.100203

Kapral, N., Saxena, R., Sule, A.A., Markle, B., 2018. Nitrofurantoin: friend or foe? BMJ Case Rep.

Kazmi, S.S.U.H., Uroosa, Warren, A., Xu, H., 2022. Insights into evaluating the toxic effects of nitrofurazone on ecological integrity in marine ecosystems using periphytic ciliate communities. Ecological Indicators 141, 109095. https://doi.org/10.1016/j.ecolind.2022.109095

Khan, M., Lively, J.A., 2020. Determination of sulfite and antimicrobial residue in imported shrimp to the USA. Aquaculture Reports 18, 100529. https://doi.org/10.1016/j.aqrep.2020.100529

Kim, J.O., Park, J.K., Kim, J.H., Jin, S.G., Yong, C.S., Li, D.X., Choi, J.Y., Woo, J.S., Yoo, B.K., Lyoo, W.S., Kim, J.-A., Choi, H.-G., 2008. Development of polyvinyl alcohol–sodium alginate gel-matrix-based wound dressing system containing nitrofurazone. International Journal of Pharmaceutics 359, 79–86. https://doi.org/10.1016/j.ijpharm.2008.03.021

Klein, E.Y., Milkowska-Shibata, M., Tseng, K.K., Sharland, M., Gandra, S., Pulcini, C., Laxminarayan, R., 2021. Assessment of WHO antibiotic consumption and access targets in 76 countries, 2000–15: an analysis of pharmaceutical sales data. The Lancet Infectious Diseases 21, 107–115. https://doi.org/10.1016/S1473-3099(20)30332-7

Klein, E.Y., Van Boeckel, T.P., Martinez, E.M., Pant, S., Gandra, S., Levin, S.A., Goossens, H., Laxminarayan, R., 2018. Global increase and geographic convergence in antibiotic consumption between 2000 and 2015. Proc. Natl. Acad. Sci. U.S.A. 115. https://doi.org/10.1073/pnas.1717295115

Klobučar, R.S., Brozovic, A., Štambuk, A., 2013. Ecotoxicological assessment of nitrofurantoin in fish cell lines, unicellular algae Desmodesmus subspicatus, and bacterial strains of Salmonella typhimurium. Fresenius Environmental Bulletin 22.

Knäbel, A., Bundschuh, M., Kreuzig, R., Schulz, R., 2016. Runoff of veterinary pharmaceuticals from arable and grassland—A comparison between predictions from model simulations and experimental studies. Agriculture, Ecosystems & Environment 218, 33–39. https://doi.org/10.1016/j.agee.2015.10.022

Kokulnathan, T., Chen, S.-M., 2020. Robust and selective electrochemical detection of antibiotic residues: The case of integrated lutetium vanadate/graphene sheets architectures. Journal of Hazardous Materials 384, 121304. https://doi.org/10.1016/j.jhazmat.2019.121304

Kong, D., Liang, B., Yun, H., Cheng, H., Ma, J., Cui, M., Wang, A., Ren, N., 2015. Cathodic degradation of antibiotics: Characterization and pathway analysis. Water Research 72, 281–292. https://doi.org/10.1016/j.watres.2015.01.025

Kong, D., Yun, H., Cui, Dan, Qi, M., Shao, C., Cui, Dichen, Ren, N., Liang, B., Wang, A., 2017. Response of antimicrobial nitrofurazone-degrading biocathode communities to different cathode potentials. Bioresource Technology 241, 951–958. https://doi.org/10.1016/j.biortech.2017.06.056

K'oreje, K.O., Kandie, F.J., Vergeynst, L., Abira, M.A., Van Langenhove, H., Okoth, M., Demeestere, K., 2018. Occurrence, fate and removal of pharmaceuticals, personal care products and pesticides in wastewater stabilization ponds and receiving rivers in the Nzoia Basin, Kenya. Science of The Total Environment 637–638, 336–348. https://doi.org/10.1016/j.scitotenv.2018.04.331

Kosmehl, T., Hallare, A.V., Reifferscheid, G., Manz, W., Braunbeck, T., Hollert, H., 2006. A novel contact assay for testing genotoxicity of chemicals and whole sediments in zebrafish embryos. Environ Toxicol Chem 25, 2097. https://doi.org/10.1897/05-460R.1

Kovalakova, P., Cizmas, L., McDonald, T.J., Marsalek, B., Feng, M., Sharma, V.K., 2020. Occurrence and toxicity of antibiotics in the aquatic environment: A review. Chemosphere 251, 126351. https://doi.org/10.1016/j.chemosphere.2020.126351

Krishnan, A.A., Thelukutla, V., Sengar, A.S., Vijayan, A., Raveendran, S., Malekadi, P., Sterk, S.S., Shanker, R., Reddy, J.S., 2023. Simultaneous determination of five metabolites of nitrofurans including the metabolite nifursol in shrimp and fish by UPLC- MS/MS: in-house method validation according to commission implementing regulation (EU) 2021/808. Food Additives & Contaminants: Part A 40, 222–234. https://doi.org/10.1080/19440049.2022.2154855

Kumar, M., Jaiswal, S., Sodhi, K.K., Shree, P., Singh, D.K., Agrawal, P.K., Shukla, P., 2019. Antibiotics bioremediation: Perspectives on its ecotoxicity and resistance. Environment International 124, 448–461. https://doi.org/10.1016/j.envint.2018.12.065

Kümmerer, K., 2009. Antibiotics in the aquatic environment – A review – Part I. Chemosphere 75, 417–434. https://doi.org/10.1016/j.chemosphere.2008.11.086

Lai, J.-H., Dhenadhayalan, N., Chauhan, A., Chien, C.-W., Yeh, J.-C., Hung, P.-Q., Lin, K.-C., 2022. Antibiotic drugs removal by visible light-driven photocatalysis using Pt/Ru nanoparticle-decorated hafnium oxide nanohybrids. Journal of Environmental Chemical Engineering 10, 108557. https://doi.org/10.1016/j.jece.2022.108557

La-Scalea, M.A., Menezes, C.M. de S., Julião, M.S. da S., Chung, M.C., Serrano, S.H.P., Ferreira, E.I., 2005. Voltammetric behavior of nitrofurazone and its hydroxymethyl prodrug with potential anti-Chagas activity. J. Braz. Chem. Soc. 16, 774–782. https://doi.org/10.1590/S0103-50532005000500015

Leitner, A., Zöllner, P., Lindner, W., 2001. Determination of the metabolites of nitrofuran antibiotics in animal tissue by high-performance liquid chromatography–tandem mass spectrometry. Journal of Chromatography A 939, 49–58. https://doi.org/10.1016/S0021-9673(01)01331-0

Leston, S., Nunes, M., Viegas, I., Lemos, M.F.L., Freitas, A., Barbosa, J., Ramos, F., Pardal, M.A., 2011. The effects of the nitrofuran furaltadone on Ulva lactuca. Chemosphere 82, 1010–1016. https://doi.org/10.1016/j.chemosphere.2010.10.067

Lewkowski, J., Rogacz, D., Rychter, P., 2019. Hazardous ecotoxicological impact of two commonly used nitrofuran-derived antibacterial drugs: Furazolidone and nitrofurantoin. Chemosphere 222, 381–390. https://doi.org/10.1016/j.chemosphere.2019.01.144

Li, H., Zhang, Z., Yang, X., Mao, X., Wang, Y., Wang, J., Peng, Y., Zheng, J., 2019. Electron Deficiency of Nitro Group Determines Hepatic Cytotoxicity of Nitrofurantoin. Chem. Res. Toxicol. 32, 681–690. https://doi.org/10.1021/acs.chemrestox.8b00362

Li, J., Peng, K., Zhang, D., Luo, C., Cai, X., Wang, Y., Zhang, G., 2020. Autochthonous bioaugmentation with non-direct degraders: A new strategy to enhance wastewater bioremediation performance. Environment International 136, 105473. https://doi.org/10.1016/j.envint.2020.105473

Li, J., Yu, Z., Warren, A., Lin, X., 2023. Predation risk affects the ecotoxicity evaluation of antibiotics: Population growth and antioxidase activity in the ciliate Paramecium jenningsi. Ecotoxicology and Environmental Safety 251, 114536. https://doi.org/10.1016/j.ecoenv.2023.114536

Li, J., Zhang, K., Zhang, H., 2018. Adsorption of antibiotics on microplastics. Environmental Pollution 237, 460–467. https://doi.org/10.1016/j.envpol.2018.02.050

Li, Zhonghui, Li, Zhoumin, Xu, D., 2017. Simultaneous detection of four nitrofuran metabolites in honey by using a visualized microarray screen assay. Food Chemistry 221, 1813–1821. https://doi.org/10.1016/j.foodchem.2016.10.099

Liu, X., Xia, F., Zhang, S., Cheng, Y., Fan, L., Kang, S., Gao, X., Sun, X., Li, J., Li, X., Zhu, L., 2023. Dual-color aggregation-induced emission nanoparticles for simultaneous lateral flow immunoassay of nitrofuran metabolites in aquatic products. Food Chemistry 402, 134235. https://doi.org/10.1016/j.foodchem.2022.134235

Liu, Y., Wang, F., Chen, X., Zhang, J., Gao, B., 2015. Cellular responses and biodegradation of amoxicillin in Microcystis aeruginosa at different nitrogen levels. Ecotoxicology and Environmental Safety 111, 138–145. https://doi.org/10.1016/j.ecoenv.2014.10.011

Livanios, K., Karampi, E.-S., Sotiriou, A., Tavernaraki, K., Styliara, P., Kainis, E., 2016. Nitrofurantoin-induced acute pulmonary toxicity: Nitrofurantoin-induced lung toxicity. Respirology Case Reports 4, 25–27. https://doi.org/10.1002/rcr2.131

López-Serna, R., Jurado, A., Vázquez-Suñé, E., Carrera, J., Petrović, M., Barceló, D., 2013. Occurrence of 95 pharmaceuticals and transformation products in urban groundwaters underlying the metropolis of Barcelona, Spain. Environmental Pollution 174, 305–315. https://doi.org/10.1016/j.envpol.2012.11.022

Luo, Y., Guo, W., Ngo, H.H., Nghiem, L.D., Hai, F.I., Zhang, J., Liang, S., Wang, X.C., 2014. A review on the occurrence of micropollutants in the aquatic environment and their fate and removal during wastewater treatment. Science of The Total Environment 473–474, 619–641. https://doi.org/10.1016/j.scitotenv.2013.12.065

Ma, F., Xu, S., Tang, Z., Li, Z., Zhang, L., 2021. Use of antimicrobials in food animals and impact of transmission of antimicrobial resistance on humans. Biosafety and Health 3, 32–38. https://doi.org/10.1016/j.bsheal.2020.09.004

Ma, Z., Liu, J., Dick, R.P., Li, H., Shen, D., Gao, Y., Waigi, M.G., Ling, W., 2018. Rhamnolipid influences biosorption and biodegradation of phenanthrene by phenanthrene-degrading strain Pseudomonas sp. Ph6. Environmental Pollution 240, 359–367. https://doi.org/10.1016/j.envpol.2018.04.125

Madigan, M.T., Bender, K.S., Buckley, D.H., Sattley, W.M., Stahl, D.A., 2018. Molecular Biology of Microbial Growth, in: Brock Biology of Microorganisms. Pearson, NY, NY.

Manzetti, S., Ghisi, R., 2014. The environmental release and fate of antibiotics. Marine Pollution Bulletin 79, 7–15. https://doi.org/10.1016/j.marpolbul.2014.01.005

Mccracken, R.J., Van Rhijn, J.A., Kennedy, D.G., 2005. The occurrence of nitrofuran metabolites in the tissues of chickens exposed to very low dietary concentrations of the nitrofurans. Food Additives and Contaminants 22, 567–572. https://doi.org/10.1080/02652030500137868

McOsker, C.C., Fitzpatrick, P.M., 1994. Nitrofurantoin: Mechanism of action and implications for resistance development in common uropathogens. Journal of Antimicrobial Chemotherapy 33, 23–30. https://doi.org/10.1093/jac/33.suppl_A.23

Mompelat, S., Le Bot, B., Thomas, O., 2009. Occurrence and fate of pharmaceutical products and by-products, from resource to drinking water. Environment International 35, 803–814. https://doi.org/10.1016/j.envint.2008.10.008

Monahan, C., Morris, D., Nag, R., Cummins, E., 2023. Risk ranking of macrolide antibiotics – Release levels, resistance formation potential and ecological risk. Science of The Total Environment 859, 160022. https://doi.org/10.1016/j.scitotenv.2022.160022

Moutiez, M., Belin, P., Gondry, M., 2017. Aminoacyl-tRNA-Utilizing Enzymes in Natural Product Biosynthesis. Chem. Rev. 117, 5578–5618. https://doi.org/10.1021/acs.chemrev.6b00523

Nakagawa, S., Kurimoto, Y., Ezumi, M., Nakatani, K., Mizunaga, S., Yamagishi, Y., Mikamo, H., 2021. In vitro and in vivo antibacterial activity of nitrofurantoin against clinical isolates of E. coli in Japan and evaluation of biological cost of nitrofurantoin resistant strains using a mouse urinary tract infection model. Journal of Infection and Chemotherapy 27, 250–255. https://doi.org/10.1016/j.jiac.2020.09.026

Nam, S.T., Kim, H.W., Kim, H.S., Park, Y.H., Lee, D., Lee, M.B., Min, K.Y., Kim, Y.M., Choi, W.S., 2018. Furaltadone suppresses IgE-mediated allergic response through the inhibition of Lyn/Syk pathway in mast cells. European Journal of Pharmacology 828, 119–125. https://doi.org/10.1016/j.ejphar.2018.03.035

Nesse, A.S., Aanrud, S.G., Lyche, J.L., Sogn, T., Kallenborn, R., 2022. Confirming the presence of selected antibiotics and steroids in Norwegian biogas digestate. Environ Sci Pollut Res 29, 86595–86605. https://doi.org/10.1007/s11356-022-21479-1

Nnabuife, O.O., Ogbonna, J.C., Anyanwu, C., Ike, A.C., Eze, C.N., Enemuor, S.C., 2022. Mixed bacterial consortium can hamper the efficient degradation of crude oil hydrocarbons. Arch Microbiol 204, 306. https://doi.org/10.1007/s00203-022-02915-9

Novelli, A., Rosi, E., 2017. Pharmacological properties of oral antibiotics for the treatment of uncomplicated urinary tract infections. Journal of Chemotherapy 29, 10–18. https://doi.org/10.1080/1120009X.2017.1380357

O'Connor, R.A., Patel, V., Lang, V., Brima, W., 2022. Systemic Inflammatory Response Syndrome from Nitrofurantoin: A Case Report. Am J Case Rep 23. https://doi.org/10.12659/AJCR.935113

Olender, D., Żwawiak, J., Zaprutko, L., 2018. Multidirectional Efficacy of Biologically Active Nitro Compounds Included in Medicines. Pharmaceuticals 11, 54. https://doi.org/10.3390/ph11020054

Organisation for Economic Co-operation and Development, 1992. Test No. 301: Ready Biodegradability, OECD Guidelines for the Testing of Chemicals, Section 3. OECD. https://doi.org/10.1787/9789264070349-en

Ossai, I.C., Ahmed, A., Hassan, A., Hamid, F.S., 2020. Remediation of soil and water contaminated with petroleum hydrocarbon: A review. Environmental Technology & Innovation 17, 100526. https://doi.org/10.1016/j.eti.2019.100526

Ouyang, X., Fan, Y., Huang, S., Liu, X., 2022. Rapid and accurate quantification and analysis of nitrofuran metabolites residues in aquatic products by ultra-high performance liquid chromatography–tandem mass spectrometry. Eur Food Res Technol 248, 2857–2864. https://doi.org/10.1007/s00217-022-04095-8

Pacholak, A., Juzwa, W., Zgoła-Grześkowiak, A., Kaczorek, E., 2023a. Multi-faceted analysis of bacterial transformation of nitrofurantoin. Science of The Total Environment 874, 162422. https://doi.org/10.1016/j.scitotenv.2023.162422

Pacholak, A., Smułek, W., Zgoła-Grześkowiak, A., Kaczorek, E., 2019. Nitrofurantoin—Microbial Degradation and Interactions with Environmental Bacterial Strains. IJERPH 16, 1526. https://doi.org/10.3390/ijerph16091526

Pacholak, A., Zdarta, A., Frankowski, R., Cybulski, Z., Kaczorek, E., 2020. Exploring Elimination Kinetics of Four 5-Nitrofuran Derivatives by Microbes Present in Rural and Municipal Activated Sludge. Water Air Soil Pollut 231, 252. https://doi.org/10.1007/s11270-020-04634-7

Pacholak, A., Zgoła-Grześkowiak, A., Kaczorek, E., 2023b. Dynamics of microbial communities during biotransformation of nitrofurantoin. Environmental Research 216, 114531. https://doi.org/10.1016/j.envres.2022.114531

Pan, M., Chu, L.M., 2017. Fate of antibiotics in soil and their uptake by edible crops. Science of The Total Environment 599–600, 500–512. https://doi.org/10.1016/j.scitotenv.2017.04.214

Patel, M., Kumar, R., Kishor, K., Mlsna, T., Pittman, C.U., Mohan, D., 2019. Pharmaceuticals of Emerging Concern in Aquatic Systems: Chemistry, Occurrence, Effects, and Removal Methods. Chem. Rev. 119, 3510–3673. https://doi.org/10.1021/acs.chemrev.8b00299

Peng, Z., Liu, X., Zhang, W., Zeng, Z., Liu, Z., Zhang, C., Liu, Y., Shao, B., Liang, Q., Tang, W., Yuan, X., 2020. Advances in the application, toxicity and degradation of carbon nanomaterials in environment: A review. Environment International 134, 105298. https://doi.org/10.1016/j.envint.2019.105298

Robinson, K., Ma, X., Liu, Y., Qiao, S., Hou, Y., Zhang, G., 2018. Dietary modulation of endogenous host defense peptide synthesis as an alternative approach to in-feed antibiotics. Animal Nutrition 4, 160–169. https://doi.org/10.1016/j.aninu.2018.01.003

Rodriguez-Mozaz, S., Vaz-Moreira, I., Varela Della Giustina, S., Llorca, M., Barceló, D., Schubert, S., Berendonk, T.U., Michael-Kordatou, I., Fatta-Kassinos, D., Martinez, J.L., Elpers, C., Henriques, I., Jaeger, T., Schwartz, T., Paulshus, E., O'Sullivan, K., Pärnänen, K.M.M., Virta, M., Do, T.T., Walsh, F., Manaia, C.M., 2020. Antibiotic residues in final effluents of European wastewater treatment plants and their impact on the aquatic environment. Environment International 140, 105733. https://doi.org/10.1016/j.envint.2020.105733

Roushani, M., Rahmati, Z., 2019. Development of electrochemical sensor based on molecularly imprinted copolymer for detection of nitrofurantoin. J IRAN CHEM SOC 16, 999–1006. https://doi.org/10.1007/s13738-018-01575-1

Shakila, R.J., Saravanakumar, R., Shanmugapriya, E., Jeyasekaran, G., 2008. Detection of Furazolidone Residues by Microbial Assay in Thermally Processed and Cold Stored Shrimp. Journal of Aquatic Food Product Technology 17, 156–172. https://doi.org/10.1080/10498850801937141

Smirnova, G.V., Oktyabrsky, O.N., 2005. Glutathione in Bacteria. Biochemistry (Moscow) 70, 1199–1211. https://doi.org/10.1007/s10541-005-0248-3

Szabó-Bárdos, E., Cafuta, A., Hegedűs, P., Fónagy, O., Kiss, G., Babić, S., Škorić, I., Horváth, O., 2020. Photolytic and photocatalytic degradation of nitrofurantoin and its photohydrolytic products. Journal of Photochemistry and Photobiology A: Chemistry 386, 112093. https://doi.org/10.1016/j.jphotochem.2019.112093

Szekeres, E., Chiriac, C.M., Baricz, A., Szőke-Nagy, T., Lung, I., Soran, M.-L., Rudi, K., Dragos, N., Coman, C., 2018. Investigating antibiotics, antibiotic resistance genes, and microbial contaminants in groundwater in relation to the proximity of urban areas. Environmental Pollution 236, 734–744. https://doi.org/10.1016/j.envpol.2018.01.107

Tacconelli, E., Carrara, E., Savoldi, A., et al., 2018. Discovery, research, and development of new antibiotics: the WHO priority list of antibiotic-resistant bacteria and tuberculosis. The Lancet Infectious Diseases 18, 318–327. https://doi.org/10.1016/S1473-3099(17)30753-3

Takahashi, M., Iizuka, S., Watanabe, T., Yoshida, M., Ando, J., Wakabayashi, K., Maekawa, A., 2000. Possible mechanisms underlying mammary carcinogenesis in female Wistar rats by nitrofurazone. Cancer Letters 156, 177–184. https://doi.org/10.1016/S0304-3835(00)00459-6

Tan, L.-R., Xia, P.-F., Zeng, R.J., Li, Q., Sun, X.-F., Wang, S.-G., 2018. Low-level concentrations of aminoglycoside antibiotics induce the aggregation of cyanobacteria. Environ Sci Pollut Res 25, 17128–17136. https://doi.org/10.1007/s11356-018-1894-5

Tian, X., Li, H., Han, D., Wen, F., Liu, H., Liu, G., Peng, K., Gong, X., Liu, X., Wang, W., Yu, H., Xu, Y., 2021. Sources, Toxicity and Detection Techniques of Semicarbazide: A Review. J. Ocean Univ. China 20, 1263–1275. https://doi.org/10.1007/s11802-021-4688-1

Tolić, K., Mutavdžić Pavlović, D., Židanić, D., Runje, M., 2019. Nitrofurantoin in sediments and soils: Sorption, isotherms and kinetics. Science of The Total Environment 681, 9–17. https://doi.org/10.1016/j.scitotenv.2019.05.054

Tran, K.M., Lee, H.-M., Thai, T.D., Shen, J., Eyun, S., Na, D., 2021. Synthetically engineered microbial scavengers for enhanced bioremediation. Journal of Hazardous Materials 419, 126516. https://doi.org/10.1016/j.jhazmat.2021.126516

Tran, N.H., Hoang, L., Nghiem, L.D., Nguyen, N.M.H., Ngo, H.H., Guo, W., Trinh, Q.T., Mai, N.H., Chen, H., Nguyen, D.D., Ta, T.T., Gin, K.Y.-H., 2019. Occurrence and risk assessment of multiple classes of antibiotics in urban canals and lakes in Hanoi, Vietnam. Science of The Total Environment 692, 157–174. https://doi.org/10.1016/j.scitotenv.2019.07.092

United Nations, 2022. Department of Economic and Social Affairs, Population Division.

Uroosa, Kazmi, S.S.U.H., Zhong, X., Xu, H., 2021. An approach to evaluating the acute toxicity of nitrofurazone on community functioning using protozoan periphytons. Marine Pollution Bulletin 173, 113066. https://doi.org/10.1016/j.marpolbul.2021.113066

U.S. Food and Drug Administration, 2020. Chemotherapeutics in aquaculture seafood compliance program.

Van Boeckel, T.P., Brower, C., Gilbert, M., Grenfell, B.T., Levin, S.A., Robinson, T.P., Teillant, A., Laxminarayan, R., 2015. Global trends in antimicrobial use in food animals. Proc. Natl. Acad. Sci. U.S.A. 112, 5649–5654. https://doi.org/10.1073/pnas.1503141112

Van Boeckel, T.P., Gandra, S., Ashok, A., Caudron, Q., Grenfell, B.T., Levin, S.A., Laxminarayan, R., 2014. Global antibiotic consumption 2000 to 2010: an analysis of national pharmaceutical sales data. The Lancet Infectious Diseases 14, 742–750. https://doi.org/10.1016/S1473-3099(14)70780-7

Van Boeckel, T.P., Glennon, E.E., Chen, D., Gilbert, M., Robinson, T.P., Grenfell, B.T., Levin, S.A., Bonhoeffer, S., Laxminarayan, R., 2017. Reducing antimicrobial use in food animals. Science 357, 1350–1352. https://doi.org/10.1126/science.aao1495

Vasquez, M.I., Hapeshi, E., Fatta-Kassinos, D., Kümmerer, K., 2013. Biodegradation potential of ofloxacin and its resulting transformation products during photolytic and photocatalytic treatment. Environ Sci Pollut Res 20, 1302–1309. https://doi.org/10.1007/s11356-012-1096-5

Vass, M., Hruska, K., Franek, M., 2008. Nitrofuran antibiotics: a review on the application, prohibition and residual analysis. Vet. Med. 53, 469–500. https://doi.org/10.17221/1979-VETMED

Wang, B., He, B., Xie, L., Cao, X., Liang, Z., Wei, M., Jin, H., Ren, W., Suo, Z., Xu, Y., 2022. A novel detection strategy for nitrofuran metabolite residues: Dual-mode competitive-type electrochemical immunosensor based on polyethyleneimine reduced graphene oxide/gold nanorods nanocomposite and silica-based multifunctional immunoprobe. Science of The Total Environment 853, 158676. https://doi.org/10.1016/j.scitotenv.2022.158676

Wang, B., Liu, J.-H., Yu, J., Lv, J., Dong, C., Li, J.-R., 2020. Broad spectrum detection of veterinary drugs with a highly stable metal-organic framework. Journal of Hazardous Materials 382, 121018. https://doi.org/10.1016/j.jhazmat.2019.121018

Williams, E.M., Triller, D.M., 2006. Recurrent Acute Nitrofurantoin-Induced Pulmonary Toxicity. Pharmacotherapy 26, 713–718. https://doi.org/10.1592/phco.26.5.713

Yang, M., Yi, J., Wei, C., Lu, Y., Yang, Y., Yang, Z., Zhao, L., Jiang, X., Tu, F., 2022. Rapid determination of nitrofuran metabolites residues in honey by ultrasonic assisted derivatization - QuEChERS - high performance liquid chromatography / tandem mass spectrometry. Journal of Food Composition and Analysis 114, 104812. https://doi.org/10.1016/j.jfca.2022.104812

Yashas, S.R., Shivaraju, H.P., Sandeep, S., Kumara Swamy, N., Gurupadayya, B., 2022. Application of yttrium molybdate tethered polypyrrole nanocomposite for the photocatalytic remediation of nitrofurantoin in water. Surfaces and Interfaces 32, 102102. https://doi.org/10.1016/j.surfin.2022.102102

Ye, S., Zeng, G., Wu, H., Zhang, Chang, Dai, J., Liang, J., Yu, J., Ren, X., Yi, H., Cheng, M., Zhang, Chen, 2017. Biological technologies for the remediation of co-contaminated soil. Critical Reviews in Biotechnology 37, 1062–1076. https://doi.org/10.1080/07388551.2017.1304357

Yu, W.-H., Chin, T.-S., Lai, H.-T., 2013. Detection of nitrofurans and their metabolites in pond water and sediments by liquid chromatography (LC)-photodiode array detection and LC-ion spray tandem mass spectrometry. International Biodeterioration & Biodegradation 85, 517–526. https://doi.org/10.1016/j.ibiod.2013.03.015

Yuan, G., Zhu, Z., Yang, P., Lu, S., Liu, H., Liu, W., Liu, G., 2020. Simultaneous determination of eight nitrofuran residues in shellfish and fish using ultra-high performance liquid chromatography–tandem mass spectrometry. Journal of Food Composition and Analysis 92, 103540. https://doi.org/10.1016/j.jfca.2020.103540

Zhang, Q.-Q., Ying, G.-G., Pan, C.-G., Liu, Y.-S., Zhao, J.-L., 2015. A comprehensive evaluation of antibiotics emission and fate in the river basins of China: Source analysis, multimedia modelling, and linkage to bacterial resistance. Environmental Science & Technology 49, 6772–6782. https://doi.org/10.1021/acs.est.5b00729

Zhang, W., Niu, Z., Yin, K., Liu, F., Chen, L., 2013. Degradation of furazolidone by bacteria Acinetobacter calcoaceticus T32, Pseudomonas putida SP1 and Proteus mirabilis V7. International Biodeterioration & Biodegradation 77, 45–50. https://doi.org/10.1016/j.ibiod.2012.11.006

Zhang, Y., Qiao, H., Chen, C., Wang, Z., Xia, X., 2016. Determination of nitrofurans metabolites residues in aquatic products by ultra-performance liquid chromatography–tandem mass spectrometry. Food Chemistry 192, 612–617. https://doi.org/10.1016/j.foodchem.2015.07.035

Zhao, R., Feng, J., Liu, J., Fu, W., Li, X., Li, B., 2019. Deciphering of microbial community and antibiotic resistance genes in activated sludge reactors under high selective pressure of different antibiotics. Water Research 151, 388–402. https://doi.org/10.1016/j.watres.2018.12.034

Zhen-Yuan, Z., Zhen-Hu, X., 2015. Removal of Four Nitrofurans Drugs from Aqueous Solution by Magnetic Multi-Wall Carbon Nanotubes. Fullerenes, Nanotubes and Carbon Nanostructures 23, 640–648. https://doi.org/10.1080/1536383X.2014.947646

Zhou, L., Li, J., Lin, X., Al-Rasheid, K.A.S., 2011. Use of RAPD to detect DNA damage induced by nitrofurazone in marine ciliate, Euplotes vannus (Protozoa, Ciliophora). Aquatic Toxicology 103, 225–232. https://doi.org/10.1016/j.aquatox.2011.03.002

Zuccato, E., Castiglioni, S., Bagnati, R., Melis, M., Fanelli, R., 2010. Source, occurrence and fate of antibiotics in the Italian aquatic environment. Journal of Hazardous Materials 179, 1042–1048. https://doi.org/10.1016/j.jhazmat.2010.03.110

Zuma, N.H., Aucamp, J., N'Da, D.D., 2019. An update on derivatisation and repurposing of clinical nitrofuran drugs. European Journal of Pharmaceutical Sciences 140, 105092. https://doi.org/10.1016/j.ejps.2019.105092

Zuma, N.H., Smit, F.J., Seldon, R., Aucamp, J., Jordaan, A., Warner, D.F., N'Da, D.D., 2020. Single-step synthesis and in vitro anti-mycobacterial activity of novel nitrofurantoin analogues. Bioorganic Chemistry 96, 103587. https://doi.org/10.1016/j.bioorg.2020.103587

Scientific activity

Author impact

- Summary Impact Factor for the journals for the year of publications: 127.166
- Citations (Apr 18, 2023): 239 (Scopus), 221 (WoS), 306 (Google Scholar)
- H-index: 9 (Scopus, WoS, Google Scholar)

Publications in journals indexed by the Journal Citation Reports

Presented in reverse chronological order

1. M. Szulc*, R. Kujawski, **A. Pacholak**, M. Poprawska, K. Czora-Poczwardowska, B. Geppert, P. Ł. Mikołajczak, *Cannabidiol as a Modulator of the Development of Alcohol Tolerance in Rats*, Nutrients 15 (2023) 7, doi:10.3390/nu15071702, **IF 6.706**
2. **A. Pacholak***, W. Juzwa, A. Zgoła-Grześkowiak, E. Kaczorek, *Multi-faceted analysis of bacterial transformation of nitrofurantoin*, Science of the Total Environment 874 (2023)162422, doi:10.1016/j.scitotenv.2023.162422, **IF 10.753**
3. **A. Pacholak***, J. Żur-Pińska, A. Piński, Q. A. Nguyen, M. Ligaj, M. Łuczak, L. D. Nghiem, E. Kaczorek, *Potential negative effect of long-term exposure to nitrofurans on bacteria isolated from wastewater*, Science of the Total Environment 872 (2023) 162199, doi: 10.1016/j.scitotenv.2023.162199, **IF 10.753**
4. **A. Pacholak***, A. Zgoła-Grześkowiak, E. Kaczorek, *Dynamics of microbial communities during biotransformation of nitrofurantoin*, Environmental Research 2016 (2023) 114531, doi:10.1016/j.envres.2022.114531, **IF 8.431**
5. W. Smułek*, M. Rojewska*, **A. Pacholak**, O. Machrowicz, K. Prochaska, E. Kaczorek, *Co-interaction of nitrofurantoin and saponins surfactants with biomembrane leads to an increase in antibiotic's antibacterial activity*, Journal of Molecular Liquids 364 (2022) 120070, doi: 10.1016/j.molliq.2022.120070, **IF 6.633**
6. **A. Pacholak***, N. Burlaga, R. Frankowski, A. Zgoła-Grześkowiak, E. Kaczorek, *Azole fungicides: (Bio)degradation, transformation products and toxicity elucidation*, Science of the Total Environment 802 (2022) 149917, doi: 10.1016/j.scitotenv.2021.149917, **IF 10.753**

7. W. Smułek*, Z. Bielan, **A. Pacholak**, A. Zdarta, A. Zgoła-Grześkowiak, A. Zielińska-Jurek, E. Kaczorek*, *Nitrofurazone Removal from Water Enhanced by Coupling Photocatalysis and Biodegradation*, International Journal of Molecular Sciences 22 (2021) 2186, doi:10.3390/ijms22042186, **IF 6.208**
8. **A. Pacholak**, Ze-Liang Gao, Xiao-Yu Gong, E. Kaczorek, You-Wei Cui*, *The metabolic pathways of polyhydroxyalkanoates and exopolysaccharides synthesized by Haloferax mediterranei in response to elevated salinity*, Journal of Proteomics 232 (2021) 104065, doi:10.1016/j.jprot.2020.104065, **IF 3.855**
9. **A. Pacholak***, N. Burlaga, U. Guzik, E. Kaczorek*, *Investigation of the bacterial cell envelope nanomechanical properties after long-term exposure to nitrofurans*, Journal of Hazardous Materials 407 (2021) 124352, doi: 10.1016/j.jhazmat.2020.124352, **IF 14.224**
10. **A. Pacholak***, N. Burlaga, E. Kaczorek, *Evaluating the Effect of Azole Antifungal Agents on the Stress Response and Nanomechanical Surface Properties of Ochrobactrum anthropi Aspcl2.2*, Molecules 25 (2020) 3348, doi:10.3390/molecules25153348, **IF 4.412**
11. **A. Pacholak**, A. Zdarta, R. Frankowski, Z. Cybulski, E. Kaczorek*, *Exploring Elimination Kinetics of Four 5-Nitrofuran Derivatives by Microbes Present in Rural and Municipal Activated Sludge*, Water, Air, & Soil Pollution 231 (2020) 252, doi: 10.1007/s11270-020-04634-7, **IF 2.520**
12. A. Zdarta*, W. Smułek, **A. Pacholak**, B. Dudzińska-Bajorek, E. Kaczorek, *Surfactant addition in diesel oil degradation – how can it help the microbes?*, Journal of Environmental Health Science and Engineering 18 (2020), doi:10.1007/s40201-020-00494-9, **IF 2.130**
13. W. Smułek*, **A. Pacholak***, E. Kaczorek*, *Modification of the Bacterial Cell Wall—Is the Bioavailability Important in Creosote Biodegradation?,* Processes 8 (2020) 147, doi:10.3390/pr8020147, **IF 2.847**
14. W. Smułek*, A. Zdarta, **A. Pacholak**, T. Runka, E. *Kaczorek, Increased biological removal of 1-chloronaphthalene as a result of exposure: a study of bacterial adaptation strategies*, Ecotoxicology and Environmental Safety 185 (2019) 109707, doi:10.1016/j.ecoenv.2019.109707, **IF 4.872**
15. **A. Pacholak**, W. Smułek, Z. Zgoła-Grześkowiak, E. Kaczorek*, *Nitrofurantoin—Microbial Degradation and Interactions with Environmental Bacterial Strains*, International Journal of Environmental Research and Public Health 16 (2019) 1526, doi:10.3390/ijerph16091526, **IF 2.849**
16. A. Zdarta*, W. Smułek, **A. Pacholak**, E. Kaczorek, *Environmental aspects of the use of Hedera helix extract in bioremediation process*, Microorganisms 7 (2019) 43, doi:10.3390/microorganisms7020043, **IF 4.152**

17. Zdarta, **A. Pacholak,** W. Smułek*, A. Zgoła-Grześkowiak, N. Ferlin, A. Bil, J. Kovensky, E. Grand*, E. Kaczorek, *Biological impact of octyl D-glucopyranoside based surfactants*, Chemosphere 217 (2019), doi:10.1016/j.chemosphere.2018.11.025, **IF 5.778**
18. **A. Pacholak,** W. Smułek*, A. Zdarta, A. Zgoła-Grześkowiak, E. Kaczorek, *Bacterial biodegradation of 4-monohalogenated diphenyl ethers in one-substrate and co-metabolic systems*, Catalysts 8 (2018) 472, doi:10.3390/catal8100472, **IF 3.444**
19. A. Zdarta*, **A. Pacholak**, M. Galikowska, W. Smułek, E. Kaczorek, *Butylbenzene and tert-Butylbenzene—Sorption on Sand Particles and Biodegradation in the Presence of Plant Natural Surfactants*, Toxins 10 (2018) 9, doi:10.3390/toxins10090338, **IF 3.895**
20. **A. Pacholak**, W. Smułek*, E.Kaczorek, *Wpływ stresu metabolicznego na biodegradację chloropochodnych toluenu i modyfikację właściwości powierzchniowych komórek szczepu Raoultella planticola SA2*, Ochrona środowiska 40 (2018) 2, **IF 0.840**
21. **A. Pacholak,** J. Simlat, A. Zgoła-Grześkowiak, E. Kaczorek*, *Biodegradation of clotrimazole and modification of cell properties after metabolic stress and upon addition of saponins*, Ecotoxicology and Environmental Safety 161 (2018), doi:10.1016/j.ecoenv.2018.06.050, **IF 4.527**
22. W. Smułek, A. Zdarta, **A. Pacholak**, A. Zgoła-Grześkowiak, Ł. Marczak, M. Jarzębski, E. Kaczorek*, *Saponaria officinalis L. extract: Surface active properties and impact on environmental bacterial strains*, Colloids and Surfaces B: Biointerfaces 150 (2017), doi:10.1016/j.colsurfb.2016.11.035, **IF 3.997**
23. **A. Pacholak**, W. Smułek, T. Jesionowski, E. Kaczorek*, *The ability of Achromobacter sp. KW1 strain to biodegrade isomers of chlorotoluene*, Journal of Chemical Technology and Biotechnology 92 (2017) 8, doi:10.1002/jctb.5221, **IF 2.587**

Publication in journal without Impact Factor and peer reviewed conference materials

1. A. Pacholak*, E. Kaczorek, *The role of selected environmental bacteria in decomposition of nitrofuran antibiotics*, Proceedings of the World Congress on New Technologies (2019), doi:10.11159/ICEPR19.134 – peer reviewed conference materials
2. E. Kaczorek*, A. Pacholak, A. Zdarta, W. Smułek, *The impact of biosurfactants on microbial cell properties leading to hydrocarbon bioavailability increase*, Colloids and Interfaces 2 (2018) 35, doi:10.3390/colloids2030035

* Denotes the corresponding author

International mobility

- The Ohio State University, USA, Aug 16, 2021 – Dec 16, 2021 (Internship)
- University of Technology Sydney, Australia, Nov 25, 2019 – Dec 06, 2019 (Summer school)
- University of Helsinki (Finland), Sep 18, 2019 – Sep 10, 2019 (Summer school)
- Beijing University of Technology, China, Sep 03, 2018 – Dec 10 2018 (Internship)

Conferences

- Oral presentations at international conferences: 10
- Poster presentations at international conferences: 9
- Oral presentations at national conferences: 7
- Poster presentations at national conferences: 15

Awards and scholarships

- START 2022 scholarship awarded by the Polish Science Foundation
- Scholarship awarded by the Kościuszko Foundation for conducting research in the USA (2021)
- Poznan City Scholarship for young researchers from the Poznan scientific community (2021)
- Best paper and oral presentation award for the paper entitled: *The role of selected environmental bacteria in decomposition of nitrofuan antibiotics* during 5th World Congress on New Technologies, Aug 18- 20, 2019, Lisbon, Portugal
- Best oral presentation award for the speech *Bioavailability as a key factor in biological degradation of xenobiotics* during XIVth Summer School for PhD Students and Young Researchers, Interfacial Phenomena in Theory and Practice, Jun, 24-28, 2019, Sudomie Resort, Poland
- Scholarship awarded by the Rector of the Poznan University of Technology for PhD students

Research projects

- Research grant SONATA 17, supported by the National Science Centre in Poland, no. 2021/43/D/NZ9/01201
  Title: *Natural insecticides used in organic farming - multiaspects evaluation of their microbiological safety*
  Principal investigator – Wojciech Smułek, investigator – **Amanda Pacholak**

- Research grant OPUS 20, supported by the National Science Centre in Poland, no. 2020/39/B/NZ9/03196
  Title: *Is there a synergistic effect of plant surfactants and antibiotics against bacterial cells?*
  Principal investigator – Ewa Kaczorek, investigator – **Amanda Pacholak**
- Research grant PRELUDIUM 15, supported by the National Science Centre in Poland, no. 2018/29/N/NZ9/01532
  Title: *Azole fungcides - biodegradation and impact on environmental bacterial strains*
  Principal investigator – **Amanda Pacholak**
- Research grant OPUS 14, supported by the National Science Centre in Poland, no. 2017/27/B/NZ9/01603
  Title: *Biodegradation of nitrofuran derivatives by environmental bacteria - from metabolic pathways to changes in genome and proteome*
  Principal investigator – Ewa Kaczorek, investigator – **Amanda Pacholak**
- Research grant supported by the National Centre for Research and Development NCBiR, no. POIR.04.01.02-00-0057/17
  Title: *Modern technology of bioremediation of soils contaminated with creosote oil in Nasycalnia Podkładów Spółka Akcyjna in Koźmin Wielkopolski (Nowoczesna technologia bioremediacji gruntów zanieczyszczonych olejem kreozotowym na terenie Nasycalni Podkładów Spółka Akcyjna w Koźminie Wielkopolskim*)
  Principal investigator at PUT – Ewa Kaczorek, investigator – **Amanda Pacholak**
- Program PROM of the Polish National Agency for Academic Exchange, no. POWR.03.03.00-00-PN13/18
  Title: *International scholarship exchange of PhD students and academic Staff*
  Principal investigator – Stefan Trzcieliński, investigator – **Amanda Pacholak**
- Subsidy for conducting research at Poznan University of Technology (2023),
  Title: *Microbiological removal of environmental pollutants by single strains and bacterial consortia (Mikrobiologiczne usuwanie zanieczyszczeń środowiskowych przez pojedyncze szczepy i konsorcja bakteryjne)*
  Principal investigator – Agata Zdarta, investigator – **Amanda Pacholak**
- Subsidy for conducting research at Poznan University of Technology (2022), grant no. 0912/SBAD/2211
  Title: *Impact of natural and anthropogenic bioactive compounds on human and environmental microbiota (Wpływ naturalnych i antropogenicznych związków bioaktywnych na mikroorganizmy tworzące mikroflorę człowieka oraz otaczające go środowisko)*
  Principal investigator – **Amanda Pacholak**
- Subsidy for conducting research at Poznan University of Technology (2021), grant no. 0912/SBAD/2115
  Title: *Biotechnological methods in assessing the properties of pharmaceuticals and new biomedical materials (Metody biotechnologiczne w ocenie właściwości farmaceutyków i nowych materiałów biomedycznych)*
  Principal investigator – Wojciech Smułek, investigator – **Amanda Pacholak**

- Subsidy for conducting research at Poznan University of Technology (2020), grant no. 0912/SBAD/2015
  Title: *The use of plant-derived compounds as protective compounds in the storage of probiotic bacteria, (Wykorzystanie związków pochodzenia roślinnego jako związków ochronnych w przechowywaniu bakterii probiotycznych)*
  Principal investigator – Wojciech Smułek, investigator – **Amanda Pacholak**
- Subsidy for conducting research at Poznan University of Technology (2019), grant no. 03/32/SBAD/0911
  Title: *Impact of selected analgesics on probiotic bacteria (Wpływ wybranych leków przeciwbólowych na bakterie probiotyczne)*
  Principal investigator – **Amanda Pacholak**
- Subsidy for conducting research at Poznan University of Technology (2018), grant no. 03/32/DSMK/0816
  Title: *Biological degradation of halogenated diphenylethers (Biologiczna degradacja halogenowych pochodnych difenyloeteru)*
  Principal investigator – Wojciech Smułek, investigator – **Amanda Pacholak**
- Subsidy for conducting research at Poznan University of Technology (2017), grant no. 03/32/DSMK/0721
  Title: *The influence of surfactants containing sugar residues on environmental microorganisms (Wpływ surfaktantów zawierających reszty cukrowe na mikroorganizmy środowiskowe)*
  Principal investigator – Agata Zdarta, investigator – **Amanda Pacholak**

Memberships

- Member of Polish Society of Microbiologists
- Member of the National Chamber of Laboratory Diagnosticians, licence to practise the profession of Laboratory Diagnostician in the Republic of Poland, no. 19767
- Member of PUT Chemistry Student's Scientific Association

Additional activity

- Co-author of 41 newly isolated bacterial strains which 16S rRNA sequences have been deposited in the GenBank database
- Member of the Organizing Committee of I, II, III and IV National Symposium on Bioorganic and Organic Chemistry and Biomaterials (2015, 2017, 2019, 2022)
- Participation in the organization of the Researchers' Night at Poznań University of Technology

Appendix A: Full text of papers

Publication P1

International Journal of
Environmental Research and Public Health

MDPI

Article

Nitrofurantoin—Microbial Degradation and Interactions with Environmental Bacterial Strains

Amanda Pacholak [1], Wojciech Smułek [1], Agnieszka Zgoła-Grześkowiak [2] and Ewa Kaczorek [1,*]

1 Institute of Chemical Technology and Engineering, Poznan University of Technology, Berdychowo 4, 60-695 Poznan, Poland; amanda.d.pacholak@doctorate.put.poznan.pl (A.P.); wojciech.smulek@put.poznan.pl (W.S.)
2 Institute of Chemistry and Technical Electrochemistry, Poznan University of Technology, Berdychowo 4, 60-965 Poznan, Poland; agnieszka.zgola-grzeskowiak@put.poznan.pl
* Correspondence: ewa.kaczorek@put.poznan.pl; Tel.: +48-61-665-3671

Received: 14 March 2019; Accepted: 26 April 2019; Published: 30 April 2019

Abstract: The continuous exposure of living organisms and microorganisms to antibiotics that have increasingly been found in various environmental compartments may be perilous. One group of antibacterial agents that have an environmental impact that has been very scarcely studied is nitrofuran derivatives. Their representative is nitrofurantoin (NFT)—a synthetic, broad-spectrum antibiotic that is often overdosed. The main aims of the study were to: (a) isolate and characterize new microbial strains that are able to grow in the presence of NFT, (b) investigate the ability of isolates to decompose NFT, and (c) study the impact of NFT on microbial cell properties. As a result, five microbial species were isolated. A 24-h contact of bacteria with NFT provoked modifications in microbial cell properties. The greatest differences were observed in *Sphingobacterium thalpophilum* P3d, in which a decrease in both total and inner membrane permeability (from 86.7% to 48.3% and from 0.49 to 0.42 μM min^{-1}) as well as an increase in cell surface hydrophobicity (from 28.3% to 39.7%) were observed. Nitrofurantoin removal by selected microbial cultures ranged from 50% to 90% in 28 days, depending on the bacterial strain. Although the isolates were able to decompose the pharmaceutical, its presence significantly affected the bacterial cells. Hence, the environmental impact of NFT should be investigated to a greater extent.

Keywords: nitrofurantoin; pharmaceutical; biodegradation; microbial strains isolation; cell membrane permeability; cell metabolic activity

1. Introduction

Being increasingly used by millions of peoples, pharmaceuticals have become an indispensable element of contemporary societies [1–3]. Many of them are purchased and consumed in quantities that exceed the real demand, and recent studies have shown that these substances are entering the natural environment. There are many ways that medicines make their way into the environment (Figure 1). These include improper drugs disposal or the inappropriate management of drug manufacturing facilities. Nevertheless, a great portion of the pharmaceuticals that are present in ecosystems comes from the drugs taken by people or animals that are excreted in an unchanged form in urine or feces [2,4,5].

Int. J. Environ. Res. Public Health **2019**, *16*, 1526

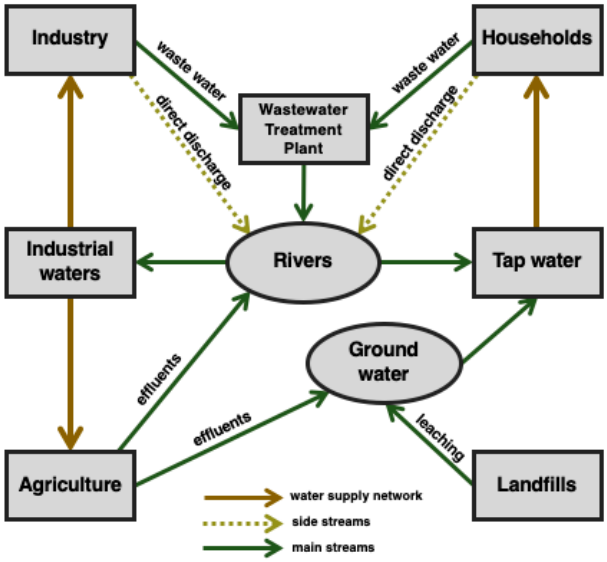

Figure 1. Sources of natural environment contamination with pharmaceuticals. Side and main streams indicate the relative amount of pharmaceutical contaminants introduced to the environment.

Although the concentrations of pharmaceuticals detected in the environment usually do not exceed safety regulations, their possible adverse impact on fauna and flora cannot be neglected. The particularly dangerous group of compounds found in the environment are antibiotics [6]. The social concerns about them are related not to their concentration in the environmental compartments, but rather to the nature of the molecules and their biological activity [4,6]. The continuous, low-level, unintentional exposure of living organisms and microorganisms to antibiotics contribute to, among other factors, the development of pathogenic bacteria resistance to these compounds [7]. Antibiotics present in the environment also affect natural microbial communities. A number of research studies have demonstrated that the presence of antibacterial pharmaceuticals influences the microbial growth, enzymatic activity, and biomass production, leading to the decrease in microbial diversity [8–14]. On the other hand, through being involved in the self-purification process of ecosystems and being able to decompose the xenobiotics, natural bacterial communities play a key role in the environmental fate of antibiotics [1,15]. By far, a considerable number of antibiotics has been tested according to their biodegradability. However, one group of antibacterial compounds whose environmental impact has been very scarcely studied is nitrofuran derivatives. They belong to synthetic, broad-spectrum antibiotics that are active against Gram-positive and Gram-negative bacteria. The most often used nitrofuran compound is nitrofurantoin (NFT): an imidazolidinedione derivative containing a distinctive 5-nitrofuran ring [7]. Its bacteriostatic and bactericidal effects are complex and not entirely understood, but might be related to the inhibition of bacterial DNA, RNA, and protein synthesis as well as the formation of reactive oxygen species [16–18].

Nitrofurans used to be applied in livestock production; however, according to their possible carcinogenic properties, its usage in the fields in question has been prohibited in the European Union since 1995. Nevertheless, they are still easily accessible and used in the treatment of urinary tract infections in humans as well as in veterinary medicine [17,19].

Since studies about the environmental effects of nitrofurantoin as well as its biodegradation are limited [20,21], the main aim of this study is to investigate the ability of environmental microbial strains to decompose nitrofurantoin and study the impact of the compound mentioned on microbial cell properties. The analyses performed include the isolation of new bacterial strains from rural and municipal activated sludge as well as their biochemical characterization. Afterwards, the biodegradation

Int. J. Environ. Res. Public Health **2019**, *16*, 1526

of nitrofurantoin by newly isolated microbes was studied with the use of HPLC-MS/MS. Moreover, microbial cell viability and changes in the inner and total membrane permeability as well as cell surface hydrophobicity after contact with nitrofuran-derived drugs were tested. To the best of our knowledge, this is the first comprehensive report on the impact of nitrofurantoin on environmental microbial strains.

2. Materials and Methods

2.1. Chemicals

For preparing all the media and aqueous solutions, ultra-purified Mili-Q water (Arium® Pro, Sartorius, Kostrzyn Wlkp., Poland) was used. The chemicals applied in the experiments, e.g., nitrofurantoin, 3-(4,5-dimethylthiazol-2-yl)-2,5-diphenyltetrazolium bromide, salts, and medium components, were of the highest purity grade (98% or greater). They were purchased from Sigma-Aldrich (Poznan, Poland).

2.2. Isolation and Identification of Bacterial Strains

The bacterial strains that are able to grow in the presence of nitrofurantoin were isolated from activated sludge samples collected aseptically from the rural waste water treatment plant (WWTP) located in Kaźmierz, Poland (52°29′41.6″ N, 16°35′08.8″ E) serving small households, and from the WWTP in Poznań, Poland (52°25′53.1″ N, 16°57′31.8″ E) collecting sewage from the municipal agglomeration. After incubation for 24 h at 30 °C, 10 mL of the activated sludge was transferred to 90 mL of sterile mineral salt medium containing 1 mL of aqueous solution of sodium succinate (20%) and nitrofurantoin (1 mg mL^{-1}). Every 7 days, the microorganisms were transferred to a fresh culture medium. The amount of nitrofurantoin was successively increased (by 1 mg L^{-1} every week for five weeks; the last three weeks, it was maintained at 5 mg L^{-1}) and sodium succinate content was decreased (by 0.125 mL every week). As a consequence, after 8 weeks, the only carbon source was nitrofurantoin at a concentration of 5 mg L^{-1}. In the next step, 0.1 mL of the cultures were seeded on Mueller–Hinton agar medium plates (bioMerieux, Warsaw, Poland), and after 24 h of incubation, a streaking technique was used to isolate the colonies formed by individual bacterial strains. After the isolation, the strains that showed the best growth in the presence of NFT were selected and identified by 16S rRNA gene sequencing in accordance with the method described in our previously published article [22]. Figure 2 reports the main isolation steps.

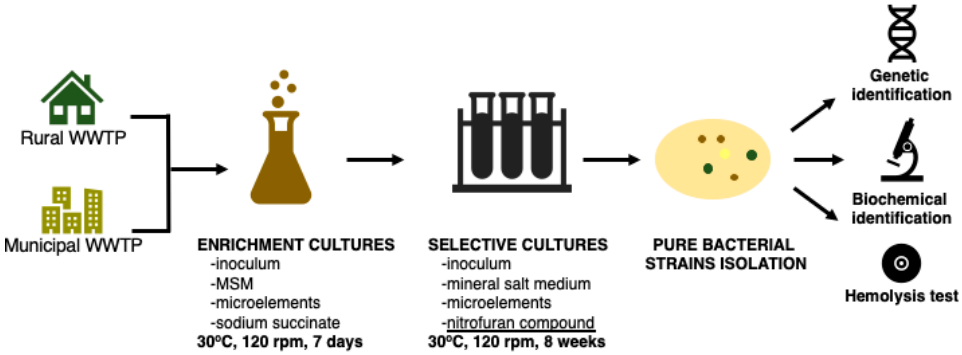

Figure 2. Isolation of microorganisms from the activated sludge—scheme of the procedure.

2.3. Biochemical Characterization of Bacterial Strains

In order to characterize the pure bacterial strains isolated from municipal and rural WWTPs, their biochemical profiles were evaluated using the Vitek 2 Compact (bioMerieux, Warsaw, Poland) system. Moreover, all the isolated strains were inoculated on plates with Columbia agar containing 5% sheep blood (bioMerieux, Warsaw, Poland). After incubation for 24 h at 30 °C, the color and

transparency of the agar medium around the bacterial colonies were observed. These observations can indicate the strains' ability to cause the lysis of red blood cells, which may be caused by the production of surface-active compounds secreted outside the cell by bacteria [23,24]. The main isolation and characterization steps are depicted in Figure 3.

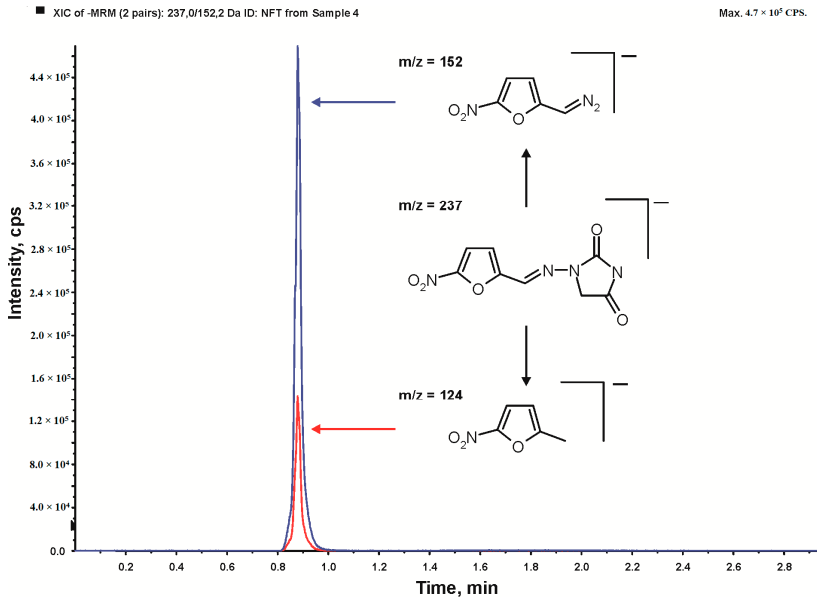

Figure 3. A typical nitrofurantoin chromatogram with two fragmentation transitions used in the multiple reaction monitoring mode.

2.4. Growing Conditions

Isolated and characterized pure bacterial strains were stored on tryptic soy agar plates at 4 °C. They were subcultivated every 21 days.

The liquid bacterial cultures used in the experiments contained 45 mL of nitrofurantoin solution prepared in mineral salt medium (2.8 mg dissolved in 500 mL of medium under sterile conditions), 5 mL of inoculum, 0.1 mL of sodium succinate (20% aqueous solution), and 0.1 mL of trace elements solution. The composition of the mineral salt medium (MSM) (composition (g L^{-1}): $Na_2HPO_4 \cdot 2H_2O$ 7.0, KH_2PO_4 2.8, NaCl 0.5, NH_4Cl 1.0) included the addition of sodium succinate and microelements ($MgSO_4 \cdot 7H_2O$ 0.35, $FeSO_4 \cdot 7H_2O$ 0.035, $CuSO_4 \cdot 7H_2O$ 0.2, $MnSO_4 \cdot 5H_2O$ 0.2, $ZnCl_2$ 0.105, $CoSO_4 \cdot 7H_2O$ 0.025, H_3BO_3 0.285).

The inocula that were used to prepare the liquid cultures were prepared by adding the loop full of cells taken from an agar plate to sterilized nutrient broth. Such mixtures were incubated at 30 °C with shaking at 120 rpm (KS 4000 ic control, IKA Werke GmbH, Staufen, Germany) for 24 h. Afterwards, the bacteria were centrifuged at 4000× *g* for 10 min (3–18K, Sigma Laborzentrifugen GmbH, Osterode am Harz, Germany) and washed twice with mineral salt medium. Finally, the cell pellet was re-suspended in sterile medium to reach the final bacteria concentration of $1 \cdot 10^9$ cfu mL^{-1} (mid log phase; optical density (OD_{600}) 1.0 at λ = 600 nm; spectrophotometer Jasco V-650, Tokyo, Japan).

The microbial cultures were incubated at 30 °C with shaking at 120 rpm over a period of time depending on the experiments (biodegradation, 28 days; cell viability and cell surface properties, 24 h). They were conducted in the sterile 250-mL Duran® Schott (Wertheim, Germany) laboratory glass bottles. All the solutions and glassware were sterilized prior to use in the experiments. In order to prevent contamination, the laminar flow cabinet was used during activities associated with biological samples.

2.5. Cell Membrane Permeability and Cell Surface Hydrophobicity

In order to evaluate the influence of the presence of NFT (initial concentration 5 mg L^{-1}) on microbial strains isolated from rural and municipal activated sludge, analyses of microbial inner membrane permeability, total membrane permeability, and cell surface hydrophobicity were performed. The methods applied includedo-nitrophenyl-β-D-galactoside assay (ONPG), crystal violet assay (CV), and congo red assay (CR). Microbial cultures with and without the addition of NFT were established as described in Section 3.3. Control samples contained mineral salt medium instead of NFT solution. After 24 h, microbial cultures were centrifuged (4000× *g*, 10 min) and washed with mineral salt medium. Afterwards, they were resuspended in MSM to obtain the OD_{600} = 1.0. The total reaction volume was 1 mL. Inner membrane permeability was tested as described previously [25] by measuring the concentration of β-galactosidase released into the solution using ONPG as a substrate. Total membrane permeability was tested according to [26] by colorimetric measurements of the uptake of crystal violet solution by microbial cells (CV assay). Cell surface hydrophobicity was analyzed by measuring the adsorption of congo red dye on the surface of microbial cells (CR assay) [27].

2.6. Microbes Viability after Contact with NFT

Evaluation of microbial cells' viability after 24-h contact between microbes and nitrofurantoin as well as control samples (cultivated in the same manner but without the addition of NFT) was performed using 3-(4,5-dimethylthiazol-2-yl)-2,5-diphenyltetrazolium bromide assay (MTT) in accordance with the method described in [28]. After 24 h, microbial cultures were centrifuged (4000× *g*, 10 min) and washed with mineral salt medium. Afterwards, they were resuspended in MSM to obtain OD_{600} values ranging from 0.1 to 0.2. The research samples contained 0.9 mL of microbial suspension and were incubated with 0.1 mL of 5 g L^{-1} MTT solution (the final concentration of MTT in the samples was 0.5 g L^{-1}) for 2 h at 30 °C. After incubation, the cultures were centrifuged at 15,000× *g*. The supernatant was discarded, and the pellet (the formazan precipitate formed by viable cells) was dissolved with 1 mL of propan-2-ol. Afterwards, the samples were centrifuged again at 4000× *g*, and the supernatant was analyzed on a UV-Vis spectrophotometer at 560 nm.

2.7. Nitrofurantoin Biodegradation with Kinetic Study

The biodegradation of nitrofurantoin by bacterial strains isolated from rural and municipal sewage was analyzed in the present study. Microbial cultures were prepared as described in Section 2.4. In order to determine the content of residual nitrofurantoin in microbial cultures, the samples were taken in 3 to 4-day intervals.

The qualitative and quantitative analysis of residual nitrofurantoin was analyzed using HPLC/MS-MS. The chromatographic system UltiMate 3000 RSLC from Dionex (Sunnyvale, CA, USA) was used. Five-µL samples were injected into a Gemini-NX C18 column (100 mm × 2.0 mm i.d.; 3 µm) from Phenomenex (Torrance, CA, USA) maintained at 35 °C. The mobile phase employed in the analysis consisted of ammonium acetate (5 10^{-3} mol L^{-1}) in water and methanol at a flow rate of 0.3 mL min^{-1}. Gradient elution was performed by linearly increasing the percentage from 75% methanol to 80% in 2 min, and then linearly increasingthe percentage to 100% in 1 min. The LC column effluent was directed to the API 4000 QTRAP triple quadrupole mass spectrometer from AB Sciex (Foster City, CA, USA) through the electrospray ionization source operating in the positive ion mode. The dwell time for each mass transition detected in the MS/MS multiple reaction monitoring mode was set to 200 ms. All the ions were detected using the following settings for the ion source and mass spectrometer: curtain gas, 10 psi; nebulizer gas, 40 psi; auxiliary gas, 40 psi; temperature, 400 °C; and collision gas, medium. The ion spray voltage was −4500 V, and the declustering potential was −60 V. The multiple reaction monitoring transitions parameters were as follows: analytical m/z = 237 → m/z = 152 (collision energy 17 eV, collision cell exit potential 10 V), confirmatory m/z = 237 → m/z = 124 (collision energy 20 eV, collision cell exit potential 10 V); see Figure 3.

Moreover, the nitrofurantoin biodegradation study was extended with kinetic analysis. According to Bekins et al. [29], zero-order calculations, first-order calculations, and the simplified Monod equation were used to calculate the biodegradation kinetics.

2.8. Statistical Analysis

All the results are reported as mean values calculated from at least three independent experiments. The statistical significance of differences between the means of research samples and control samples (without the addition of NFT) were determined by one-way analysis of variance (ANOVA) with Tukey's range test applied as posthoc analysis. Differences with $p < 0.05$ were considered statistically significant. The calculations were performed using Statistica v13 (StatSoft, Cracow, Poland).

3. Results and Discussion

3.1. Isolation and Identification of Microbial Strains

The microorganisms used in our research were isolated from samples of activated sludge (AS) taken from municipal and rural waste water treatment plants (WWTPs). In order to isolate pure bacterial strains, selective liquid cultures were established and inoculated with a given sludge sample. After eight weeks of cultivation, 18 bacterial strains were isolated from the rural AS, and 13 were isolated from the municipal one. Thereafter, the strains that showed the best growth in the presence of NFT were selected and identified by 16S rRNA gene sequencing. From the rural WWTP, only two strains were able to use the NFT as the only carbon and energy source, and they were identified as *Sphingomonas paucimobilis* (K3a) and *Ochrobactrum antrophi* (K3b). Both strains are often found in activated sludge [30,31], and are recognized as efficient biodegraders of biocides such as triclocarban (*Sphingomonas* strain described by [32]), triclosan (two *Sphingomonas* strains investigated by [33]), oxytetracycline (*Ochrobactrum* sp. KSS10 studied by [34]), sulfamethoxazole (*Ochrobactrum* sp. SMX-PM1-SA1 isolated by [35]), or erythromycin (*Ochrobactrum* sp. described by [36]). In municipal WWTP activated sludge, three strains showing the capability of degrading nitrofurantoin were found: *Rhizobium radiobacter* (P4c), *Pseudomonas aeruginosa* (P4a), and *Sphingobacterium thalpophilum* (P3d). *R. radiobacter* has been previously recognized as degrading several dyes [37,38]; the second strain is an ubiquitous environmental bacteria displaying great biodegradation potential [39,40]. However, the strain from the *Sphingobacterium thalpophilum* genus was found in activated sludge fed with pharmaceutical waste water [41].

Furthermore, for all the isolated strains, the biochemical profile was evaluated using a Vitek2® system with a GN Colorimetric Identification Card. The results of differentiating reactions are presented in Table 1. The Vitek2® system (bioMerieux, Warsaw, Poland) provides information about 48 characteristic biochemical reactions. Among them, 23 were common for all the investigated strains. The strains belong to different genera, and the variety of biochemical profiles is comprehensible. However, L-proline arylamidase and tyrosine arylamidase assimilation were observedin all the strains.

The next step of the microbial strains' characterization was the analysis of their ability to produce hemolysins. For that purpose, microbial strains were grown on Columbia agar containing 5% sheep blood (bioMerieux, Warsaw, Poland) using the streaking technique. Among the tested strains, only *P. aeruginosa* (P4a) caused the complete lysis of the blood cells (β-hemolysis). However, the lysis could be observed in the place of the massive growth of bacteria only. Presumably, the amount of hemolysins produced by the strain was too small to cause the rupture of red blood cells where the single colonies were formed. Moreover, *O. antrophi* (K3b) displayed α-hemolysis because the agar under the colony was dark and greenish. The agar under the colonies of *S. paucimobilis* (K3a), *R. radiobacter* (P4c), and *S. thalpophilum* (P3d) was unchanged. It means that those strains did not induce hemolysis (i.e., were non-hemolytic).

Table 1. The differentiating reactions from Vitek2® GN Colorimetric Identification Card (bioMerieux, Warsaw, Poland) for strains coming from the rural WWTP: *Sphingomonas paucimobilis* (K3a), *Ochrobactrum antrophi* (K3b) and the municipal wastewater treatment plant (WWTP): *Rhizobium radiobacter* (P4c), *Pseudomonas aeruginosa* (P4a), and *Sphingobacterium thalpophilum* (P3d).

Strain	APPA	ILATk	GlyA	O129R	ADO	dMAL	dTAG	AGLU	PyrA	AGLTp	dTRE	SUCT
K3a	+	+	−	−	−	+	−	+	+	−	−	−
K3b	−	+	+	−	+	−	+	−	+	−	−	+
P4c	−	−	+	−	−	−	−	−	+	−	−	−
P4a	−	+	−	+	−	−	−	−	−	+	(+)	−
P3d	−	−	−	−	−	−	−	+	−	−	−	−
	IMLTa	IARL	dGLU	dMNE	CIT	ELLM	GGT	URE	MNT	CMT	BAlap	BGUR
K3a	−	−	+	−	+	−	−	+	−	−	−	−
K3b	−	−	−	−	−	+	−	+	−	−	+	−
P4c	−	+	−	−	−	+	−	+	−	−	−	−
P4a	+	−	+	+	+	−	+	−	+	+	+	−
P3d	−	−	−	−	−	−	−	+	−	−	−	+

APPA—Ala-Phe-Pro-arylamidase; ILATk—L-lactatealkalinisation; GlyA—glycinearylamidase; O129R—O/129 resisitance (comp. vibrio); ADO—adonitol; dMAL—D-maltose; dTAG—D-tagatose; AGLU—alpha-glucosidase; PyrA—L-pyrrolydonyl-arilamidase; AGLTp—glutamylarylamidasepNA; dTRE—D-trehalose; SUCT—succinatealkalinisation; IMLTa—L-malateassimilation; dMNE—D-mannitol; CIT—citrate (sodium); ELLM—Ellman; GGT—gamma-glutamyl-transferase; URE—urease; MNT—malonate; CMT—coumarate; BAIap—β-alaninearylamidasepNA; BGUR—β-glucoronidase.

3.2. Inner and Total Membrane Permeability

The experiments performed within the study included the analysis of inner and total membrane permeability. The parameters were tested in cells subjected to 24-h contact with nitrofurantoin (initial concentration 5 mg L^{-1}), and those that were cultivated under the same conditions but without the addition of NFT. All the experiments were performed in independent quadruplicates. Afterwards, the statistical analysis was performed, and statistically significant differences were indicated. The results of experiments are depicted in Figure 4.

One-way analysis of variance (ANOVA) and further posthoc tests showed that nitrofurantoin did not cause any modifications in the inner membrane permeability of the K3a strain ($p = 0.992054$) (Figure 4a). The average value of the parameter tested was 0.10 μM min^{-1}. However, statistically significant differences in inner membrane permeability were observed in microbial cells of strains K3b, P4c, P3d, and P4a between control samples and samples with NFT. The strongest difference was observed in K3b and P3d strains (both p-values < 0.001). In both strains, the permeability of the inner membrane was lower after contact with NFT. A different situation was observed in the cells of the P4c and P4a strains: permeability was significantly greater in the microbial cultures with nitrofurantoin compared to the culture that contained mineral salt medium only. Increases from 0.03 to 0.05 μM min^{-1} and from 0.07 to 0.14 μM min^{-1} were observed. What is more, within the five microbial strains tested, P4c was characterized by the smallest inner membrane permeability, and P3d had the greatest.

The results of the inner membrane permeability measurements obtained within the present study are similar to those of Guven et al. (2005), who investigated the effect of various antibiotics and pesticides on the inner membrane permeability of *E. coli* ML 35 using the same method as in the present article. Their experiments revealed that neither gramicidin D nor ampicillin modify the activity of the enzyme β-galactosidase in the ML 35 strain [42]. This means that the presence of those antibiotics did not influence the permeability of the ML 35 membrane, which is similar to how nitrofurantoin did not modify the permeability of the K3a and P4c strains. On the other hand, Rajasekaran et al. (2019) have performed the experiments on antimicrobial peptides and their analogs. They checked, among other factors, the β-galactosidase activity in the *E. coli* strain after contact with the peptides. They observed an increase or no change in the membrane permeability of the inner membrane [43]. In our studies, nitrofurantoin induced a statistically significant increase in the permeability of the inner membrane in only one (P4a) of the five strains.

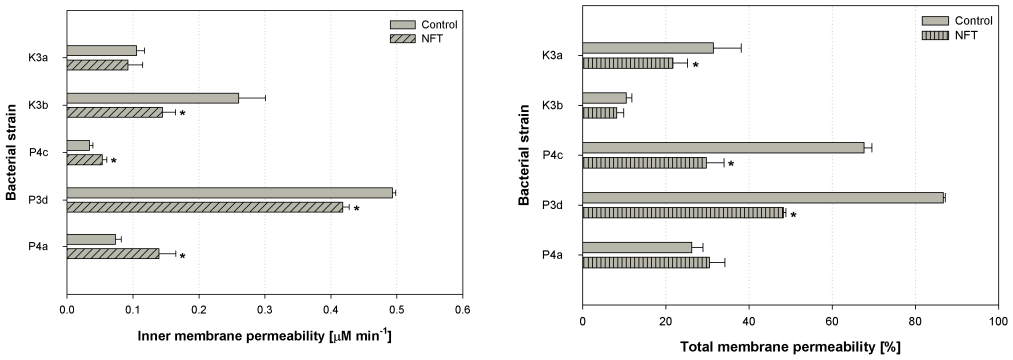

Figure 4. Changes in inner membrane permeability (**a**) and total membrane permeability (**b**) in five microbial strains subjected and not subjected to contact with nitrofurantoin; *Sphingomonas paucimobilis* (K3a), *Ochrobactrum antrophi* (K3b), *Rhizobium radiobacter* (P4c), *Pseudomonas aeruginosa* (P4a), and *Sphingobacterium thalpophilum* (P3d); stars (*) above the columns indicate statistical differences among groups (samples treated with nitrofurantoin (NFT) vs. untreated controls, $p < 0.05$, ANOVA followed by Tukey's range test); results are reported as mean values calculated from three independent experiments.

Figure 4b depicts the results of modifications of the total membrane permeability after the addition of nitrofurantoin (these groups are described as 'NFT'). The greatest differences between the control samples and samples containing nitrofurantoin were observed in the P4c and P3d strains ($p < 0.001$ for both strains). The presence of NFT provoked a reduction in total membrane permeability by 40% of the microbial cells mentioned. A statistically significant modification in total membrane permeability was noticed also for the K3a strain (a decrease from 31.4% to 21.7%, $p = 0.038384$). However, no changes were observed in the case of K3b ($p = 0.996302$) and P4a ($p = 0.838065$). Interestingly, the same direction of changes in both inner and total membrane permeability was observed for P3d (a statistically significant decrease in the presence of NFT) and P4a (a statistically significant increase in the presence of NFT), as well as K3a and K3b (a decrease in the presence of NFT); however, for the last two strains, the modifications were not significant for at least one parameter. Moreover, it should be highlighted that among all the strains tested, *S. thalpophilum* (P3d) was characterized by the greatest permeability change for both the bacterial total and inner membrane (in both the 'Control' and 'NFT' samples).

In general, the contact of bacteria cells with antimicrobial agents often causes an increase in the total membrane permeability. For example, ciprofloxacin and rhamnolipids provoked an increase of crystal violet uptake by *S. aureus* and *E. coli* cells [44]. Similarly, Bharali et al. (2013) observed rhamnolipids enhancing the membrane permeability of *K. pneumonie* cells [45]. However, ranbezolid, the pharmaceutical containing a nitrofuran ring in its molecule, did not affect *S. aureus* membrane integrity, but rather strongly damaged the membrane of *S. epidermidis* [46].

Most often, the increase of cellular membrane permeability is related to toxic effect of the xenobiotics on the cell and leads to its rupture [47]. On the other hand, it can facilitate the uptake of these compounds, and can be useful in biodegradation processes, as observed in the research of Qiu et al. [48]. Moreover, it should be mentioned that the permeability of the bacterial inner membranes decreased after contact with NFT in the K3b and P3d strains, and the permeability of the total membrane was statistically reduced in the K3a, P4c, and P3d strains. These results can suggest that the bacteria initiated a cellular defense mechanism against the exogenous substance and tried to prevent the xenobiotics molecules from entering into the cell [49].

3.3. Cell Surface Hydrophobicity

An important parameter of the bacterial cell surface that may indicate the chemical compound bioavailability to microbial cells is the cell surface hydrophobicity (CSH). In our research, the CSH

was tested using colorimetric congo red assay [27]. The results are presented in Figure 5. Among all the strains tested, *S. paucimobilis* (K3a) was characterized by the highest CSH (62.1%), as measured in the control samples. The presence of NFT provoked a decrease in the hydrophobicity of K3a to 36.2% ($p < 0.001$). A statistically significant reduction in the parameter in question was also noticed in P4c; however, an increase in CSH was observed in P3d. Considering K3b and P4a, no significant changes in the cell surface hydrophobicity were investigated. However, it should be noted that the cells of K3b were characterized by strongly hydrophilic properties (CSH between 5.3–6.8%), but the P4a cells were slightly hydrophobic (CSH around 31.3%).

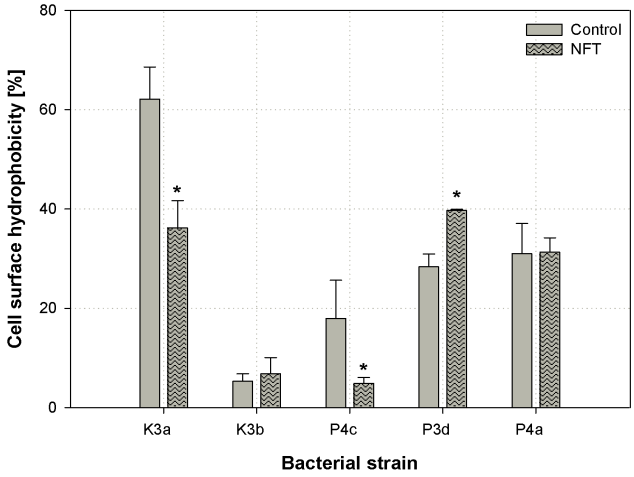

Figure 5. Changes in cell surface hydrophobicity in five microbial strains subjected and not subjected to contact with nitrofurantoin: *Sphingomonas paucimobilis* (K3a), *Ochrobactrum antrophi* (K3b), *Rhizobium radiobacter* (P4c), *Pseudomonas aeruginosa* (P4a), and *Sphingobacterium thalpophilum* (P3d); stars (*) above the columns indicate statistical differences among groups (samples treated with NFT vs. untreated controls, $p < 0.05$, ANOVA followed by Tukey's range test); the results are reported as mean values calculated from three independent experiments.

The carbon source may strongly affect the cell surface hydrophobicity. In turn, the bioavailability of the compound to be degraded may be increased [50]. However, the number of factors influencing the cell surface hydrophobicity impedes the easy interpretation of the mechanism of modification of bacteria cells' surface properties [51]. The alteration in cell surface hydrophobicity is clearly noticeable in the presence of hydrophobic pollutants such as diesel oil [52]. What is important, the pharmaceuticals, such as ibuprofen, also can modify the hydrophobicity of the bacterial cell surface [53]. Similarly, the presence of nitrofurantoin provoked changes in the CSH of the bacteria tested. It may indicate remodeling the outer layers of bacterial cells and changes in substrate bioavailability. However, phenomena occurring during the assimilation of a degraded compound are complex, and modifications of CSH do not have to directly affect changes in biodegradability.

3.4. Cytotoxity Analysis of NFT

Microbial cells viability is an important parameter during the evaluation of the xenobiotic's toxicity. In the present paper, the MTT (3-(4,5-dimethylthiazol-2-yl)-2,5-diphenyltetrazolium bromide) method was used in order to observe the effect of nitrofurantoin presence on the metabolic activity of newly isolated microbial strains [28]. The results are presented as MTT reducing units (MRU) in Figure 6.

The one-way ANOVA test and Tukey's range test indicated that nitrofurantoin provoked a significant decrease in the cell metabolic activity of strains K3a, K3b, P4c, and P4a (p-value < 0.001,

all four strains). The strongest difference was observed for P4c, where the relative number of metabolically active cells decreased from 2.55 to 1.12 MRU [-]. However, the slightest decrease that was still significant was noticed for the P4a strain. Considering the microbial strain isolated from the municipal WWTP, *S. thalpophilum* P3d, no notable changes in cells metabolic activity were noticed between the sample with MSM and the one with NFT. It should be noticed that a slight increase in metabolic activity was noticed in the P3d strain after contact with NFT; however, the difference was not significant ($p = 0.614344$).

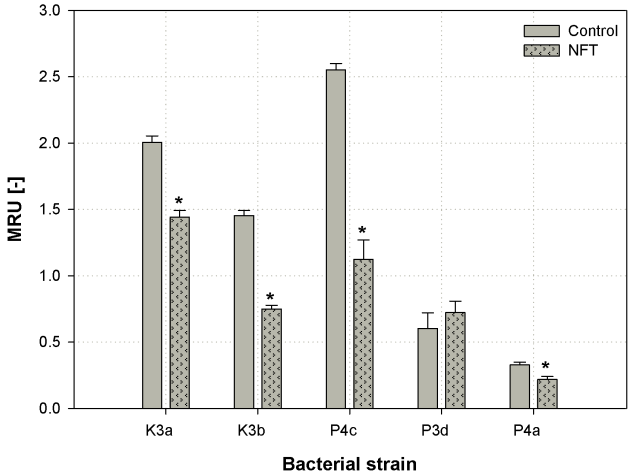

Figure 6. Modifications of microbial cells' viability in microbial cultures subjected and not subjected to contact with nitrofurantoin after 24 h of cultivating: *Sphingomonas paucimobilis* (K3a), *Ochrobactrum antrophi* (K3b), *Rhizobium radiobacter* (P4c), *Pseudomonas aeruginosa* (P4a), and *Sphingobacterium thalpophilum* (P3d); stars (*) above the columns indicate statistical differences among groups (samples treated with NFT vs. untreated controls, $p < 0.05$, ANOVA followed by Tukey's range test); results are reported as mean values calculated from three independent experiments.

Zhang et al. (2013) investigated the effect of another nitrofuran derivative—furazolidone—on microbial metabolic activity. The results showed that the relative cytotoxicity of the compound in question ranged from 6% to 36%, regarding the bacterial strain tested [54]. Another study published by Bergheim et al. (2015) showed that antibiotics are highly toxic to the *Pseudomonas putida* strain. High toxicity was associated with the low degradability of those compounds [3]. Such correlation did not have a place in our research. Although the presence of antimicrobial exogenous compounds decreased cells' viability, its biodegradation by the strains tested was still efficient (see Section 3.5). Itis interesting that the highest decrease in cells' metabolic activity (P4c) was not observed in the strain that had the smallest degradation rate (P4a).

3.5. Nitrofurantoin Removal

The next stage of the research was devoted to the analysis of the degradation potential of nitrofurantoin by the isolated bacterial strains. The highest removal rate was observed for all the strains within the first two days of cultivation (Figure 7). However, microorganisms from the rural WWTP, *S. paucimobilis* K3a and *O. antrophi* K3b, displayed the highest nitrofurantoin removal efficiency. Both strains utilized nearly 90% of the initial amount of the pharmaceutical in two days. At the end of the experiments, on the 28th day, the concentration of the degraded compound was reduced to 0.22 mg L^{-1} and 0.34 mg L^{-1} in cultures with K3a and K3b, respectively. Analyzing the results obtained for the strains of municipal WWTP origin, the most effective degradation was conducted by the P4c strain. The concentration of nitrofurantoin was reduced to 0.78 mg L^{-1} in four weeks (84% of the initial

NFT concentration was utilized). At the same time, the concentration of NFT measured in cultures containing P3d and P4a on the 28th day was 1.48 and 2.49 mg L^{-1}, which corresponded to 70% and 50% removal efficiency, respectively.

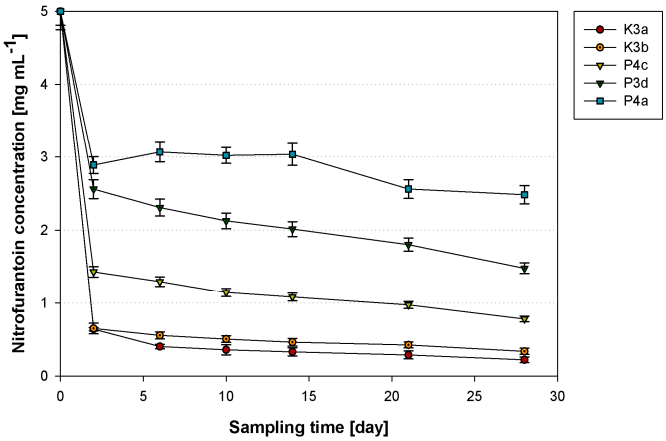

Figure 7. The nitrofurantoin removal in cultures with strains *Sphingomonas paucimobilis* (K3a), *Ochrobactrum antrophi* (K3b), *Rhizobium radiobacter* (P4c), *Pseudomonas aeruginosa* (P4a), and *Sphingobacterium thalpophilum* (P3d); results are reported as the mean values calculated from three independent experiments.

An important aspect of nitrofurantoin degradation is its relation to microbial cell properties. Reorganizations of cellular structures are expected to depend on bacterial species. As described above, microbial strains identified as *S. paucimobilis* K3a and *O. antrophi* K3b exhibited the greatest degradation ability. However, the response of these bacterial cells to the presence of nitrofurantoin was equivocal. We observed that in K3a, a high degradation was accompanied by the modification of the cells surface toward hydrophilic properties, and total membrane permeability toward significantly lower values. Nevertheless, the permeability of the inner membrane has not been changed. A different situation was noticed in the case of K3b, where a high degradation rate was accompanied by a significant decrease in inner membrane permeability, and the other parameters (total membrane permeability and cell surface hydrophobicity) have not been changed. On the other hand, the lowest nitrofurantoin removal rate was observed for *P. aeruginosa* P4a. In this case, the contact of bacterial cells with nitrofurantoin induced a statistically significant increase in both the inner and total membrane permeability. It is interesting that among all the strains tested, P4a was the strain that was characterized by the lowest metabolic activity, which was additionally reduced after cells' exposure to nitrofurantoin. The strain in question was also the only one that exhibited β-hemolysis. The results obtained indicate a variety of changes in the properties of the tested strains. Different observations can be explained by the different mechanisms of uptake of the substrate.

The information about the biodegradation of nitrofurantoin and other nitrofuran-derived compounds is scarce. Among the articles published in the last decade, only [54] studied furazolidone biodegradation by bacterial strains *Acinetobacter calcoaceticus* T32, *Pseudomonas putida* SP1, and *Proteus mirabilis* V7. On the second day of the experiment, the concentration of the compound in the cultures decreased significantly, and was lower than 30% of the initial concentration. Moreover, it is worth mentioning that Samuelsen et al. (1991) have analyzed the impact of furazolidone on microorganisms from aquaculture sediments, and noted that the half-life of furazolidone (at initial concentration of 400 μg mL^{-1}) did not exceed 18 h. However, an addition of the compound tested strongly reduced the number of autochthonic bacteria in the sediment [55].

Table 2 presents the results of an NFT degradation kinetic study calculated for individual microorganisms. The calculations results accurately match the Monod model, which allowed

determining the main constants in an equation describing the above-mentioned kinetic model. A half-saturation constant (K_s) representing the calculated substrate concentration at which its biotransformation is half the maximum value had the highest value for the P4c, P3d, and P4d strains (2.87, 3.68, and 4.09 mg L^{-1}, respectively). In contrast, the lowest values did not exceed 2.63 mg L^{-1}, and were found for two strains of rural WWTP origin. The distribution of substrate utilization rate (v_m) values among the tested bacteria was relatively similar to the K_s distribution. Microorganisms from the municipal activated sludge exhibited relatively low utilization rates (0.01 mg L^{-1} day^{-1}). The strains from the rural activated sludge had higher values of v_m: 0.02 and 0.06 mg L^{-1} day^{-1} for K3b and K3a, accordingly.

Table 2. The kinetics parameters according to the Monod equation describing nitrofurantoin biodegradation by strains *Sphingomonas paucimobilis* (K3a), *Ochrobactrum antrophi* (K3b), *Rhizobium radiobacter* (P4c), *Pseudomonas aeruginosa* (P4a), and *Sphingobacterium thalpophilum* (P3d).

Bacterial Strain	Half-Saturation Constant K_s [mg L^{-1}]	Substrate Utilization Rate v_m [mg L^{-1} day^{-1}]	R^2
K3a	2.13	0.02	0.99
K3b	2.63	0.06	0.99
P4c	2.87	0.01	0.99
P3d	3.68	0.01	0.99
P4a	4.09	0.01	0.99

The kinetics of antimicrobial agents' biodegradation have been analyzed by several researchers; however, this has never been studied in relation to nitrofurantoin. What is more, the results of antibiotics biodegradation have not always fitted the Monod model. For example, the sulfadiazine biodegradation by *Arthrobacter* spp. followed first-order decay kinetics [56]. In contrast, Cheyns et al. [57] after an analysis of atrazine biodegradation suggested that the Monod equation fits better. Hence, the obtained results are important, because the proper kinetics model can help predict the biodegradation capacity of microorganisms [57,58].

4. Conclusions

Both microbial consortia used (municipal and rural WWTPs' activated sludge) contained microbial strains that were capable of using NFT as a source of carbon and energy. Among the microbes isolated, the best nitrofurantoin removal efficiency was displayed by *S. paucimobilis* K3a and *O. antrophi* K3b (on average, 90% of the initial concentration of NFT was reduced in 28 days). Nitrofurantoin induced a decrease in both theTMP and CSH of the K3a strain. In general, the microorganisms that had their permeability lowered in the presence of NFT were characterized by lower cell metabolic activity.

Author Contributions: Conceptualization, A.P. and W.S.; methodology, A.P., W.S., A.Z.-G.; investigation, A.P., A.Z.-G.; writing—original draft preparation, A.P. and W.S.; writing—review and editing, E.K.; supervision, E.K.

Funding: This research was funded by the National Science Center, Poland, grant number 2017/27/B/NZ9/01603.

Conflicts of Interest: The authors declare no conflict of interest.

References

1. Grenni, P.; Ancona, V.; Caracciolo, A.B. Ecological effects of antibiotics on natural ecosystems: A review. *Microchem. J.* **2018**, *136*, 25–39. [CrossRef]
2. Caracciolo, A.B.; Topp, E.; Grenni, P. Pharmaceuticals in the environment: Biodegradation and effects on natural microbial communities. A review. *J. Pharm. Biomed. Anal.* **2015**, *106*, 25–36. [CrossRef] [PubMed]
3. Bergheim, M.; Gminski, R.; Spangenberg, B.; Debiak, M.; Bürkle, A.; Mersch-Sundermann, V.; Kümmerer, K.; Gieré, R. Antibiotics and sweeteners in the aquatic environment: biodegradability, formation of phototransformation products, and in vitro toxicity. *Environ. Sci. Pollut.* **2015**, *22*, 18017–18030. [CrossRef] [PubMed]

4. Edhlund, B.L.; Arnold, W.A.; McNeill, K. Aquatic photochemistry of nitrofuran antibiotics. *Environ. Sci. Technol.* **2006**, *40*, 5422–5427. [CrossRef]
5. Li, Y.; Dang, Z.; Huang, Y.; Yang, C.; Guo, C. Effects of cytotoxicity of erythromycin on PAH-degrading strains and degrading efficiency. *RSC Adv.* **2016**, *6*, 114396–114404.
6. Kümmerer, K. Antibiotics in the aquatic environment—A review—Part I. *Chemosphere* **2009**, *75*, 417–434. [CrossRef]
7. Biošić, M.; Škorić, I.; Beganović, J.; Babić, S. Nitrofurantoin hydrolytic degradation in the environment. *Chemosphere* **2017**, *186*, 660–668. [CrossRef]
8. Santos, F.; Mucha, A.P.; Alexandrino, D.A.; Almeida, C.M.R.; Carvalho, M.F. Biodegradation of enrofloxacin by microbial consortia obtained from rhizosediments of two estuarine plants. *J. Environ. Manag.* **2019**, *231*, 1145–1153. [CrossRef]
9. Harrabi, M.; Alexandrino, D.A.; Aloulou, F.; Elleuch, B.; Liu, B.; Jia, Z.; Almeida, C.M.R.; Mucha, A.P.; Carvalho, M.F. Biodegradation of oxytetracycline and enrofloxacin by autochthonous microbial communities from estuarine sediments. *Sci. Total. Environ.* **2019**, *648*, 962–972. [CrossRef]
10. Liu, N.; Hou, T.; Yin, H.; Han, L.; Huang, G. Effects of amoxicillin on nitrogen transformation and bacterial community succession during aerobic composting. *J. Hazard. Mater.* **2019**, *362*, 258–265. [CrossRef]
11. Jepsen, R.; He, K.; Blaney, L.; Swan, C. Effects of antimicrobial exposure on detrital biofilm metabolism in urban and rural stream environments. *Sci. Total. Environ.* **2019**, *666*, 1151–1160. [CrossRef]
12. Zhang, J.; Li, W.; Chen, J.; Qi, W.; Wang, F.; Zhou, Y. Impact of biofilm formation and detachment on the transmission of bacterial antibiotic resistance in drinking water distribution systems. *Chemosphere* **2018**, *203*, 368–380. [CrossRef]
13. Lv, G.; Li, Z.; Elliott, L.; Schmidt, M.J.; MacWilliams, M.P.; Zhang, B. Impact of tetracycline-clay interactions on bacterial growth. *J. Hazard. Mater.* **2019**, *370*, 91–97. [CrossRef]
14. Du, B.; Wang, R.; Yang, Q.; Hu, H.; Li, X.; Duan, X. Impact of tetracycline on the performance and abundance of functional bacteria of a lab-scale anaerobic-aerobic wastewater treatment system. *Biochem. Eng. J.* **2018**, *138*, 98–105. [CrossRef]
15. Manzetti, S.; Ghisi, R. The environmental release and fate of antibiotics. *Mar. Pollut.* **2014**, *79*, 7–15. [CrossRef]
16. Vumma, R.; Bang, C.S.; Kruse, R.; Johansson, K.; Persson, K. Antibacterial effects of nitric oxide on uropathogenic *Escherichia coli* during bladder epithelial cell colonization—A comparison with nitrofurantoin. *J. Antibiot.* **2016**, *69*, 183–186. [CrossRef]
17. Purohit, V.; Basu, A.K. Mutagenicity of Nitroaromatic Compounds. *Chem. Toxicol.* **2000**, *13*, 673–692. [CrossRef]
18. Kijima, A.; Ishii, Y.; Takasu, S.; Matsushita, K.; Kuroda, K.; Hibi, D.; Suzuki, Y.; Nohmi, T.; Umemura, T. Chemical structure-related mechanisms underlying in vivo genotoxicity induced by nitrofurantoin and its constituent moieties in gpt delta rats. *Toxicology* **2015**, *331*, 125–135. [CrossRef]
19. Vass, M.; Hruska, K.; Fránek, M. Nitrofuran antibiotics: a review on the application, prohibition and residual analysis. *Vet. Med.* **2008**, *53*, 469–500. [CrossRef]
20. Lewkowski, J.; Rogacz, D.; Rychter, P. Hazardous ecotoxicological impact of two commonly used nitrofuran-derived antibacterial drugs: Furazolidone and nitrofurantoin. *Chemosphere* **2019**, *222*, 381–390. [CrossRef]
21. Wang, Y.; Chan, K.K.J.; Chan, W. Plant uptake and metabolism of nitrofuran antibiotics in spring onion grown in nitrofuran—Contaminated soil. *J. Agric. Food Chem.* **2017**, *65*, 4255–4261. [CrossRef]
22. Kaczorek, E.; Sałek, K.; Guzik, U.; Dudzińska-Bajorek, B. Cell surface properties and fatty acids composition of *Stenotrophomonas maltophilia* under the influence of hydrophobic compounds and surfactants. *New Biotechnol.* **2013**, *30*, 173–182. [CrossRef]
23. Youssef, N.H.; Duncan, K.E.; Nagle, D.P.; Savage, K.N.; Knapp, R.M.; McInerney, M.J. Comparison of methods to detect biosurfactant production by diverse microorganisms. *J. Microbiol. Methods* **2004**, *56*, 339–347. [CrossRef]
24. Hassanshahian, M. Isolation and characterization of biosurfactant producing bacteria from Persian Gulf (Bushehr provenance). *Mar. Pollut.* **2014**, *86*, 361–366. [CrossRef]
25. Pacholak, A.; Simlat, J.; Zgoła-Grześkowiak, A.; Kaczorek, E. Biodegradation of clotrimazole and modification of cell properties after metabolic stress and upon addition of saponins. *Ecotoxicol. Environ. Saf.* **2018**, *161*, 676–682. [CrossRef]

26. Devi, K.P.; Sakthivel, R.; Nisha, S.A.; Suganthy, N.; Pandian, S.K. Eugenol alters the integrity of cell membrane and acts against the nosocomial pathogen Proteus mirabilis. *Arch. Pharmacal* **2013**, *36*, 282–292. [CrossRef]
27. Ambalam, P.; Kondepudi, K.K.; Nilsson, I.; Wadström, T.; Ljungh, Å. Bile stimulates cell surface hydrophobicity, Congo red binding and biofilm formation of *Lactobacillus* strains. *FEMS Microbiol. Lett.* **2012**, *333*, 10–19. [CrossRef]
28. Wang, H.; Cheng, H.; Wang, F.; Wei, D.; Wang, X. An improved 3-(4,5-dimethylthiazol-2-yl)-2,5-diphenyl tetrazolium bromide (MTT) reduction assay for evaluating the viability of *Escherichia coli* cells. *J. Microbiol. Methods* **2010**, *82*, 330–333. [CrossRef]
29. Bekins, B.A.; Warren, E.; Godsy, E.M. A Comparison of Zero-Order, First-Order, and Monod Biotransformation Models. *Ground Water* **1998**, *36*, 261–268. [CrossRef]
30. Poszytek, K.; Karczewska-Golec, J.; Ciok, A.; Decewicz, P.; Dziurzynski, M.; Gorecki, A.; Jakusz, G.; Krucon, T.; Lomza, P.; Romaniuk, K.; et al. Genome-Guided Characterization of *Ochrobactrum* sp. POC9 enhancing sewage sludge utilization—biotechnological potential and biosafety considerations. *Int. J. Environ. Res. Public. Health* **2018**, *15*, 1501. [CrossRef]
31. Wang, X.S.; Huang, L.P.; Li, Y.; Chen, J.; He, W.; Miao, H.H. Uptake of Cr (VI) by *Sphingomonas paucimobilis* Biomass from Aqueous Solutions. *Sci. Technol.* **2010**, *45*, 681–686.
32. Thelusmond, J.-R.; Strathmann, T.J.; Cupples, A.M. Carbamazepine, triclocarban and triclosan biodegradation and the phylotypes and functional genes associated with xenobiotic degradation in four agricultural soils. *Sci. Total. Environ.* **2019**, *657*, 1138–1149. [CrossRef] [PubMed]
33. Kim, Y.-M.; Murugesan, K.; Schmidt, S.; Bokare, V.; Jeon, J.-R.; Kim, E.-J.; Chang, Y.-S. Triclosan susceptibility and co-metabolism—A comparison for three aerobic pollutant-degrading bacteria. *Bioresour. Technol.* **2011**, *102*, 2206–2212. [CrossRef]
34. Shao, S.; Hu, Y.; Cheng, J.; Chen, Y. Degradation of oxytetracycline (OTC) and nitrogen conversion characteristics using a novel strain. *Chem. Eng. J.* **2018**, *354*, 758–766. [CrossRef]
35. Mulla, S.I.; Hu, A.; Sun, Q.; Li, J.; Suanon, F.; Ashfaq, M.; Yu, C.-P. Biodegradation of sulfamethoxazole in bacteria from three different origins. *J. Environ. Manag.* **2018**, *206*, 93–102. [CrossRef] [PubMed]
36. Zhang, W.; Qiu, L.; Gong, A.; Yuan, X. Isolation and characterization of a high-efficiency erythromycin A-degrading Ochrobactrum sp. strain. *Mar. Pollut.* **2017**, *114*, 896–902. [CrossRef]
37. Telke, A.; Kalyani, D.; Jadhav, J.; Govindwar, S. Kinetics and mechanism of reactive Red 141 degradation by a bacterial isolate *Rhizobium radiobacter* MTCC 816. *Acta Chim. Slov.* **2008**, *55*, 320–329.
38. Parshetti, G.; Saratale, G.; Telke, A.; Govindwar, S. Biodegradation of hazardous triphenylmethane dye methyl violet by *Rhizobium radiobacter* (MTCC 8161). *J. Basic Microbiol.* **2009**, *49*, S36–S42. [CrossRef]
39. Radó, J.; Kaszab, E.; Petrovics, T.; Pászti, J.; Kriszt, B.; Szoboszlay, S. Characterization of environmental *Pseudomonas aeruginosa* using multilocus sequence typing scheme. *J. Med Microbiol.* **2017**, *66*, 1457–1466. [CrossRef]
40. Sindu, P.A.; Gautam, P. Studies on the biofilm produced by *P. aeruginosa* grown in different metal fatty acid salt media and its application in biodegradation of fatty acids and bioremediation of heavy metal ions. *Can. J. Microbiol.* **2017**, *63*, 61–73. [CrossRef]
41. Rozitis, D.; Strade, E. COD reduction ability of microorganisms isolated from highly loaded pharmaceutical wastewater pre-treatment process. *J. Mater. Environ. Sci.* **2015**, *6*, 507–512.
42. Guven, K.; Yolcu, M.; Gul-Guven, R.; Erdogan, S.; De Pomerai, D. The effects of organic pesticides on inner membrane permeability in *Escherichia coli* ML35. *Cell Boil. Toxicol.* **2005**, *21*, 73–81. [CrossRef]
43. Rajasekaran, G.; Dinesh Kumar, S.; Nam, J.; Jeon, D.; Kim, Y.; Lee, C.W.; Park, I.-S.; Shin, S.Y. Antimicrobial and anti-inflammatory activities of chemokine CXCL14-derived antimicrobial peptide and its analogs. *Biochim. Biophys. Acta Biomembr.* **2019**, *1861*, 256–267. [CrossRef]
44. Sana, S.; Datta, S.; Biswas, D.; Sengupta, D. Assessment of synergistic antibacterial activity of combined biosurfactants revealed by bacterial cell envelop damage. *Biochim. Biophys. Acta Biomembr* **2018**, *1860*, 579–585. [CrossRef]
45. Bharali, P.; Saikia, J.; Ray, A.; Konwar, B. Rhamnolipid (RL) from *Pseudomonas aeruginosa* OBP1: A novel chemotaxis and antibacterial agent. *Colloids Surf. B Biointerfaces* **2013**, *103*, 502–509. [CrossRef]
46. Kalia, V.; Miglani, R.; Purnapatre, K.P.; Mathur, T.; Singhal, S.; Khan, S.; Voleti, S.R.; Upadhyay, D.J.; Saini, K.S.; Rattan, A.; et al. Mode of Action of ranbezolid against Staphylococci and structural modeling studies of its interaction with ribosomes. *Antimicrob. Agents Chemother.* **2009**, *53*, 1427–1433. [CrossRef]

47. Heipieper, H.J.; Neumann, G.; Cornelissen, S.; Meinhardt, F. Solvent-tolerant bacteria for biotransformations in two-phase fermentation systems. *Appl. Microbiol. Biotechnol.* **2007**, *74*, 961–973. [CrossRef]
48. Qiu, S.; Xu, H.; Xu, S.; Ma, F. The effect of tourmaline on cell membrane of nitrosomonaseuropaea and biodegradation of micropollutant: The effect of tourmaline on cell membrane. *Surf. Interface Anal.* **2014**, *46*, 564–569. [CrossRef]
49. Branco, M.R.; Marinho, H.S.; Cyrne, L.; Antunes, F. Decrease of H_2O_2 plasma membrane permeability during adaptation to H_2O_2 in *Saccharomyces cerevisiae*. *J. Biol. Chem.* **2004**, *279*, 6501–6506. [CrossRef]
50. Kaczorek, E.; Pacholak, A.; Zdarta, A.; Smułek, W. The impact of biosurfactants on microbial cell properties leading to hydrocarbon bioavailability increase. *Colloids Interfaces* **2018**, *2*, 35. [CrossRef]
51. Krasowska, A.; Sigler, K. How microorganisms use hydrophobicity and what does this mean for human needs? *Front. Microbiol.* **2014**, *4*, 1–7. [CrossRef]
52. Smułek, W.; Zdarta, A.; Guzik, U.; Dudzińska-Bajorek, B.; Kaczorek, E. *Rahnella* sp. strain EK12: Cell surface properties and diesel oil biodegradation after long-term contact with natural surfactants and diesel oil. *Microbiol. Res.* **2015**, *176*, 38–47. [CrossRef]
53. Oliveira, I.M.; Borges, A.; Borges, F.; Simões, M. Repurposing ibuprofen to control *Staphylococcus aureus* biofilms. *Eur. J. Med. Chem.* **2019**, *166*, 197–205. [CrossRef]
54. Zhang, W.; Niu, Z.; Yin, K.; Liu, F.; Chen, L. Degradation of furazolidone by bacteria *Acinetobacter calcoaceticus* T32, *Pseudomonas putida* SP1 and *Proteus mirabilis* V7. *Int. Biodeterior. Biodegrad.* **2013**, *77*, 45–50. [CrossRef]
55. Samuelsen, O.B.; Solheim, E.; Lunestad, B.T. Fate and microbiological effects of furazolidone in a marine aquaculture sediment. *Sci. Total. Environ.* **1991**, *108*, 275–283. [CrossRef]
56. Deng, Y.; Mao, Y.; Li, B.; Yang, C.; Zhang, T. Aerobic Degradation of sulfadiazine by *Arthrobacter* spp.: kinetics, pathways, and genomic characterization. *Environ. Sci. Technol.* **2016**, *50*, 9566–9575. [CrossRef]
57. Cheyns, K.; Mertens, J.; Diels, J.; Smolders, E.; Springael, D. Monod kinetics rather than a first-order degradation model explains atrazine fate in soil mini-columns: Implications for pesticide fate modelling. *Environ. Pollut.* **2010**, *158*, 1405–1411. [CrossRef]
58. Sniegowski, K.; Mertens, J.; Diels, J.; Smolders, E.; Springael, D. Inverse modeling of pesticide degradation and pesticide-degrading population size dynamics in a bioremediation system: Parameterizing the Monod model. *Chemosphere* **2009**, *75*, 726–731. [CrossRef]

Publication P2

Journal of Hazardous Materials 407 (2021) 124352

Contents lists available at ScienceDirect

Journal of Hazardous Materials

journal homepage: www.elsevier.com/locate/jhazmat

Research Paper

Investigation of the bacterial cell envelope nanomechanical properties after long-term exposure to nitrofurans

Amanda Pacholak [a,*], Natalia Burlaga [a], Urszula Guzik [b], Ewa Kaczorek [a,*]

[a] Institute of Chemical Technology and Engineering, Poznan University of Technology, Berdychowo 4, 60-965 Poznan, Poland
[b] University of Silesia in Katowice, Faculty of Natural Science, Institute of Biology, Biotechnology and Environmental Protection, Jagiellońska 28, 40 032 Katowice, Poland

ARTICLE INFO

Editor: Dr. T Meiping

Keywords:
Atomic force microscopy
Bacterial cell mechanics
Young's modulus
Stiffness
Adhesion
Membrane permeability
Bacterial cell wall

ABSTRACT

Antibiotic residues in the environment may negatively affect biological communities in the natural ecosystems. However, their influence on environmental bacterial strains has not been thoroughly investigated. In this study, two representatives of 5-nitrofuran antibiotics (nitrofurantoin and furaltadone) were investigated in terms of their long-term influence on the cell envelopes of newly isolated environmental bacterial strains (*Sphingobacterium caeni* FTD2, *Achromobacter xylosoxidans* NFZ2 and *Pseudomonas hibiscicola* FZD2). A 12-month exposure of bacterial cells to nitrofurans at a concentration of 20 mg L^{-1} induced changes in the cell structure and texture (bacteria under stress conditions showed a loss of their original shape and seemed to be vastly inflated, the cells increased average surface roughness after exposure to NFT and FTD, respectively). AFM observations allowed the calculation of the bacterial cell nanomechanical properties. Significant increase in adhesion energy of bacteria after prolonged contact with nitrofurantoin was demonstrated. Changes in the permeability of bacterial membrane, fatty acids' composition and bacterial cell surface hydrophobicity were determined. Despite visible bacterial adaptation to nitrofurans, prolonged presence of pharmaceuticals in the environment has led to significant alterations in the cells' structures which was particularly visible in *P. hibiscicola*.

1. Introduction

The pollution of the environment with hazardous materials is one of the most essential environmental issues of the 21st century. The best evidence of this is a rapidly growing number of publications focused on the characterization of these materials, their environmental fate, removal and monitoring (Angeles et al., 2020a; Charuaud et al., 2019; Hahladakis et al., 2018; Kokulnathan and Chen, 2020; Kumar et al., 2019; Tran et al., 2018). A group of substances which increasingly have been resealed into the environment are antimicrobial compounds. Antibiotics constitute the largest proportion of the drugs produced globally and are believed to be the most successful group of pharmaceuticals discovered (Kokulnathan and Chen, 2020; Kumar et al., 2019). It has been recently reported that between 2000 and 2015 the worldwide antibiotic consumption increased by 65% and is expected to be up to 200% higher than the 42 billion defined daily doses estimated in 2015 (Klein et al., 2018). These substances have not been only used for the treatment of animals' and humans' infections, they had been also commonly applied in husbandry and farming.

Despite unequivocal benefits provided for humans and animals, antibiotics may pose serious problems when released into the environment. First of all, their presence in the natural environment promotes the worldwide escalation of antibiotic resistance genes and antibiotic resistance bacteria (Berendonk et al., 2015). In addition, the antibiotics residues consumed in products of animal origin or drinking water may induce changes in the structure of human intestinal microflora leading to development of opportunistic pathogens (Ben et al., 2020).

Therefore, their usage in livestock production has been restricted in the European Union since 2006 and in the United Stated since 2017 (Kokulnathan and Chen, 2020; Robinson et al., 2018). Despite the limitations implemented, various antibiotics and their residues have been recently detected in various water bodies, e.g. the influents and effluents of wastewater treatments plants (Angeles et al., 2020b; Tran et al., 2018), groundwater and river water (Kim et al., 2018) or drinking water (Ben et al., 2020; Charuaud et al., 2019).

One of the main classes of the widely used antibiotics which

* Corresponding authors.
E-mail addresses: amanda.d.pacholak@doctorate.put.poznan.pl (A. Pacholak), burlaganatalia@gmail.com, natalia.burlaga@doctorate.put.poznan.pl (N. Burlaga), urszula.guzik@us.edu.pl (U. Guzik), ewa.kaczorek@put.poznan.pl (E. Kaczorek).

https://doi.org/10.1016/j.jhazmat.2020.124352
Received 28 June 2020; Received in revised form 14 October 2020; Accepted 19 October 2020
Available online 24 October 2020

environmental impact is very scarcely studied are 5-nitrofuran derivatives (5-NFs). The main compounds from the 5-NFs family are nitrofurantoin, nitrofurazone, furazolidone and furaltadone (Kokulnathan and Chen, 2020; Kumar et al., 2019). 5-NFs have been employed as pharmaceuticals, food additives, conservatives as well as in the livestock production since 1940s.

Nitrofurantoin (N-(5-nitro-2- furfurylidene)-1-aminohydantoin, NFT) has been used for the treatment of acute and chronic lower UTI since 1953. Despite the fact that the drug is known for its rare adverse effects which include pulmonary fibrosis and hepatitis, 90% of patients treated with NFT have recovered with no complications (Muller et al., 2017; Wijma et al., 2019). The bioavailability of NFT is 90%, it's elimination half-live is smaller than one hour and 27–50% of the drug is excreted non-metabolized in the urine. NFT has a bactericidal effect against Gram-negative uropathogens such as *E. coli* or *E. faecalis* (Novelli and Rosi, 2017).

Introduced in 1958, furaltadone (5-morpholinomethyl-3-(5-nitrofurfurylideneamino)-2-oxazolidinonem, FTD) has been mainly known as veterinary drug used for the treatment and prophylaxis of bacterial diseases in aquatic organisms. FTD is active against Gram-negative and Gram-positive bacteria. The drug is believed to be unstable and rapidly metabolized into 3-amino-5-methylmorpholino-2-oxazolidinone (AMOZ). Both FTD and AMOZ have been reported to show mutagenic, teratogenic and carcinogenic properties for humans (Zuma et al., 2019).

Nowadays, the usage of 5-NFs in husbandry and farming has been strictly prohibited in many countries (Kokulnathan and Chen, 2020). Nevertheless, they are still legally produced due to their effectiveness and low production costs. They are also easily available for the treatment of human and veterinary bacterial infections. Presumed excessive misuse of these drugs as well as illegal application in livestock production are the main reasons of the continuous release of their residues into the environment (Zhang et al., 2019). Having entered the natural environmental compartments, the antibiotics affect humans, animals and plants. However, they also directly influence environmental bacteria which play essential roles in the global ecosystem (Kumar et al., 2019).

A multilayered structure that separates the bacterial cell's plasma from the outside environment is called the bacterial cell envelope. The cell envelope of Gram-negative bacteria is composed of the inner cell membrane, the periplasmic space containing cell wall composed of a thin layer of peptidoglycan and the outer cell membrane containing lipopolysaccharide. (Silhavy et al., 2010). As this envelope interacts with exocellular environment directly, a characterization of its detailed structure and modifications provides essential information for understanding the mechanisms of interaction of xenobiotics with bacterial cells.

Although xenobiotics are believed to negatively affect bacterial cells, the exact mechanism of their interactions with bacterial surfaces remains unclear (Ahmed et al., 2020). Previous studies revealed that pharmaceuticals contribute to modification of bacterial cell membrane permeability, cell wall elasticity or fatty acids composition (Cai et al., 2019; Mohamed et al., 2016; Pogoda et al., 2017; Uzoechi and Abu-Lail, 2020; Yu and Zhao, 2020).

Recently, the traditional biochemical methods of bacterial cell properties evaluation have been complemented with novel powerful techniques which allow determination of biological samples at the nanometer scale (Dorobantu and Gray, 2010; El-Kirat-Chatel et al., 2020; Müller and Dufrêne, 2011; Núñez et al., 2005). Such an approach was implemented in our research whose aim was to investigate the impact of two NFs representatives (nitrofurantoin and furaltadone) on the modification of cell envelope of Gram-negative bacteria newly isolated from the activated sludge. The bacteria used in the experiments were characterized by relatively good growth in the presence of NFT and FTD. Moreover, these species have been found in different environmental compartments and some of them have shown the potential application in the bioremediation of various micropollutants (Li et al., 2009; Manzoor et al., 2019; Nam et al., 2015; Singh and Singh, 2011; Sun et al., 2013). The bacteria isolated were subjected to the long-term exposure to NFT and FTD and the effect of the exposure on bacterial cell envelopes was investigated. The novel tools and techniques were applied in the research presented (such as TEM microscopy and AFM microscopy) which allowed detailed studies of modifications in microbial surface triggered by long-term exposure of bacteria to pharmaceuticals. AFM observations allowed also the calculation of bacterial cells roughness and cell nanomechanical properties. To the best of our knowledge, this study is the first to report changes in nanomechanical properties of bacterial cells after long-term exposure to antibiotics. Moreover, changes in the permeability of the fatty acids' composition and bacterial cell surface hydrophobicity as well as bacterial total and inner membrane permeability were studied. The knowledge obtained within the research presented may help enhance our understanding of pharmaceuticals that pose a threat to the environment and human health.

2. Materials and methods

2.1. Chemicals

Nitrofurantoin, furaltadone and all other chemicals were purchased from Sigma-Aldrich (Sigma-Aldrich, St. Louis, MO, USA), microbiological media were obtained from bioMérieux (Warsaw, Poland). All chemical reagents and solvents were of the highest analytical grade and used without further purification. All required solutions were prepared using ultra-purified Milli-Q water (Arium® Pro, Sartorius, Kostrzyn Wlkp., Poland).

The aqueous solutions and glassware were steam sterilized before using them in the experiments. Non-autoclavable solutions were filter sterilized (0.22 μm) (Captiva EconoFilters, Agilent, CA, USA). In order to prevent contamination, a biological safety cabinet (Labculture® Class II, Esco, Singapore) was used during activities associated with biological samples.

2.2. Bacterial strains and growing conditions

The bacterial strains used in the experiments were isolated from the activated sludge samples collected aseptically from the municipal wastewater treatment plant in Poznań, Poland (52°25′53.1′ N, 16°57′31.8′ E) using a selective cultures method (selective agents: NFT or FTD) in accordance with the procedure described previously (Pacholak et al., 2019).

After isolation process, the microbial growth of the single bacterial strains was monitored through culture optical density by measuring absorption spectrophotometrically at 600 nm (Multiskan 152 Sky Microplate Spectrophotometer, Thermo Fisher Scientific, Waltham, MA, USA). Three bacterial strains which showed the best growth in the presence of NFT and FTD were selected to further experiments. The strains were identified using biochemical (Vitek® 2 system, bioMérieux, Warsaw, Poland) and molecular techniques which allowed determination of their taxonomic affiliations (Kaczorek et al., 2013). Their 16S rRNA gene sequences have been deposited in the GenBank database under the following accession numbers: *Sphingobacterium caeni* FTD2 (Sph, GenBank: MK493331.1); *Achromobacter xylosoxidans* NFZ2 (Acb, GenBank: MK493330.1); *Pseudomonas hibiscicola* FZD2 (Psd, GenBank: MK493329.1).

In order to induce a long-term stress response, the bacteria isolated were cultivated overall for 12 months on the Mueller–Hinton (MH) solid media supplemented with nitrofurantoin (20 mg L^{-1}) or furaltadone (20 mg L^{-1}). The bacteria were subcultivated every 14 days in order to provide fresh nutrients and a selective agent (NFT or FTD). Simultaneously, the reference samples were cultivated on the MH agar plates without the addition of 5-NFs (bioMérieux, Warsaw, Poland). The reference bacterial strains were sub-cultivated to the new MH media as

often as the bacteria treated with nitrofurans. Such activities allowed determine the impact of prolonged contact of microorganisms with selected pharmaceuticals on the changes in the bacterial cell envelope (Fig. S1). After 12 months of continuous cultivation of bacteria in the presence of NFT and FTD, the cells under stress conditions (exposed to NFT or FTD) and the reference bacteria (non-exposed) were subjected to topography measurements (AFM and TEM imaging), analysis of their surface mechanical and biochemical properties (bacterial inner and total membrane permeability, Congo Red adsorption and fatty acids composition). Each experiment was preceded by liquid cultures preparation. The cultures were carried out in 250 mL DURAN® laboratory glass bottles containing 45 mL of minimal medium (composition: Na_2HPO_4 7.0; KH_2PO_4 2.8; NaCl 0.5; NH_4Cl 1.0 g L^{-1}), microelements solution ($FeSO_4{\cdot}7H_2O$ 35.0; $MgSO_4{\cdot}7H_2O$ 350.0; $MnSO_4{\cdot}5H_2O$ 200.0; $CuSO_4{\cdot}7H_2O$ 200.0; $CoSO_4{\cdot}7H_2O$ 25.0; H_3BO_3 285.0; ZnCl 105.0 mg L^{-1}), 5 mL of inoculum (cells freshly grown on agar plates, washed with sterile medium, optical density adjusted to 1.0 ± 0.1), 0.1 mL 20% sodium succinate as a source of carbon, nitrofurantoin or furaltadone (the final concentration 5 mg L^{-1}). The cultures were incubated in 30 °C with shaking (120 rpm) for 48 h to obtain cells in the exponential growth phase.

2.3. Preparation of bacterial samples for AFM analysis

Long-term treated (NFTs and FTDs) and untreated (Ctrl) cells from liquid cultures were washed three times with sterile DPBS (Dulbecco's Phosphate-Buffered Saline) solution. The pellets were gently resuspended in DPBS to obtain cells' concentration of 1×10^8 cfu mL^{-1}, and subsequently the cells were rinsed with distilled water. 10 µl of a given bacterial suspension was placed on a freshly cleaved mica surface and left to dry in air at room temperature for 2 h before imaging. The mica was attached to a steel puck using double-sided adhesive tape and then was transferred into the sample stage on the AFM microscope.

2.4. Bacterial cells surface characterization by AFM

An atomic force microscope (Park NX10, Park Systems Corp., Suwon, Korea) was implemented in the experiments to analyze changes in the cell topography of three bacterial strains subjected to long-term exposure to 5-NFs. The surface plots were made to provide a three-dimensional perspective of the surface, from which changes in the bacterial surface were analyzed and roughness parameters were calculated. Measurements were performed using non-contact mode using All-in-One cantilever, type D (BudgetSensors, Sofia, Bulgaria) with nominal resonance frequency of 350 kHz and nominal force constant of 40 N m^{-1}. The scan size was set to 5×5 µm^2 with sampling of 512 lines for each image and scan rate of 0.4–0.5 Hz. For each sample, at least three measurements of 10×10 µm^2 were performed in different positions in order to localize the bacterial cells and choose the best view of sample positioning. The measurements were performed in air at room temperature (about 22 °C). The results of imaging were further investigated by Gwyddion open-source software.

2.5. Surface roughness determination by AFM

Surface roughness was calculated from single cell images over a linear profile of the cell in the central region of the given cells, from images of 5×5 µm size. For each experimental setup at least 25 cells were included in calculations. Three height parameters (Ra, RMS, R3z) and one spacing parameter (λq) were chosen as indicative of bacterial cell surface modifications:

- the average roughness (Ra) – which represents the average arithmetical height of the profile;
- root mean square roughness (RMS) – being the root mean square of the height values of the profile;
- average roughness depth (R3z) – the third highest peak to third deepest valley height, this parameter omits the two highest peaks and the two lowest valleys, it measures the vertical variation of the third highest peak from the third deepest valley over the evaluation length;
- wavelength of the profile (λq) – root mean square of the average wavelength (the parameter that relates the average roughness with the individual frequencies and amplitudes of the local peaks and valleys) of the profile.

The parameters in question are expressed in nm. The final results are expressed as the median of the replicates and the error bars indicate 95% CI.

2.6. Mechanical properties of bacteria determination by AFM

PinPoint™ Nanomechanical Mode from Park Systems enabled evaluation of high-resolution data using force-distance spectroscopy with simultaneous measurements of topographical data. This allowed calculation of changes in selected quantitative nanomechanical properties of bacterial cells. The median loading force was 270 nN with a constant approach and retract velocity of 30 µm s^{-1}. The cells nanomechanical properties include parameters as follows: adhesion energy, adhesion force, deformation, energy dissipation, elastic modulus, stiffness and elastic modulus. For each experimental setup at least 25 cells were included in calculations.

2.7. TEM analysis

The morphology of the non-exposed and 5-nitrofurans exposed cells were also characterized by transmission electron microscopy using Transmission Electron Microscope HT7700 (Hitachi, Tokyo, Japan). Each bacterial suspension was placed on a copper grid coated with carbon film and negatively stained with 2% tungstic acid. Such prepared cells were left to dry in air at room temperature for 2 h before imaging.

2.8. Changes in the bacterial cell envelope

The experiments determining the impact of 5-NFs 12-month exposure on modifications of bacterial cell envelope were performed on the bacteria exposed to NFT, bacteria exposed to FTD and the reference bacteria. Additionally, modifications in the cell membrane permeability and Congo Red adsorption were measured in reference samples subjected to 7-day contact with NFT or FTD (short-term exposure) in minimal medium.

The experiments in question include: (i) Analysis of the cellular fatty acid profiles. Fatty acids' isolation and identification were conducted according to (Kaczorek et al., 2013). (ii) Modifications of the bacterial total and inner membrane permeability; (iii) adsorption of the Congo Red dye (cell surface hydrophobicity). The measurements of the total membrane permeability were based on the changes of Crystal Violet uptake by bacterial cells. The ones of the inner membrane permeability were based on determination of the release of β-galactosidase from the cell interior. Cell surface hydrophobicity measured bacterial cell capability of adsorbing hydrophobic dye Congo Red (Congo Red Assay). The last three tests were performed as described previously (Pacholak et al., 2019) with some modifications. The reaction volume was reduced to 0.2 mL, the reactions were carried out in the 96-well plates and spectrophotometric measurements were done using Microplate Spectrophotometer (Multiskan 152 Sky, Thermo Fisher Scientific, Waltham, MA, USA).

2.9. Statistical analysis

The results of the experiments are reported as median values calculated from at least three independent experiments (biological repetitions

– three independent samples inoculated at day 0). For each biological sample, three technical repetitions were performed. A statistical significance of differences between the means of test samples and reference samples was determined by two-way analysis of variance and Tukey's test for multiple comparisons. P-values calculated report up to three digits after the decimal point and are described in the graphs as follows. Significance level was 5%. The calculations were performed using GraphPad Prism (GraphPad Software, LLC, San Diego, CA, USA).

3. Results

3.1. Morphology and topography of bacterial cells

Representative AFM phase measurements before and after 12-month exposure to NFT and FTD of *Sphingobacterium caeni* FTD2, *Achromobacter xylosoxidans* NFZ2 and *Pseudomonas hibiscicola* FZD2 are shown in Fig. 1a–c. The images of cells of all strains exposed to NFT or FTD exhibited considerable modifications of bacterial cells shape in comparison to control samples, indicating changes in cells surface structure induced by prolonged exposure to pharmaceuticals. Measurements of the cells under stress conditions (both NFT- and FTD-exposed cells) evidenced a smooth, homogenous surface topography in all directions,

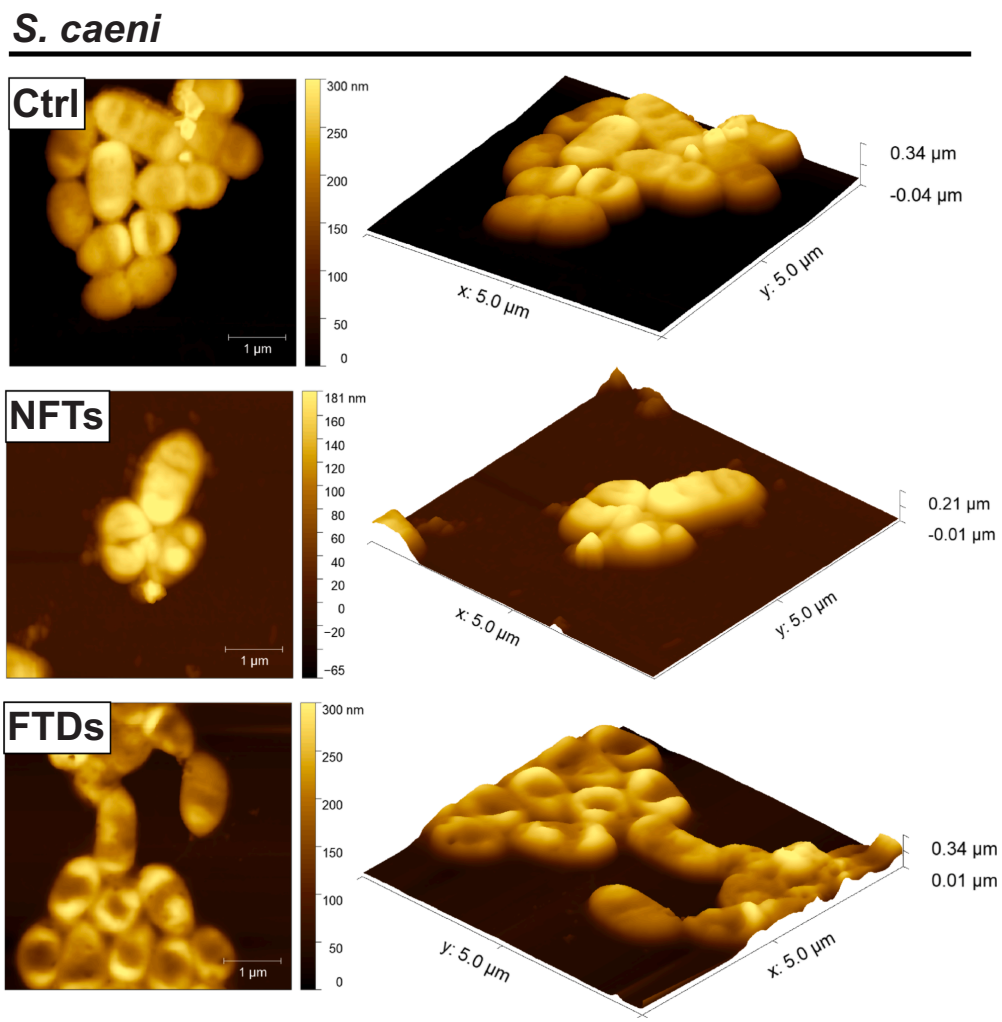

Fig. 1. Representative surface three-dimensional plots (5 µm × 5 µm) and height images illustrating the bacterial topography after 12-month exposure to nitrofurantoin or furaltadone. Bacterial strains: (a) *Sphingobacterium caeni* FTD2, (b) *Achromobacter xylosoxidans* NFZ2 and (c) *Pseudomonas hibiscicola* FZD2 (*Psd*). Ctrl – control samples (bacteria not exposed to nitrofurans); NFTs – bacteria after 12-month exposure to nitrofurantoin; FTDs – bacteria after 12-month exposure to furaltadone.

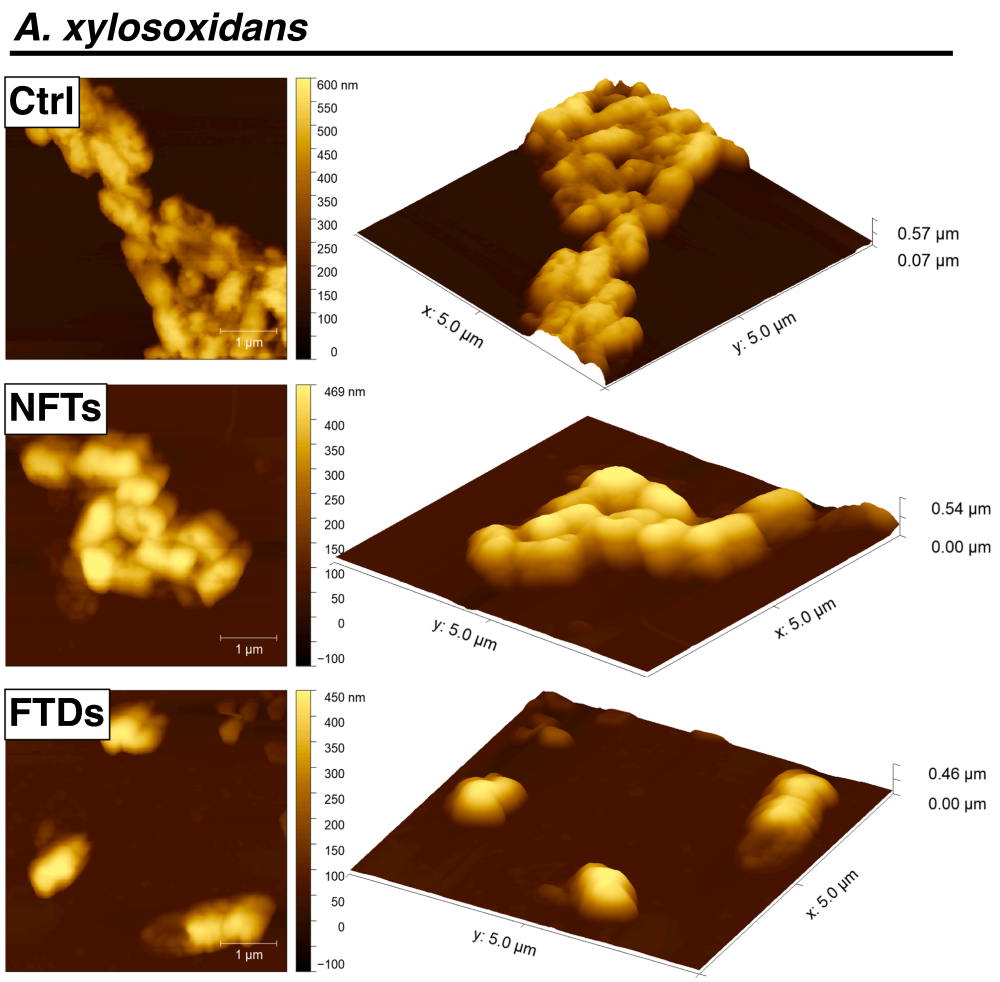

Fig. 1. (*continued*).

especially in the case of *S. caeni* (Fig. 1a). Bacteria were homogenous and no obvious damage in the cells subjected to prolonged exposure to nitrofurans was observed. An increase in the length of the cells under stress conditions in comparison to control samples was observed for all strains except for NFT-treated *S. caeni* (Table 1). In particular, NFT-exposed and FTD-exposed cells of *A. xylosoxidans* showed a loss of their original shape and seemed to be vastly inflated. Irregular cells architecture which could be attributed to cells damage can be observed in AFM pictures (Fig. 1b). This phenomenon was also strongly observed in the case of *P. hibiscicola* strain whose the cells became more spherical. The control cells of all strains tested showed strong aggregation which was not always observed in the case of bacteria under stress conditions. The smallest differences between control samples and treated samples were noted for *S. caeni strain*.

Fig. 2 represents bacterial morphology of the cells of *S. caeni*, *A. xylosoxidans* and *P. hibiscicola* measured by transmission electron microscopy. The cell surfaces of bacteria in the images are intact, stained well and the cells have mostly unimpaired cell envelopes. The bacterial surface of control cells (Fig. 2a, d, g) is slightly waved. The cells of all strains exposed to NFT (Fig. 2b, e, h) and FTD (Fig. 2c, f, i) exhibit considerable modifications in comparison to control samples, indicating changes in cells surface structure. *S. caeni* control cells (Fig. 2a) exhibit elongated worm-like morphology and are characterized by a wide, dark-colored boundary which could be attributed to the presence of extracellular substances secreted by the cells. Such observations have been also noticed for *S. caeni* exposed to NFT. A complete loss of dark boundary around the cell was noticed for FTD-treated *S. caeni* cells. The lengths of NFT- and FTD-exposed *S. caeni* cells have increased, the cells seem to be fluffier and inflated in comparison to control samples. The control cells of *A. xylosoxidans* (Fig. 2d) exhibit a slightly elongated morphology. There are dark condensed structures visible in the middle of the cells. Heterogeneous appearance of the cytoplasm, presence of condensed spots and septal rings (circle) as well as disintegration and thickening of the cell wall (arrow) can be observed in *A. xylosoxidans* after treatment with NFT (Fig. 2e). The morphological changes in FTD-treated cells (heterogeneous appearance of the cytoplasm and

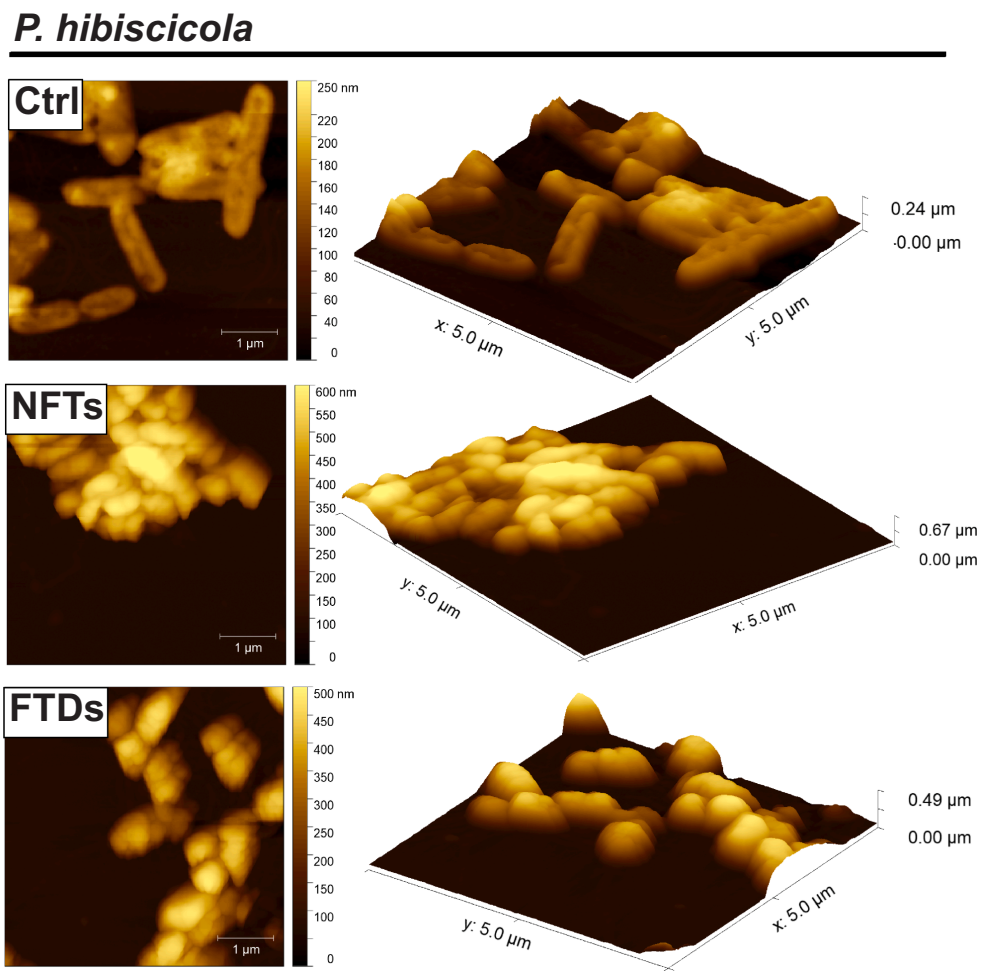

Fig. 1. (*continued*).

Table 1
Dimensions of individual cells calculated from AFM images. The results are presented as the mean value ± standard deviation.

Strain	Sample	Cell length [µm]	Cell width [µm]	Cell height [µm]
Sph	Ctrl	1.40 ± 0.24	0.75 ± 0.12	0.31 ± 0.13
	NFTs	1.42 ± 0.21	0.89 ± 0.05	0.17 ± 0.01
	FTDs	**1.10 ± 0.16****	0.75 ± 0.07	0.13 ± 0.05
Acb	Ctrl	0.88 ± 0.13	0.41 ± 0.08	0.35 ± 0.02
	NFTs	**1.02 ± 0.11***	0.52 ± 0.04	0.39 ± 0.07
	FTDs	**1.14 ± 0.15*****	**0.70 ± 0.10*****	0.34 ± 0.03
Psd	Ctrl	1.40 ± 0.27	0.50 ± 0.03	0.10 ± 0.02
	NFTs	**0.78 ± 0.17*****	0.30 ± 0.08	**0.17 ± 0.10***
	FTDs	**0.80 ± 0.25*****	0.58 ± 0.07	0.32 ± 0.06

Asterisks indicate a statistically significant difference (treated cells vs. control cells) calculated using one-way ANOVA: P-value: < 0.001(***); (0.001; 0.01 > (**); > 0.01 (*).

condensed spots, Fig. 2f) of *A. xylosoxidans* appear to be similar to those induced by NFT-treated ones. The TEM images of *P. hibiscicola* strain show that the shape and surface structure of the cells after treatment with NFT (Fig. 2h) and FTD (Fig. 2i) resemble that of control cells (Fig. 2g) – they exhibit elongated morphology and the structure is waved. However, the cells under stress conditions seem to have slightly increased width and reduced length. Moreover, the images of treated cells show intracellular inclusion bodies, which can be seen as light gray irregularly shaped circles.

3.2. Bacterial cell surface roughness determination by AFM

Bacterial surface roughness parameters are summarized in Fig. 3. Among all strains tested, the highest initial roughness was calculated for *A. xylosoxidans*. The prolonged exposure of bacterial cells to nitrofuran antibiotics contributed to the substantial increase of roughness average (Ra). The average roughness of *S. caeni* increased from 3.1± 0.4 nm (Ctrl) to average 4.5 nm (FTDs, NFTs). There was no difference between

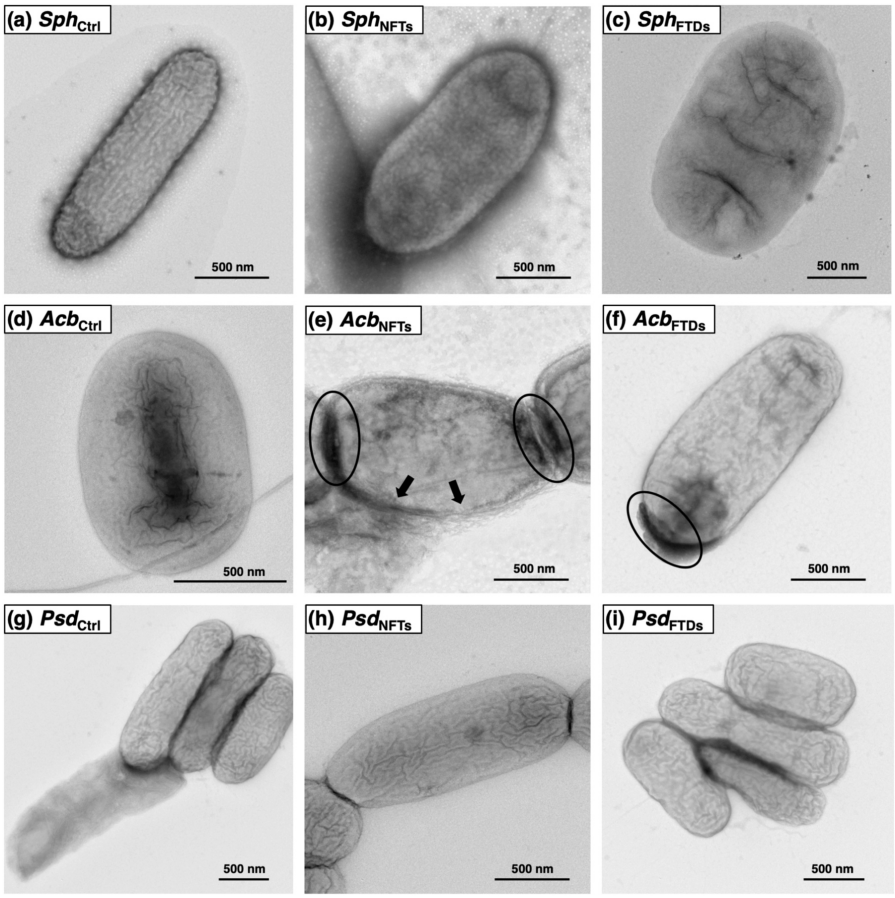

Fig. 2. TEM images of bacterial cells illustrating the morphology of three bacterial strains after 12-month exposure to nitrofurantoin or furaltadone. Bacterial strains: *Sphingobacterium caeni* FTD2 (*Sph*), *Achromobacter xylosoxidans* NFZ2 (*Acb*) and *Pseudomonas hibiscicola* FZD2 (*Psd*). Ctrl – control samples (bacteria not exposed to nitrofurans); NFTs – bacteria after 12-month exposure to nitrofurantoin; FTDs – bacteria after 12-month exposure to furaltadone.

NFT- and FTD-exposed cells. Similar observations were made for *P. hibiscicola, however,* the average Ra of treated bacteria was twice as high as that of control cells ($P < .001$), Regarding *A. xylosoxidans*, prolonged exposure to FTD did not induce statistically significant changes in the average roughness of the bacterial cells. Different observations were made for root mean square roughness (RMS). The parameter in question did not exhibit such significant modifications as Ra. The statistical differences between samples were calculated only in the case of *P. hibiscicola*. RMS of the control cells was 3.4 ± 0.7 nm and a substantial increase to 6.9 ± 1.6 nm was observed in NFT-treated cells ($P < .001$) and to 6.6 ± 0.7 nm in FTD-treated cells ($P < .001$). On the other hand, the modifications of average roughness depth (R3z) of all strains tested resemble these of Ra: a significant increase in NFT- and FTD-exposed cells in comparison to Ctrl of *S. caeni as well as P. hibiscicola*, and significant difference between NFT-exposed and FTD-exposed cells of *A. xylosoxidans*. 12-month exposure of the cells to nitrofurans induced significant alterations in the wavelength of the profile (λq) of NFT-treated *A. xylosoxidans* for which a substantial increase was calculated in comparison to control sample.

3.3. Bacterial cell surface nanomechanical properties determination by AFM

The violin plots in Fig. 4 show the frequency distribution of the data obtained for bacterial mechanical properties measurements. These include adhesion energy, adhesion force, deformation, elastic modulus and stiffness. The initial adhesion energy calculated for control samples was different for each strain tested. *S. caeni* was characterized by the lowest value (75.8 ± 9.0 aJ) and *P. hibiscicola* by the highest one (100.1 ± 10.3 aJ). Bacteria subjected to prolonged contact with nitrofurantoin significantly increased adhesion energy in comparison to control samples (all samples, Ctrl vs. NFTs, $P < .001$). The average adhesion energy for these bacteria was at least 130 aJ. Bacteria exposed to furaltadone had always lower adhesion energy than the ones exposed to nitrofurantoin (all samples, NFTs vs. FTDs, $P < .001$). When compared the bacteria after treatment with furaltadone to control samples, a statistically significant difference was observed only for *P. hibiscicola* (increase from 100.1 ± 10.3 to 121.6 ± 10.2 aJ).

Regarding adhesion force, the average initial value was again the

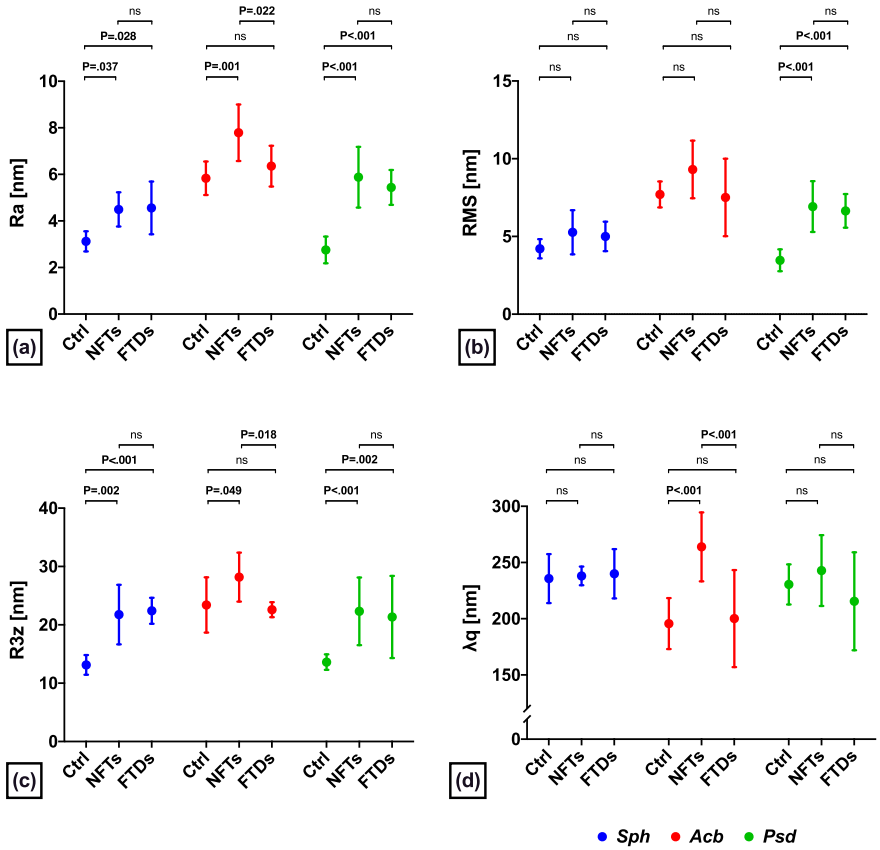

Fig. 3. Cell surface roughness parameters of *Sphingobacterium caeni* FTD2 (*Sph*, blue color in the graphs), *Achromobacter xylosoxidans* NFZ2 (*Acb*, red color in the graphs) and *Pseudomonas hibiscicola* FZD2 (*Psd*, green color in the graphs). Ctrl – control samples (bacteria not exposed to nitrofurans); NFTs – bacteria after 12-month exposure to nitrofurantoin; FTDs – bacteria after 12-month exposure to furaltadone. Ra – the average roughness; RMS – root mean square roughness, R3z – average roughness depth; λq – wavelength of the profile. The results are expressed as the mean of the replicates and the error bars indicate 95% CI. P-values in bold indicate statistically significant difference; ns – not significant. (For interpretation of the references to color in this figure legend, the reader is referred to the web version of this article.)

lowest in *S. caeni* (19.08 ± 2.2 nN) and the highest in *P. hibiscicola* (34.21 ± 1.41 nN). The prolonged contact with 5-NF induced alterations of bacterial adhesion force in all strains tested, however, the strongest ones were noted for *A. xylosoxidans*. An increase from 21.16 ± 0.93 nN to 33.32 ± 2.91 nN ($P < .001$) was noted for NFT-exposed cells and to 24.79 ± 2.25 nN for FTD-exposed cells ($P < .001$). A long-term contact of *S. caeni* strain with nitrofurans induced a statistically significant decrease in adhesion force in the case of furaltadone. Different observations were made for *P. hibiscicola* in which a statistically significant increase in adhesion force was noted after treatment with nitrofurantoin. The adhesion force of FTD-treated cells was similar to that of control cells.

Analysis of the deformation of the cell envelope using atomic force microscopy has provided some information about elastic properties of bacterial cells. A significant increase in deformation was noted for NFT-exposed cells of all strains in comparison to control samples ($P < .001$). These cells showed significant heterogenicity which is exhibited by considerable difference between 25th and 75th percentile (dotted lines in the violin plots). When the bacteria were subjected to prolonged contact with FTD, the deformation of *S. caeni* cells was not significantly different from that of untreated cells. Statistically significant alterations of deformation of the cells under stress conditions were visible in the case of *A. xylosoxidans* and *P. hibiscicola*. Bacterial 12-month exposure to both, NFT and FTD, provoked a statistically significant increase in deformation of both strains in question (*A. xylosoxidans*: Ctrl vs. NFTs, FTDs, $P < .001$; *P. hibiscicola*: Ctrl vs. NFTs, FTDs and NFTs vs. FTDs, $P < .001$).

Elastic properties of bacterial cells expressed by elastic modulus (Young's modulus, Y) are presented in Fig. 4d. The control samples of all strains tested had the lowest capacity to undergo elongation or compression. Among them, the lowest average elastic modulus was calculated for *A. xylosoxidans* (0.38 ± 0.06 GPa). The prolonged contact of the bacterial strains with NFT or FTD has undoubtedly increased their elastic properties. The cells of *S. caeni* and *P. hibiscicola* treated with nitrofurantoin exhibited higher difference between control samples than the cells of these strains treated with furaltadone. The average values of Young's moduli of these cells were 2.38 ± 0.10 GPa and 2.02 ± 0.29 GPa, respectively. The Young's modulus of NFT-treated

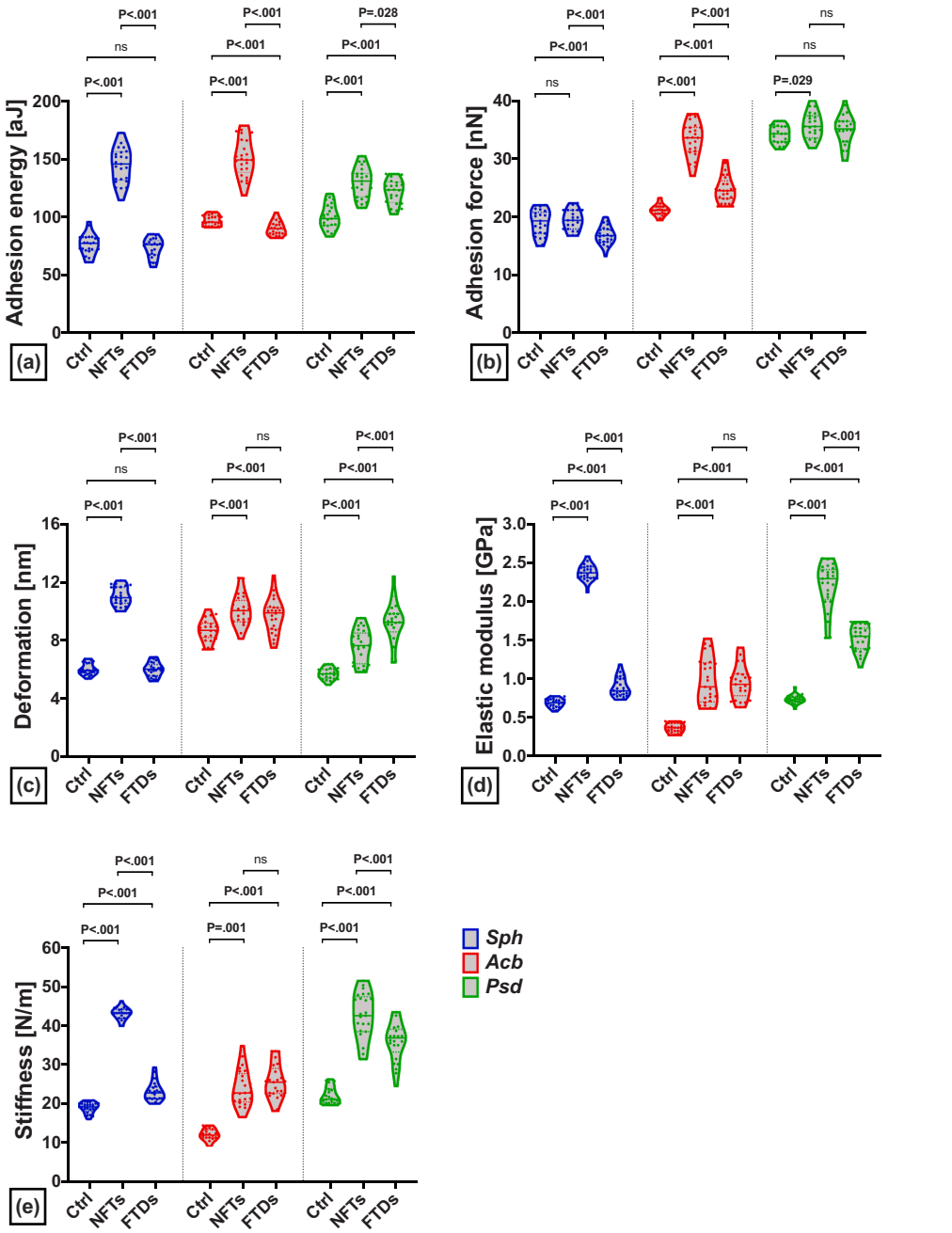

Fig. 4. Surface nanomechanical properties of the bacterial cells of *Sphingobacterium caeni* FTD2 (*Sph,* blue color in the graphs), *Achromobacter xylosoxidans* NFZ2 (*Acb,* red color in the graphs) and *Pseudomonas hibiscicola* FZD2 (*Psd,* green color in the graphs). Ctrl – control samples (bacteria not exposed to nitrofurans); NFTs – bacteria after 12-month exposure to nitrofurantoin; FTDs – bacteria after 12-month exposure to furaltadone. Box upper and lower lines represent maximum and minimum value, midline is sample median, dotted lines in the box stand for quartiles. P-values in bold indicate statistically significant difference; ns – not significant. (For interpretation of the references to color in this figure legend, the reader is referred to the web version of this article.)

A. xylosoxidans cells was similar to that of FTD-treated cells with the average value of 0.97 GPa. It is worth to emphasize that the cells which showed significant alterations on Young's modulus, exhibited also considerable heterogenicity.

The prolonged exposure of bacterial cells to the presence of nitrofuran antibiotics induced modifications of stiffness, the last surface nanomechanical property measured. The direction of these modifications was similar to that of elastic modulus. Statistically significant changes were noted for all strains which had the stiffness increased under stress conditions. In the case of *S. caeni* and *A. xylosoxidans* the treatment with NFT induced stronger alterations than the treatment with FTD. Different observations were made for *A. xylosoxidans*, where both antibiotics affected the bacterial cell stiffness similarly.

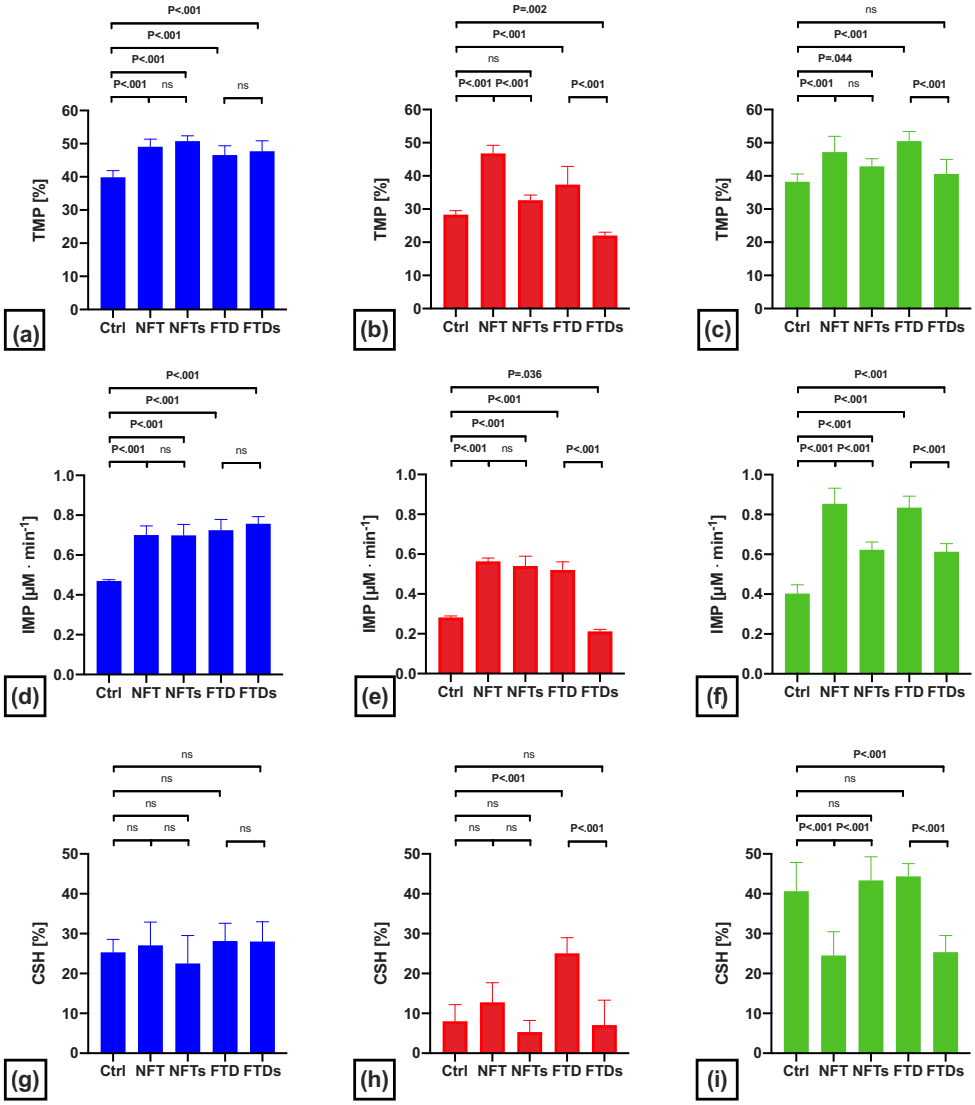

Fig. 5. Cell surface properties of *Sphingobacterium caeni* FTD2 (*Sph,* blue color in the graphs), *Achromobacter xylosoxidans* NFZ2 (*Acb,* red color in the graphs) and *Pseudomonas hibiscicola* FZD2 (*Psd,* green color in the graphs). TMP – total membrane permeability, IMP – inner membrane permeability, CSH – cell surface hydrophobicity. Ctrl – control samples (bacteria not exposed to nitrofurans); NFT – bacteria after short-term contact with nitrofurantoin; NFTs – bacteria after 12-month exposure to nitrofurantoin; FTD – bacteria after short-term exposure to furaltadone; FTDs – bacteria after 12-month exposure to furaltadone. The results are expressed as the mean of the replicates and the error bars indicate 95% CI. P-values in bold indicate statistically significant difference; ns – not significant. (For interpretation of the references to color in this figure legend, the reader is referred to the web version of this article.)

3.4. Modifications of the cell membrane permeability and cell surface hydrophobicity

The next part of the experiments performed was devoted to analyzes of changes in the total and inner membrane permeability as well as bacterial cell surface hydrophobicity. The results of the tests are presented in Fig. 5. Total membrane permeability (TMP) of *S. caeni* was the lowest in control sample (39.9 ± 1.9%) and a substantial increase by around 10% was noted for all other samples ($P < .001$). However, there was no significant difference between these samples in the total permeability of bacterial membrane. Different observations were made for *A. xylosoxidans* and *P. hibiscicola*. In these strains, the highest modifications of TMP were observed between control samples and bacteria after short-term contact with pharmaceuticals as well as between bacteria in question and the ones after 12-month exposure to selected nitrofurans. Short-term exposure to nitrofurantoin and furaltadone induced significant increase in TMP in comparison to Ctrl (Ctrl vs. NFT and Ctrl vs. FTD, $P < .001$, both strains). However, by comparison with bacteria after short-term exposure, bacteria after 12-month exposure with nitrofurans have the TMP lowered.

The directions of the modifications of the inner membrane permeability (IMP) measurements were similar to these of the TMP. Ctrl sample of *S. caeni* had the lowest permeability of the inner membrane and considerable increase in permeability was noted for all other samples in comparison to Ctrl ($P < .001$). The same situation was observed in the case of *A. xylosoxidans* except for bacteria after long-term exposure to FTD where statistically significant reduction of IMP was observed when compared to both reference sample and bacteria (Ctrl vs. FTDs, $P = .038$; FTD vs. FTDs, $P < .001$). The strongest alterations of inner membrane permeability were measured for *P. hibiscicola*. Exposure of each cell line to nitrofurantoin or furaltadone resulted in increased IMP. Nevertheless, the highest values were noted for samples after short-term contact with pharmaceuticals. It seems that these bacteria had not adapted to the presence of nitrofurans in their environment and the pharmaceuticals might have induced a disintegration of bacterial membrane.

Experiments on adsorption of Congo Red dye by bacterial cells allowed indicate cells adhesion properties. Among all strains tested, the highest modifications were noted for *P. hibiscicola.* This strain was characterized by the most hydrophobic properties. Short-term exposure to NFT and long-term exposure to FTD provoked significant reductions in its hydrophobic properties. The bacteria of *A. xylosoxidans* were hydrophilic. Prolonged exposure of *Acb* cells to nitrofurans provoked a reduction of hydrophobic properties and a short-term exposure induced an increase in these properties, however modifications were statistically significant only between control samples and samples after short-term exposure to furaltadone (Ctrl vs. FTD, $P < .001$) as well as between the samples in question and FTDs (FTD vs. FTDs, $P < .001$). Moreover, no statistically significant changes were measured for *S. caeni*, the mean cell surface hydrophobicity of these cell ranged between 22.5 ± 6.7 and 28.1 ± 4.3%.

3.5. Fatty acids profiles

In order to determine the effect of long-term exposure of nitrofurantoin or furaltadone on whole cell-derived fatty acids profiles of *S. caeni*, *A. xylosoxidans* and *P. hibiscicola,* fatty acids methyl esters were isolated from these bacteria exposed and non-exposed to a given 5-NF. The identified fatty acids were divided into two major groups: unsaturated and saturated and fatty acids. The second group included: straight-chain, hydroxy, cyclopropane and branched fatty acids. Fig. 6 presents the total percentage of the fatty acids and shows the compositional changes during growth of examined strains in the presence of nitrofurantoin or furaltadone for 12 months. For *A. xylosoxidans* strain in the presence of both NFT and FTD, a significant reduction in the percentage share of cyclopropane fatty acids and increase in the percentage share of unsaturated fatty acids as compared to the control cells were observed. As a consequence, the changes in the saturated/unsaturated fatty acids ratio for this strain were observed (21.88, 9.45, 8.67 for Ctrl, NFTs and FTDs, respectively). The treatment with nitrofurantoin or furaltadone of *S. caeni,* induced an increase in the percentage share of straight-chain fatty acids only. Most changes in the fatty acid profiles were observed in *P. hibiscicola* strain. However, in this case an increase in the saturated/unsaturated fatty acids ratio from 3.28 (Ctrl) to 5.87 (NFTs) and 5.53 (FTDs) was observed. The only fatty acids which had not been affected by nitrofurans belong to hydroxylated fatty acids group.

4. Discussion

Antimicrobial compounds are among the most widely used pharmaceuticals worldwide. Their residual amounts in the natural environment may negatively affect environmental bacterial strains and subsequently promote ecosystems' imbalance. An important issue that should be highlighted is the fact that nitrofurans attract less scientific attention regarding their environmental fate and impact than the other antibiotics. In this study, two representatives of 5-nitrofuran derivatives were investigated in terms of their long-term influence on the cell envelopes of newly isolated environmental bacterial strains.

First of all, we analyzed changes in the bacterial cell morphology and topography of the cells subjected to a 12-month exposure to NFT and

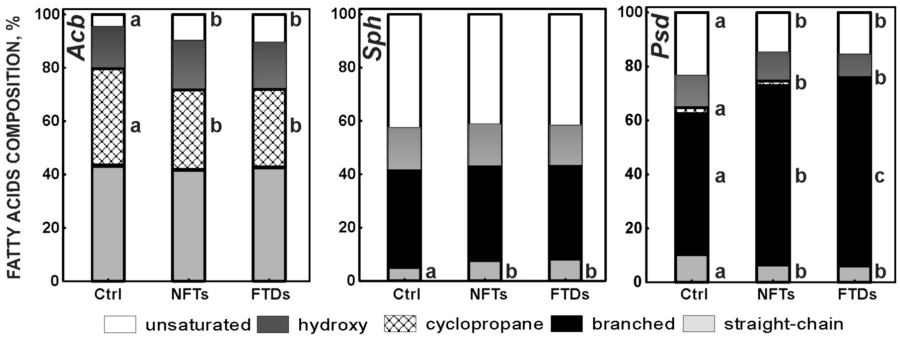

Fig. 6. Changes in the fatty acids' composition induced by prolonged exposure to nitrofurans. Bacterial strains: *Sphingobacterium caeni* FTD2 (*Sph*), *Achromobacter xylosoxidans* NFZ2 (*Acb*) and *Pseudomonas hibiscicola* FZD2 (*Psd*). Experimental setups: Ctrl – control samples (bacteria not exposed to nitrofurans); NFTs – bacteria after 12-month exposure to nitrofurantoin; FTDs – bacteria after 12-month exposure to furaltadone.

FTD using an atomic force microscopy and transmission electron microscopy. The results obtained were compared to control cells, which had not been previously subjected to such exposure. The research revealed that all bacterial strains tested have undergone significant modifications in terms of cells structure and shape. In general, bacteria under stress conditions seemed to be inflated and their surface has been more undulating than that of untreated control cells (Figs. 1 and 2). In most cases bacteria after NFT exposure behaved differently than the ones after FTD exposure, suggesting that these two nitrofuran compounds do not affect bacterial cell in the same way. However, the exact mechanism of changes in the cell shape after bacterial adaptation to the presence of antibiotics detected in this research is currently unknown and requires further investigation. Modification of bacterial surface in response to the presence of xenobiotics has also been observed by Ahmed et al., (2020). They measured cell topography and morphology of some beneficial soil bacteria exposed to antimicrobial agents. Irregular cells architecture, cells heterogenicity, leakage of the cellular content and cellular damage after exposure to nanoparticles were measured using AFM and TEM. In our research slight damage of bacterial cells exposed to 5-NFs could have been observed in the case of A. *xylosoxidans*. The most essential difference between the studies of Ahmed et al., (2020) and ours is the time of bacterial exposure to antimicrobial agents. In our studies bacterial cells have been cultivated continuously in the presence of xenobiotics for 12 months while in the studies of Ahmed et al., (2020) the cultivation time varied from 12 to 48 h. The latter points to a powerful and efficient adaptative capability of bacterial strains employed in our research, in particular *S. caeni*, and can be an explanation of different observations. It is also worth highlighting that the massive release of extracellular polymeric substance as well as elevated biofilm formation are important adaptative responses of bacteria living in the harsh environments. Such strategies may help them survive in the presence of xenobiotics and might have been implemented by the strains employed in our studies (Cai et al., 2018; Ma et al., 2017; Ouyang et al., 2020). Moreover, the difference in the nature of the compounds studied cannot be neglected.

Another significant point for consideration in bacterial topography characterization is the cell texture. Surface texture is measured by surface roughness, which in turn is represented by different quantitative parameters, among which roughness average (Ra) is the most widely used (De Oliveira et al., 2012). Nevertheless, in order to fully characterize a surface, more sophisticated parameters should be used (like R3z, RMS). Surface topography has been known to strongly affect bacterial attachment which is greatly connected to biofilm formation (Cheng et al., 2019; Wu et al., 2018). Studies on the bacterial cell surface roughness are becoming more current, however, the available papers mostly focus on Ra, whilst a deep analysis of other important roughness parameters is also essential. Most often than not, treatment of bacterial cells with xenobiotics results in increased cell surface roughness. Soon et al., (2009) observed a substantial increase in the Ra of *A. baumanii* after treatment with colistin. In another study, Ahmed et al., (2020) observed a substantial increase in the Ra of three bacterial strains after treatment with Ag- and ZnO-nanoparticles. Moreover, Uzoechi and Abu-Lail (2020) measured increased RMS of two *E. coli* strains after treatment with antibiotics in comparison to untreated cells. In the studies presented here, a statistically significant increase in Ra and R3z of all strains exposed to NFT and FTD in comparison to Ctrl was observed except for FTD-treated *A. xylosoxidans*. Increase in the cell surface roughness might have indicated cell membrane destruction, however, TEM and AFM images do not indicate unquestionable leakage of cell content or membrane damage. Increased cell surface roughness can also result from increased production of biopolymers on the bacterial surface. These biopolymers are believed to support the bacterial membrane integrity (Uzoechi and Abu-Lail, 2020; Limoli et al., 2020).

Surface roughness parameters of *A. xylosoxidans* were not significantly affected by prolonged exposure to furaltadone. In contrast, significant modifications of nanomechanical properties and changes in the topographical features were noted for this strain. Moreover, *A. xylosoxidans* was the only strain exhibiting slight disintegration and thickening of the cell wall which was visible in the microscopic images. Different observations were noted for *P. hibiscicola* and *S. caeni* in which a substantial increase in surface roughness parameters was calculated for the cells cultivated under stress conditions. Changes in the surface roughness were accompanied by modifications of nanomechanical properties (Fig. 4) as well as membrane permeability (Fig. 5c, f) and CR adsorption (Fig. 5i). Therefore, there is evidence suggesting that these modifications might have arisen from the adaptative response occurring in the cells.

Studies that focus on quantitative evaluation of the mechanical properties of bacterial cells are limited (Auer and Weibel, 2017; Uzoechi and Abu-Lail, 2020). To the best of our knowledge, changes in nanomechanical properties of bacterial cells after long-term exposure to antibiotics have not yet been investigated. The parameters tested include adhesion energy, adhesion force, deformation, elastic modulus and stiffness. Peptidoglycan, the main component of the bacterial cell wall is believed to be one of the key elements that influence cells mechanical properties (Auer and Weibel, 2017; Dorobantu and Gray, 2010). Previous studies investigating changes in the bacterial adhesion in response to the presence of antibiotics have shown an increase in adhesion force after treatment with pharmaceuticals which was consistent with an increase in the cell roughness (Uzoechi and Abu-Lail, 2020; Laskowski et al., 2018). However, in the research presented here; the adhesion force increased with the increasing surface roughness for two of three strains tested. These include *A. xylosoxidans* and *P. hibiscicola*. Substantial changes in the adhesion force were mainly observed for bacteria after prolonged exposure to NFT. The increase in adhesion is often attributed to the leakage of the bacterial cell content. The leakage is believed to be caused not only by the presence of antimicrobial agents but also by AFM tip penetrating inside the cytoplasm (Uzoechi and Abu-Lail, 2020). Another strategy that explains changes in adhesion force assumes modification of bacterial cell surface hydrophobicity in order to increase bacterial adhesion to various surfaces. This phenomenon was measured by (Uzoechi and Abu-Lail, 2020, 2019). This shows that the studies of bacterial cells mechanics taken together with classic biochemical research provide complex information about bacterial cell behavior (Araújo et al., 2019). In our research the results of adhesion energy were consistent with the results of the cell surface hydrophobicity for *S. caeni* after 12-month exposure to FTD.

Understanding remodeling of the cell wall in response to pharmaceuticals and correlation of structural mechanics with changes in biochemical properties are significant in cellular microbiology (Dorobantu and Gray, 2010). An important parameter is bacterial cell elasticity which can be expressed by elastic modulus, stiffness and deformation (Fig. 4c–e). Gaveau et al., (2017) noted a decrease in Young's modulus after treatment with antibiotics of three Gram-positive and Gram-negative strains. The values were not higher than 800 kPa for untreated and 380 kPa for treated cells. These values differ significantly from the results presented in Fig. 4d, because Gaveau et al., (2017) measured these properties in liquid medium and we measured modifications of elastic properties on dry cells. Measurements of the bacterial mechanics strongly depend on the experimental conditions and significant differences are visible in values measured by various techniques. For example, dehydrating and imaging in air may lead to increase in cell stiffness and change the properties of the envelope which may be the reason of high values of elastic modulus obtained in our research. Hence it is extremely important to compare data between the samples prepared similarly and measured by the same method (Araújo et al., 2019; Auer and Weibel, 2017). In another study, the cells with a damaged membrane were characterized by an elastic modulus twice as high as that of bacteria with unimpaired cells membranes (Cerf et al., 2009). Moreover, Uzoechi and Abu-Lail (2020) suggest that increased elasticity may reflect impermeability in cellular membrane. In our research increased Young's modulus was accompanied by enhanced total membrane

permeability of NFT- and FTD-treated *S. caeni* as well as NFT-exposed *P. hibiscicola*. Moreover, the directions of changes of elastic modulus were similar to those of the inner membrane permeability for all long-term exposed strains except for *A. xylosoxidans* exposed to FTD. On the one hand, these directional modifications may indicate damaged cell membranes, however, cell imaging with AFM and TEM microscopy did not indicate cell impairment, especially of *S. caeni* cells.

Young's Modulus variations measured before and after antibiotic treatment can also be attributed to the cell wall stiffness modifications. In the studies of Pogoda et al., (2017), *Bacillus subtilis* cells exhibited increased stiffness, adhesion force and Young's modulus, after treatment with antimicrobial agents called ceragenins. Apart from antimicrobials agents which directly interact with bacterial membranes, there are other cell mechanics modulators. These include: a degree of cross-linking of peptidoglycan; the level of expression of genes connected to cell mechanics (Auer et al., 2016); the presence of proteins in the cell wall that affect mechanical properties of the cell by altering the cross-linking and glycan chain length of peptidoglycan (penicilin-binding proteins, OMpA, Tol-Pal complex) (Auer and Weibel, 2017). The examples mentioned may be also involved in the mechanism of the cell wall stiffness enhancement.

It has been suggested that more homogenous population of bacterial cells indicates better bacterial adaptation to external stimuli (Uzoechi and Abu-Lail, 2020). In our research, some bacterial cells showed considerable heterogenicity in such parameters as adhesion energy, elastic modulus or stiffness. This phenomenon has often repeated in the same type samples.

The main components of the Gram-negative bacterial cell envelope contribute to the mechanical stability of the cell and serve as barrier that facilitates transport of molecules between the surrounding environment and the cell (Hwang et al., 2018). Many studies have reported changes in the bacterial cell membrane permeability after exposure to antibiotics (Ferreira and Kasson, 2019; Krishnamoorthy et al., 2017; Mohamed et al., 2016; Pacholak et al., 2019; Yu and Zhao, 2020). However, the experiments focusing on the changes in membrane permeability after long-term adaptation of bacteria to the presence of pharmaceuticals are limited. Ahmed et al., (2020) measured changes in the bacterial inner membrane permeability using the same method as here. After exposure to nanoparticles, the β-galactosidase activity significantly increased. Bacterial β-galactosidase is an intracellular enzyme which is often measured to observe the cell damage triggered by stressor molecules (Ahmed et al., 2020). We observed increased release of β-galactosidase in all samples treated with antibiotics in comparison to control samples. Most often than not, bacteria under short-term stress revealed stronger impairment of cell membrane in comparison to those subjected to long-term stress. In our previous study, we demonstrated that exposure of environmental bacterial strains to nitrofurantoin increased bacterial cell surface hydrophobicity (Pacholak et al., 2019). Moreover, the enhanced hydrophobicity was correlated with higher degradation efficiency. This may indicate that higher hydrophobic properties facilitate the uptake of xenobiotics by bacterial cells. In the research presented here modifications of cell surface hydrophobicity were different for each strain.

It is well known, that the major adaptive response of the bacterial cells to toxic compound is to keep the fluidity of their membranes at a constant value. Such stabilization of membrane fluidity prevents the loss of the mechanical and chemical properties of the lipid bilayer (Di Pasqua et al., 2006; Nowak et al., 2016). Adaptation of bacterial cell membranes to changing environmental conditions is also manifested by changing the composition of fatty acids. This may be regulated by the degree of unsaturation, the chain length, branching or cyclisation of bacterial membrane fatty acids (Bajerski et al., 2017; Eberlein et al., 2018). The obtained results confirm the previous reports that changes occurring in the profile of fatty acids under the influence of xenobiotics are an individual feature of bacterial strains (Mrozik et al., 2005; Nowak et al., 2016).

The research presented in this work have provided information about possible interactions of selected nitrofuran derivatives with autochthonous, beneficial bacterial strains in the natural environment. The results have proven that prolonged exposure of bacterial strains to nitrofurantoin and furaltadone contribute to significant modifications of bacterial inner membrane and outer membrane. The latter may contribute to natural ecosystems imbalance. Therefore, we are confident that the environmental impact of nitrofurans requires further investigation.

5. Conclusions

As a conclusion, in this study, we have demonstrated that prolonged exposure of bacterial cell to antibiotics is able to induce changes in the bacterial cell envelope, as evaluated with microscopic and biochemical methods. Electron microscopy and atomic force microscopy revealed morphological changes induced by 12-month exposure of bacteria to the presence of nitrofurantoin or furaltadone. Nanomechanical properties of environmental bacterial strains have been altered after 12-month bacterial exposure to nitrofurans. Modifications of the bacterial cell structure were strongly modulated by the nature of the pharmaceutical's molecule and the bacterial cell type. In most of the cases, nitrofurantoin provoked stronger remodeling of the cells structure than furaltadone, which was particularly visible in the measurements of surface roughness and nanomechanical properties. Among all strains tested, *Pseudomonas hibiscicola* FZD2 showed most significant alterations in cell texture and surface properties after prolonged exposure to nitrofurans. Despite visible multilevel adaptation occurring in the cells, the prolonged presence of nitrofurans in the environment leads to significant alterations in the cell structure. The knowledge obtained within the research presented help enhance our understanding of nitrofurans that attract little scientific attention but pose a threat to the environment and human health.

CRediT authorship contribution statement

Amanda Pacholak: Conceptualization, Methodology, Validation, Formal analysis, Investigation, Writing – Original Draft, Writing – review & editing, Visualization. **Natalia Burlaga**: Formal analysis, Investigation, Writing – Original Draft, Visualization. **Urszula Guzik**: Formal analysis, Investigation, Writing – Original Draft. **Ewa Kaczorek**: Conceptualization, Resources, Writing – review & editing, Supervision, Project administration, Funding acquisition.

Funding

This work was supported by National Science Centre, Poland, grant number 2017/27/B/NZ9/01603.

Declaration of Competing Interest

The authors declare that they have no known competing financial interests or personal relationships that could have appeared to influence the work reported in this paper.

Appendix A. Supplementary material

Supplementary data associated with this article can be found in the online version at doi:10.1016/j.jhazmat.2020.124352.

References

Ahmed, B., Ameen, F., Rizvi, A., Ali, K., Sonbol, H., Zaidi, A., Khan, M.S., Musarrat, J., 2020. Destruction of cell topography, morphology, membrane, inhibition of respiration, biofilm formation, and bioactive molecule production by nanoparticles of Ag, ZnO, CuO, TiO_2, and Al_2O_3 toward beneficial soil bacteria. ACS Omega 5, 7861–7876. https://doi.org/10.1021/acsomega.9b04084.

Angeles, L.F., Islam, S., Aldstadt, J., Saqeeb, K.N., Alam, M., Khan, M.A., Johura, F.-T., Ahmed, S.I., Aga, D.S., 2020a. Retrospective suspect screening reveals previously ignored antibiotics, antifungal compounds, and metabolites in Bangladesh surface waters. Sci. Total Environ. 712, 136285 https://doi.org/10.1016/j.scitotenv.2019.136285.

Angeles, L.F., Mullen, R.A., Huang, I.J., Wilson, C., Khunjar, W., Sirotkin, H.I., McElroy, A.E., Aga, D.S., 2020b. Assessing pharmaceutical removal and reduction in toxicity provided by advanced wastewater treatment systems. Environ. Sci. Water Res. Technol. 6, 62–77. https://doi.org/10.1039/C9EW00559E.

Araújo, G.R. de S., Viana, N.B., Gómez, F., Pontes, B., Frases, S., 2019. The mechanical properties of microbial surfaces and biofilms. Cell Surf. 5, 100028 https://doi.org/10.1016/j.tcsw.2019.100028.

Auer, G.K., Lee, T.K., Rajendram, M., Cesar, S., Miguel, A., Huang, K.C., Weibel, D.B., 2016. Mechanical genomics identifies diverse modulators of bacterial cell stiffness. Cell Syst. 2, 402–411. https://doi.org/10.1016/j.cels.2016.05.006.

Auer, G.K., Weibel, D.B., 2017. Bacterial cell mechanics. Biochemistry 56, 3710–3724. https://doi.org/10.1021/acs.biochem.7b00346.

Bajerski, F., Wagner, D., Mangelsdorf, K., 2017. Cell membrane fatty acid composition of Chryseobacterium frigidisoli PB4T, isolated from Antarctic Glacier forefield soils, in response to changing temperature and pH conditions. Front. Microbiol. 8. https://doi.org/10.3389/fmicb.2017.00677.

Ben, Y., Hu, M., Zhang, X., Wu, S., Wong, M.H., Wang, M., Andrews, C.B., Zheng, C., 2020. Efficient detection and assessment of human exposure to trace antibiotic residues in drinking water. Water Res. 175, 115699 https://doi.org/10.1016/j.watres.2020.115699.

Berendonk, T.U., Manaia, C.M., Merlin, C., Fatta-Kassinos, D., Cytryn, E., Walsh, F., Bürgmann, H., Sørum, H., Norström, M., Pons, M.-N., Kreuzinger, N., Huovinen, P., Stefani, S., Schwartz, T., Kisand, V., Baquero, F., Martinez, J.L., 2015. Tackling antibiotic resistance: the environmental framework. Nat. Rev. Microbiol. 13, 310–317. https://doi.org/10.1038/nrmicro3439.

Cai, L., Wu, D., Xia, J., Shi, H., Kim, H., 2019. Influence of physicochemical surface properties on the adhesion of bacteria onto four types of plastics. Sci. Total Environ. 671, 1101–1107. https://doi.org/10.1016/j.scitotenv.2019.03.434.

Cai, P., Liu, X., Ji, D., Yang, S., Walker, S.L., Wu, Y., Gao, C., Huang, Q., 2018. Impact of soil clay minerals on growth, biofilm formation, and virulence gene expression of Escherichia coli O157:H7. Environ. Pollut. 243, 953–960. https://doi.org/10.1016/j.envpol.2018.09.032.

Cerf, A., Cau, J.-C., Vieu, C., Dague, E., 2009. Nanomechanical properties of dead or alive single-patterned bacteria. Langmuir 25, 5731–5736. https://doi.org/10.1021/la9004642.

Charuaud, L., Jarde, E., Jaffrezic, A., Thomas, M.-F., Le Bot, B., 2019. Veterinary pharmaceutical residues from natural water to tap water: sales, occurrence and fate. J. Hazard. Mater. 361, 169–186. https://doi.org/10.1016/j.jhazmat.2018.08.075.

Cheng, Y., Feng, G., Moraru, C.I., 2019. Micro- and nanotopography sensitive bacterial attachment mechanisms: a review. Front. Microbiol. 10, 191. https://doi.org/10.3389/fmicb.2019.00191.

De Oliveira, R.R.L., Albuquerque, D.A.C., Cruz, T.G.S., Yamaji, F.M., Leite, F.L., 2012. Measurement of the nanoscale roughness by atomic force microscopy: basic principles and applications. In: Bellitto, V. (Ed.), Atomic Force Microscopy – Imaging, Measuring and Manipulating Surfaces at the Atomic Scale. InTech. ⟨https://doi.org/10.5772/37583⟩.

Di Pasqua, R., Hoskins, N., Betts, G., Mauriello, G., 2006. Changes in membrane fatty acids composition of microbial cells induced by addiction of thymol, carvacrol, limonene, cinnamaldehyde, and eugenol in the growing media. J. Agric. Food Chem. 54, 2745–2749. https://doi.org/10.1021/jf052722l.

Dorobantu, L.S., Gray, M.R., 2010. Application of atomic force microscopy in bacterial research. Scanning 32, 74–96. https://doi.org/10.1002/sca.20177.

Eberlein, C., Baumgarten, T., Starke, S., Heipieper, H.J., 2018. Immediate response mechanisms of gram-negative solvent-tolerant bacteria to cope with environmental stress: cis-trans isomerization of unsaturated fatty acids and outer membrane vesicle secretion. Appl. Microbiol. Biotechnol. 102, 2583–2593. https://doi.org/10.1007/s00253-018-8832-9.

El-Kirat-Chatel, S., Beaussart, A., Mathelié-Guinlet, M., Dufrêne, Y.F., 2020. The importance of force in microbial cell adhesion. Curr. Opin. Colloid Interface Sci. 47, 111–117. https://doi.org/10.1016/j.cocis.2019.12.010.

Ferreira, R.J., Kasson, P.M., 2019. Antibiotic uptake across gram-negative outer membranes: better predictions towards better antibiotics. ACS Infect. Dis. 5, 2096–2104. https://doi.org/10.1021/acsinfecdis.9b00201.

Gaveau, A., Coetsier, C., Roques, C., Bacchin, P., Dague, E., Causserand, C., 2017. Bacteria transfer by deformation through microfiltration membrane. J. Membr. Sci. 523, 446–455. https://doi.org/10.1016/j.memsci.2016.10.023.

Hahladakis, J.N., Velis, C.A., Weber, R., Iacovidou, E., Purnell, P., 2018. An overview of chemical additives present in plastics: migration, release, fate and environmental impact during their use, disposal and recycling. J. Hazard. Mater. 344, 179–199. https://doi.org/10.1016/j.jhazmat.2017.10.014.

Hwang, H., Paracini, N., Parks, J.M., Lakey, J.H., Gumbart, J.C., 2018. Distribution of mechanical stress in the Escherichia coli cell envelope. Biochim. Biophys. Acta (BBA) – Biomembr. 1860, 2566–2575. https://doi.org/10.1016/j.bbamem.2018.09.020.

Kaczorek, E., Sałek, K., Guzik, U., Dudzińska-Bajorek, B., 2013. Cell surface properties and fatty acids composition of Stenotrophomonas maltophilia under the influence of hydrophobic compounds and surfactants. New Biotechnol. 30, 173–182. https://doi.org/10.1016/j.nbt.2012.09.003.

Kim, C., Ryu, H.-D., Chung, E.G., Kim, Y., 2018. Determination of 18 veterinary antibiotics in environmental water using high-performance liquid chromatography-q-orbitrap combined with on-line solid-phase extraction. J. Chromatogr. B 1084, 158–165. https://doi.org/10.1016/j.jchromb.2018.03.038.

Klein, E.Y., Van Boeckel, T.P., Martinez, E.M., Pant, S., Gandra, S., Levin, S.A., Goossens, H., Laxminarayan, R., 2018. Global increase and geographic convergence in antibiotic consumption between 2000 and 2015. Proc. Natl. Acad. Sci. USA 115, E3463–E3470. https://doi.org/10.1073/pnas.1717295115.

Kokulnathan, T., Chen, S.-M., 2020. Robust and selective electrochemical detection of antibiotic residues: the case of integrated lutetium vanadate/graphene sheets architectures. J. Hazard. Mater. 384, 121304 https://doi.org/10.1016/j.jhazmat.2019.121304.

Krishnamoorthy, G., Leus, I.V., Weeks, J.W., Wolloscheck, D., Rybenkov, V.V., Zgurskaya, H.I., 2017. Synergy between active efflux and outer membrane diffusion defines rules of antibiotic permeation into gram-negative bacteria. mBio 8. mBio 01172-17, e01172-17. https://doi.org/10.1128/mBio.01172-17.

Kumar, M., Jaiswal, S., Sodhi, K.K., Shree, P., Singh, D.K., Agrawal, P.K., Shukla, P., 2019. Antibiotics bioremediation: perspectives on its ecotoxicity and resistance. Environ. Int. 124, 448–461. https://doi.org/10.1016/j.envint.2018.12.065.

Laskowski, D., Strzelecki, J., Pawlak, K., Dahm, H., Balter, A., 2018. Effect of ampicillin on adhesive properties of bacteria examined by atomic force microscopy. Micron 112, 84–90. https://doi.org/10.1016/j.micron.2018.05.005.

Li, W., Dai, Y., Xue, B., Li, Y., Peng, X., Zhang, J., Yan, Y., 2009. Biodegradation and detoxification of endosulfan in aqueous medium and soil by Achromobacter xylosoxidans strain CS5. J. Hazard. Mater. 167, 209–216. https://doi.org/10.1016/j.jhazmat.2008.12.111.

Limoli, D.H., Jones, C.J., Wozniak, D.J., 2020. Bacterial Extracellular Polysaccharides in Biofilm Formation and Function 19.

Ma, W., Peng, D., Walker, S.L., Cao, B., Gao, C.-H., Huang, Q., Cai, P., 2017. Bacillus subtilis biofilm development in the presence of soil clay minerals and iron oxides. npj Biofilms Microbiomes 3, 4. https://doi.org/10.1038/s41522-017-0013-6.

Manzoor, M., Gul, I., Ahmed, I., Zeeshan, M., Hashmi, I., Amin, B.A.Z., Kallerhoff, J., Arshad, M., 2019. Metal tolerant bacteria enhanced phytoextraction of lead by two accumulator ornamental species. Chemosphere 227, 561–569. https://doi.org/10.1016/j.chemosphere.2019.04.093.

Mohamed, Y.F., Abou-Shleib, H.M., Khalil, A.M., El-Guink, N.M., El-Nakeeb, M.A., 2016. Membrane permeabilization of colistin toward pan-drug resistant gram-negative isolates. Braz. J. Microbiol. 47, 381–388. https://doi.org/10.1016/j.bjm.2016.01.007.

Mrozik, A., Łabużek, S., Piotrowska-Seget, Z., 2005. Changes in fatty acid composition in Pseudomonas putida and Pseudomonas stutzeri during naphthalene degradation. Microbiol. Res. 160, 149–157. https://doi.org/10.1016/j.micres.2004.11.001.

Muller, A.E., Verhaegh, E.M., Harbarth, S., Mouton, J.W., Huttner, A., 2017. Nitrofurantoin's efficacy and safety as prophylaxis for urinary tract infections: a systematic review of the literature and meta-analysis of controlled trials. Clin. Microbiol. Infect. 23, 355–362. https://doi.org/10.1016/j.cmi.2016.08.003.

Müller, D.J., Dufrêne, Y.F., 2011. Atomic force microscopy: a nanoscopic window on the cell surface. Trends Cell Biol. 21, 461–469. https://doi.org/10.1016/j.tcb.2011.04.008.

Nam, I.-H., Kim, Y., Cho, D., Kim, J.-G., Song, H., Chon, C.-M., 2015. Effects of heavy metals on biodegradation of fluorene by a *Sphingobacterium* sp. strain (KM-02) isolated from polycyclic aromatic hydrocarbon-contaminated mine soil. Environ. Eng. Sci. 32, 891–898. https://doi.org/10.1089/ees.2015.0037.

Novelli, A., Rosi, E., 2017. Pharmacological properties of oral antibiotics for the treatment of uncomplicated urinary tract infections. J. Chemother. 29, 10–18. https://doi.org/10.1080/1120009X.2017.1380357.

Nowak, A., Greń, I., Mrozik, A., 2016. Changes in fatty acid composition of Stenotrophomonas maltophilia KB2 during co-metabolic degradation of monochlorophenols. World J. Microbiol. Biotechnol. 32, 198. https://doi.org/10.1007/s11274-016-2160-y.

Núñez, M.E., Martin, M.O., Chan, P.H., Duong, L.K., Sindhurakar, A.R., Spain, E.M., 2005. Atomic force microscopy of bacterial communities. In: Methods in Enzymology. Elsevier, pp. 256–268. ⟨https://doi.org/10.1016/S0076-6879(05)97015-8⟩.

Ouyang, K., Mortimer, M., Holden, P.A., Cai, P., Wu, Y., Gao, C., Huang, Q., 2020. Towards a better understanding of Pseudomonas putida biofilm formation in the presence of ZnO nanoparticles (NPs): role of NP concentration. Environ. Int. 137, 105485 https://doi.org/10.1016/j.envint.2020.105485.

Pacholak, A., Smułek, W., Zgoła-Grześkowiak, A., Kaczorek, E., 2019. Nitrofurantoin—microbial degradation and interactions with environmental bacterial strains. IJERPH 16, 1526. https://doi.org/10.3390/ijerph16091526.

Pogoda, K., Piktel, E., Deptuła, P., Savage, P.B., Lekka, M., Bucki, R., 2017. Stiffening of bacteria cells as a first manifestation of bactericidal attack. Micron 101, 95–102. https://doi.org/10.1016/j.micron.2017.06.011.

Robinson, K., Ma, X., Liu, Y., Qiao, S., Hou, Y., Zhang, G., 2018. Dietary modulation of endogenous host defense peptide synthesis as an alternative approach to in-feed antibiotics. Anim. Nutr. 4, 160–169. https://doi.org/10.1016/j.aninu.2018.01.003.

Silhavy, T.J., Kahne, D., Walker, S., 2010. The bacterial cell envelope. Cold Spring Harb. Perspect. Biol. 2, 1–16. https://doi.org/10.1101/cshperspect.a000414.

Singh, N.S., Singh, D.K., 2011. Biodegradation of endosulfan and endosulfan sulfate by Achromobacter xylosoxidans strain C8B in broth medium. Biodegradation 22, 845–857. https://doi.org/10.1007/s10532-010-9442-0.

Soon, R.L., Nation, R.L., Hartley, P.G., Larson, I., Li, J., 2009. Atomic force microscopy investigation of the morphology and topography of colistin-heteroresistant acinetobacter baumannii strains as a function of growth phase and in response to colistin treatment. AAC 53, 4979–4986. https://doi.org/10.1128/AAC.00497-09.

Sun, L.-N., Zhang, J., Chen, Q., He, J., Li, S.-P., 2013. Sphingobacterium caeni sp. nov., isolated from activated sludge. Int. J. Syst. Evolut. Microbiol. 63, 2260–2264. https://doi.org/10.1099/ijs.0.046987-0.

Tran, N.H., Reinhard, M., Gin, K.Y.-H., 2018. Occurrence and fate of emerging contaminants in municipal wastewater treatment plants from different geographical regions-a review. Water Res. 133, 182–207. https://doi.org/10.1016/j.watres.2017.12.029.

Uzoechi, S.C., Abu-Lail, N.I., 2020. Variations in the morphology, mechanics and adhesion of persister and resister E. coli cells in response to ampicillin: AFM study. Antibiotics 9, 235. https://doi.org/10.3390/antibiotics9050235.

Uzoechi, S.C., Abu-Lail, N.I., 2019. The effects of β-lactam antibiotics on surface modifications of multidrug-resistant Escherichia coli: a multiscale approach. Microsc. Microanal. 25, 135–150. https://doi.org/10.1017/S1431927618015696.

Wijma, R.A., Fransen, F., Muller, A.E., Mouton, J.W., 2019. Optimizing dosing of nitrofurantoin from a PK/PD point of view: what do we need to know? Drug Resist. Updates 43, 1–9. https://doi.org/10.1016/j.drup.2019.03.001.

Wu, S., Zhang, B., Liu, Y., Suo, X., Li, H., 2018. Influence of surface topography on bacterial adhesion: a review (review). Biointerphases 13, 060801. https://doi.org/10.1116/1.5054057.

Yu, M., Zhao, Y., 2020. Cell permeability, β-lactamase activity, and transport contribute to high level of resistance to ampicillin in Lysobacter enzymogenes. Appl. Microbiol. Biotechnol. 104, 1149–1161. https://doi.org/10.1007/s00253-019-10266-7.

Zhang, X., Zhang, D., He, K., 2019. Combining an effective immuno-affinity column with ELISA for reliable and visual detection of furaltadone metabolites in aquatic products. Anal. Methods 11, 1270–1275. https://doi.org/10.1039/C8AY02597E.

Zuma, N.H., Aucamp, J., N'Da, D.D., 2019. An update on derivatisation and repurposing of clinical nitrofuran drugs. Eur. J. Pharm. Sci. 140, 105092 https://doi.org/10.1016/j.ejps.2019.105092.

Publication P3

Environmental Research 216 (2023) 114531

Contents lists available at ScienceDirect

Environmental Research

journal homepage: www.elsevier.com/locate/envres

Dynamics of microbial communities during biotransformation of nitrofurantoin

Amanda Pacholak [a,*], Agnieszka Zgoła-Grześkowiak [b], Ewa Kaczorek [a]

[a] Institute of Chemical Technology and Engineering, Poznan University of Technology, Poland
[b] Institute of Chemistry and Technical Electrochemistry, Poznan University of Technology, Poland

ARTICLE INFO

Keywords:
Antibiotic
Bacteria
Degradation
Metagenomics
Nitrofuran
Transformation products

ABSTRACT

The purpose of this research was to investigate the biodegradation of nitrofurantoin (NFT), a typical nitrofuran antibiotic of potential carcinogenic properties, by two microbial communities derived from distinct environmental niches – mountain stream (NW) and seaport water (SS). The collected environmental samples represent the reserve of the protected area with no human intervention and the contaminated area that concentrates intense human activities. The structure, composition, and diversity of the communities were analyzed at three timepoints during NFT biodegradation. *Comamonadaceae* (43.2%) and *Pseudomonadaceae* (19.6%) were the most abundant families in the initial NW sample. The top families in the initial SS sample included *Aeromonadaceae* (31.4%) and *Vibrionaceae* (25.3%). The proportion of the most abundant families in both consortia was remarkably reduced in all samples treated with NFT. The biodiversity significantly increased in both consortia treated with NFT suggesting that NFT significantly alters community structure in the aquatic systems. In this study, NFT removal efficiency and transformation products were also studied. The biodegradation rate decreased with the increasing initial NFT concentration. Biodegradation followed similar pathways for both consortia and led to the formation of transformation products: 1-aminohydantoin, semicarbazide (SEM), and hydrazine (HYD). SEM and HYD were detected for the first time as NFT biotransformation products. This study demonstrates that the structure of the microbial community may be directly correlated with the presence of NFT. Enchanced biodiversity of the microbial community does not have to be correlated with increase in functional capacity, such as the ability to biodegradation because higher biodiversity corresponded to lower biodegradation. Our findings provide new insights into the effect of NFT contamination on aquatic microbiomes. The study also increases our understanding of the environmental impact of nitrofuran residues and their biodegradation.

1. Introduction

Pollution of the natural environment with chemical compounds poses one of the largest dangers to humanity. Many anthropogenic chemicals are toxic after release into the biosphere and geosphere which poses direct risks to all living organisms (Gruber, 2018; Naidu et al., 2021). Pesticides, antibiotics, growth-promoters and other substances have been detected in the human food chain at levels that are higher than acceptable (Dinh et al., 2020; Griboff et al., 2020; Mccracken et al., 2005; Tang et al., 2021; Wu et al., 2021). This contamination is a challenging problem that needs to be utterly addressed (Al-Waili et al., 2012).

Researchers have studied the occurrence, fate, and risk assessment of various antibiotics in natural environments (S. Li et al., 2019; Wang et al., 2020; Xu et al., 2021). Important classes of antibiotic compounds include β-lactams, tetracyclines, aminoglycosides, macrolides, glycopeptides, sulfonamides, quinolones, and nitrofurans (Kumar et al., 2019; Kümmerer, 2009). Among antibiotics listed, nitrofurans (5-NFs) are given less attention even though they might pose carcinogenic properties. 5-NFs are bactericidal, broad-spectrum antimicrobial agents. In the

Abbreviations: AHD, 1-aminohydantoin; AHD-NBA, 2-nitrobenzaldehyde derivative of 1-aminohydantoin; ESI, electrospray ion source; HYD, hydrazine; NBA-HYD-NBA, 2-nitrobenzaldehyde derivative of hydrazine; NBA, 2-nitrobenzaldehyde; NFT, nitrofurantoin; NW, mountain stream water sample; OECD, The Organization for Economic Co-operation and Development; PCoA, principal coordinates analysis; RT, room temperature; SEM, semicarbazide; SEM-NBA, 2-nitrobenzaldehyde derivative of semicarbazide; SS, seaport water sample; TPs, transformation products; 5-NFs, (5-)nitrofurans.

* Corresponding author.
E-mail address: amanda.pacholak@put.poznan.pl (A. Pacholak).

https://doi.org/10.1016/j.envres.2022.114531
Received 20 June 2022; Received in revised form 1 October 2022; Accepted 5 October 2022
Available online 13 October 2022

past they were used in the husbandry of livestock as growth promoters, however, this practice is now prohibited in many countries. The representatives of the 5-NFs family include nitrofurantoin (NFT), nitrofurazone, furazolidone and furaltadone (Kokulnathan and Chen, 2020). The alleged excessive misuse of 5-NFs as well as illicit application in agriculture promote their continuous discharge into the natural environment.

The environmental fate of 5-NFs (as well as many other antibiotics) is not fully understood. A phenomenon that involves most pharmaceutical pollutants and occurs in nature over time is bioremediation. This is the process of using biological organisms such as bacteria, yeast, and fungi, to decompose hazardous substances into less toxic or nontoxic substances (Chandran et al., 2020; Techtmann and Hazen, 2016). Natural biodegradation, based on the indigenous consortia is usually slow but at the same time much more sustainable than other remediation technologies (Chandran et al., 2020; Jørgensen, 2011). Another important factor that needs to be addressed is microbial adaptation to chemical compounds. Bacterial exposure to environmental pollutants plays a key role in this complex process. It is generally believed that microbial adaptation may stimulate biodegradation of organic pollutants, however, its impact on biodegradation requires further investigation (Poursat et al., 2019).

Microorganisms that degrade contaminants interact with other community members and the surrounding environment. Physicochemical parameters of the ecosystem (e.g., availability of growth- and biomass-limiting nutrients, temperature, pH, light, and presence of other pollutants) are among crucial factors limiting bioremediation efficiency. Other factors that determine the rate and the extent of remediation technologies are related to the biological properties of microbial communities (e.g. their structure, tolerance to toxicity, activity, surface properties) and characteristics of the pollutants (e.g. concentration, molecular structure, physicochemical properties) (Head et al., 2006; Ossai et al., 2020; Zainab et al., 2020).

Mixed microbial communities have the most powerful potential to metabolize the complex mixtures of the organic compounds in the polluted area. (Jördening and Winter 2005). Importantly, the primary biodegradation of antibiotics by microbial consortia is often incomplete and leads to formation of transformation products (TPs). These can remain unchanged in the ecosystems for a long time and show higher toxicity than the parent compounds (Zainab et al., 2020).

The composition of microbial communities changes dynamically during biodegradation (Wang et al., 2018; Xiong et al., 2019). Understanding and monitoring microbial community dynamics allows for optimal microbiome selection and may help detect common patterns associated with bioremediation. The importance of learning about these modifications lies in the possibility of targeting groups of microorganisms that control environmental concentrations of pollutants to increase their activity to accelerate bioremediation efficiency (Head et al., 2006). Molecular biology approaches such as fingerprinting of communities, metagenomics, proteomics, transcriptomics, metabolomics, or detection of specific enzymes associated with decomposition of pollutants enable deep insight into the microbial world inhabiting a particular ecosystem. This progressively allows for improving the reliability, monitoring, and effectiveness of natural remediation processes (Kouzuma and Watanabe, 2011).

Metagenomics generally relies on the analysis of the total genomic content of a microbial community (Chandran et al., 2020). Some studies have demonstrated the functional and structural responses of bacterial communities during treatment with anthropogenic contaminants (Dong et al., 2022; Xiong et al., 2019). However, relatively little is known about the interactions of environmental microorganisms with antibiotic pollutants, especially 5-NFs.

We hypothesized that bacterial exposure to environmental pollutants plays a significant role in biodegradation of NFT. The goal of this study was (a) to understand the biodegradation of NFT by bacterial communities derived from two distinct environmental niches, and (b) to investigate the effect of NFT on the composition and diversity of the bacterial consortia. This study demonstrates, for the first time, the effect of NFT contamination on aquatic microbiomes. The study also increases our understanding of the environmental impact of 5-NFs and their biodegradation.

2. Materials and methods

2.1. Chemical reagents

Standards (i.e. NFT, 1-aminohydantoin, semicarbazide), microbiological media components (i.e. minimal microbial growth medium), organic solvents (i.e. HPLC grade methanol), and all other reagents were purchased from Merck (Darmstadt, Germany) unless otherwise stated. Brain Heart Infusion broth (BHI) was from bioMerieux (Warsaw, Poland). The chemicals were of the highest analytical grade (at least 99%) and used without further purification. The solutions were prepared using ultra-purified Milli-Q water (Arium® Pro, Sartorius, Kostrzyn Wlkp., Poland). The glassware and autoclavable solutions were steam sterilized. Other solutions were filter sterilized using Captiva 0.22 μm EconoFilters (Agilent, CA, USA). A biological safety cabinet (Labculture® Class II, Esco, Singapore) was used during activities associated with bacterial samples.

2.2. Sampling sites description, preparation of cultures inoculum, and growing conditions

The water samples were collected from two distinct environmental niches – the mountain stream and seaport water in May 2019. The mountain stream water sample (NW) was collected from the area nearby Siklawica Waterfall in Tatra National Park in Poland (geographical location: 49°15′34″N 19°55′44″E). It represents the reserve of the protected area with no human intervention. The seaport water sample (SS) was collected from the area of the Port of Gdańsk, one of the largest seaports on the Baltic Sea located on the southern coast of Gdańsk Bay in Poland (geographical location 54°23′36″N 18°40′12″E). The seaport represents the area that concentrates diverse human activities and receives numerous contaminants including petroleum hydrocarbons, pesticides, microplastic, and metals.

The water samples were collected by aseptic sampling technique using sterile bottles, containers, and sterile disposable gloves. Water was sampled away from the bank, from approximately 30 cm below the water surface. Exposure of water samples, sampling equipment, and the interior of sampling containers to the environment was minimized. The collected samples were stored in iceboxes with freezer packs and delivered to the laboratory on the same day. The procedures of water samples collection were adapted from guidelines provided by The New South Wales Department of Primary Industries (NSW Department of Primary Industries, 2019).

Samples were aerated at room temperature (RT) on a horizontal shaker (Chemland, Stargard, Poland) for 24 h at 120 rpm. The enrichment cultures were established by adding 1 mL of the initial samples to 9 mL of half-strength BHI broth. Microbial suspensions were incubated overnight at RT. Next, the cells were washed twice with sterile Dulbecco's phosphate-buffered saline and resuspended in the buffer to adjust the optical density at 600 nm to 1.0 ± 0.1 using Multiskan 152 Sky Microplate Spectrophotometer (Thermo Fisher Scientific, Waltham, MA, USA). Such prepared microbial suspensions were used for inoculation to start the microbial cultures.

2.3. Liquid cultures preparation

The liquid cultures were prepared in sterile 250 mL Duran® laboratory bottles. The cultures components included: 45 mL of NFT solution prepared directly in a minimal medium, 0.1 mL of microelements solution, 0.1 mL of 20% sodium succinate (easily absorbed source of

carbon and energy for the microbes), and 5 mL of inoculum. Four concentrations of NFT were chosen for testing: 5, 10, 15 and 20 mg · L^{-1}. The composition of the microelements solution and the medium solution containing phosphates buffered at pH 7.4 was described previously (Pacholak et al., 2020a). The sterile abiotic control samples were obtained by autoclaving the biomass at 121 °C for 15 min and addition of 2% sodium azide to inhibit the proliferation of bacteria. The cultures were incubated at RT on a horizontal shaker in the dark. The removal efficiency was measured for 28 days according to the guidelines of The Organization for Economic Co-operation and Development (OECD).

2.4. Samples collection, TPs derivatization, and LC-MS/MS analysis

To investigate the biodegradation rate, detect degradation products and analyze shifts in the microbial communities, 1.5mL samples were collected aseptically from the cultures every few days. Day 0 samples were collected after 1h incubation to ensure the initial equilibration and homogeneity of the sample. The samples were centrifuged at 13,000 g for 2 min. Cell debris was used for bacterial DNA extraction, supernatants were used for chromatographic analyses. To calculate the degradation rate, the supernatants were diluted with HPLC grade methanol and filtered using 0.2 μm polytetrafluoroethylene membrane syringe filters (Agilent, Santa Clara, CA, USA). Disposable Injekt® Solo syringes were provided by B. Braun (Melsungen AG, Hessen, Germany). The filtered samples were analyzed qualitatively and quantitatively for the residual NFT using liquid chromatography coupled with mass spectrometry (LC-MS/MS). To detect degradation products, the supernatants were derivatized. The detailed protocols of NFT metabolites derivatization and LC-MS/MS analysis are presented in the Supplementary Information. To determine total organic matter removal, measurements of ultraviolet absorption at 254 nm wavelength were also performed as the literature reports a high correlation between UV absorption at 254 nm and Total Organic Carbon (TOC) content (Albrektienė et al., 2012; Frankowski et al., 2021).

2.5. Bacterial DNA extraction, PCR amplification and sequencing

DNA was isolated from each sample in duplicate using GenElute™ Bacterial Genomic DNA Kit (NA2100) provided by Sigma-Aldrich (St. Louis, MO, USA). The purity and concentration of the DNA samples were examined by measuring absorbance at 260 nm, 280 nm and 320 nm on Multiskan 152 Sky Microplate Spectrophotometer (Thermo Fisher Scientific, Waltham, MA, USA). DNA quality was evaluated by electrophoresis on a 0.8% agarose gel. The DNA samples were stored at −80 °C before use. To evaluate the microbial community structure in the cultures, iTag sequencing of 16S rRNA genes was performed. The detailed protocol of sequencing is presented in the Supplementary Information.

Data availability: Sequences are available in the NCBI Sequence Read Archive (BioProject no. PRJNA845907).

2.6. Statistical analysis

GraphPad Prism (GraphPad Software, LLC, San Diego, CA, USA) was used to analyze the differences in the residual NFT and TPs. The data are expressed as the mean ± standard deviation. All data were normally distributed and had equal variances according to Shapiro-Wilk and Levene's tests. A statistical significance of differences between the means of the samples was determined by a two-way analysis of variance followed by Tukey's range test (the significance level of 5%). Shifts within and between the microbial communities' structures were determined by alpha and beta diversity calculated based on the OTUs tables. The bioinformatics analysis was performed with R software, using the following packages: phyloseq, vegan and dendextend. The Observed OTUs, Chao1, ACE, Shannon and Simpson indices were used to analyze the alpha diversity of each bacterial community at each timepoint analyzed. The similarity patterns between the bacterial communities were analyzed by beta diversity based on Bray-Curtis ordination. Graphs were created using GraphPad Prism (GraphPad Software, LLC, San Diego, CA, USA) and heatmapper online software (Babicki et al., 2016).

3. Results

3.1. NFT primary biodegradation

Fig. 1a shows the biodegradation rate by the microbial consortia present in the mountain stream (NW) sample. The highest removal rate was observed during the first day of the process for all concentrations tested. The culture with the lowest initial content of NFT (5 mg · L^{-1}) was characterized by the highest removal of the antibiotic. The average removal after 12 h of incubation was 92.3 ± 0.1%. The consortium collected from water in the National Park area was able to completely degrade 5 mg · L^{-1} NFT in less than two days. A similar situation was observed for the NW culture with an initial concentration of 10 mg · L^{-1} NFT. On average, 78.2 ± 1.3% of NFT was removed from the culture in 12 h, 90.4 ± 0.7% in 24 h, and a complete removal was observed on the 4th cultivation day. In the 15 mg · L^{-1} culture, 79.0 ± 1.4% of NFT was degraded after 24 h. The elimination of NFT was progressively increasing, reaching 94.0 ± 0.5% on the 28th day. The lowest degradation was observed in the cultures that contained the highest initial NFT concentration (20 mg · L^{-1}). In the 24-h cultures the residual NFT content was 37.1% (62.9 ± 0.5% biodegradation). Total removal of NFT has not been achieved, in 28-day cultures 88.3 ± 1.0% biodegradation was measured.

Fig. 1b shows the results of NFT primary biodegradation by bacteria collected from the seaport water (SS) sample. They showed significantly lower degradation capabilities than the bacteria from the mountain stream, however, the effect of NFT concentration on degradation ability was similar. The cultures with the lowest initial NFT content showed the highest removal and the cultures with the highest initial NFT concentration showed the lowest biodegradation. A complete removal has

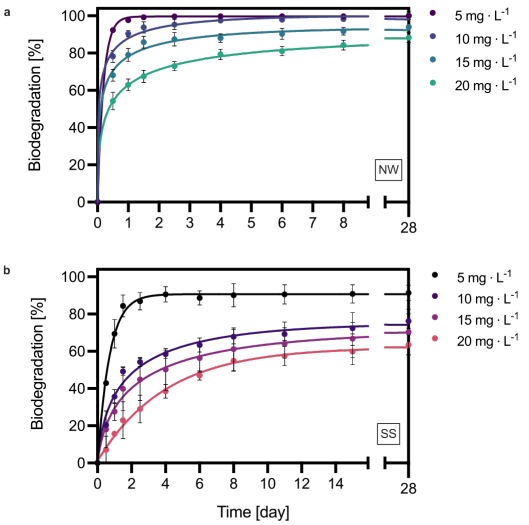

Fig. 1. The biodegradation rate by two microbial consortia at four initial concentrations of NFT: 5, 10, 15 and 20 mg · L^{-1}. (a) Mountain stream water sample (NW) represents the bacterial community collected from the protected area with no human intervention. (b) Seaport water sample (SS) represents the bacterial community collected from the seaport area that receives numerous contaminants.

never been measured for SS bacterial consortium. In a 5 mg · L^{-1} culture, the highest decrease (69.4 ± 3.0%) in NFT concentration was measured on the first day and was followed by the steady gradual elimination of NFT. After reaching a peak of 90.6 ± 1.7% removal in a 4-day culture, NFT concentration remained relatively stable by the end of the experiment (0.4 mg · L^{-1}). In the 10 mg · L^{-1} cultures, the average NFT removal after 12 h of incubation was 20.5 ± 0.5%. 24-hour incubation resulted in 35.6 ± 1.5% NFT removal. This was followed by a gradual decrease in NFT concentration, reaching the average value of 2.4 mg · L^{-1} at the end of the cultivation period (76.3 ± 1.6% biodegradation). The bacterial cultures incubated with 15 mg · L^{-1} NFT showed different biotransformation rates than the ones with lower initial content of NFT. Here, NFT elimination was steady and gradual throughout the entire time. The average biodegradation after 24 h was 27.6 ± 1.9%. This value doubled on the sixth day. The final removal rate was 70.3 ± 4.9% with a residual NFT concentration of 4.5 mg · L^{-1}. A similar characteristic of the antibiotic elimination rate was observed for the sample with a 20 mg · L^{-1} initial concentration. The average biodegradation in the cultures after 12 h was only 7.0 ± 3.0%. 24-hour culture resulted in 15.7 ± 0.2% NFT removal. The residual NFT concentration was 7.3 mg · L^{-1} after 28 days of incubation. In addition, concentrations measured in the abiotic control samples showed that after 28 days no more than 5% of the NFT was abiotically removed from the culture medium.

Separate analyses were performed to estimate dynamic changes of TOC content in the bacterial cultures. The results show a considerable difference between NW and SS communities (Supplementary Information). The calculated TOC decreased with time for most of the samples and the greatest decline was noted between 4th and 11th day. The higher initial concentration of NFT in the microbial cultures, the higher TOC was calculated.

3.2. NFT transformation products

According to the OECD, primary biodegradation is defined as the modification of the structure of the chemical compound that results in the loss of the specific properties of that compound. Primary biodegradation is also referred to as biotransformation. In this study, the TPs of NFT primary biodegradation by two microbial consortia were identified. For this purpose, the LC-MS/MS system was used. To increase the concentrations of TPs and allow for detection of secondary transformation products, and a more accurate proposition of degradation pathway, TPs were analyzed at the highest initial concentration of NFT. We suggest that these TPs may be formed because of cleavage at the carbon-carbon bond linking the aromatic 5-nitrofuran ring and the specific tail group in the NFT molecule as well as modification of the side ring moiety. The suggested TPs of NFT biodegradation include 1-aminohydantoin (AHD), semicarbazide (SEM) and hydrazine (HYD) (Fig. 2).

LC-MS/MS analysis of the samples collected from the bacterial cultures derivatized with 2-nitrobenzaldehyde (NBA) confirmed our assumptions (Supplementary Information). In the chromatograms, the TPs

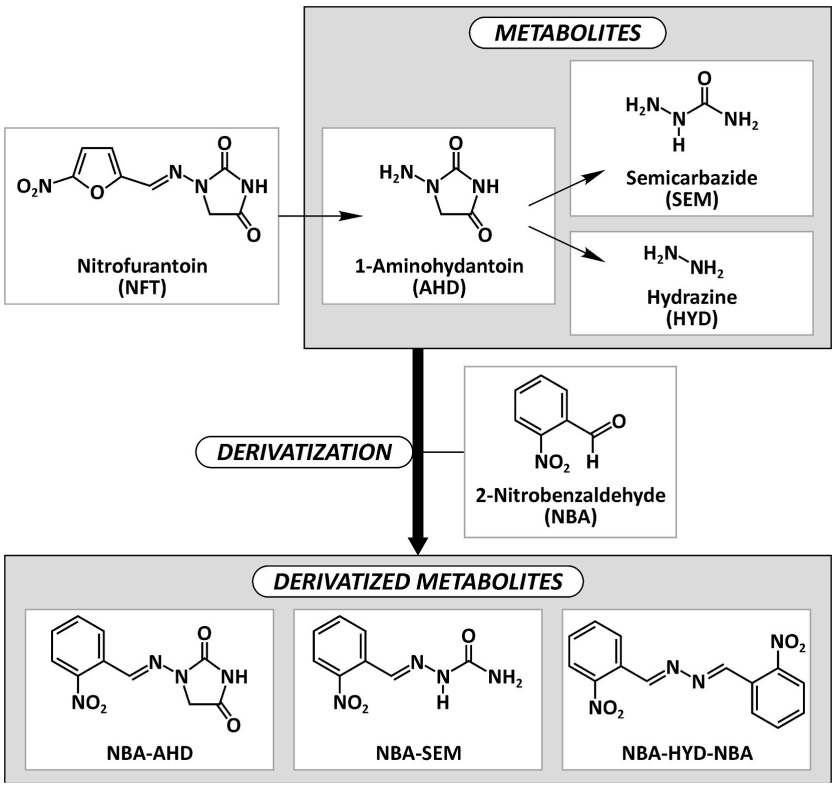

Fig. 2. Degradation pathway - a scheme of the derivatization process for NFT metabolites. AHD-NBA is the 2-nitrobenzaldehyde derivative of 1-aminohydantoin, SEM-NBA is the 2-nitrobenzaldehyde derivative of semicarbazide, NBA-HYD-NBA is the 2-nitrobenzaldehyde derivative of hydrazine (both NH2 groups of hydrazine were derivatized).

were identified at m/z values corresponding to the protonated NBA derivatives (AHD-NBA, SEM-NBA, and NBA-HYD-NBA). NBA-AHD conjugate was found at m/z = 249 and NBA-SEM at m/z = 209, while HYD was observed as the protonated molecule derivatized from its both ends, i.e. NBA-HYD-NBA at m/z = 299 (Supplementary Information). AHD was assumed to be the primary transformation product, which was then transformed into two secondary TPs: SEM and HYD. Hydrazine as a product of NFT degradation was observed for the first time in this study. Biodegradation of NFT followed similar pathways for both consortia and led to the formation of similar TPs.

Fig. 3 shows the changes in AHD and SEM content during NFT biodegradation. A significant increase in the concentration of AHD in both microbial consortia was measured during the first four days of the biodegradation process. This is consistent with the results of primary biodegradation (Fig. 1) which show that the highest increase in NFT elimination rate was observed during the first four incubation days. The peak in AHD content was followed by a gradual decrease until the end of the process. A microbial consortium that showed better degradation efficiency (NW), exhibited a higher concentration of AHD than the consortium with lower biodegradation (SS).

SEM, a secondary NFT biodegradation product generated by the decomposition of AHD, was identified in samples with both consortia. The SEM signal increased over time in both cultures. The highest increase of the SEM signal in NW bacterial consortium was noted in the first four incubation days. This is contrary to the SS consortium, where the SEM signal was gradually increasing. The SEM signal in the SS consortium was significantly higher than that in the NW consortium. This indicates that SS could have metabolized NFT to a lower extent, but its mineralization was more complete. Both TPs have been found in the samples even in the 20-day bacterial cultures indicating that they were not completely transformed. The remaining TPs in the bacterial cultures could be of environmental concern.

3.3. Shifts in microbial communities during NFT biodegradation

3.3.1. NGS sequencing results

Seven NW and six SS DNA samples were subjected to metagenomic sequencing. A total of 1,936,497 raw 16S rRNA reads were obtained. Merging and quality filtering reduced the total number of sequences to 1,524,952 reads with an average of 117,304 reads per sample. Bacterial sequences were predominant in each sample (>99.5%). At least 99% sequence similarity was measured in 73.8 ± 1.4% of total reads (109,925 reads on average). The remaining reads were associated with archaeal 16S sequences which were excluded from further analyses. In the NW consortium 74.3 ± 0.9% of reads were classified at taxonomic levels from phylum to family and 50.5 ± 10.4% were classified at the genus level. In the SS consortium at least 72.5 ± 2.4% of reads were classified at taxonomic levels from phylum to family and 48.7 ± 9.1% were classified at the genus level. The bacterial profiles of each bacterial community were constructed by extracting the bacterial reads among samples at various taxonomic levels from phylum to genus. The relative abundance at the family level in the samples is illustrated in Fig. 4a.

3.3.2. The mountain stream (NW) bacterial community

All NW cultures were dominated by species within phyla *Proteobacteria* and *Bacteroidetes*. Of the *Proteobacteria*, classes *Gammaproteobacteria* and *Betaproteobacteria* dominated the communities (Fig. 4a).

Flavobacteriia was the most abundant class in the *Bacteroidetes* phylum. The top five families in the control NW sample at day 0 were *Comamonadaceae* (43.2%), *Pseudomonadaceae* (19.6%), [*Weeksellaceae*] (12.1%), *Enterobacteriaceae* (9.1%), and *Xanthomonadaceae* (7.0%). The proportion of the two largest families was remarkably reduced in all treatments. On the 4th cultivation day, the proportion of *Pseudomonadaceae* was higher than on the 28th day in 5 and 10 mg · L^{-1} samples, however, it increased with increasing NFT concentration. A significant increase in the proportion of *[Weeksellaceae]* to 43.5% and 40.0% was

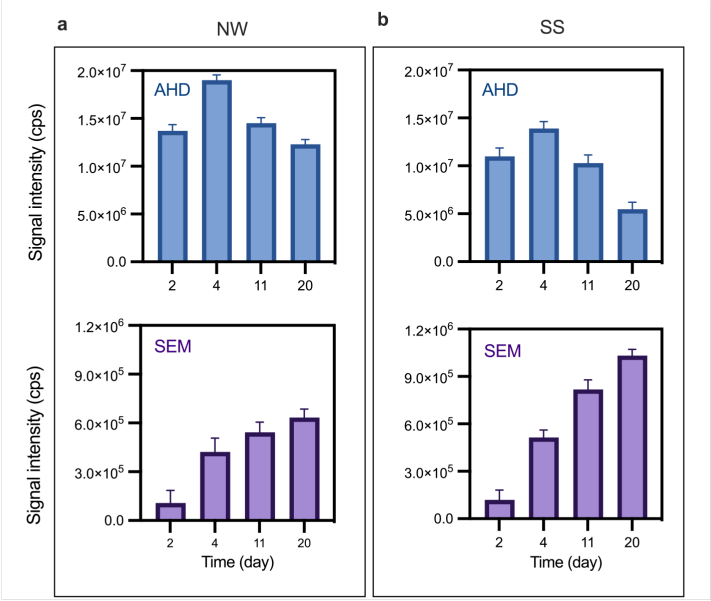

Fig. 3. Changes in the analytical signal of 1-aminohydantoin (AHD) and semicarbazide (SEM) during NFT biodegradation. (a) Mountain stream water sample (NW) represents the bacterial community collected from the protected area with no human intervention. (b) Seaport water sample (SS) represents the bacterial community collected from the seaport area that receives numerous contaminants. The numbers 2, 4, 11, and 20 indicate the sample collection days.

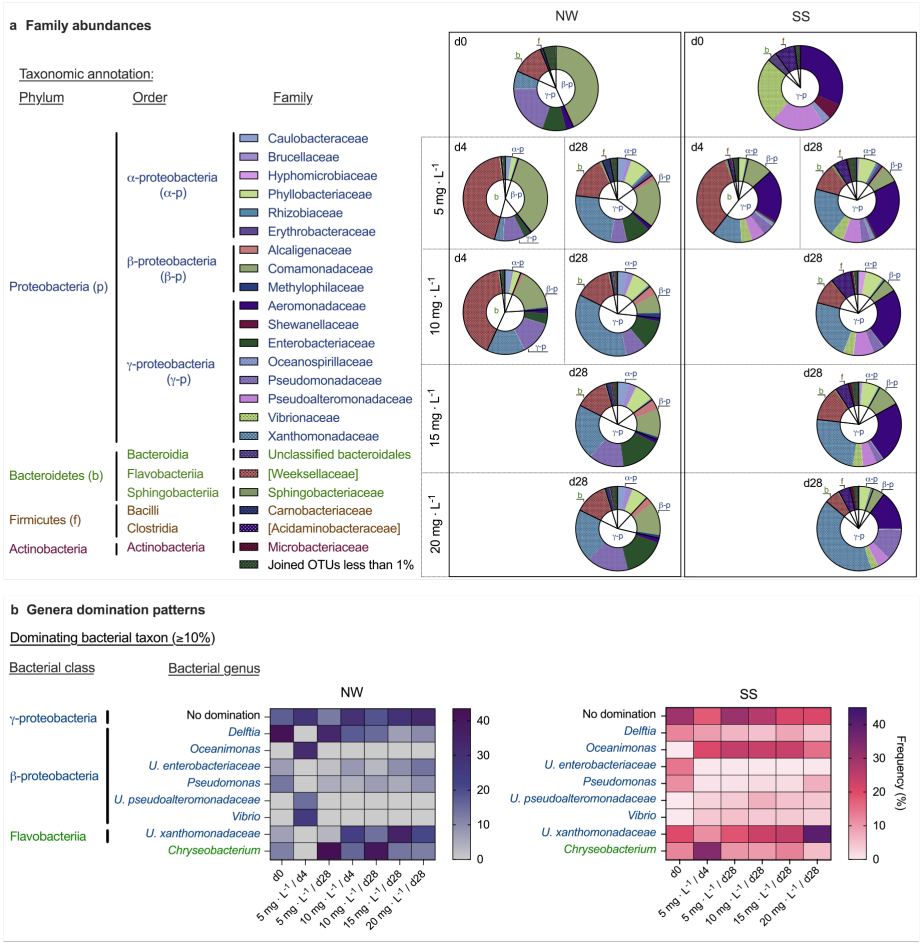

Fig. 4. Comparison of taxonomic differences in two bacterial communities treated with NFT (5, 10, 15 and 20 mg · L^{-1}). Mountain stream water sample (NW) represents the bacterial community collected from the protected area with no human intervention. Seaport water sample (SS) represents the bacterial community collected from the seaport area that receives numerous contaminants. The numbers d0, d4, and d28 indicate the sample collection days. (a) Relative abundance (above 1%) of the 16S rRNA gene sequence at the family level. The classifications with less than 1% abundance are gathered into the category "Joined OTUs less than 1%". (b) Domination matrices between bacterial taxa defined as relative abundance of a bacterial genus ≥10%.

observed in the 4-day cultures treated with 5 and 10 mg · L^{-1} NFT, while the relative abundance was 12.1% in the control sample at day 0.

A longer incubation time (28 days) resulted in a decrease in the relative abundance of *[Weeksellaceae]* in all NFT-treated samples. Significant alterations in the abundance of *Enterobacteriaceae* and *Xanthomonadaceae* were also observed. *Enterobacteriaceae* decreased on day 4 in both 5 and 10 mg · L^{-1} NFT. *Xanthomonadaceae* abundance decreased in cultures treated with 5 mg · L^{-1} to 3.4% and increased in 10 mg · L^{-1} cultures to 14.7%. *Xanthomonadaceae* dominated all cultures on the 28th day reaching the proportion of 20.1–37.7%. *Caulobacteraceae*, *Brucellaceae*, *Phyllobacteriaceae*, and *Alcaligenaceae* were below 1% at the initial sampling day, however, an increase in their proportion was observed after treatment with NFT.

To further explore these observations, we assessed co-domination patterns between bacterial genera in each culture (Fig. 4b). Co-domination is defined here as the presence of species at 10% relative abundance or higher. In the initial NW sample (d0) the most abundant genus was *Delftia* sp. reaching 42.6% and comprising about 99% of the *Comamonadaceae* family which was also the most abundant in the NW consortium. The two other top genera in the NW consortium included *Pseudomonas* sp. (13.5%) and *Chryseobacterium* sp. (12.1%). The specific bacterial species were unidentified within these two genera. In the 4-day culture at the initial concentration of NFT 5 mg · L^{-1} co-dominance of two species was observed, *Oceanimonas* sp. (31.4%) and *Vibrio* sp. (25.2%). The situation has changed in 28-day samples where again co-domination of *Delftia* sp. and *Chryseobacterium* sp. was measured. A similar situation was noted in 10 mg · L^{-1} samples, but the proportions of these genera were lower than in 5 mg · L^{-1} cultures. In 15 mg · L^{-1} cultures, an unclassified genus within the *Xanthomonadaceae* family was the most abundant (35.5%). The other genera that showed abundance above 10% included *Chryseobacterium* (13.8%) and an unclassified genus within the *Enterobacteriaceae* family. In 20 mg · L^{-1} treatment,

domination of an unclassified genus from *Xanthomonadaceae* was observed. The other genera that showed similar abundance between 10 and 14% included unclassified *Enterobacteriaceae, Chryseobacterium, Delftia* sp., and *Pseudomonas* sp. The proportion of the genera that did not show any domination increased with the concentration of NFT suggesting that NFT promotes greater biodiversity within bacterial cultures.

3.3.3. Seaport seawater (SS) bacterial community

The SS consortia were composed of species within phyla *Proteobacteria, Bacteroidetes, Firmicutes*, and *Actinobacteria* as plotted in Fig. 4a. Of the *Proteobacteria*, class *Gammaproteobacteria* dominated the communities. Class *Flavobacteriia* dominated within the *Bacteroidetes* phylum. The top five families in the control SS sample at day 0 were *Aeromonadaceae*, *Vibrionaceae*, *Pseudoalteromonadaceae*, [*Acidaminobacteraceae*], and *Shewanellaceae*. The proportion of the three largest families remarkably decreased in the samples treated with NFT compared with the control. The greater the initial NFT concentration, the lower proportion of these families in the microbial community was detected. *[Weeksellaceae], Xanthomonadaceae, Pseudomonadaceae, Comamonadaceae* and *Phyllobacteriaceae* were more abundant in all communities treated with NFT than in the control community. The greatest increase was noted for *[Weeksellaceae]* (33.9%, 5 mg · L^{-1}/d4) and *Xanthomonadaceae* (40.5%, 20 mg · L^{-1}/d28). These two families were barely detected in the control sample. The relative abundance of the *[Weeksellaceae]* family decreased with time by at least 3-fold in 5 mg · L^{-1} bottles. In 28-day microbial communities *[Weeksellaceae]* proportion was the highest at the lowest concentration of NFT (5 mg · L^{-1}) and the lowest at the highest NFT concentration (20 mg · L^{-1}). On the contrary, the proportion of *Xanthomonadaceae* significantly increased over time and NFT concentration.

Domination and co-domination patterns in the SS sample, plotted in Fig. 4b, indicate that the most abundant group (29.6%) in the initial SS sample included bacterial genera with no domination. The top five genera with domination between 11 and 20% included two unclassified genera within the *Xanthomonadaceae* and *Enterobacteriaceae* families, *Delftia* sp., *Pseudomonas* sp. and *Chryseobacterium* sp. In the 4-day 5 mg · L^{-1} consortium co-dominance of *Chryseobacterium* and *Oceanimonas* was observed. Interestingly, the proportion of *Oceanimonas* was enriched or remained stable at greater NFT concentration, and *Chryseobacterium* remarkably decreased reaching 5.5% in 28-day 20 mg · L^{-1} culture. In 10 and 15 mg · L^{-1} treatments, co-domination of *Oceanimonas* and unclassified genus within the *Xanthomonadaceae* family was measured. The relative abundance of the latter substantially increased with the increasing content of NFT. Within *Oceanimonas* genus, *Shewanella algae* was detected with the proportion of 6.23% in the initial sample. The abundance of *S. algae* decreased to 0.5% in NFT-treated cultures.

3.3.4. Alpha and beta diversity of the microbial consortia

To estimate the richness and diversity of each bacterial consortium treated with NFT as well as differences in bacterial composition between the samples, alpha and beta diversity indices were calculated. The richness (Observed OTUs, Chao1, ACE) and diversity (Shannon and Simpson) indices were used to analyze the alpha diversity of each bacterial community (Supplementary Information). The lowest OTUs in both consortia were measured in the initial samples at day 0. OTUs in the NW consortium were significantly higher than in the SS consortium. The OTUs indices significantly increased in all samples treated with NFT. Both Chao1 and ACE indices were the lowest in the initial samples in both consortia. They increased by around 40% in the NW consortium in NFT-treated samples. In the SS consortium, the two indices increased by at least 2-fold in all NFT-treated samples.

In both NS and SS consortia, Shannon and Simpson indices remarkably reduced in 4-day NFT-treated cultures in comparison to the initial samples. In the NW consortium, these indices were higher in 10 mg · L^{-1} cultures than in the 5 mg · L^{-1} ones. The highest values were calculated in 28-day cultures. In the SS consortium, Shannon and Simpson indices decreased with the increasing initial concentration of NFT. The initial NW (samples collected at day 0) was characterized by higher richness and lower diversity as opposed to SS. NFT-treated samples significantly increased Observed OTUs, Chao1, and ACE indices in both consortia.

The similarity patterns between the bacterial communities were analyzed by beta diversity based on Bray-Curtis ordination (PCoA) as shown in Fig. 5a and b. Fig. 5a shows that the samples from the same consortium are clustered together in many cases. PCoA analysis suggests that the NW consortium exhibited higher PCoA1 values, accounting for 61.2% of the variation. The SS community sampled upon experiment initiation (SS, d0) was distinctly different from the others. Using PCoA analysis data, we found a significant separation based on the period of communities' incubation with NFT. Both communities exhibited a significant variation over time. The samples isolated from 28-day cultures were ordinated closer to one another indicating that they were more similar than those ordinated further away (4-day samples). The NW communities in 28-day samples clustered together in the bottom right quadrant and they were more like each other than the corresponding communities in the SS cultures. The differences in the NFT treatments were also observed in a cluster dendrogram presented in Fig. 5b. Beta diversity heatmap compares the species of communities' differences between the samples. The larger the index, the more differences between the samples. The samples from each consortium clustered together. The distances of samples were smaller in the NW consortium than in the SS consortium. The distance between 15 and 20 mg · L^{-1} cultures of the NW consortium collected on the 28th day was the smallest. The largest differences were observed between the initial SS consortium and all NW samples.

4. Discussion

This study focused on the biodegradation of NFT by two distinct environmental consortia, and the determination of NFT degradation products. The microbial consortia were isolated from two aqueous environmental niches: the National Park in Southern Poland and the seaport in Northern Poland. Protected areas, such as national parks, wilderness areas and nature reserves, due to their long-term protection are expected to be a mainstay of biodiversity conservation. Unfortunately, in recent years, the loss of biodiversity in the protected areas has been reported (Abessa et al., 2018; Butchart et al., 2010; Watson et al., 2014). Protected areas should be characterized by low concentration of anthropogenic pollutants. We hypothesized that microorganisms present in the water bodies of such pristine areas have not been exposed to anthropogenic contaminants, therefore, they might not have the adaptative mechanisms developed. Therefore, the bacteria could be very sensitive to chemical residues and exhibit low biodegradation potential. On the other hand, we expected that the aqueous environmental compartments, such as seaport water, contain microorganisms that have higher biodegradation potential. The microorganisms were expected to have adaptive responses greatly developed to survive in adverse environments due to the numerous contaminants they receive. Our conception was based, among other, on the papers written by Zhang et al. (2018) and Poursat et al. (2019) who suggested that increased concentration of toxic pollutants enhances bacterial adaptation which stimulates biodegradation efficiency. According to Thouand et al. (2011), diverse microbial consortia are more efficient in the biodegradation of anthropogenic substances. The results presented here were unexpected because NFT biodegradation by microorganisms in the NW sample was significantly more efficient than biodegradation by microbes in the SS sample (Fig. 1). A complete NFT primary biodegradation by the NW consortium has been achieved in samples with the two lowest initial concentrations of NFT (5 and 10 mg · L^{-1}) as opposed to the analogic samples containing the SS consortium. Moreover, in the cultures with the highest initial NFT concentration (20 mg · L^{-1}), the NW consortium degraded more NFT (88.1 ± 1.0%) than the SS consortium (63.5 ±

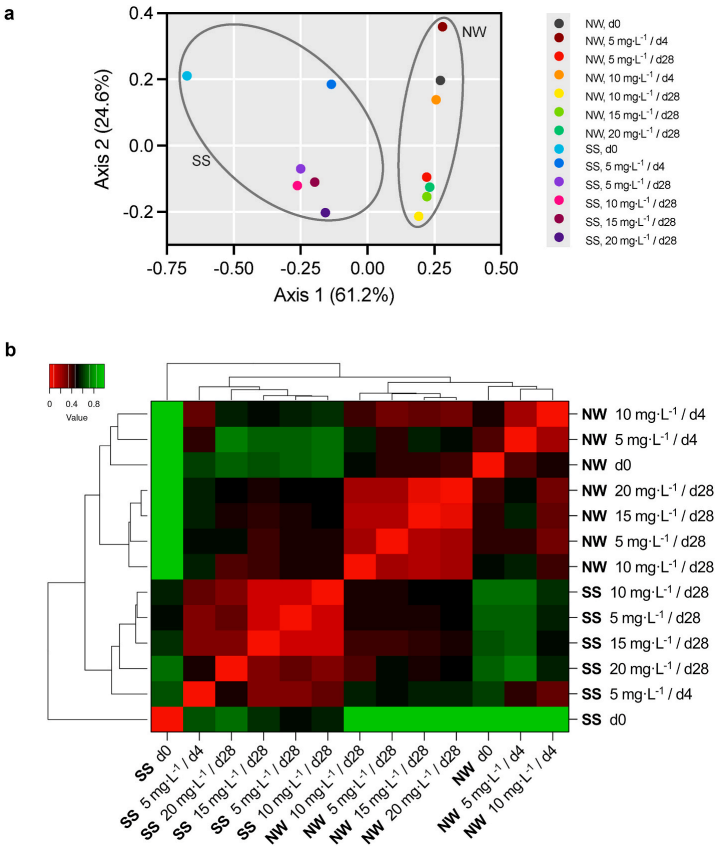

Fig. 5. Beta diversity of two bacterial communities treated with NFT at a concentration of 5, 10, 15 and 20 mg · L^{-1} calculated using the Bray–Curtis dissimilarity index. Mountain stream water sample (NW) represents the bacterial community collected from the protected area with no human intervention. Seaport water sample (SS) represents the bacterial community collected from the seaport area that receives numerous contaminants. The numbers d0, d4, and d28 indicate the sample collection days. (a) Principal coordinate analysis of the communities. Objects that are ordinated closer together have smaller dissimilarity values than those ordinated further apart. (b) Heatmap comparing the species of communities' differences between the samples.

2.2%). By contrast, our previous studies on the biodegradation of four 5-NFs by the activated sludge collected from the municipal and rural wastewater treatment plants (WWTPs) show that the consortia from the municipal WWTP were characterized by greater degradation potential than the microbes from the rural WWTP (Pacholak et al., 2020b). However, metagenomic analysis of municipal microorganisms that were exposed to a greater concentration of pollutants showed increased biodiversity in comparison with microorganisms that had lower exposure to the anthropogenic contaminants which reflects the results presented here. Recently, many researchers have focused on the biological removal of antibiotic pollutants from the environment, however, information about the biological degradation of 5-NFs is limited (Liao et al., 2017; Shi et al., 2021; Zhu et al., 2021). It has been reported that 5-NFs are unstable and rapidly metabolized *in vivo* (Gong et al., 2020; Khan and Lively, 2020; Yuan et al., 2020). Due to this instability, their level in the environment may be difficult to determine. In our samples, NFT was detected unmetabolized after 28 days of incubation with microorganisms, and this certainly proves that this antibiotic is quite stable and not easily degradable. No articles to our knowledge describe the NFT biodegradation capacity of the natural environmental consortia. Therefore, further studies are needed.

The primary biodegradation of anthropogenic substances may lead to the formation of TPs that can remain unchanged in the ecosystems for a long time (Zainab et al., 2020). In this study, the proposed TPs of NFT biodegradation include AHD, SEM, and HYD. We suggest that their formation resulted from the cleavage at the carbon-carbon bond linking the aromatic 5-nitrofuran ring and the specific tail group in the NFT molecule as well as modification of the side ring moiety. AHD is a well-known metabolite of NFT formed by higher organisms. It has been frequently determined in animal products due to its ability to bind tissue proteins, and therefore, is used to monitor the residues of NFs in animal products (Li et al., 2017; Sheng et al., 2013; Yuan et al., 2020). Another product of NFT transformation detected here was SEM which previously has been a known intermediate in the degradation of nitrofurazone, another antibiotic from the nitrofuran group. Neither AHD nor SEM was detected as TPs in biodegradation experiments before. This may be due to very limited information about NFT biodegradation. Szabó-Bárdos et al. (2020), however, detected AHD as a product of NFT photocatalytic degradation. This suggests that the mechanism of biological NFT removal may be similar to physicochemical degradation. Importantly, both compounds were detected in the natural environment which proves their persistence (Goessens et al., 2022; Yu et al., 2013). HYD, a well-known precursor to blowing agents, pesticides and pharmaceuticals, was detected in our study as a secondary product of NFT biodegradation. HYD is known for its genotoxic and carcinogenic properties (Wang et al., 2016). The similarity of the chemical structure of NFT with other 5-NFs (such as nitrofurazone, furazolidone, and furaltadone) suggests that HYD might be formed during the biodegradation of these compounds as well. In this study, the TPs from NFT biodegradation were still detected in 20-day cultures. This indicates that NFT was not

completely transformed. The content of primary biodegradation product (AHD) decreased with time and secondary biodegradation product (SEM) slightly increased with time. This indicates that TPs would remain unchanged in water for a long time. The remaining TPs in the bacterial cultures could be of environmental concern because they often show higher toxicity than the parent compound. Increased toxicity of TPs of various xenobiotics has been recently documented (Gutowski et al., 2015; Pacholak et al., 2022; Sosa-Martínez et al., 2020).

In addition to the biodegradation studies, the bacterial biodiversity and composition of the two bacterial communities were examined in this study. The composition of the consortia was determined from the phylum to the species level. In total, 6 phyla, 13 classes, 31 orders, 65 families, 119 genera, and 134 species were found in our samples. *Proteobacteria* was the most dominant phylum in both communities followed by *Bacteroidetes*. Similar results were found previously in soil, marsh sediments and aquaculture water by other authors (Li et al., 2022; Seeley et al., 2020; Wongkiew et al., 2022). Based on alpha and beta diversity measures, the increasing concentration of NFT resulted in differences in the overall bacterial community diversities. All alpha diversity indices indicate that NFT-treated SS consortia were more diverse than the NW consortia. The biodiversity significantly increased in both consortia treated with NFT compared to the initial samples. These findings are not supported by Li et al. (2019) who found out that the biodiversity of the natural microbial communities decreased significantly during the biodegradation of hydrocortisone and dexamethasone. Our results, however, clearly demonstrate that NFT contamination affects the composition of aqueous microbial communities and microbial community structure may be directly correlated with the presence of this antibiotic. Other authors also suggested that anthropogenic pollutants shape the structure of microbial communities (Bourhane et al., 2022; Li et al., 2022; Seeley et al., 2020). Significant variations in the bacterial community composition may also be caused by differences in pH, salinity, and TOC concentration of the outside environment. In general, *Acidobacteria* dominate environments with acidic pH, the neutralophilic bacteria grow well at pH values 5.5 to 9. Despite many researchers studied effect of pH on the bacterial communities, the mechanisms by which pH acts on the composition and biodiversity of bacterial communities are still poorly understood (Rousk et al., 2010; Yavitt et al., 2021). Rath et al. (2019) found high community salt tolerance is positively correlated with *Bacteroidetes* and the *Gammaproteobacteria*. Effect of salinity on the structure of bacterial community has been investigated also by other authors, however, the research is often focused on the soil microbiome (Bai et al., 2020; Kaartokallio et al., 2005; Li et al., 2021).

Previous studies show that microorganisms responsible for antibiotics degradation are broadly distributed taxonomically, including *Proteobacteria*, *Firmicutes*, *Cyanobacteria*, *Bacteroidetes*, *Chloroflexi*, and *Acidobacteria* (Kumar et al., 2019; Liao et al., 2017; Zhu et al., 2021). Changes in the microbial composition of both microbial consortia studied indicate that the *Xanthomonadaceae* family was significantly enriched in all samples treated with NFT in comparison with the initial consortia. Moreover, the proportion of *Xanthomonadaceae* was higher in the cultures where the complete primary biodegradation was measured (Fig. 4a). The unclassified *Xanthomonadaceae* species showed domination in these cultures. This suggests that the strain in question could be one of the main drivers of NFT biodegradation in the NW consortium. Previous studies show that the species in the *Xanthomonadaceae* family (i.e. *Pseudoxanthomonas* sp. strain NyZ600, *Stenotrophomonas maltophilia* DT1) are responsible for the biodegradation of recalcitrant compounds, such as polymers, hydrocarbons and pharmaceuticals (Bell et al., 2013; Leng et al., 2016; Thelusmond et al., 2016; Yue et al., 2021). On the other hand, the proportion of *Comamonadaceae* and *Pseudomonadaceae* significantly decreased in NW in the treated samples of the NW consortium suggesting that these species did not contribute to biodegradation. The *Weeksellaceae* family remarkably increased in the 4-day cultures which was followed by a strong reduction in the abundance of these microbes. This suggests that the *Weeksellaceae* family could have been responsible for the primary biodegradation of NFT. *Chryseobacterium,* a genus from the *Weeksellaceae* family, has been detected as one of the dominating genera in bacterial cultures. The *Chryseobacterium* species are known degraders of many xenobiotics, including fungicides (carbendazim) (Silambarasan and Abraham, 2020), keratin waste (Gurav et al., 2020), or herbicides (glyphosate) (Zhang et al., 2022). The results presented here indicate that NFT contamination may lead to an increased abundance of the *Chryseobacterium* species.

5-NFs are generally known as old antibiotics, and their use has increased recently. They are very broad-spectrum antibiotics and this multiactivity allows the repurposing of these drugs from agricultural chemicals and basic antibiotics to efficient pharmaceuticals against human life-threatening diseases. The alleged excessive misuse and the illegal application in husbandry contribute to 5-NFs continuous release into the natural environment, which may negatively affect all living organisms. The negative impact of 5-NFs on the environmental bacteria has been investigated in our previous papers (Pacholak et al., 2020a, 2020b; Smułek et al., 2022; Zdarta et al., 2021), however, it still raises many questions and requires further investigation. In the last few years, scientists have been increasingly interested in the environmental impact of antibiotics. The greatest attention has been drawn to tetracyclines, sulfonamides, macrolides, and beta-lactams. 5-NFs are among the few antibiotic groups whose environmental impact is not sufficiently understood. Fulfilling the research gap in this field will contribute to better understanding of the environmental impact of 5-NFs and their biodegradation. This, in turn, could be helpful in designing the bioremediation technologies.

5. Conclusions

Investigation of NFT biodegradation and shifts in the microbial communities' compositions revealed that aqueous bacterial communities are likely influenced by NFT. There were clear deviations between the two communities. The initial microbial consortium from the contaminated aquatic systems was more diverse than the consortium isolated from the pristine area. Through our analysis, we also revealed that an increase in microbial community diversity does not have to be correlated with an increase in functional capacity, such as the ability to biodegradation. In this study, higher biodiversity corresponded to lower biodegradation. In addition, bacterial exposure to environmental pollutants was not related with increased NFT biodegradation. The highest removal efficiency was observed for microbial communities at the lowest NFT concentration. Besides, among TPs formed during biodegradation, HYD was reported for the first time. Higher primary degradation of NFT was followed by a higher concentration of primary TPs and lower concentration of secondary TPs, however, lower primary degradation of NFT was followed by low concentration of primary TPs and high concentration of secondary TPs. Our results demonstrate that NFT contamination affects the composition of aqueous microbial communities and microbial community structure may be directly correlated with the presence of this antibiotic. The study also increased understanding of the environmental impact of 5-NFs and their biodegradation.

Credit author statement

Amanda Pacholak: Conceptualization, Methodology, Validation, Formal analysis, Investigation, Resources; Writing – Original Draft, Writing – review & editing, Visualization, **Agnieszka Zgoła-Grzeskowiak**: Conceptualization (LC-MS/MS analysis), Investigation (LC-MS/MS analysis), Methodology, Writing – review & editing, Validation (LC-MS/MS analysis), **Ewa Kaczorek**: Conceptualization, Resources, Writing – review & editing, Supervision, Project administration, Funding acquisition.

Declaration of competing interest

The authors declare that they have no known competing financial interests or personal relationships that could have appeared to influence the work reported in this paper.

Data availability

Data will be made available on request.

Acknowledgments

This study was funded in whole by National Science Centre in Poland, grant number 2017/27/B/NZ9/01603). Amanda Pacholak is grateful for financial support from the Foundation for Polish Sciences (FNP).

Appendix A. Supplementary data

Supplementary data to this article can be found online at https://doi.org/10.1016/j.envres.2022.114531.

References

Abessa, D.M.S., Albuquerque, H.C., Morais, L.G., 2018. Pollution status of marine protected areas worldwide and the consequent toxic effects are unknown. Environ. Pollut. 1450–1459. https://doi.org/10.1016/j.envpol.2018.09.129.

Albrektienė, R., Rimeika, M., Zalieckienė, E., Šaulys, V., Zagorskis, A., 2012. Determination of organic matter by UV absorption in the ground water. J. Environ. Eng. Landsc. Manag. 20, 163–167. https://doi.org/10.3846/16486897.2012.674039.

Al-Waili, N., Salom, K., Al-Ghamdi, A., Ansari, M.J., 2012. Antibiotic, pesticide, and microbial contaminants of honey: human health hazards. Sci. World J. 1–9. https://doi.org/10.1100/2012/930849, 2012.

Babicki, S., Arndt, D., Marcu, A., Liang, Y., Grant, J.R., Maciejewski, A., Wishart, D.S., 2016. Heatmapper: web-enabled heat mapping for all. Nucleic Acids Res. 44, 147–153. https://doi.org/10.1093/nar/gkw419.

Bai, Y., Ren, P., Feng, P., Yan, H., Li, W., 2020. Shift in rhizospheric and endophytic bacterial communities of tomato caused by salinity and grafting. Sci. Total Environ. 734, 139388 https://doi.org/10.1016/j.scitotenv.2020.139388.

Bell, T.H., Yergeau, E., Juck, D.F., Whyte, G., Greer, L.W.C., 2013. Alteration of microbial community structure affects diesel biodegradation in an Arctic soil. FEMS Microbiol. Ecol. 85, 51–61. https://doi.org/10.1111/1574-6941.12102.

Bourhane, Z., Lanzén, A., Cagnon, C., Ben Said, O., Mahmoudi, E., Coulon, F., Atai, E., Borja, A., Cravo-Laureau, C., Duran, R., 2022. Microbial diversity alteration reveals biomarkers of contamination in soil-river-lake continuum. J. Hazard Mater. 421, 126789 https://doi.org/10.1016/j.jhazmat.2021.126789.

Butchart, S.H.M., Walpole, M., Collen, B., van Strien, A., Scharlemann, J.P.W., Almond, R.E.A., Baillie, J.E.M., Bomhard, B., Brown, C., Bruno, J., Carpenter, K.E., Carr, G.M., Chanson, J., Chenery, A.M., Csirke, J., Davidson, N.C., Dentener, F., Foster, M., Galli, A., Galloway, J.N., Genovesi, P., Gregory, R.D., Hockings, M., Kapos, V., Lamarque, J.-F., Leverington, F., Loh, J., McGeoch, M.A., McRae, L., Minasyan, A., Morcillo, M.H., Oldfield, T.E.E., Pauly, D., Quader, S., Revenga, C., Sauer, J.R., Skolnik, B., Spear, D., Stanwell-Smith, D., Stuart, S.N., Symes, A., Tierney, M., Tyrrell, T.D., Vié, J.-C., Watson, R., 2010. Global biodiversity: indicators of recent declines. Science 328, 1164–1168. https://doi.org/10.1126/science.1187512.

Chandran, H., Meena, M., Sharma, K., 2020. Microbial biodiversity and bioremediation assessment through omics approaches. Front. Environ. Chem. 1, 570326 https://doi.org/10.3389/fenvc.2020.570326.

Dinh, Q.T., Munoz, G., Vo Duy, S., Tien Do, D., Bayen, S., Sauvé, S., 2020. Analysis of sulfonamides, fluoroquinolones, tetracyclines, triphenylmethane dyes and other veterinary drug residues in cultured and wild seafood sold in Montreal, Canada. J. Food Compos. Anal. 94, 103630 https://doi.org/10.1016/j.jfca.2020.103630.

Dong, Y., Wu, S., Fan, H., Li, X., Li, Y., Xu, S., Bai, Z., Zhuang, X., 2022. Ecological selection of bacterial taxa with larger genome sizes in response to polycyclic aromatic hydrocarbons stress. J. Environ. Sci. 112, 82–93. https://doi.org/10.1016/j.jes.2021.04.027.

Frankowski, R., Płatkiewicz, J., Stanisz, E., Grześkowiak, T., Zgoła-Grześkowiak, A., 2021. Biodegradation and photo-Fenton degradation of bisphenol A, bisphenol S and fluconazole in water. Environ. Pollut. 289, 117947 https://doi.org/10.1016/j.envpol.2021.117947.

Goessens, T., De Baere, S., Deknock, A., De Troyer, N., Van Leeuwenberg, R., Martel, A., Pasmans, F., Goethals, P., Lens, L., Spanoghe, P., Vanhaecke, L., Croubels, S., 2022. Agricultural contaminants in amphibian breeding ponds: occurrence, risk and correlation with agricultural land use. Sci. Total Environ. 806, 150661 https://doi.org/10.1016/j.scitotenv.2021.150661.

Gong, J., Li, J., Yuan, H., Chu, B., Lin, W., Cao, Q., Zhao, Q., Fang, R., Li, L., Xiao, G., 2020. Determination of four nitrofuran metabolites in gelatin Chinese medicine using dispersive solid phase extraction and pass-through solid phase extraction coupled to ultra high performance liquid chromatography-tandem mass spectrometry. J. Chromatogr. B 1146, 122018. https://doi.org/10.1016/j.jchromb.2020.122018.

Griboff, J., Carrizo, J.C., Bonansea, R.I., Valdés, M.E., Wunderlin, D.A., Amé, M.V., 2020. Multiantibiotic residues in commercial fish from Argentina. The presence of mixtures of antibiotics in edible fish, a challenge to health risk assessment. Food Chem. 332, 127380 https://doi.org/10.1016/j.foodchem.2020.127380.

Gruber, K., 2018. Cleaning up pollutants to protect future health. Nature 555, S20–S22. https://doi.org/10.1038/d41586-018-02481-5.

Gurav, R., Bhatia, S.K., Choi, T.-R., Park, Y.-L., Park, J.Y., Han, Y.-H., Vyavahare, G., Jadhav, J., Song, H.-S., Yang, P., Yoon, J.-J., Bhatnagar, A., Choi, Y.-K., Yang, Y.-H., 2020. Treatment of furazolidone contaminated water using banana pseudostem biochar engineered with facile synthesized magnetic nanocomposites. Bioresour. Technol. 297, 122472 https://doi.org/10.1016/j.biortech.2019.122472.

Gutowski, L., Olsson, O., Leder, C., Kümmerer, K., 2015. A comparative assessment of the transformation products of S-metolachlor and its commercial product Mercantor Gold® and their fate in the aquatic environment by employing a combination of experimental and in silico methods. Sci. Total Environ. 506–507, 369–379. https://doi.org/10.1016/j.scitotenv.2014.11.025.

Head, I.M., Jones, D.M., Röling, W.F.M., 2006. Marine microorganisms make a meal of oil. Nat. Rev. Microbiol. 4, 173–182. https://doi.org/10.1038/nrmicro1348.

Jördening, H.-J., Winter, J., 2005. Environmental Biotechnology: Concepts and Applications. Wiley-VCH, Weinheim.

Jørgensen, K.S., 2011. In situ bioremediation. In: Comprehensive Biotechnology. Elsevier, pp. 59–67. https://doi.org/10.1016/B978-0-08-088504-9.00372-X.

Kaartokallio, H., Laamanen, M., Sivonen, K., 2005. Responses of Baltic Sea ice and open-water natural bacterial communities to salinity change. Appl. Environ. Microbiol. 71, 4364–4371. https://doi.org/10.1128/AEM.71.8.4364-4371.2005.

Khan, M., Lively, J.A., 2020. Determination of sulfite and antimicrobial residue in imported shrimp to the USA. Aquaculture Reports 18, 100529. https://doi.org/10.1016/j.aqrep.2020.100529.

Kokulnathan, T., Chen, S.-M., 2020. Robust and selective electrochemical detection of antibiotic residues: the case of integrated lutetium vanadate/graphene sheets architectures. J. Hazard Mater. 384, 121304 https://doi.org/10.1016/j.jhazmat.2019.121304.

Kouzuma, A., Watanabe, K., 2011. Molecular approaches for the analysis of natural attenuation and bioremediation. In: Comprehensive Biotechnology. Elsevier, pp. 25–36. https://doi.org/10.1016/B978-0-08-088504-9.00375-5.

Kumar, M., Jaiswal, S., Sodhi, K.K., Shree, P., Singh, D.K., Agrawal, P.K., Shukla, P., 2019. Antibiotics bioremediation: perspectives on its ecotoxicity and resistance. Environ. Int. 124, 448–461. https://doi.org/10.1016/j.envint.2018.12.065.

Kümmerer, K., 2009. Antibiotics in the aquatic environment – a review – Part I. Chemosphere 75, 417–434. https://doi.org/10.1016/j.chemosphere.2008.11.086.

Leng, Y., Bao, J., Chang, G., Zheng, H., Li, Xingxing, Du, J., Snow, D., Li, Xu, 2016. Biotransformation of tetracycline by a novel bacterial strain *Stenotrophomonas maltophilia* DT1. J. Hazard Mater. 318, 125–133. https://doi.org/10.1016/j.jhazmat.2016.06.053.

Li, S., Ju, H., Zhang, J., Chen, P., Ji, M., Ren, J., Zhao, S., 2019. Occurrence and distribution of selected antibiotics in the surface waters and ecological risk assessment based on the theory of natural disaster. Environ. Sci. Pollut. Res. 26, 28384–28400. https://doi.org/10.1007/s11356-019-06060-7.

Li, W., Chen, X., Cai, Z., Li, M., Liu, Z., Gong, H., Yan, M., 2022. Characteristics of microplastic pollution and analysis of colonized-microbiota in a freshwater aquaculture system. Environ. Pollut. 306, 119385 https://doi.org/10.1016/j.envpol.2022.119385.

Li, X., Ma, M., Rene, E.R., Ma, W., Zhang, P., 2019. Changes in microbial communities during the removal of natural and synthetic glucocorticoids in three types of river-based aquifer media. Environ. Sci. Pollut. Res. 26, 33953–33962. https://doi.org/10.1007/s11356-018-2748-x.

Li, X., Wang, A., Wan, W., Luo, X., Zheng, L., He, G., Huang, D., Chen, W., Huang, Q., 2021. High salinity inhibits soil bacterial community mediating nitrogen cycling. Appl. Environ. Microbiol. 87, e01366-21 https://doi.org/10.1128/AEM.01366-21.

Li, Zhonghui, Li, Zhoumin, Xu, D., 2017. Simultaneous detection of four nitrofuran metabolites in honey by using a visualized microarray screen assay. Food Chem. 221, 1813–1821. https://doi.org/10.1016/j.foodchem.2016.10.099.

Liao, X., Zou, R., Li, B., Tong, T., Xie, S., Yuan, B., 2017. Biodegradation of chlortetracycline by acclimated microbiota. Process Saf. Environ. Protect. 109, 11–17. https://doi.org/10.1016/j.psep.2017.03.015.

Mccracken, R.J., Van Rhijn, J.A., Kennedy, D.G., 2005. The occurrence of nitrofuran metabolites in the tissues of chickens exposed to very low dietary concentrations of the nitrofurans. Food Addit. Contam. 22, 567–572. https://doi.org/10.1080/02652030500137868.

Naidu, R., Biswas, B., Willett, I.R., Cribb, J., Kumar Singh, B., Paul Nathanail, C., Coulon, F., Semple, K.T., Jones, K.C., Barclay, A., Aitken, R.J., 2021. Chemical pollution: a growing peril and potential catastrophic risk to humanity. Environ. Int. 156, 106616 https://doi.org/10.1016/j.envint.2021.106616.

NSW Department of Primary Industries, 2019. Water Collection Guidelines for Microbiological Testing [WWW Document]. https://www.dpi.nsw.gov.au/_data/assets/pdf_file/0009/856008/water-collection-guidelines-for-microbiological-testing.pdf. accessed 9.30.22.

Ossai, I.C., Ahmed, A., Hassan, A., Hamid, F.S., 2020. Remediation of soil and water contaminated with petroleum hydrocarbon: a review. Environ. Technol. Innovat. 17, 100526 https://doi.org/10.1016/j.eti.2019.100526.

Pacholak, A., Burlaga, N., Frankowski, R., Zgoła-Grześkowiak, A., Kaczorek, E., 2022. Azole fungicides: (Bio)degradation, transformation products and toxicity

elucidation. Sci. Total Environ. 802, 149917 https://doi.org/10.1016/j.scitotenv.2021.149917.
Pacholak, A., Burlaga, N., Guzik, U., Kaczorek, E., 2020a. Investigation of the bacterial cell envelope nanomechanical properties after long-term exposure to nitrofurans. J. Hazard Mater. 124352 https://doi.org/10.1016/j.jhazmat.2020.124352.
Pacholak, A., Zdarta, A., Frankowski, R., Cybulski, Z., Kaczorek, E., 2020b. Exploring elimination kinetics of four 5-nitrofuran derivatives by microbes present in rural and municipal activated sludge. Water Air Soil Pollut. 231, 252. https://doi.org/10.1007/s11270-020-04634-7.
Poursat, B.A.J., van Spanning, R.J.M., de Voogt, P., Parsons, J.R., 2019. Implications of microbial adaptation for the assessment of environmental persistence of chemicals. Crit. Rev. Environ. Sci. Technol. 49, 2220–2255. https://doi.org/10.1080/10643389.2019.1607687.
Rath, K.M., Fierer, N., Murphy, D.V., Rousk, J., 2019. Linking bacterial community composition to soil salinity along environmental gradients. ISME J. 13, 836–846. https://doi.org/10.1038/s41396-018-0313-8.
Rousk, J., Bååth, E., Brookes, P.C., Lauber, C.L., Lozupone, C., Caporaso, J.G., Knight, R., Fierer, N., 2010. Soil bacterial and fungal communities across a pH gradient in an arable soil. ISME J. 4, 1340–1351. https://doi.org/10.1038/ismej.2010.58.
Seeley, M.E., Song, B., Passie, R., Hale, R.C., 2020. Microplastics affect sedimentary microbial communities and nitrogen cycling. Nat. Commun. 11, 2372. https://doi.org/10.1038/s41467-020-16235-3.
Sheng, L.-Q., Chen, M.-M., Chen, S.-S., Du, N.-N., Liu, Z.-D., Song, C.-F., Qiao, R., 2013. High-performance liquid chromatography with fluorescence detection for the determination of nitrofuran metabolites in pork muscle. Food Addit. Contam. 30, 2114–2122. https://doi.org/10.1080/19440049.2013.849387.
Shi, Y., Lin, H., Ma, J., Zhu, R., Sun, W., Lin, X., Zhang, J., Zheng, H., Zhang, X., 2021. Degradation of tetracycline antibiotics by *Arthrobacter nicotianae* OTC-16. J. Hazard Mater. 403, 123996 https://doi.org/10.1016/j.jhazmat.2020.123996.
Silambarasan, S., Abraham, J., 2020. Biodegradation of carbendazim by a potent novel *Chryseobacterium* sp. JAS14 and plant growth promoting *Aeromonas caviae* JAS15 with subsequent toxicity analysis. 3 Biotech 10, 326. https://doi.org/10.1007/s13205-020-02319-w.
Smułek, W., Rojewska, M., Pacholak, A., Machrowicz, O., Prochaska, K., Kaczorek, E., 2022. Co-interaction of nitrofurantoin and saponins surfactants with biomembrane leads to an increase in antibiotic's antibacterial activity. J. Mol. Liq. 364, 120070 https://doi.org/10.1016/j.molliq.2022.120070.
Sosa-Martínez, J.D., Balagurusamy, N., Montañez, J., Peralta, R.A., Moreira, R. de, Bracht, A., Peralta, R.M., Morales-Oyervides, L., 2020. Synthetic dyes biodegradation by fungal ligninolytic enzymes: process optimization, metabolites evaluation and toxicity assessment. F.P.M. J. Hazard Mater. 400, 123254 https://doi.org/10.1016/j.jhazmat.2020.123254.
Szabó-Bárdos, E., Cafuta, A., Hegedüs, P., Fónagy, O., Kiss, G., Babić, S., Škorić, I., Horváth, O., 2020. Photolytic and photocatalytic degradation of nitrofurantoin and its photohydrolytic products. J. Photochem. Photobiol. Chem. 386, 112093 https://doi.org/10.1016/j.jphotochem.2019.112093.
Tang, F.H.M., Lenzen, M., McBratney, A., Maggi, F., 2021. Risk of pesticide pollution at the global scale. Nat. Geosci. 14, 206–210. https://doi.org/10.1038/s41561-021-00712-5.
Techtmann, S.M., Hazen, T.C., 2016. Metagenomic applications in environmental monitoring and bioremediation. J. Ind. Microbiol. Biotechnol. 43, 1345–1354. https://doi.org/10.1007/s10295-016-1809-8.
Thelusmond, J.-R., Strathmann, T.J., Cupples, A.M., 2016. The identification of carbamazepine biodegrading phylotypes and phylotypes sensitive to carbamazepine exposure in two soil microbial communities. Sci. Total Environ. 571, 1241–1252. https://doi.org/10.1016/j.scitotenv.2016.07.154.
Thouand, G., Durand, M.-J., Maul, A., Gancet, C., Blok, H., 2011. New concepts in the evaluation of biodegradation/persistence of chemical substances using a microbial inoculum. Front. Microbiol. 2 https://doi.org/10.3389/fmicb.2011.00164.
Wang, G., Zhou, S., Han, X., Zhang, L., Ding, S., Li, Y., Zhang, D., Zarin, K., 2020. Occurrence, distribution, and source track of antibiotics and antibiotic resistance genes in the main rivers of Chongqing city, southwest China. J. Hazard Mater. 389, 122110 https://doi.org/10.1016/j.jhazmat.2020.122110.
Wang, J., Yang, S., Zhang, K., 2016. A simple and sensitive method to analyze genotoxic impurity hydrazine in pharmaceutical materials. J. Pharmaceut. Biomed. Anal. 126, 141–147. https://doi.org/10.1016/j.jpba.2016.04.038.
Wang, Z., Xu, Z., Li, X., 2018. Biodegradation of methamphetamine and ketamine in aquatic ecosystem and associated shift in bacterial community. J. Hazard Mater. 359, 356–364. https://doi.org/10.1016/j.jhazmat.2018.07.039.
Watson, J.E.M., Dudley, N., Segan, D.B., Hockings, M., 2014. The performance and potential of protected areas. Nature 515, 7. https://doi.org/10.1038/nature13947.
Wongkiew, S., Chaikaew, P., Takrattanasaran, N., Khamkajorn, T., 2022. Evaluation of nutrient characteristics and bacterial community in agricultural soil groups for sustainable land management. Sci. Rep. 12, 7368. https://doi.org/10.1038/s41598-022-09818-1.
Wu, Q., Pan, C.-G., Wang, Y.-H., Xiao, S.-K., Yu, K.-F., 2021. Antibiotics in a subtropical food web from the Beibu Gulf, South China: occurrence, bioaccumulation and trophic transfer. Sci. Total Environ. 751, 141718 https://doi.org/10.1016/j.scitotenv.2020.141718.
Xiong, Y., Mason, O.U., Lowe, A., Zhou, C., Chen, G., Tang, Y., 2019. Microbial community analysis provides insights into the effects of tetrahydrofuran on 1,4-dioxane biodegradation. Appl. Environ. Microbiol. 85, e00244-19 https://doi.org/10.1128/AEM.00244-19.
Xu, M., Wang, F., Sheng, H., Stedtfeld, R.D., Li, Z., Hashsham, S.A., Jiang, X., Tiedje, J. M., 2021. Does anaerobic condition play a more positive role in dissipation of antibiotic resistance genes in soil? Sci. Total Environ. 757, 143737 https://doi.org/10.1016/j.scitotenv.2020.143737.
Yavitt, J.B., Roco, C.A., Debenport, S.J., Barnett, S.E., Shapleigh, J.P., 2021. Community organization and metagenomics of bacterial assemblages across local scale pH gradients in northern forest soils. Microb. Ecol. 81, 758–769. https://doi.org/10.1007/s00248-020-01613-7.
Yu, W.-H., Chin, T.-S., Lai, H.-T., 2013. Detection of nitrofurans and their metabolites in pond water and sediments by liquid chromatography (LC)-photodiode array detection and LC-ion spray tandem mass spectrometry. Int. Biodeterior. Biodegrad. 85, 517–526. https://doi.org/10.1016/j.ibiod.2013.03.015.
Yuan, G., Zhu, Z., Yang, P., Lu, S., Liu, H., Liu, W., Liu, G., 2020. Simultaneous determination of eight nitrofuran residues in shellfish and fish using ultra-high performance liquid chromatography–tandem mass spectrometry. J. Food Compos. Anal. 92, 103540 https://doi.org/10.1016/j.jfca.2020.103540.
Yue, W., Yin, C.-F., Sun, L., Zhang, J., Xu, Y., Zhou, N.-Y., 2021. Biodegradation of bisphenol-A polycarbonate plastic by *Pseudoxanthomonas* sp. strain NyZ600. J. Hazard Mater. 416, 125775 https://doi.org/10.1016/j.jhazmat.2021.125775.
Zainab, S.M., Junaid, M., Xu, N., Malik, R.N., 2020. Antibiotics and antibiotic resistant genes (ARGs) in groundwater: a global review on dissemination, sources, interactions, environmental and human health risks. Water Res. 187, 116455 https://doi.org/10.1016/j.watres.2020.116455.
Zdarta, A., Smułek, W., Bielan, Z., Zdarta, J., Nguyen, L.N., Zgoła-Grześkowiak, A., Nghiem, L.D., Jesionowski, T., Kaczorek, E., 2021. Significance of the presence of antibiotics on the microbial consortium in wastewater – the case of nitrofurantoin and furazolidone. Bioresour. Technol. 339, 125577 https://doi.org/10.1016/j.biortech.2021.125577.
Zhang, B., Xu, X., Zhu, L., 2018. Activated sludge bacterial communities of typical wastewater treatment plants: distinct genera identification and metabolic potential differential analysis. Amb. Express 8, 184. https://doi.org/10.1186/s13568-018-0714-0.
Zhang, W., Li, J., Zhang, Y., Wu, X., Zhou, Z., Huang, Y., Zhao, Y., Mishra, S., Bhatt, P., Chen, S., 2022. Characterization of a novel glyphosate-degrading bacterial species, *Chryseobacterium* sp. Y16C, and evaluation of its effects on microbial communities in glyphosate-contaminated soil. J. Hazard Mater. 432, 128689 https://doi.org/10.1016/j.jhazmat.2022.128689.
Zhu, T., Su, Z., Lai, W., Zhang, Y., Liu, Y., 2021. Insights into the fate and removal of antibiotics and antibiotic resistance genes using biological wastewater treatment technology. Sci. Total Environ. 776, 145906 https://doi.org/10.1016/j.scitotenv.2021.145906.

Supplementary information (P3)

SUPPLEMENTARY MATERIAL

Dynamics of microbial communities during biotransformation of nitrofurantoin

Submitted to

Environmental Research

By

Amanda Pacholak[a], Agnieszka Zgoła-Grześkowiak[b], Ewa Kaczorek[a]

[a] Institute of Chemical Technology and Engineering, Poznan University of Technology, Poland

[b] Institute of Chemistry and Technical Electrochemistry, Poznan University of Technology, Poland

* Corresponding author:

Email: amanda.pacholak@put.poznan.pl

Phone: +48 61 665 3686

S1. Procedure of NFT metabolites derivatization

1 mL of 0.1 M HCl and 0.1 mL of 100 mM 2-nitrobenzaldehyde (NBA) methanol solution were added to 1 mL of the collected sample. The samples were mixed for 5 min and incubated at 37°C for 16 hours. Then they were cooled to RT and 0.5 mL of 0.2 M Na_2HPO_4 and 0.1 mL of 1 M NaOH were added. The samples were then extracted twice with ethyl acetate following which the solvent was evaporated using a steady stream of nitrogen gas. The dry residues were redissolved in 1 mL of 40% HPLC grade methanol and analyzed by LC-MS/MS.

S2. Procedure of liquid chromatography-mass spectrometry

Primary biodegradation and identification of degradation products were performed using a chromatographic system UltiMate 3000 HPLC (Dionex, Sunnyvale, CA, USA) coupled with a 4000 QTRAP mass spectrometer manufactured by ABSciex (Foster City, CA, USA). 5 µL samples were injected into a column Gemini-NX C18 (100 mm × 2.0 mm I.D.; 3 µm) purchased from Phenomenex (Torrance, CA, USA) maintained at 35°C. The mobile phase consisted of 5 mM ammonium acetate in water and methanol at a flow rate of 0.3 mL · min^{-1} in two different elution gradients, depending on the analysis performed. Gradient elution for NFT biodegradation was performed by linearly increasing methanol percentage from 75% to 80% in 2 min, and then linearly increasing the percentage to 100% in 1 min. Methanol gradient elution for detection of derivatized NFT transformation products was as follows: 1 minute 30%, then in 4 minutes increase to 100%, and the phase composition was maintained for another 2 minutes. The electrospray (ESI) ion source operated in positive and negative modes. Nitrogen was used in both the source and the mass spectrometer. The following parameters of the ESI source and mass spectrometer were used: curtain gas pressure 10 psi, nebulization gas pressure 40 psi, auxiliary gas pressure 45 psi, source temperature 450°C, ESI voltage ±4500 V. Chromatograms were collected in the MRM mode and enhanced product ion mode in a 50 – 500 m/z range. Selected ions were fragmented in the enhanced product ion mode. The detected and confirmed mass transitions and specific parameters of each analyte are summarised in Table S1.

Table S1. Parameters of mass spectrometric detection characteristic of the analytes

Analyte	Parent ion	DP[a] [V]	Multiple reaction monitoring transitions					
			Analytical	CE[b] [eV]	CXP[c] [V]	Confirmatory	CE [eV]	CXP [V]
NFT	$[M-H]^-$	-60	237 → 152	-17	-10	237 → 124	-20	-10
NBA-AHD	$[M+H]^+$	70	249 → 134	18	7	249 → 178	22	10
NBA-SEM	$[M+H]^+$	40	209 → 166	14	9	209 → 192	17	11

DP[a] - declustering potential, CE[b] - collision energy, CXP[c] – collision cell exit potential

S3. Procedure of PCR amplification and sequencing

To evaluate the microbial community structure in the cultures, iTag sequencing of 16S rRNA genes was performed. In total, the microbial communities in 13 samples were analyzed. Bacterial V3-V4 16S rDNA regions were amplified from 2.5 µL of DNA samples diluted to 5 ng μL^{-1} using the following primers:

341F:5' **TCGTCGGCAGCGTCAGATGTGTATAAGAGACAG**CCTACGGGNGGCWGCAG,

785R:5' **GTCTCGTGGGCTCGGAGATGTGTATAAGAGACAG**GACTACHVGGGTATCTAATCC.

The primers contain Illumina adaptor sequence (bold) and V3-V4 16S rRNA locus-specific sequence. All steps including amplification, indexing and library quantification were performed according to the protocol provided by Illumina "16S Metagenomic Sequencing Library Preparation" with one modification: Q5 High-Fidelity Polymerase (New England Biolabs) was used. Next Generation Sequencing was performed using the Illumina MiSeq System in 2 x 300 PE (paired ends) mode. Quality filtering of the reads and classification to the species level was performed using the QIIME package according to the GreenGenes (v.13_8) reference database.

16S V3 and V4 Amplicon Workflow is presented in figure S1.

The components of amplicon PCR [in square brackets volume used for 1 reaction is indicated]:

- Microbial DNA (5 ng/µl) [2.5 µl]
- Amplicon PCR Forvard Primer 1 µM [5 µl]

- Amplicon PCR Reverse Primer 1 µM [5 µl]
- 2 x KAPA HiFi HotStart Ready Mix [12.5 µl]

The PCR program details:

- 95°C for 3 minutes
- 25 cycles of:
    - — 95°C for 30 seconds
    - — 55°C for 30 seconds
    - — 72°C for 30 seconds
- 72°C for 5 minutes
- Hold at 4°C

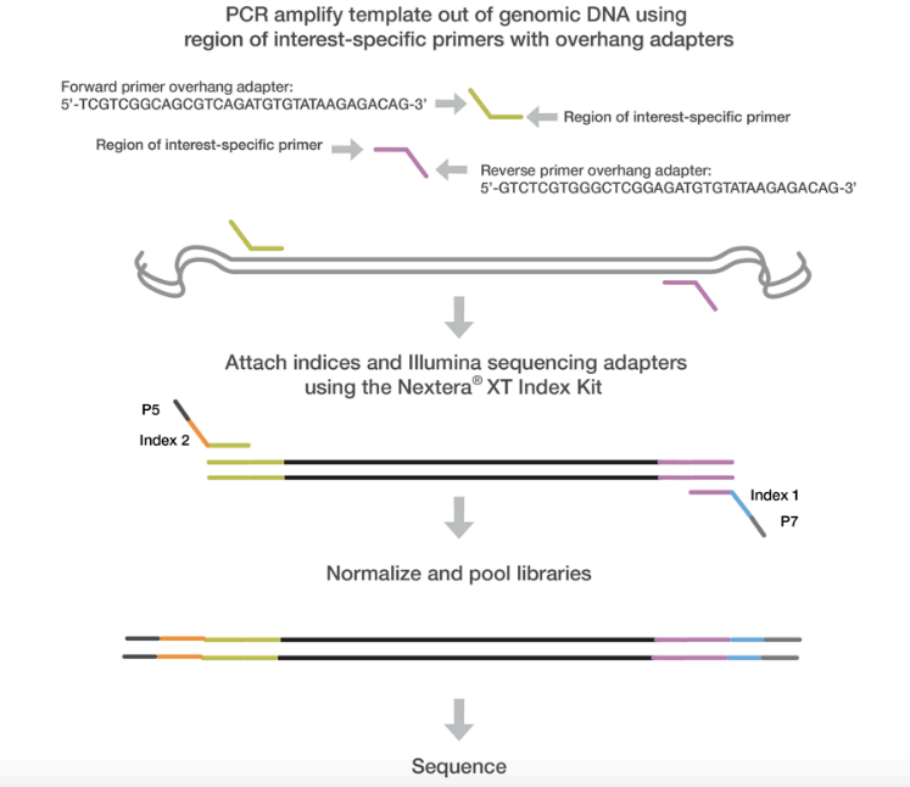

Figure S1. 16S V3 and V4 Amplicon Workflow

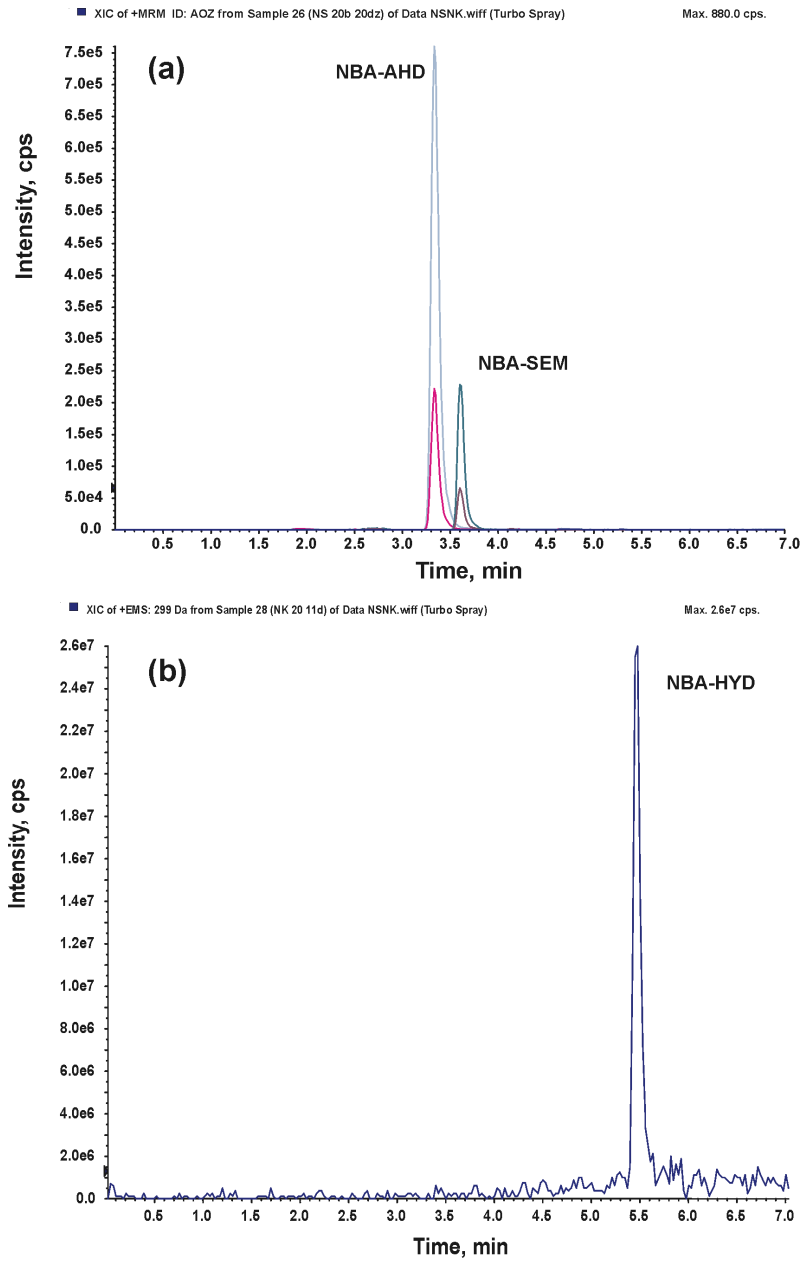

Figure S2 – Typical chromatograms of the derivatized degradation products. (a) 1-aminohydantoin and semicarbazide multiple reaction monitoring chromatogram, (b) hydrazine extracted from the enhanced mass spectra chromatogram.

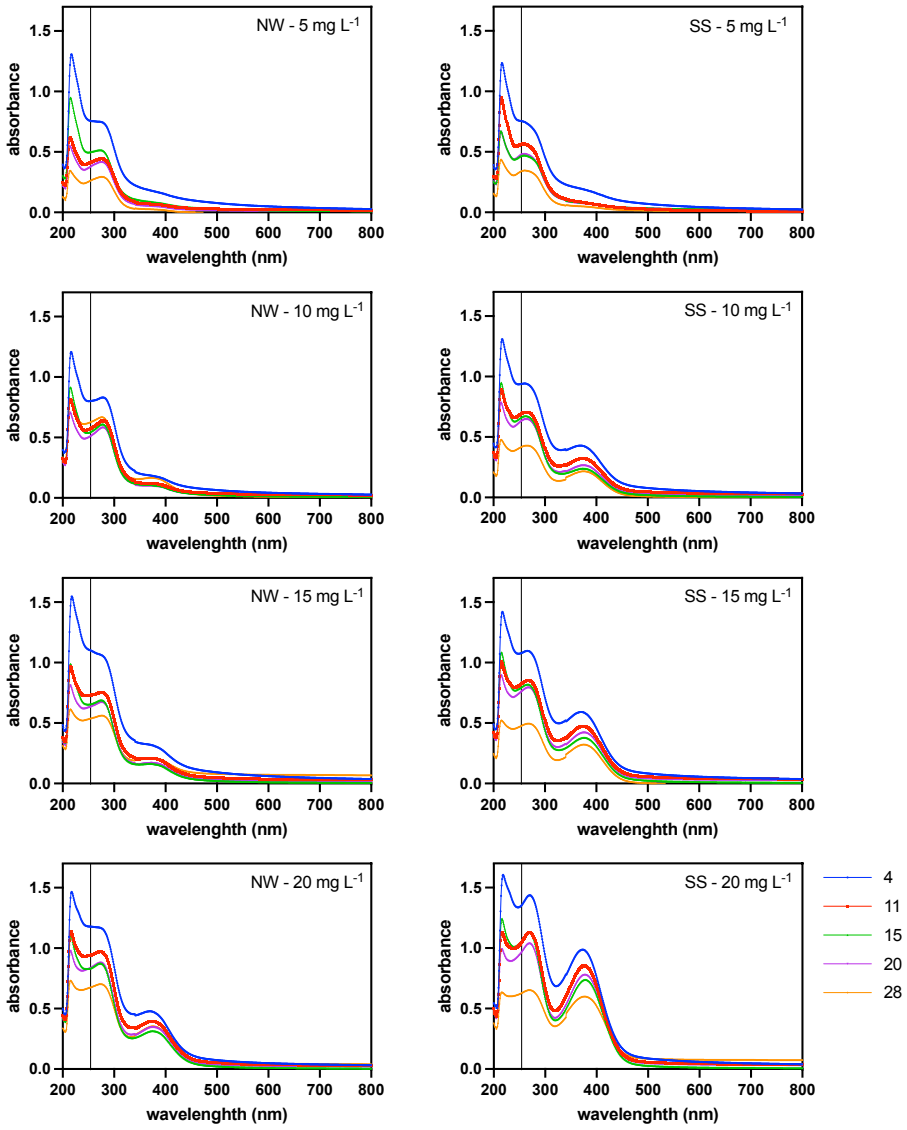

Figure S3 – UV-Vis Spectra of the culture medium during biodegradation experiments at four initial concentrations of NFT: 5, 10, 15 and 20 mg L-1. Mountain stream water sample (NW) represents the bacterial community collected from the protected area with no human intervention. Seaport water sample (SS) represents the bacterial community collected from the seaport area that receives numerous contaminants. Different colors and numbers (2, 4, 11, 20, and 28) indicate the sample collection days.

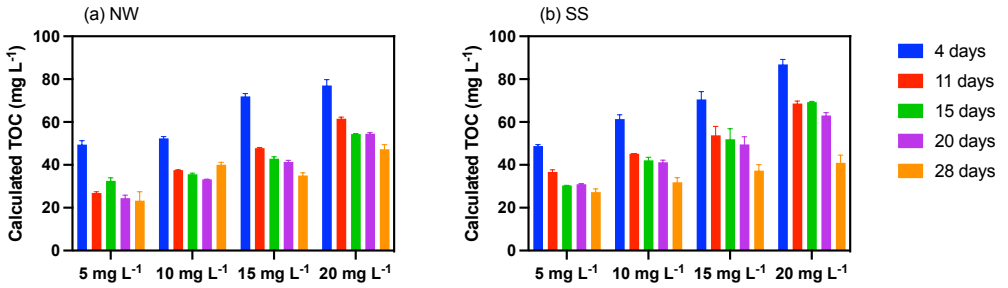

Figure S4 – TOC concentration calculated based on the UV_{254} absorption of the culture medium of biodegradation experiments at four initial concentrations of NFT: 5, 10, 15 and 20 mg L^{-1}. Mountain stream water sample (NW) represents the bacterial community collected from the protected area with no human intervention. Seaport water sample (SS) represents the bacterial community collected from the seaport area that receives numerous contaminants. Different colors and numbers (2, 4, 11, 20, and 28) indicate the sample collection days.

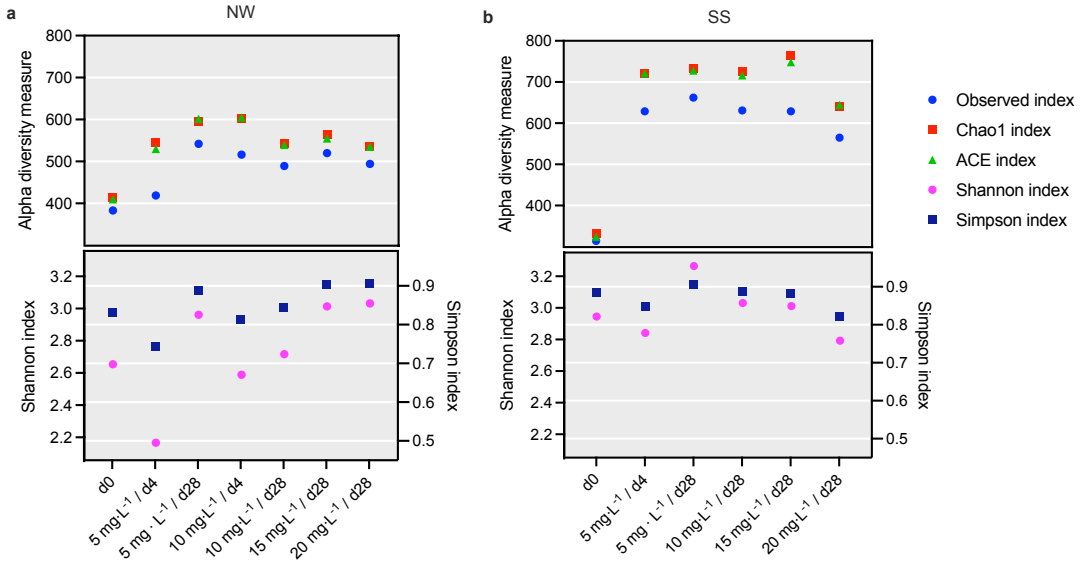

Figure S5 – Alpha diversity indices of two bacterial communities treated with NFT at a concentration of 5, 10, 15 and 20 mg L^{-1}. NW represents the bacterial community collected from the mountain stream, the protected area with no human intervention. SS represents the bacterial community collected from the seaport area that receives numerous contaminants.

Publication P4

Science of the Total Environment 872 (2023) 162199

Contents lists available at ScienceDirect

Science of the Total Environment

journal homepage: www.elsevier.com/locate/scitotenv

Potential negative effect of long-term exposure to nitrofurans on bacteria isolated from wastewater

Amanda Pacholak [a,*], Joanna Żur-Pińska [b,c], Artur Piński [c], Quynh Anh Nguyen [d], Marta Ligaj [e], Magdalena Luczak [f], Long D. Nghiem [d], Ewa Kaczorek [a]

[a] Institute of Chemical Technology and Engineering, Poznan University of Technology, Poland
[b] Biotechnology Centre, The Silesian University of Technology, Gliwice, Poland
[c] Institute of Biology, Biotechnology and Environmental Protection, Faculty of Natural Sciences, University of Silesia in Katowice, Poland
[d] Centre for Technology in Water and Wastewater, School of Civil and Environmental Engineering, University of Technology Sydney, New South Wales, Australia
[e] Department of Non-Food Products Quality and Packaging Development, Institute of Quality Science, Poznan University of Economics and Business, Poland
[f] Institute of Bioorganic Chemistry, Polish Academy of Sciences, Poznan, Poland

HIGHLIGHTS

- Whole genome sequencing was used to characterize bacteria isolated from wastewater.
- Exposure to nitrofurans altered metabolomic characteristics of the strains.
- Metabolomic analysis revealed 184 differentially accumulated metabolites.
- Electrochemical analysis showed DNA damage and possible mutagenesis.
- Protein disruption and cellular oxidative stress were observed.

GRAPHICAL ABSTRACT

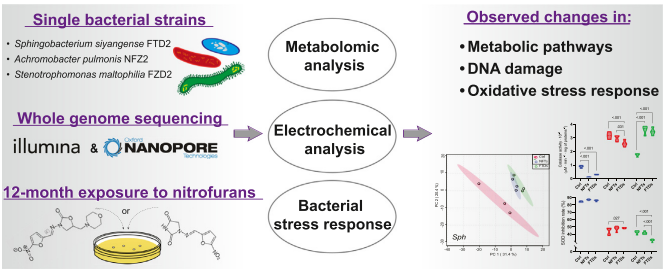

ARTICLE INFO

Editor: Dimitra A Lambropoulou

Keywords:
Enzymatic activity
Metabolomic profile
Nitrofuran exposure
Oxidative DNA damage
Whole genome sequencing

ABSTRACT

Nitrofurans are broad-spectrum bactericidal agents used in a large quantity for veterinary and human therapy. This study reports the long-term impact of two nitrofuran representatives, nitrofurantoin (NFT) and furaltadone (FTD) on the bacterial strains *Sphingobacterium siyangense* FTD2, *Achromobacter pulmonis* NFZ2, and *Stenotrophomonas maltophilia* FZD2, isolated from a full-scale wastewater treatment plant. Bacterial whole genome sequencing was used for preliminary strains characterization. The metabolomic, electrochemical, and culture methods were applied to understand changes in the bacterial strains after 12-month exposure to nitrofurans. The most significantly altered metabolic pathways were observed in amino acid and sugar metabolism, and aminoacyl-tRNA biosynthesis. Disrupted protein biosynthesis was measured in all strains treated with antibiotics. Prolonged exposure to NFT and FTD also triggered mutagenic effects, affected metabolic activity, and facilitated oxidative stress within the cells. Nitrofuran-induced oxidative stress was evidenced from an elevated activity of catalase and glutathione S-transferases. NFT and FTD elicited similar but not identical responses in all analyzed strains. The results obtained in this study provide new insights into the potential risks of the prolonged presence of antimicrobial compounds in the environment and contribute to a better understanding of the possible impacts of nitrofuran antibiotics on the bacterial cells.

* Corresponding author.
E-mail address: amanda.pacholak@put.poznan.pl (A. Pacholak).

http://dx.doi.org/10.1016/j.scitotenv.2023.162199
Received 26 September 2022; Received in revised form 25 January 2023; Accepted 8 February 2023
Available online 13 February 2023

1. Introduction

Industrial chemicals have contributed significantly to economic development and living standards of the modern world. Not surprisingly, many of them are ubiquitous in wastewater and wastewater-impacted water bodies, at a trace level of up to a few $\mu g \cdot L^{-1}$ (Luo et al., 2014; Tran et al., 2019). At a sufficiently high level, they present notable human health and ecological concerns. Examples include endocrine disrupting effect caused by synthetic hormones and several other industrial chemicals (Giulivo et al., 2016). In particular, their impact on the microbial community can be significant, although, to date, it has only been examined in a very few studies (Rodríguez et al., 2018).

Conventional cultivation-dependent microbiological methods have recently been complemented with powerful multi-omics approaches and other modern analytical techniques such as microscopy, electrochemistry, mass spectrometry and bioinformatics (Gutleben et al., 2018). Omics technologies allow for comprehensive analysis of the cells' complete genetic or molecular profiles (Palazzotto and Weber, 2018), while bioinformatics can be used to develop genomic and proteomic databases for better understanding of the detailed microbial components and their functions (Bansal, 2005).

Combining novel and conventional methods enables us to better characterize the bacterial species and describe their responses to a changing environment (Marx, 2017; Vilanova and Porcar, 2016). The application of various complementary methods may prove helpful for the prediction of the effect of environmental pollution on natural bacterial habitats and improve our understanding of the consequences of anthropogenic processes on the natural environment.

Excessive consumption of antibiotics (over 100,000 tons per annum) has contributed to a heightened risk of environmental pollution. Their presence in the natural environment promotes the spreading of antibiotic resistance by bacteria. Recently, antibiotic resistance genes have been found in various natural environments using information extracted from multi-omics data (Gutleben et al., 2018; Nguyen et al., 2021). Antimicrobial resistance is not the only concern regarding the pollution of ecosystems with antibiotics. The presence of antimicrobial compounds in the environment may result in ecological toxicity and disturb the balance of the microbial ecosystem. It accelerates, among others, oxidative damage within microbial cells (Chen et al., 2019). Oxidative stress occurs through excessive reactive oxygen species (ROS) formation by partial reduction of oxygen. Oxidative damage can have a destructive effect on proteins, nucleic acids, cellular components, and processes, disrupting normal physiology and leading to cell death. The reduction of oxidative stress in the cells can be achieved by producing enzymes (e.g. catalases, superoxide dismutase, peroxiredoxins) that react with ROS and neutralize them into harmless products (Ezraty et al., 2017).

Nitrofurans (5-NFs) are broad-spectrum, bactericidal antibiotics used to treat urinary tract infections caused by Gram-negative pathogens. Nitrofurans include nitrofurantoin (NFT), furaltadone (FTD), nitrofurazone, furazolidone and many other compounds that contain a 5-nitrofuran ring. They have been used in livestock husbandry since the 1940s, but this practice is now prohibited in many countries due to potential carcinogenic properties of some nitrofurans (Kokulnathan and Chen, 2020). The alleged excessive misuse and the illegal application in husbandry contribute to the continuous release of nitrofurans into the natural environment, which may negatively affect all living organisms (Zhang et al., 2019). Nitrofurans are among the few antibiotic groups whose environmental impact is not sufficiently understood, and data on their concentration in the environment is limited.

To address the above identified gap, two representatives of nitrofurans, specifically NFT and FTD, were investigated in terms of their long-term influence on the bacterial strains. The bacteria used in this study were isolated from the municipal activated sludge and exposed to 5-NFs for 12 months as reported previously (Pacholak et al., 2020a). The strains used in this study were characterized by high tolerance and showed relatively good growth in the presence of 5-NFs. These species have been found in many environmental compartments, and some of them have shown the potential application in the bioremediation of anthropogenic contaminants (Ahmad et al., 2018; Gao et al., 2014; Xiong et al., 2020). Our previous results have proven that prolonged exposure of the strains to NFT and FTD causes significant modifications of the bacterial cell wall which may contribute to natural ecosystem imbalance (Pacholak et al., 2020a). This was the basis for a deeper investigation of nitrofurans impact towards these environmental species. Consequently, experimental work was carried out to support two hypotheses: (H1) Prolonged exposure of bacterial strains isolated from wastewater to nitrofuran antibiotics leads to significant alterations of cell metabolism; and (H2) the effect can be compound specific. Genomic analysis of the strains served as the basis of their further investigation of underlying genetic aspects of response to nitrofurans. To verify the hypotheses, this study applied a combination of molecular biology, electrochemical, and culture methods to functionally analyze the bacteria subjected to prolonged exposure to 5-NFs. Metabolomics analysis was used to analyze selective metabolites in cell extracts. This study aimed to reveal the effects of 12-month continuous exposure of the strains to selected 5-NFs on DNA damage, metabolic activity, and stress response within the cells. The results provide new insights into the potential risks of the prolonged presence of antimicrobial compounds in the environment and provide some information on the possible impacts of 5-NFs on the bacterial cells.

2. Materials and methods

2.1. Chemicals, bacterial strains, and growth conditions

All chemicals were of analytical grade and purchased from Merck (Darmstadt, Germany) unless stated otherwise. They were used without any further purification. Microbiological media were from bioMérieux (Warsaw, Poland). Loading buffer for agarose electrophoresis was from A&A Biotechnology (Gdynia, Poland), SYBR™ Gold Nucleic Acid Gel Stain from Thermo Fisher Scientific (Waltham, MA, USA), and Nova 100 bp DNA ladder from Novazym (Poznan, Poland). Ultra-purified Milli-Q water (Arium® Pro, Sartorius, Kostrzyn Wlkp., Poland) was used to prepare all solutions in this study. The glassware was autoclaved before use. Non-autoclavable solutions were filter-sterilized (0.22 μm) using Captiva EconoFilters from Agilent (Santa Clara, CA, USA).

Three bacterial strains, namely *Sphingobacterium siyangense* FTD2 (hereafter referred to as *Sph*, NCBI accession number: CP080574), *Achromobacter pulmonis* NFZ2 (*Acb*, JAIFOT010000000), and *Stenotrophomonas maltophilia* FZD2 (*Stm*, CP080573) were isolated from the municipal wastewater treatment plant in Poznan (Poland) using a previously described protocol (Pacholak et al., 2020a). These strains were continuously cultivated in the presence of either NFT or FTD ($20\ mg \cdot L^{-1}$) for 12 months to induce long-term stress response. Cultures of these bacteria without any NFT and FTD were also maintained as the control. Media composition, cultures components and growing conditions were described previously (Pacholak et al., 2020a).

2.2. DNA isolation

DNA was extracted using the GenElute® Bacterial DNA extraction kit from Merck (Darmstadt, Germany). The purity and concentration of DNA extracted from the bacterial cells were determined by spectrophotometry using a NanoDrop OneC (Thermo Fisher Scientific, Waltham, MA, USA). DNA was subjected to electrophoresis (Biometra Compact XS/S, Analytik Jena, Jena, Germany) in 1 % agarose gel in TAE buffer (40 mM Tris-acetate, 1 mM EDTA, pH 8.3). The gel was stained with the SYBR Gold Nucleic Acid Gel Stain, and DNA was visualized by scanning gels on Biorad Gel Doc XR Imaging System (Bio-Rad Laboratories, Hercules, CA, USA).

Quality of DNA samples was confirmed by spectrophotometry before any further analysis (sequencing and electrochemical analysis). DNA concentration was measured at 260 nm using a Multiskan 152 Sky Microplate Spectrophotometer (Thermo Fisher Scientific, Waltham, MA, USA)

according to the Lambert–Beer law. DNA purity was evaluated at 230, 260, and 280 nm. The ratios of 260/280 and 260/230 were 1.81 ± 0.04 and 2.1 ± 0.07, respectively. These are within the expected range of pure DNA.

2.3. Bacterial genome sequencing

The genomic libraries were prepared according to the standard protocol implemented by Genomed (Warsaw, Poland). The genomic DNA was fragmented using Covaris E210 ultrasonicator (Covaris, Woburn, MA, USA), and libraries for Illumina were prepared using NEBNext Ultra II DNA Library Prep Kit for Illumina (New England Biolabs, Ipswich, MA, USA) while for MinION (OxfordNanopore, Oxford, Great Britain) using Ligation Sequencing Kit 1D (SQK-LSK108). Sequencing was conducted on MinION equipment and SpotON Flow Cell Mk I (R9.4) plates. For pair-end MiSeq sequencing, MiSeq Reagent Kit v3 (Illumina, San Diego, CA, USA) was utilized according to the manufacturer's protocol. The reads from MiSeq were filtered with Cutadapt (version 3.0) (Martin, 2011) while assessment of sequencing quality was performed by FastQC. For analysis of the MinION data Guppy toolkit (version 4.0.15) was used (Ueno et al., 2003). Finally, de novo assembly was performed with the Unicycler program (version 0.4.7) (Wick et al., 2017). The sequencing results were deposited in National Center for Biotechnology Information (NCBI) database under PRJNA752031 BioProject. The assessment of genomic data quality was performed with BUSCO (version 5.3.2) (Manni et al., 2021).

2.4. Phylogenetic analysis and secondary metabolite gene clusters prediction

Phylogenetic trees were constructed by extracting and aligning the core proteomes of isolated strains and type strains using M1CR0B1AL1Z3R (Avram et al., 2020). Poorly aligned regions were removed using Gblocks (version 0.91b) (Talavera and Castresana, 2007). A maximum-likelihood phylogenetic tree was inferred using MEGA (version 10.2.6) (Kumar et al., 2018) using the Jones-Taylor-Thornton matrix-based model (Jones et al., 1992) and 1000 bootstraps. To predict biosynthetic gene clusters for secondary metabolite synthesis Antibiotic and Secondary Metabolite Analysis Shell (antiSMASH) version 6.1.1 was utilized (Blin et al., 2019, 2017). The functional analysis of sequenced genomes was performed with EggNOG-mapper (version 2.1.7) (Huerta-Cepas et al., 2019).

2.5. Bacterial response to prolonged exposure to antibiotics

2.5.1. Metabolomic analysis

The cells from 48-hour liquid cultures were rinsed twice with sterile Dulbecco's phosphate-buffered saline, centrifuged for 10 min (3000*g* at 4 °C) using an Eppendorf 5910R Centrifuge, and resuspended in the buffer to adjust the optical density at 600 nm to 2.0 ± 0.1 using Multiskan 152 Sky Microplate Spectrophotometer (Thermo Fisher Scientific, Waltham, MA, USA). 5 mL of the cell suspensions were rinsed once with cold water and resuspended in 2 mL of fresh portion of cold water. Such prepared bacterial suspensions were used for cell disintegration. Sonication was performed on the Ultrasonic Homogenizer (Sonoplus HD 3100, Bandelin, Germany), using the following settings: power 75 W, 5 s ON/5 s OFF pulses, +4 °C water bath. The total sonication time was 5 min 20 s. Next, 1 mL of each cell suspension was extracted with 4 mL of methanol. The samples were vortexed for 5 min, sonicated for 10 min and precipitated at −20 °C for 60 min. Then they were centrifuged for 10 min at 10,000*g*, and 700 μL of supernatant was transferred into the new tubes and evaporated. The dried extracts were derivatized with 50 μL of methoxyamine hydrochloride in pyridine (20 mg·mL^{-1}) at 37 °C for 90 min with agitation (950 rpm). Next, 80 μL of MSTFA was added and the mixtures were incubated at 37 °C for 30 min with agitation (950 rpm). Samples were centrifuged (10 min, 10,000*g*) and analyzed by gas chromatography mass spectrometry (GC/MS) in splitless mode (1 μL injection). Each sample was prepared in two technical replicates. Quality control (QC) samples were prepared by mixing 10 μL of each sample together. One QC sample was injected every 5 samples.

The GC/MS analysis was performed using TRACE 1310 Gas Chromatograph (Thermo Fisher Scientific, Waltham, MA, USA) coupled with TSQ8000 Mass Spectrometer (Thermo Fisher Scientific, Waltham, MA, USA). In-source fragmentation was performed with 70 eV energy. Mass spectra were recorded in the mass range 35–1000 *m/z*. All spectra were subjected to automatic peak detection, deconvolution, retention index calculation and library search by MSDial software, version 4.60. The obtained profiles were normalized by the LOESS algorithm using QC samples in MSDial. The alkane series mixture (C-11 to C-33) was used to correct retention time and to determine the retention index for each compound.

2.5.2. Detection of DNA damage

Electrochemical measurements were performed using the potentiostat PGSTAT12 with GPES version 4.9 software (Eco Chemie, Utrecht, the Netherlands) and a three-electrode system consisting of a carbon paste working electrode (CPE), Ag/AgCl (3 M KCl) reference electrode, and a platinum wire counter electrode. The CPE (1 mm diameter) was made from carbon paste prepared by mixing the graphite powder with mineral oil at a ratio of 70:30 (*w*/*w*) using a method described previously (Ligaj et al., 2008). The surface of the working electrode was regenerated before use by removing the outer layer of carbon paste and polishing it to a smooth finish on a frosted glass microscope slide. After that, the CPE surface was pretreated by applying a potential of +1.7 V for 60 s in 0.05 M phosphate buffer with 0.01 M KCl (pH 7.0). For the electrochemical analysis of the genetic material damage, the electrodes were immersed for 2 min in a phosphate buffer containing DNA isolated from bacteria at a concentration of 10 μg·mL^{-1}, with the applied potential of +0.5 V. The measurements were carried out using the square wave voltammetry (SWV) with the parameters: step potential of 0.01 V, the amplitude of 0.04 V, frequency of 100 Hz, and volume of 80 μL.

To confirm genetic polymorphism occurring within the cells, random amplification of polymorphic DNA (RAPD-PCR) was performed. The detailed procedure is presented in Supplementary Information 1.

2.5.3. Bacterial stress response

Lipid peroxidation (LPX), the activity of superoxide dismutase (SOD), catalase (CAT), and glutathione S-transferases (GSTs) were measured to analyze the bacterial stress response to the prolonged exposure to NFT and FTD. LPX level, SOD, and CAT activities were quantified spectrophotometrically according to protocols adapted from Żur et al. (2021). GSTs activity was measured as described previously (Pacholak et al., 2020b) using a microplate reader (Multiskan 152 Sky Microplate Spectrophotometer, Thermo Fisher Scientific, Waltham, MA, USA). The procedure for relative metabolic activity is presented in Supplementary Information 1. To determine the level of LPX, SOD, and CAT activity, the liquid cultures were lysed by sonication, while the protein contents in the crude extracts were determined using the Bradford method. To measure GSTs activity, proteins were extracted using CelLytic™ B Plus Kit purchased from Merck and their concentration was determined by PierceTM BCA Protein Assay from Thermo Fisher Scientific.

2.6. Statistical and bioinformatics analysis

The results of the experiments are reported as the mean ± 95 % confidence interval calculated from at least three independent experiments (biological replicates). To analyze differences in the control and treated samples in electrochemical and biochemical experiments, GraphPad Prism (GraphPad Software, LLC, San Diego, CA, USA) was used. All data were normally distributed and had equal variances according to Shapiro-Wilk and Levene's tests. A statistical significance of differences between the means of the samples was determined by two-way ANOVA followed by Tukey's range test (the significance level of 5 %). Statistical analyzes of metabolomic profiles were performed using Perseus 1.6.15 (Cox and Mann, 2008) and MetaboAnalyst 5.0. (Xia et al., 2009) to identify differentially accumulated metabolites (DAMs). Quantitative spectral data were log transformed. Then, the significance of differences between groups was

estimated using either the two-sample *t*-test or one-way ANOVA. A *p*-value of <0.05 was considered statistically significant. Multivariate analyzes were carried out by untargeted principal component analysis (PCA), partial least squares discriminant analysis (PLS-DA), and hierarchical clustering. For hierarchical clustering and heat map visualization, the data were normalized to a *Z*-score. Functional analysis was performed utilizing MetaboAnalyst software and the KEGG database to determine the top canonical pathways and biological processes affected in each comparison. The cut-off value of the metabolic pathway impact was set to 0.5, and pathways with a value >0.5 were selected as the potential key metabolic pathways. There is no universal cut-off suitable for all analyses because different data generate different results. Therefore, in this study, significant changes are identified as metabolic pathways with $p < 0.05$ ($-\log10(p) > 1.3$) and pathways located in the top right region (pathway impact > 0.5) (Chong et al., 2019; Xia and Wishart, 2011). The graphs were created using GraphPad Prism (GraphPad Software, LLC, San Diego, CA, USA) and MetaboAnalyst software.

3. Results and discussion

3.1. Bacterial isolation and whole genome sequencing

In this study, three bacterial strains were isolated from wastewater collected from the municipal wastewater treatment plant. Phylogenetic analysis based on whole genome sequencing was used to identify the strains, namely *Sph*, *Acb*, and *Stm* (as described in Section 2.1). Phylogenetic trees constructed are presented in Supplementary Information 1, Fig. S1-1. Whole genome sequencing allowed for assembly of circular chromosomes for *Sph* and *Stm* and assembly of *Acb* genome into two contigs. The genomic data quality assessment performed using BUSCO shows high-quality completeness for all three sequenced genomes being 99.8 % for *Sph* and *Stm* and 99.7 % for *Acb* (Supplementary Information 2, Tab. 1). The genomes mining with antiSMASH revealed seven biosynthetic gene clusters in Sph, nine in *Acb*, and four in *Stm* (Supplementary Information 2, Tab. 2). No biosynthetic gene clusters were found to be common for all analyzed strains, with exception of aryl polyenes cluster, which is one of the most widespread family of bacterial biosynthetic gene clusters. Aryl polyenes are involved in various processes such as aggregation, adhesion to surfaces, and biofilm formation (Johnston et al., 2021). The functional analysis performed with the EggNOG-mapper of genes present in the genomes of analyzed strains was also performed (Supplementary Information 2, Tab. 3–6).

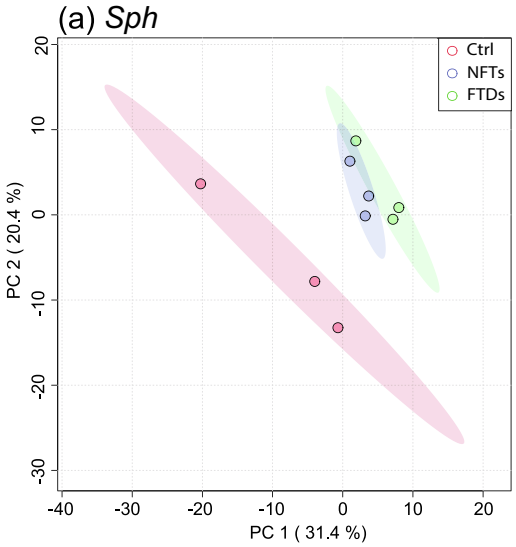

Fig. 1. PCA model comparing metabolomic profiles for *Sph* - *Sphingobacterium siyangense* FTD2 (a), *Acb* - *Achromobacter pulmonis* NFZ2 (b), and *Stm* - *Stenotrophomonas maltophilia* FZD2 (c) strains among three sample groups: Ctrl – control cells (red), NFTs/FTDs – cells exposed to nitrofurantoin (blue)/furaltadone (green). The percentage of variance is shown in parentheses on each axis. (For interpretation of the references to colour in this figure legend, the reader is referred to the web version of this article.)

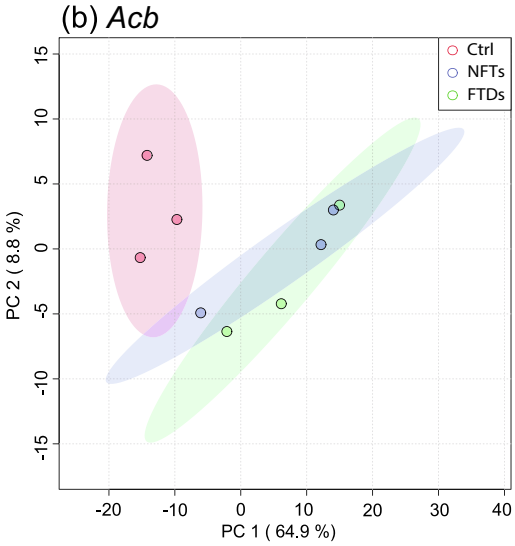

Fig. 1 (*continued*).

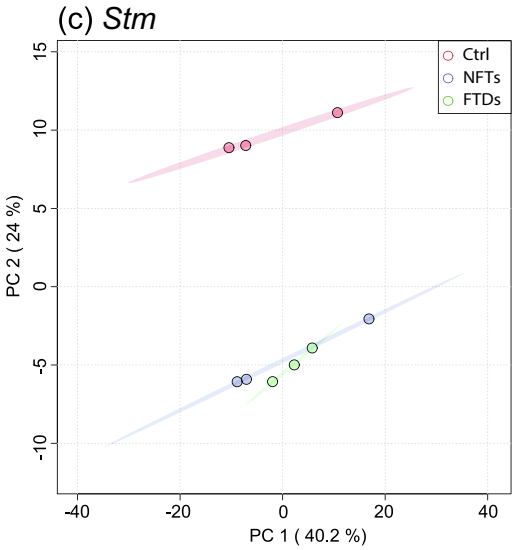

Fig. 1 (*continued*).

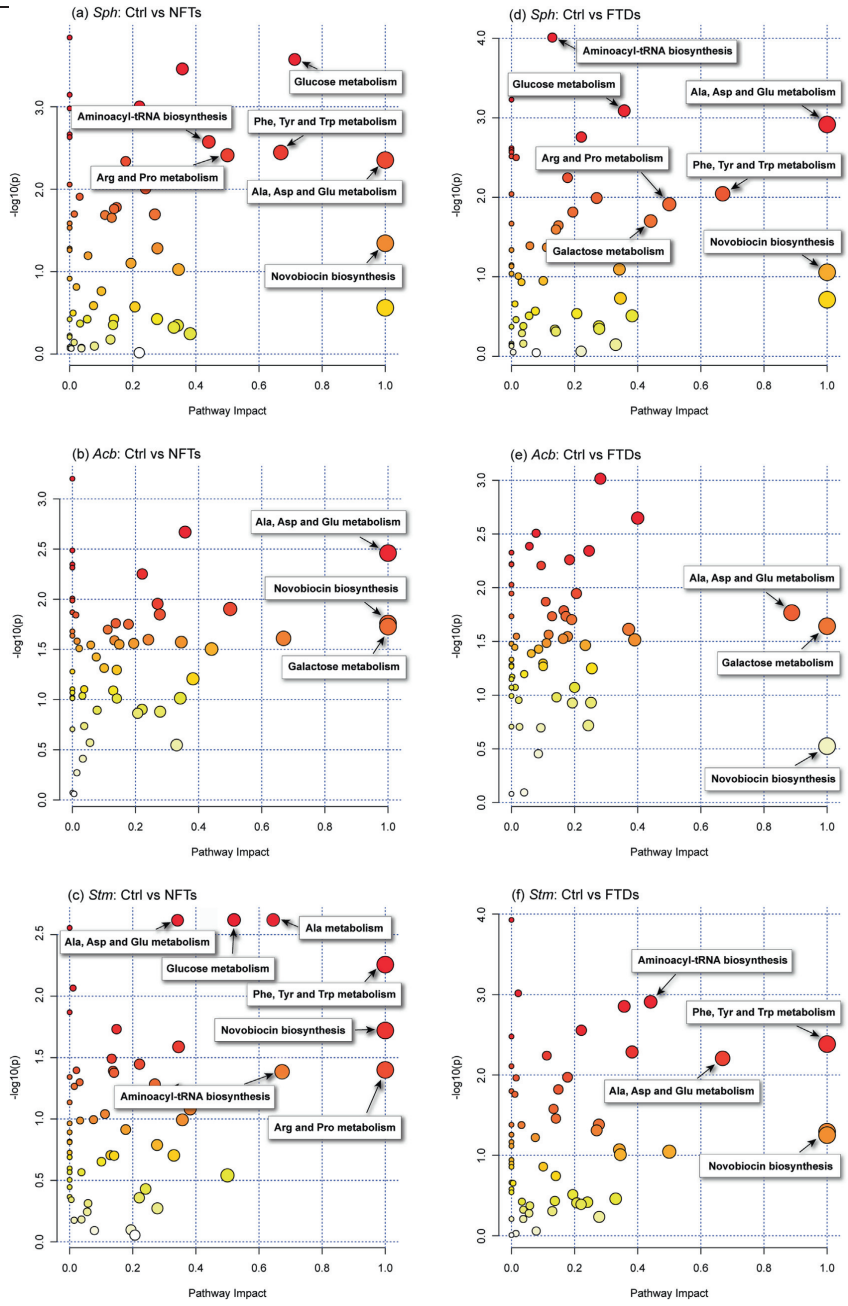

Fig. 2. Summary of the metabolic pathway analysis for *Sphingobacterium siyangense* FTD2 (*Sph*), *Achromobacter pulmonis* NFZ2 (*Acb*), and *Stenotrophomonas maltophilia* FZD2 (*Stm*) strains among three sample groups: Ctrl vs NFTs (a–c) and Ctrl vs FTDs (d–f). Ctrl – control cells, NFTs/FTDs – cells exposed to nitrofurantoin/furaltadone. The matched pathways are arranged by the pathway impact values on the x-axis and *p*-values on the y-axis. Darker red colour shows significant statistical difference while lighter yellow colour shows less significant statistical difference. The node radius represents pathway impact (the cumulative percentage of matched metabolites in each pathway), which is also shown in relative numerical scale from 0 to 1 in the horizontal axis. (For interpretation of the references to colour in this figure legend, the reader is referred to the web version of this article.)

The *Sph* strain belongs to the *Sphingobacterium siyangense* species (previously identified as *Sphingobacterium caeni*), for which only a few strains were isolated, SY1^{T} (=KCTC 22131T = CGMCC 1.6855T) from farm soil, PDNC006 from plastic debris and T12B17 from soil (Davis et al., 2019; Lee et al., 2013; Liu et al., 2008). The *Acb* strain was identified as *Achromobacter pulmonis* (previously identified as *Achromobacter xylosoxidans*), for which the genomes of three other strains were sequenced to date. The *A. pulmonis* strains LMG 26696 and LMG 26788 were isolated from sputum of cystic fibrosis patients, and the ANB-1 strain was isolated from soil contaminated by pesticides. The ANB-1 strain exhibits aniline degradation abilities (Davis et al., 2019; Vandamme et al., 2013). The *Stm* strain belongs to the *Stenotrophomonas maltophilia* species, which is a ubiquitous bacterium in water, soil, plant-associated habitats, animal tissues, and the human body. The *S. maltophilia* strains are known as degraders of various xenobiotics and are characterized by intrinsic resistance to various groups of antibiotics (Berg and Martinez, 2015; Pinski et al., 2020). Indeed, *Pseudomonas* species, which are closely phylogenetically related to *Stenotrophomonas* genus, are naturally resistant to NFT (Saati-Santamaría et al., 2021).

The significance of this study is justified by several factors. First, bacteria isolated from wastewater are good indicators to understand the effect of prolonged exposure to nitrofurans. These strains have been already employed in bioremediation and biodegradation studies. Antibiotics residues can affect bacterial cells and therefore it is important to understand the response of single strains to these chemicals.

3.2. Metabolomic profile

GC/MS analysis of metabolites showed a total of 1371 signals corresponding to the compounds in the mass range from 35 to 1000 Da. The PCA analysis was performed to understand the aggregation of the samples and the general metabolomic profile of each group (Fig. 1). In the PCA models derived from all three strains, the control samples clustered separately from both the FTDs and NFTs, indicating that they had strikingly different metabolomic characteristics. The most visible separation between the control and treated samples was found for the *Stm* strain (Fig. 1c) and the smallest separation was observed for the *Acb* strain (Fig. 1b). The samples exposed to NFT and FTD were ordinated closer to one another, eliciting a similar but not identical response in all analyzed strains.

Further analysis revealed 184 DAMs that differed significantly among the strains and the treatments. These metabolites were classified as amino acids and derivatives (27 compounds), long chain fatty acids (11), o-glycosyl compounds (6), fatty acids methyl esters (6), hexoses (5) and others (Supplementary Information 1, Fig. S1-2; Supplementary Information 2, Tab. 7 and 8). All DAMs were subjected to the functional bioinformatic analysis to investigate if certain pathways or processes are significantly different between the control and treated samples.

Fig. 2 shows significant impact of long-term nitrofuran exposure on metabolic pathways of the strains. The most significantly altered pathways were observed in amino acid (Ala, Asp, Glu, Phe, Tyr, Trp, Arg and Pro) metabolism, sugar (glucose, galactose) metabolism, aminoacyl-tRNA (aa-tRNA) biosynthesis and novobiocin biosynthesis. Asp and Glu metabolism was the only pathway observed in all three strains that was significantly affected by both NFT and FTD treatment. A total of eight metabolic pathways were identified as related to NFT-prolonged exposure. Seven pathways were detected in the *Stm* strain (Ctrl vs NFTs), five pathways in *Sph* and three in the *Acb* strain (Fig. 2). The common pathway of great importance for all strains that was impaired in response to NFT exposure was novobiocin biosynthesis. The most significant alteration was measured in the *Stm* strain, and least important alteration was found for *Sph*. A total of seven metabolic pathways were identified as related to FTD-prolonged exposure: all pathways were identified in the *Sph* strain, two in *Acb* and three in *Stm*. The smallest differences in the metabolic pathway analysis were noted for NFTs vs FTDs comparisons indicating that the bacterial response to the prolonged presence of these antibiotics was similar. A significant difference between NFT and FTD treatment were observed in *Acb* strain for Phe metabolism only.

Variations in concentration of differentially accumulated amino acids among three sample groups are shown in Fig. 3. Accumulation of most amino acids and derivatives significantly decreased in cells of all strains exposed to FTD and NFT except for Trp, Ile, DL-2,3-Diaminopropionic acid and 1-Amino-1-cyclopentanecarboxylic acid. In the *Sph* strain, Trp and DL-2,3-Diaminopropionic acid increased after both NFT and FTD exposure, Ile

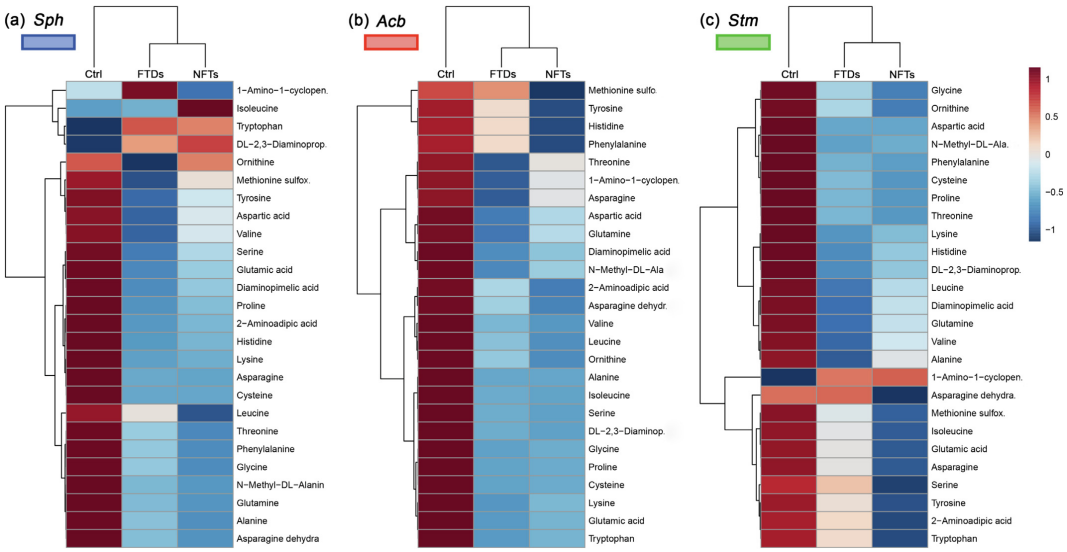

Fig. 3. Differences in abundance of differentially accumulated amino acids among three sample groups based on normalized intensity of the compounds. Ctrl – control cells, NFTs/FTDs – cells exposed to nitrofurantoin/furaltadone. *Sph* - *Sphingobacterium siyangense* FTD2 (a), *Acb* - *Achromobacter pulmonis* NFZ2 (b), *Stm* - *Stenotrophomonas maltophilia FZD2* (c). The scale bar represents normalized intensity of the compounds. A complete list of metabolites is presented in Supplementary Information 2, Table 7.

increased after treatment with NFT, and 1-Amino-1-cyclopentanecarboxylic acid increased in FTD-treated samples. The latter increased also in NFT- and FTD-exposed samples of the *Stm* strain. For the *Acb* strain cells, the lower accumulation of all protein-building amino acids was observed in response to both antibiotics.

Significantly decreased accumulation in response to prolonged exposure to both NFT and FTD in cells of all three strains was also noted for capric acid. Accumulation of some DAMs increased in the bacterial cells exposed to the examined antibiotics. For example, the level of dodecanol increased in response to prolonged exposure to NFT, and S-adenosyl-L-methionine increased in response to prolonged exposure to both NFT and FTD in cells of all three strains.

The most affected metabolites found in metabolomic analysis are components of biological pathways involved in amino-acid and sugar metabolism as well as aa-tRNA biosynthesis. It has been proposed that nitrofurantoin's mechanism of action is based on the ability to bind to ribosomes and inhibit the activity of enzymes involved in the synthesis of DNA and RNA, however, a detailed mode of antimicrobial action of 5-NFs is still unclear (Blass, 2015; Huttner et al., 2015). NFT was found to inhibit total protein synthesis by non-specific reaction with both ribosomal proteins and rRNA (McOsker and Fitzpatrick, 1994). A significant decline in the abundancy of protein-building amino acids in response to NFT and FTD was noted which is in agreements with the proposed mode of action of these antibiotics.

Aa-tRNAs are ubiquitous compounds responsible for delivering amino acids for protein synthesis at the ribosome. Aa-tRNAs are also involved in several other cellular processes such as protein biosynthesis, cell wall formation or cell envelope remodeling (Moutiez et al., 2017). In this study, several amino acids involved in aa-tRNAs biosynthesis were downregulated in response to NFT- or FTD-exposure. The largest number of downregulated amino acids was noted for the *Sph* strain in response to the NFT treatment. The smallest number of downregulated amino acids was found for the *Stm* strain in response to NFT treatment. The results of this research are consistent with those of our previous paper, which demonstrated that long-term exposure of cells to NFT causes stronger remodeling of the cells structure than FTD (Pacholak et al., 2020a). To the best of our knowledge, this is a first study to highlight the role of the aa-tRNA biosynthesis pathway in the bacterial response to nitrofuran antibiotics. Nevertheless, a recent study showed that aa-tRNA biosynthesis was one of the pathways that dominated in microbial communities residing in sediments collected from the estuaries of rivers in China with various degrees of chemical pollution (Lu et al., 2017).

Interesting results were also obtained for the metabolism of glutathione (GSH), a tripeptide which plays important role in bacterial redox-regulation and adaptation to stress in bacterial cells (Smirnova and Oktyabrsky, 2005). The metabolomic analysis showed eight compounds (amino acids, mono- and dialkylamines) involved in metabolism of GSH. These compounds include glycine, glutamic acid, cysteine, 5-oxoproline, spermidine, ornithine, putrescine, and cadaverine (Fig. 4). Exposure of all strains to NFT and FTD resulted in decreased accumulation of these metabolites. The most notable changes were noted for glycine and glutamic acid in the *Sph* and *Acb* strain. The fewest modifications were observed in the *Stm* strain.

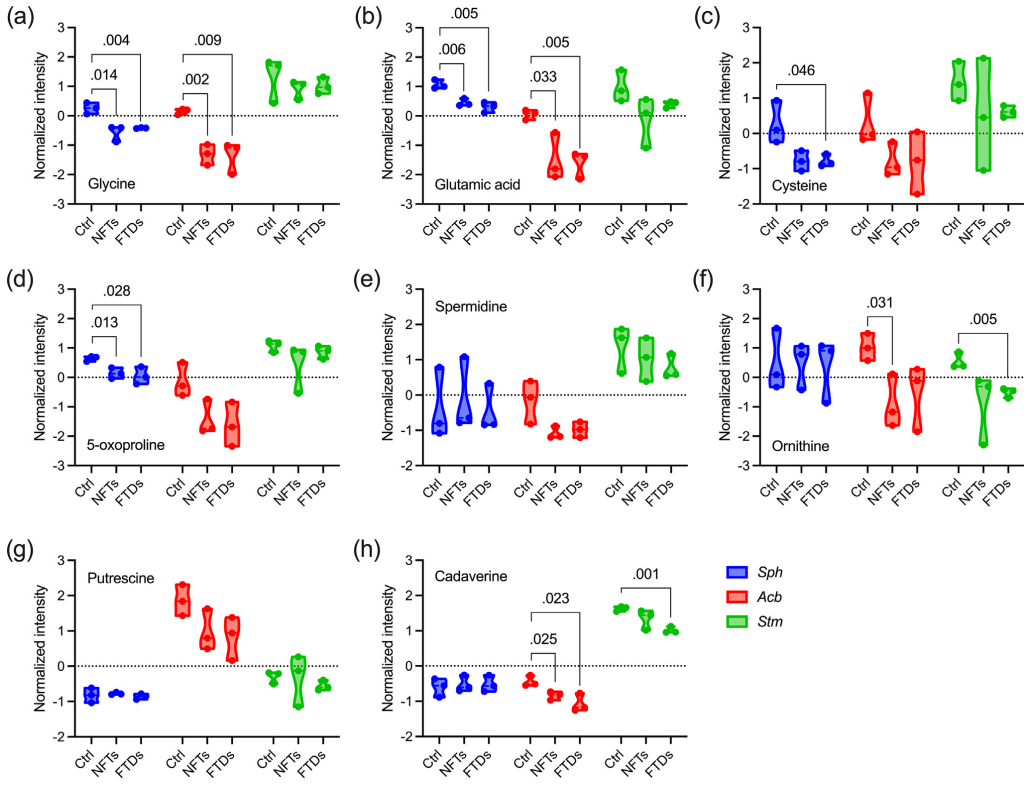

Fig. 4. Normalized intensity of peaks of the compounds involved in GSH metabolism. Ctrl – control cells, NFTs/FTDs – cells exposed to nitrofurantoin/furaltadone. *Sph* - *Sphingobacterium siyangense* FTD2, *Acb* - *Achromobacter pulmonis* NFZ2, *Stm* - *Stenotrophomonas maltophilia FZD2*.

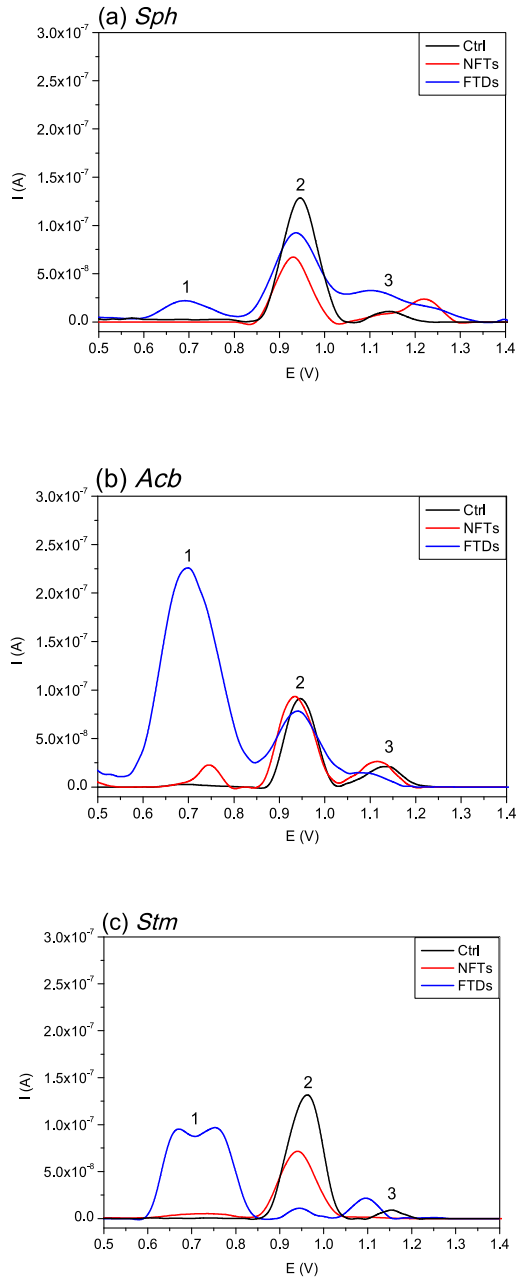

Fig. 5. Square wave voltammogram of DNA isolated from *Sph* - *Sphingobacterium siyangense* FTD2 (a), *Acb* - *Achromobacter pulmonis* NFZ2 (b), *Stm* – *Stenotrophomonas maltophilia* FZD2 (c). Ctrl – control cells, NFTs/FTDs – cells exposed to nitrofurantoin/furaltadone. Signals signs: 1 – 8-oxodG, 2 – guanine, 3 – adenine.

Significant changes in the accumulation of the compounds involved in GSH metabolism together with modified LPX, SOD, CAT, and GSTs (Section 3.4) reflect that bacterial exposure to 5-NFs decreases cell ability to cope with environmental stress. This was specifically visible in the *Sph* strain for which the strongest decline in the parameters in question were visible.

To further investigate the metabolomic characteristics of the strains and correlate these data with the genetic information provided by the whole genome sequencing, the KEGG analysis of the identified DAMs was performed. The pathways of GSH metabolism and aa-tRNA biosynthesis with the genes present in each strain and detected DAMs are summarized in Supplementary Information 1, Figs. S1-3 to S1-8. Five and six downregulated metabolites involved in the GSH metabolic pathway were revealed in the *Sph* and *Acb* strains. In the *Stm* strain, no DAMs were detected in response to NFT-prolonged exposure, and two DAMs were detected in response to FTD-prolonged exposure. The largest number of downregulated metabolites involved in the aa-tRNA pathway was detected in the *Sph* strain exposed to NFT, the smallest number was observed in the NFT-exposed *Stm* strain. Upregulated metabolites were not detected in both pathways.

3.3. Electrochemical detection of DNA damage

Fig. 5 shows the voltametric signals of nucleobases of DNA extracted from the bacterial cells. Under the measurement conditions applied, the 8-oxodG, guanine, and adenine signals were observed at the potential regions at +0.7 V (signal 1), +0.95 V (signal 2) and +1.15 V (signal 3). Out of all signals present in the voltammograms, the peaks coming from the nucleobases in question indicated the strength of guanine oxidation and the formation of 8-oxodG, which, represents 5-NFs long-term mutagenic effect on the genetic material. Fig. 5a shows the signals of nucleobases oxidation in DNA isolated from the *Sph* strain. The long-term exposure of the strain with NFT and FTD generated a significant reduction in the electric current of guanine. A loss of the guanine peak was accompanied by a strong signal appearance at +0.7 V in FTD-treated samples only. The results of voltametric analysis of DNA isolated from the *Acb* are shown in Fig. 5b. The long-term exposure with NFT and FTD generated a formation of signals at the potential region +0.7 V, indicating the presence of 8-oxodG (signal 1). The signal was more intense after treatment of the strains with FTD. The signal of adenine after treatment with FTD decreased while no change was observed in DNA extracted from NFT-treated cells of the *Acb* strain. FTD-treated samples of the *Stm* strain demonstrated a decreased guanine peak and two strong, distinct oxidation signals at potential maxima of approximately 0.65 V and 0.75 V, as exemplified in Fig. 5c. The adenine signal was shifted towards the lower potential, indicating breaking the hydrogen bonds between the nucleotide base pairs in double-stranded DNA. The samples exposed to NFT were also characterized by decreased guanine peak, but the signal was negligible due to its electrochemical oxidation. There was no adenine signal present. The changes in the DNA of the strains exposed to NFT or FTD were confirmed by RAPD-PCR as illustrated in Supplementary Information 1 (Fig. S1-9).

Electrochemical detection of DNA damage revealed 5-NFs long-term mutagenic effect on the bacterial strains investigated in this study. For all analyzed DNA samples, an increased width of guanine signals was observed, which indicates the breaking of some hydrogen bonds stabilizing the double-stranded structure of DNA and is observed as a result of dsDNA intercalation. In addition, the 8-oxodG signal was observed in the analyzed genetic material, which was particularly evident in long-term response to FTD, indicating a potentially mutagenic effect of these antibiotics (Bruskov, 2002). It is generally known that 5-NFs participate in generating ROS and NO through their nitro group reduction (Zolla and Timperio, 2005). The obtained results confirmed the influence of 5-NFs on the oxidative damage of bacterial genetic material (Hájková et al., 2017).

3.4. The bacterial stress response to the long-term presence of 5-NFs

Fig. 6 shows the bacterial stress response to the prolonged exposure to nitrofurans in terms of LPX, SOD, CAT, and GSTs activities. LPX refers to

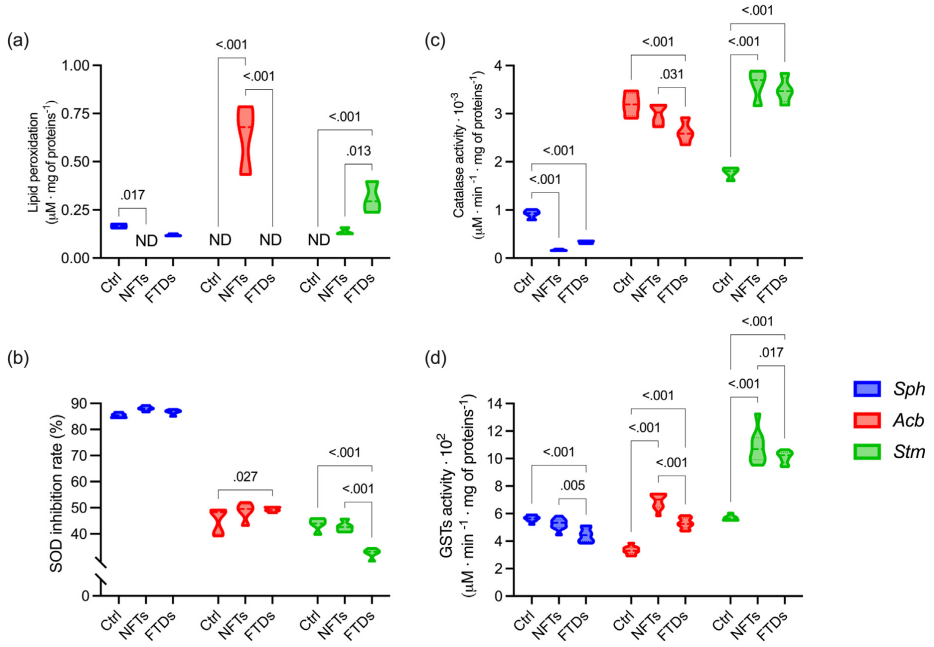

Fig. 6. The specific level of lipid peroxidation (a), superoxide dismutase inhibition rate (b), catalase activity (c), and glutathione S-transferases activity (d). *Sph* - *Sphingobacterium siyangense* FTD2, *Acb* - *Achromobacter pulmonis* NFZ2, *Stm* – *Stenotrophomonas maltophilia* FZD2. Ctrl – control cells, NFTs/FTDs – cells exposed to nitrofurantoin/furaltadone.

the oxidative degradation of lipids. SOD and CAT protect cells from oxidative damage by ROS while GSTs play a key role in cell detoxification.

Each strain subjected to the long-term exposure to NFT or FTD responded differently to the increasing concentration of each antibiotic (Supplementary Information 1, Fig. S1-10). The *Sph* strain was characterized by the increased relative metabolic activity (RMA) when cultivated at concentrations of NFT ranging from 5 to 15 mg·L^{-1}. No significant modifications in the RMA of *Sph*-FTDs were observed at concentrations of 5–15 mg·L^{-1} FTD. Cultivation of the *Sph*-NFTs strain and *Sph*-FTDs strain at 20 mg·L^{-1} of NFT or FTD reduced RMA of the cells. RMA of the *Acb*-NFTs strain cultivated with NFT was strikingly lower than that in the control cells regardless of the antibiotic concentration. Cultivation of the *Acb*-FTDs strain at a concentration of 10 mg·L^{-1} or higher induced a significant reduction in its RMA. No significant effect of NFT concentration on the RMA of the *Stm*-NFTs strain was detected. The increased concentration of FTD did not result in decreased RMA of the *Stm* strain.

In addition to the potential effects of NFT and FTD on metabolic activity, there is also evidence of bacterial stress response to the presence of these antibiotics. Results in Fig. 6 are related cells cultivated with 5 mg·L^{-1} of NFT or FTD. Fig. 6a shows changes in LPX induced by long-term exposure of the *Sph*, *Acb*, and *Stm* strains to NFT and FTD. LPX was determined by the detection of MDA produced as a result of oxidative degradation of lipids. The results revealed different patterns of MDA synthesis for each treatment. For the *Sph* strain, LPX has been detected for the control and the cells exposed to FTD. For the *Acb* strain, LPX was observed only for cells treated with NFT. For the *Stm* strain both treatments induced LPX, which has not been observed in the control cells. In bacteria, NFTs are transformed into highly reactive electrophiles which may inhibit the bacterial protein synthesis which was confirmed in this study by metabolomic analysis. Besides, LPX induction in the bacteria exposed to NFTs and FTDs was strictly strain specific. The lack or very low LPX may be related to the insignificant involvement of cytochrome P450 in 5-NFs metabolism.

Fig. 6b shows modifications of the SOD inhibition rate occurring in the tested strains. No statistically significant differences in SOD were observed for the *Sph* strain, however, the observed values of SOD were the highest among the tested strains, reaching up to 90 %. This suggests that high dismutase activity is an intrinsic trait of *Sphingobacterium* sp. A statistically significant increase in SOD was noted for FTDs in comparison to Ctrl for the *Acb* strain. Exposure to NFT did not affect SOD. Among all tested strains, the *Stm* strain was characterized by the lowest SOD. Exposure to FTD significantly reduced SOD, however, no change was observed for the *Stm*-NFTs cells.

Catalase, an enzyme responsible for neutralization of ROS, protects the cells from the toxic by-products of oxygen metabolism. In this study, the lowest activity of CAT was observed for the *Sph* strain (Fig. 6c). Both NFTs and FTDs exposure resulted in decreased CAT. A similar situation was observed for the *Acb* strain, however, in this case CAT was much higher, reaching up to 3000 μM·min^{-1}·mg of proteins^{-1} for the control. The opposite situation was observed for the *Stm* strain which significantly increased CAT in response to NFTs and FTDs treatment. Difference between NFTs and FTDs was not statistically significant.

The activity of GSTs in the control cells was the lowest in the *Acb* strain and the highest in the *Sph* strain. Long-term exposure of the *Sph* to FTD resulted in a decreased activity of GSTs; there was no significant difference between the control and the NFTs. Different observations were made for two other strains, which significantly increased the GSTs activity when cultivated under stress conditions. Exposure to NFT resulted in more potent induction of the GSTs enzymatic pathways than exposure to FTD in both strains.

The highest oxidative stress measured by the GSTs, CAT activity level was observed for the *Stm* strain, especially pronounced for antibiotics

treated cells. The obtained results for the *Stm* strain confirm the previous reports by Bagnyukova et al. (2006) that CAT activity increases with elevated LPX products concentrations.

4. Conclusions

Results from this study provide new insights into possible impacts of selected nitrofurans on beneficial bacterial strains isolated from wastewater. Prolonged exposure of bacterial strains to nitrofurantoin (NFT) and furaltadone (FTD) altered metabolomic characteristics, disrupted protein biosynthesis, triggered mutagenic effects, and promoted oxidative stress within the cells. Downregulated amino acids and derivatives were the main differentially accumulated metabolites. Aminoacyl t-RNA biosynthesis, which plays a key role in protein biosynthesis was one of the most significantly altered pathways. Nitrofurans-induced oxidative stress was evident through elevated levels of glutathione S-transferases and catalase. NFT and FTD showed similar mechanisms of action towards environmental bacteria. Interactions of these antibiotics with the bacterial cells depends more on characteristics of the strain than properties of the individual nitrofurans.

Supplementary data to this article can be found online at https://doi.org/10.1016/j.scitotenv.2023.162199.

CRediT authorship contribution statement

Amanda Pacholak: Conceptualization, Methodology, Validation, Formal analysis, Investigation, Resources, Writing – original draft, Writing – review & editing, Visualization. **Joanna Żur-Pińska:** Methodology, Investigation, Writing – original draft, Writing – review & editing. **Artur Piński:** Formal analysis, Data curation, Writing – original draft, Writing – review & editing. **Quynh Anh Nguyen:** Data curation, Writing – review & editing. **Marta Ligaj:** Methodology, Investigation, Writing – original draft, Writing – review & editing, Visualization. **Magdalena Luczak:** Methodology, Formal analysis, Investigation, Data curation. **Long D. Nghiem:** Resources, Writing – review & editing, Supervision. **Ewa Kaczorek:** Writing – review & editing, Supervision, Project administration, Funding acquisition.

Data availability

Data will be made available on request.

Declaration of competing interest

The authors declare that they have no known competing financial interests or personal relationships that could have appeared to influence the work reported in this paper.

Acknowledgments

This work was supported by National Science Centre, Poland, grant number 2017/27/B/NZ9/01603. Amanda Pacholak and Quynh Anh Nguyen participated in the program PROM of the Polish National Agency for Academic Exchange (grant number POWR.03.03.00-00-PN13/18). The program was co-financed from the European Social Fund within the Operational Program Knowledge Education Development, non-competitive project entitled "International scholarship exchange of PhD students and academic staff" executed under the Activity 3.3 specified in the application for funding of project No. POWR.03.03.00-00-PN13/18. Amanda Pacholak is grateful for financial support from the Foundation for Polish Science (FNP).

References

Ahmad, F., Anwar, S., Firdous, S., Da-Chuan, Y., Iqbal, S., 2018. Biodegradation of bispyribac sodium by a novel bacterial consortium BDAM: optimization of degradation conditions using response surface methodology. J. Hazard. Mater. 349, 272–281. https://doi.org/10.1016/j.jhazmat.2017.12.065.

Avram, O., Rapoport, D., Portugez, S., Pupko, T., 2020. M1CR0B1AL1Z3R—a user-friendly web server for the analysis of large-scale microbial genomics data. Access Microbiol. 2. https://doi.org/10.1099/acmi.ac2020.po1014.

Bagnyukova, T., Chahrak, O., Lushchak, V., 2006. Coordinated response of goldfish antioxidant defenses to environmental stress. Aquat. Toxicol. 78, 325–331. https://doi.org/10.1016/j.aquatox.2006.04.005.

Bansal, A.K., 2005. Bioinformatics in microbial biotechnology – a mini review. Microb. Cell Factories 4, 19. https://doi.org/10.1186/1475-2859-4-19.

Berg, G., Martinez, J.L., 2015. Friends or foes: can we make a distinction between beneficial and harmful strains of the Stenotrophomonas maltophilia complex? Front.Microbiol. 6. https://doi.org/10.3389/fmicb.2015.00241.

Blass, B.E., 2015. Case studies in drug discovery. Basic Principles of Drug Discovery And Development. Elsevier, pp. 499–529 https://doi.org/10.1016/B978-0-12-411508-8.00013-X.

Blin, K., Medema, M.H., Kottmann, R., Lee, S.Y., Weber, T., 2017. The antiSMASH database, a comprehensive database of microbial secondary metabolite biosynthetic gene clusters. Nucleic Acids Res. 45, 555–559. https://doi.org/10.1093/nar/gkw960.

Blin, K., Pascal Andreu, V., de los Santos, E.L.C., Del Carratore, F., Lee, S.Y., Medema, M.H., Weber, T., 2019. The antiSMASH database version 2: a comprehensive resource on secondary metabolite biosynthetic gene clusters. Nucleic Acids Res. 47, 625–630. https://doi.org/10.1093/nar/gky1060.

Bruskov, V.I., 2002. Heat-induced formation of reactive oxygen species and 8-oxoguanine, a biomarker of damage to DNA. Nucleic Acids Res. 30, 1354–1363. https://doi.org/10.1093/nar/30.6.1354.

Chen, X., Yin, H., Li, G., Wang, W., Wong, P.K., Zhao, H., An, T., 2019. Antibiotic-resistance gene transfer in antibiotic-resistance bacteria under different light irradiation: implications from oxidative stress and gene expression. Water Res. 149, 282–291. https://doi.org/10.1016/j.watres.2018.11.019.

Chong, J., Wishart, D.S., Xia, J., 2019. Using MetaboAnalyst 4.0 for comprehensive and integrative metabolomics data analysis. Curr. Protoc. Bioinformatics 68. https://doi.org/10.1002/cpbi.86.

Cox, J., Mann, M., 2008. MaxQuant enables high peptide identification rates, individualized P.P.B.-range mass accuracies and proteome-wide protein quantification. Nat. Biotechnol. 26, 1367–1372. https://doi.org/10.1038/nbt.1511.

Davis, J.J., Wattam, A.R., Aziz, R.K., et al., 2019. The PATRIC Bioinformatics Resource Center: expanding data and analysis capabilities. Nucleic Acids Res. 48, 606–612. https://doi.org/10.1093/nar/gkz943.

Ezraty, B., Gennaris, A., Barras, F., Collet, J.-F., 2017. Oxidative stress, protein damage and repair in bacteria. Nat. Rev. Microbiol. 15, 385–396. https://doi.org/10.1038/nrmicro.2017.26.

Gao, J., Ye, J., Ma, J., Tang, L., Huang, J., 2014. Biosorption and biodegradation of triphenyltin by Stenotrophomonas maltophilia and their influence on cellular metabolism. J. Hazard. Mater. 276, 112–119. https://doi.org/10.1016/j.jhazmat.2014.05.023.

Giulivo, M., Lopez de Alda, M., Capri, E., Barceló, D., 2016. Human exposure to endocrine disrupting compounds: their role in reproductive systems, metabolic syndrome and breast cancer.A review. Environ. Res. 151, 251–264. https://doi.org/10.1016/j.envres.2016.07.011.

Gutleben, J., Chaib De Mares, M., van Elsas, J.D., Smidt, H., Overmann, J., Sipkema, D., 2018. The multi-omics promise in context: from sequence to microbial isolate. Crit. Rev. Microbiol. 44, 212–229. https://doi.org/10.1080/1040841X.2017.1332003.

Hájková, A., Barek, J., Vyskočil, V., 2017. Electrochemical DNA biosensor for detection of DNA damage induced by hydroxyl radicals. Bioelectrochemistry 116, 1–9. https://doi.org/10.1016/j.bioelechem.2017.02.003.

Huerta-Cepas, J., Szklarczyk, D., Heller, D., Hernández-Plaza, A., Forslund, S.K., Cook, H., Mende, D.R., Letunic, I., Rattei, T., Jensen, L.J., von Mering, C., Bork, P., 2019. eggNOG 5.0: a hierarchical, functionally and phylogenetically annotated orthology resource based on 5090 organisms and 2502 viruses. Nucleic Acids Res. 47, 309–314. https://doi.org/10.1093/nar/gky1085.

Huttner, A., Verhaegh, E.M., Harbarth, S., Muller, A.E., Theuretzbacher, U., Mouton, J.W., 2015. Nitrofurantoin revisited: a systematic review and meta-analysis of controlled trials. J. Antimicrob. Chemother. 70, 2456–2464. https://doi.org/10.1093/jac/dkv147.

Johnston, I., Osborn, L.J., Markley, R.L., McManus, E.A., Kadam, A., Schultz, K.B., Nagajothi, N., Ahern, P.P., Brown, J.M., Claesen, J., 2021. Identification of essential genes for Escherichia coli aryl polyene biosynthesis and function in biofilm formation. npj BiofilmsMicrobiomes 7, 56. https://doi.org/10.1038/s41522-021-00226-3.

Jones, D.T., Taylor, W.R., Thornton, J.M., 1992. The rapid generation of mutation data matrices from protein sequences. Bioinformatics 8, 275–282. https://doi.org/10.1093/bioinformatics/8.3.275.

Kokulnathan, T., Chen, S.-M., 2020. Robust and selective electrochemical detection of antibiotic residues: the case of integrated lutetium vanadate/graphene sheets architectures. J. Hazard. Mater. 384, 121304. https://doi.org/10.1016/j.jhazmat.2019.121304.

Kumar, S., Stecher, G., Li, M., Knyaz, C., Tamura, K., 2018. MEGA X: molecular evolutionary genetics analysis across computing platforms. Mol. Biol. Evol. 35, 1547–1549. https://doi.org/10.1093/molbev/msy096.

Lee, D.-H., Hur, J.S., Kahng, H.-Y., 2013. Sphingobacterium cladoniae sp. nov., isolated from lichen, Cladonia sp., and emended description of Sphingobacterium siyangense. Int. J. Syst. Evol. Microbiol. 63, 755–760. https://doi.org/10.1099/ijs.0.038844-0.

Ligaj, M., Tichoniuk, M., Filipiak, M., 2008. Detection of bar gene encoding phosphinothricin herbicide resistance in plants by electrochemical biosensor. Bioelectrochemistry 74, 32–37. https://doi.org/10.1016/j.bioelechem.2008.03.003.

Liu, R., Liu, H., Zhang, C.-X., Yang, S.-Y., Liu, X.-H., Zhang, K.-Y., Lai, R., 2008. Sphingobacterium siyangense sp. nov., isolated from farm soil. Int. J. Syst. Evol. Microbiol. 58, 1458–1462. https://doi.org/10.1099/ijs.0.65696-0.

Lu, X.-M., Chen, C., Zheng, T.-L., 2017. Metagenomic insights into effects of chemical pollutants on microbial community composition and function in estuarine sediments receiving polluted river water. Microb. Ecol. 73, 791–800. https://doi.org/10.1007/s00248-016-0868-8.

Luo, Y., Guo, W., Ngo, H.H., Nghiem, L.D., Hai, F.I., Zhang, J., Liang, S., Wang, X.C., 2014. A review on the occurrence of micropollutants in the aquatic environment and their fate and removal during wastewater treatment. Sci. Total Environ. 473–474, 619–641. https://doi.org/10.1016/j.scitotenv.2013.12.065.

Manni, M., Berkeley, M.R., Seppey, M., Zdobnov, E.M., 2021. BUSCO: assessing genomic data quality and beyond. Curr.Protoc. 1. https://doi.org/10.1002/cpz1.323.

Martin, M., 2011. Cutadapt removes adapter sequences from high-throughput sequencing reads. EMBnet J. 17, 10. https://doi.org/10.14806/ej.17.1.200.

Marx, V., 2017. Microbiology: the return of culture. Nat. Methods 14, 37–40. https://doi.org/10.1038/nmeth.4107.

McOsker, C.C., Fitzpatrick, P.M., 1994. Nitrofurantoin: mechanism of action and implications for resistance development in common uropathogens. J. Antimicrob. Chemother. 33, 23–30. https://doi.org/10.1093/jac/33.suppl_A.23.

Moutiez, M., Belin, P., Gondry, M., 2017. Aminoacyl-tRNA-utilizing enzymes in natural product biosynthesis. Chem. Rev. 117, 5578–5618. https://doi.org/10.1021/acs.chemrev.6b00523.

Nguyen, A.Q., Vu, H.P., Nguyen, L.N., Wang, Q., Djordjevic, S.P., Donner, E., Yin, H., Nghiem, L.D., 2021. Monitoring antibiotic resistance genes in wastewater treatment: current strategies and future challenges. Sci. Total Environ. 783, 146964. https://doi.org/10.1016/j.scitotenv.2021.146964.

Pacholak, A., Burlaga, N., Guzik, U., Kaczorek, E., 2020a. Investigation of the bacterial cell envelope nanomechanical properties after long-term exposure to nitrofurans. J. Hazard. Mater., 124352 https://doi.org/10.1016/j.jhazmat.2020.124352.

Pacholak, A., Burlaga, N., Kaczorek, E., 2020b. Evaluating the effect of azole antifungal agents on the stress response and nanomechanical surface properties of Ochrobactrum anthropi Aspcl2.2. Molecules 25, 3348. https://doi.org/10.3390/molecules25153348.

Palazzotto, E., Weber, T., 2018. Omics and multi-omics approaches to study the biosynthesis of secondary metabolites in microorganisms. Curr. Opin. Microbiol. 45, 109–116. https://doi.org/10.1016/j.mib.2018.03.004.

Pinski, A., Zur, J., Hasterok, R., Hupert-Kocurek, K., 2020. Comparative genomics of Stenotrophomonas maltophilia and Stenotrophomonas rhizophila revealed characteristic features of both species. Int. J. Mol. Sci. 21, 4922. https://doi.org/10.3390/ijms21144922.

Rodríguez, J., Gallampois, C.M.J., Timonen, S., Andersson, A., Sinkko, H., Haglund, P., Berglund, Å.M.M., Ripszam, M., Figueroa, D., Tysklind, M., Rowe, O., 2018. Effects of organic pollutants on bacterial communities under future climate change scenarios. Front. Microbiol. 9, 2926. https://doi.org/10.3389/fmicb.2018.02926.

Saati-Santamaría, Z., Peral-Aranega, E., Velázquez, E., Rivas, R., García-Fraile, P., 2021. Phylogenomic analyses of the Genus Pseudomonas lead to the rearrangement of several species and the definition of new genera. Biology 10, 782. https://doi.org/10.3390/biology10080782.

Smirnova, G.V., Oktyabrsky, O.N., 2005. Glutathione in bacteria. Biochemistry 70, 1199–1211. https://doi.org/10.1007/s10541-005-0248-3 (Moscow).

Talavera, G., Castresana, J., 2007. Improvement of phylogenies after removing divergent and ambiguously aligned blocks from protein sequence alignments. Syst. Biol. 56, 564–577. https://doi.org/10.1080/10635150701472164.

Tran, N.H., Hoang, L., Nghiem, L.D., Nguyen, N.M.H., Ngo, H.H., Guo, W., Trinh, Q.T., Mai, N.H., Chen, H., Nguyen, D.D., Ta, T.T., Gin, K.Y.-H., 2019. Occurrence and risk assessment of multiple classes of antibiotics in urban canals and lakes in Hanoi,Vietnam. Sci. Total Environ. 692, 157–174. https://doi.org/10.1016/j.scitotenv.2019.07.092.

Ueno, Y., Arita, M., Kumagai, T., Asai, K., 2003. Processing sequence annotation data using the Lua programming language. Genome Informa. 14, 154–163 PMID: 15706530.

Vandamme, P., Moore, E.R.B., Cnockaert, M., De Brandt, E., Svensson-Stadler, L., Houf, K., Spilker, T., LiPuma, J.J., 2013. Achromobacter animicus sp. nov., Achromobacter mucicolens sp. nov., Achromobacter pulmonis sp. nov. and Achromobacter spiritinus sp. nov., from human clinical samples. Syst. Appl. Microbiol. 36, 1–10. https://doi.org/10.1016/j.syapm.2012.10.003.

Vilanova, C., Porcar, M., 2016. Are multi-omics enough? Nat. Microbiol. 1, 16101. https://doi.org/10.1038/nmicrobiol.2016.101.

Wick, R.R., Judd, L.M., Gorrie, C.L., Holt, K.E., 2017. Unicycler: resolving bacterial genome assemblies from short and long sequencing reads. PLoS Comput. Biol. 13, 1005595. https://doi.org/10.1371/journal.pcbi.1005595.

Xia, J., Psychogios, N., Young, N., Wishart, D.S., 2009. MetaboAnalyst: a web server for metabolomic data analysis and interpretation. Nucleic Acids Res. 37, 652–660. https://doi.org/10.1093/nar/gkp356.

Xia, J., Wishart, D.S., 2011. Web-based inference of biological patterns, functions and pathways from metabolomic data using MetaboAnalyst. Nat. Protoc. 6, 743–760. https://doi.org/10.1038/nprot.2011.319.

Xiong, W., Yin, C., Wang, Y., Lin, S., Deng, Z., Liang, R., 2020. Characterization of an efficient estrogen-degrading bacterium Stenotrophomonas maltophilia SJTH1 in saline-, alkaline-, heavy metal-contained environments or solid soil and identification of four 17β-estradiol-oxidizing dehydrogenases. J. Hazard. Mater. 385, 121616. https://doi.org/10.1016/j.jhazmat.2019.121616.

Zhang, X., Zhang, D., He, K., 2019. Combining an effective immuno-affinity column with ELISA for reliable and visual detection of furaltadone metabolites in aquatic products. Anal. Methods 11, 1270–1275. https://doi.org/10.1039/C8AY02597E.

Zolla, L., Timperio, A.M., 2005. Involvement of active oxygen species in protein and oligonucleotide degradation induced by nitrofurans. Biochem. Cell Biol. 83, 166–175. https://doi.org/10.1139/o05-023.

Żur, J., Marchlewicz, A., Piński, A., Guzik, U., Wojcieszyńska, D., 2021. Degradation of diclofenac by new bacterial strains and its influence on the physiological status of cells. J. Hazard. Mater. 403, 124000. https://doi.org/10.1016/j.jhazmat.2020.124000.

Supplementary information 1 (P4)

Supplementary Information 1

Potential negative effect of long-term exposure to nitrofurans on bacteria isolated from wastewater

Submitted to

Science of the Total Environment

By

Amanda Pacholak [a*], Joanna Żur-Pińska [bc], Artur Piński [c], Quynh Anh Nguyen [d], Marta Ligaj [e], Magdalena Luczak [f], Long D. Nghiem [d], Ewa Kaczorek [a]

[a] Institute of Chemical Technology and Engineering, Poznan University of Technology, Poland

[b] Biotechnology Centre, The Silesian University of Technology, Gliwice, Poland

[c] Institute of Biology, Biotechnology and Environmental Protection, Faculty of Natural Sciences, University of Silesia in Katowice, Poland

[d] Centre for Technology in Water and Wastewater, School of Civil and Environmental Engineering, University of Technology Sydney, New South Wales, Australia

[e] Department of Non-Food Products Quality and Packaging Development, Institute of Quality Science, Poznan University of Economics and Business, Poland

[f] Institute of Bioorganic Chemistry, Polish Academy of Sciences, Poznan, Poland

* Corresponding author: e-mail: amanda.pacholak@put.poznan.pl, phone: +48 61 665 3686

Contents

1. Methodology

1.1. RAPD-PCR procedure

Sixty primers were screened for presence of distinct and consistent bands. The following primers were used:

P01 CAGGCCCTTC	P16 TGCTCTGCCC	P31 AAAGCTGCGG	P46 ACCTGAACGG
P02 TGCCGAGCTG	P17 GGTGACGCAG	P32 TGTCATCCCC	P47 TTGGCACGGG
P03 AGTCAGCCAC	P18 GTCCACACGG	P33 AAGCCTCGTC	**P48 GTGTGCCCCA**
P04 AATCGGGCTG	P19 TGGGGGACTC	P34 TGCGTGCTTG	P49 CTCTGGAGAC
P05 AGGGGTCTTG	P20 CTGCTGGGAC	P35 GACGGATCAG	P50 GGTCTACACC
P06 GGTCCCTGAC	P21 TTCGAGCCAG	P36 CACACTCCAG	P51 AGCGCCATTG
P07 GAAACGGGTG	P22 GTGAGGCGTC	P37 TTCCCCCCAG	P52 CACCGTATCC
P08 GTGACGTAGG	P23 GGGGGTCTTT	P38 TGAGTGGGTG	P53 GGGGTGACGA
P09 GGGTAACGCC	P24 CCGCATCTAC	P39 GTTGCCAGCC	P54 CTTCCCCAAG
P10 GTGATCGCAG	P25 GATGACCGCC	P40 ACTTCGCCAC	P55 CATCCGTGCT
P11 GTTTCGCTCC	P26 GAACGGACTC	P41 ACCGCGAAGG	P56 AGGGCGTAAG
P12 TGATCCCTGG	P27 GTCCCGACGA	P42 GGACCCAACC	**P57 TTTCCCACGG**
P13 CATCCCCCTG	P28 TGGACCGGTG	P43 GTCGCCGTCA	P58 GAGAGCCAAC
P14 GGACTGGAGT	P29 CTCACCGTCC	**P44 TCTGGTGAGG**	P59 CTGGGGACTT
P15 TGCGCCCTTC	P30 TGTCTGGGTG	P45 TGAGCGGACA	P60 ACCCGGTCAC

Seven primers were found useful:

Number	Sequence	Number of the primer in the paper
P04	5`-AAT CGG GCT G-3`	P1
P44	5`-TCT GGT GAG G-3`	P2
P03	5`-AGT CAG CCA C-3`	P3
P48	5`-GTG TGC CCC A-3`	P4
P57	5`-TTT CCC ACG G-3`	P5
P01	5`-CAG GCC CTT C-3`	P6
P02	5`-TGC CGA GCT G-3`	P7

The components of PCR reaction:

- 10 ng template DNA,
- buffer Tris–KCl (20 mM Tris–HCl, 50 mM KCl, pH 8.4)
- 2 mM $MgCl_2$,
- 1 μM primer,
- 1 mM dNTP,
- 5 U of *Taq* DNA polymerase (each reaction)
- sterile deionized water to a total volume of 25 μl.

The PCR program details:

- 95°C for 3 minutes
- 30 cycles of:
    - 92°C for 30 seconds
    - 31-40°C for 30 seconds
    - 72°C for 60 seconds
- 72°C for 5 minutes
- Hold at 4°C

PCR amplified DNA fragments were separated by electrophoresis in agarose gel (1.5%) and stained with ethidium bromide (20 μg 100 ml^{-1}). A sample without DNA was included as a negative control in each experiment. Electrophoretic profile was visualized under UV radiation with BIO-RAD transilluminator. Sizes of DNA fragments were estimated by comparison with standard Ladder 100-10,000 bp. Electrophoretic profiles were analyzed for polymorphism based on the presence and absence of DNA bands on agarose gel.

RAPD-PCR analysis was performed with the kind assistance of Dr. Beata Dudzińska-Bajorek from Hipolit Cegielski State College of Higher Education in Gniezno, Poland.

1.2. Metabolic activity procedure

Cell metabolic activity was measured after 24 h of bacterial exposure to NFT and FTD at a concentration of 5, 10, 15, and 20 mg L^{-1} using 3-(4,5-dimethylthiazol-2-yl)-2,5-diphenyltetrazolium bromide (MTT) assay.

Bacterial cultures were washed two times and resuspended in Dulbecco's Phosphate Buffered Saline (DPBS), the optical density was adjusted to 0.2 ±0.02. Next, 200 µL of the cell suspension was transferred into the sample wells of the sterile 96-well microplate and optical density at a wavelength 600 nm was measured. MTT solution (5 mg mL^{-1} solution in sterile water) was added to the wells using multichannel pipette. Mixtures were incubated for 2 h in 30 °C in the dark with shaking on an orbital shaker. Later, the cells were centrifuged (4500× g, 30 min, 20 °C, Centrifuge 5910R, Eppendorf, Germany), supernatants were carefully discarded, and the remaining cell pellets were suspended in dimethyl sulfoxide (200 µL). Following a 15-min incubation, the microplates were centrifuged again (4000× g, 15 min) and 150 µL of supernatant from each well was transferred to a new microplate and absorbance at 560 nm was measured. The higher absorbance of the solution indicated the greater number of viable, metabolically active cells in the sample well. The metabolic activity is defined in MTT reducing units (MRU) and was calculated according to following equation:

$$MRU = \frac{A_{560} \cdot SV}{TV} \cdot \frac{K}{OD_{600}} \; [-]$$

where:

A_{560}—absorbance of the formazan dissolved in DMSO;

SV — the volume of the test sample [mL];
TV — total volume of the reaction mixture [mL];
K — dilution factor;
OD_{600} — optical density of the bacterial cells collected from the cultures.

Results are presented as relative metabolic activity which is defined here as the ratio between the activity of test samples (bacteria exposed to nitrofurans) and the activity of the control samples (bacteria not exposed to nitrofurans).

2. Additional results

2.1. Phylogenetic trees

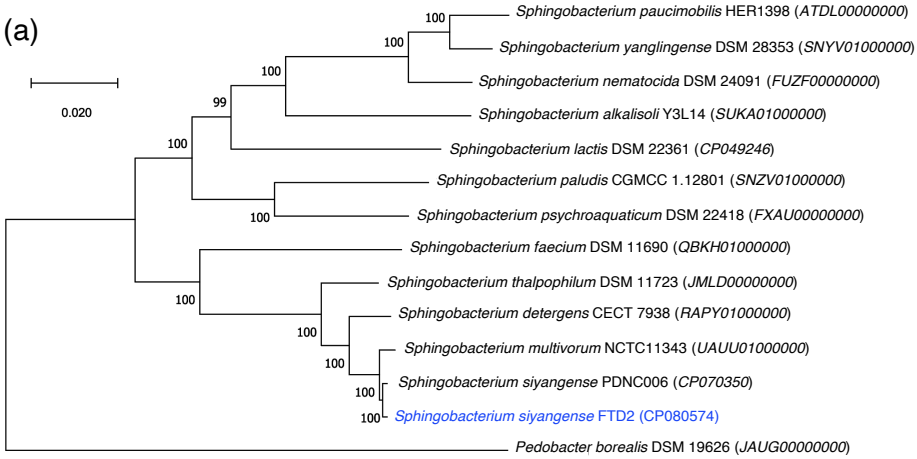

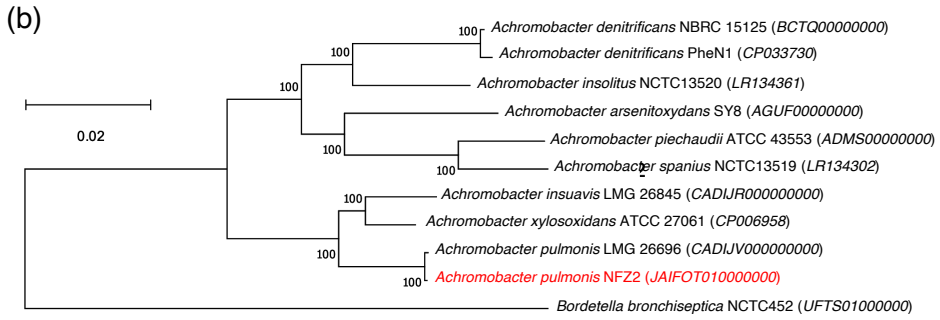

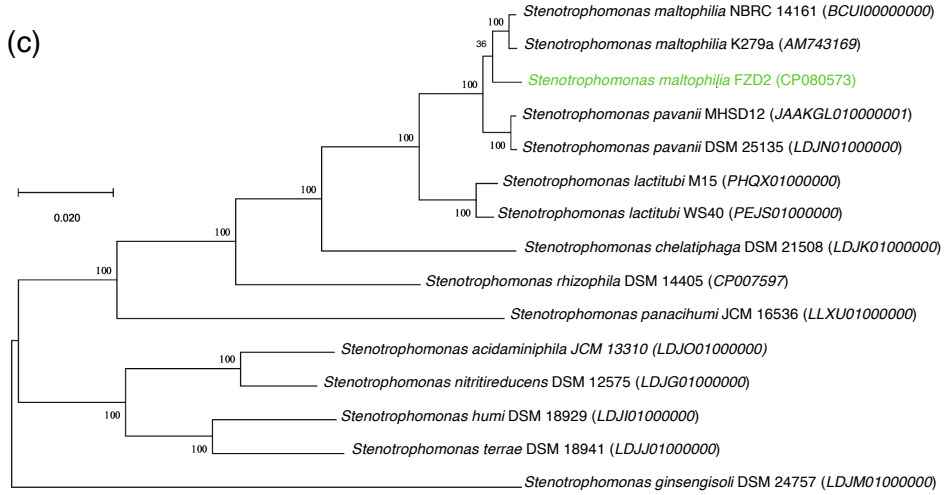

Fig. S1-1. Phylogenetic tree based on alignment of the core proteomes of three strains: *Sphingobacterium siyangense* FTD2 (based on 162 core genes which yield 52,915 amino acids) (a), *Achromobacter pulmonis* NFZ2 (1541 genes, 496,172 amino acids) (b), and *Stenotrophomonas maltophilia* FZD2 (780 genes, 269,641 amino acids) (c). The NCBI accession numbers for genomes are shown in brackets. The tree was constructed using the maximum likelihood method. The scale bars indicate 1% nucleotide sequence divergence.

2.2. Gene ontology category function groups

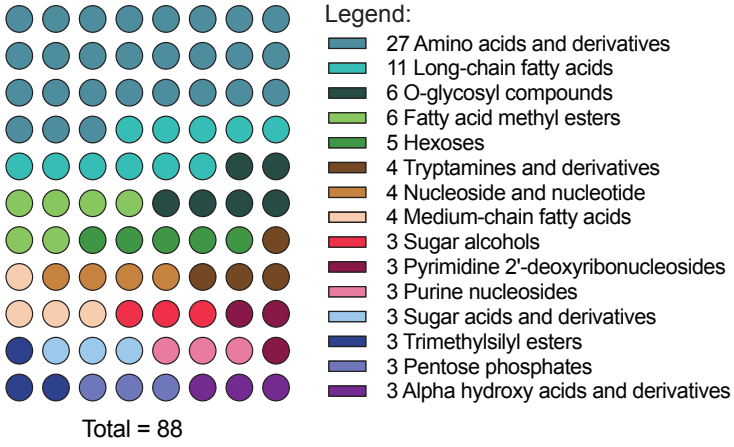

Fig. S1.2. Top significant gene ontology category function groups of the analysed strains (each group contains at least 3 differentially accumulated metabolites (DAMs)). Values labelled in a legend depict the number of the metabolites in each group.

2.3. Pathways of GSH metabolism (a) and aa-tRNA biosynthesis

(a) Sph, Ctrl vs NFTs, GSH metabolism

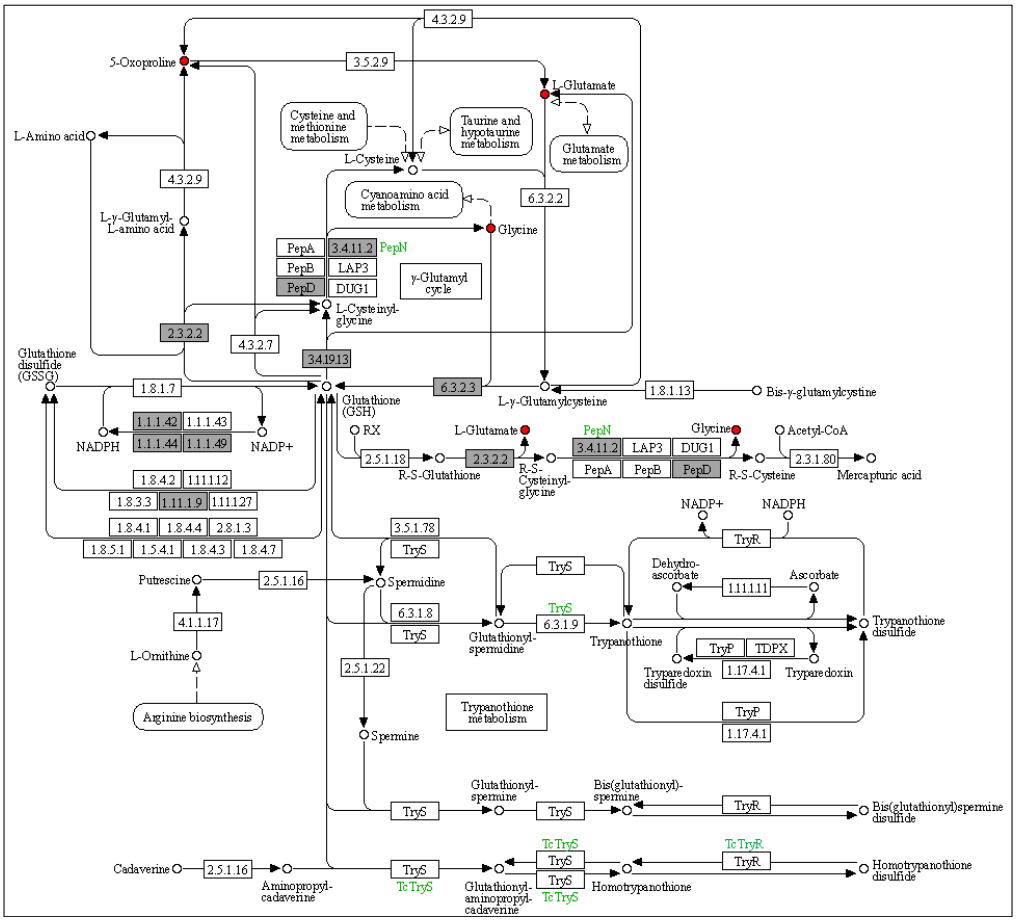

(b) Sph, Ctrl vs NFTs, aa-tRNA biosynthesis

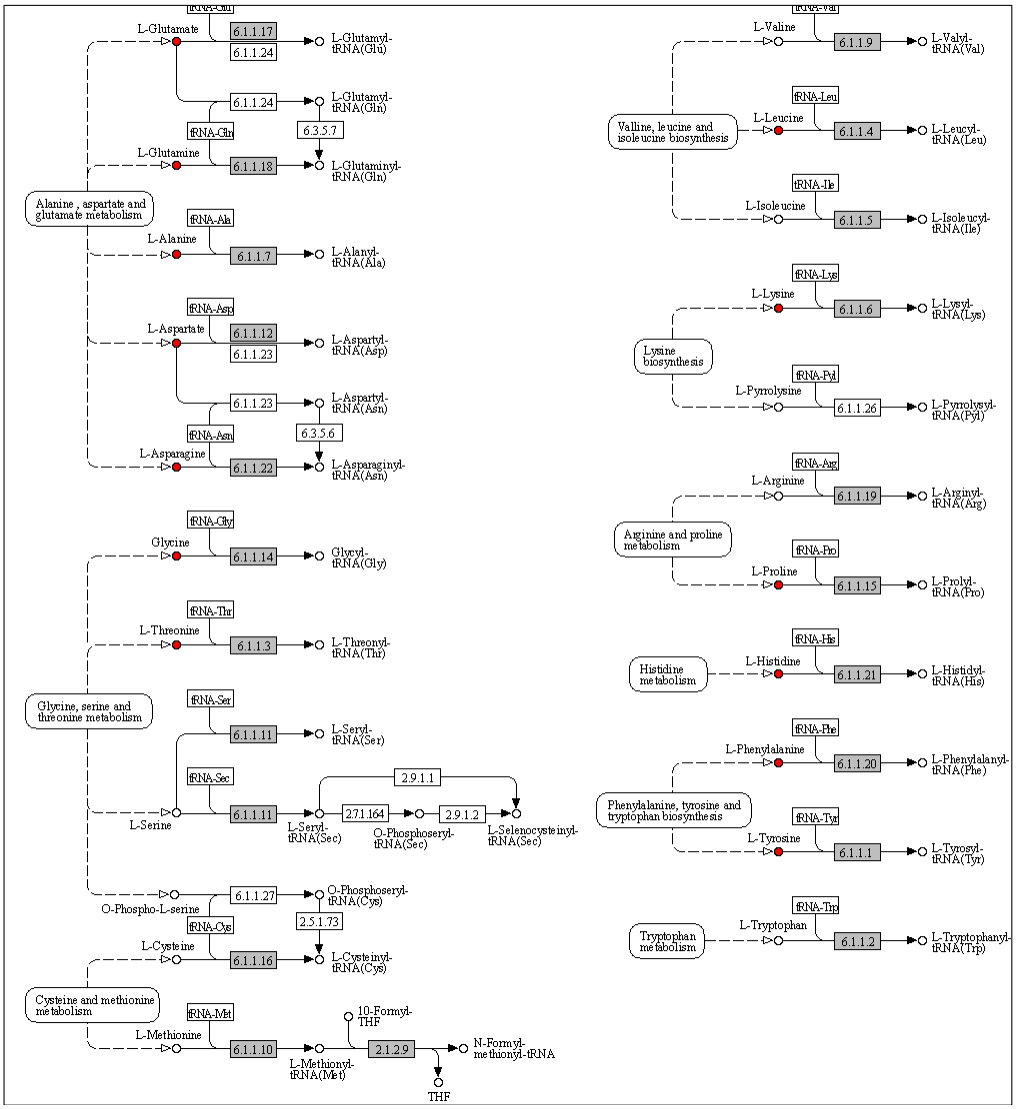

Fig. S1-3. Pathways of GSH metabolism (a) and aa-tRNA biosynthesis (b) in the *Sphingobacterium siyangense* FTD2 (Sph) in response to prolonged exposure to NFT. The genes are marked in gray and the downregulated compounds in red. No upregulated compounds involved in the pathways were observed.

(a) Sph, Ctrl vs FTDs, GSH metabolism

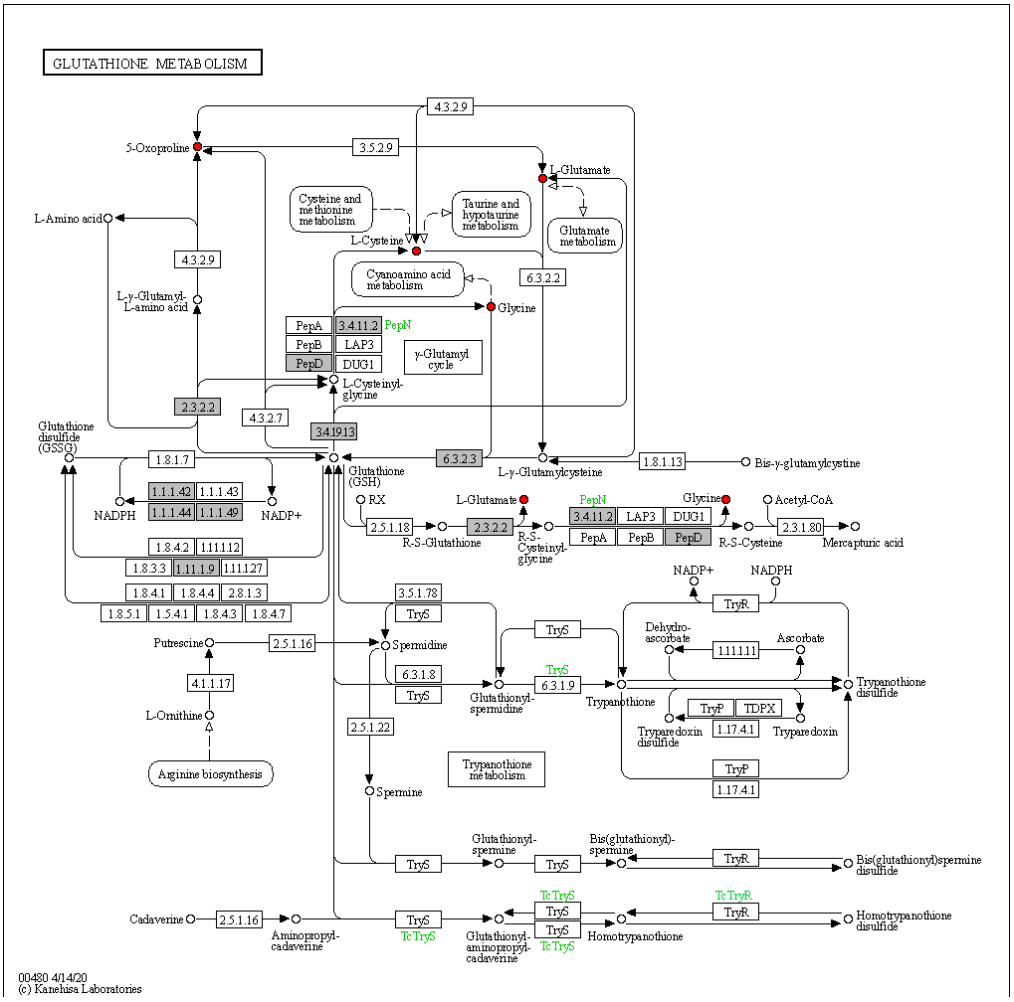

(b) Sph, Ctrl vs FTDs, aa-tRNA biosynthesis

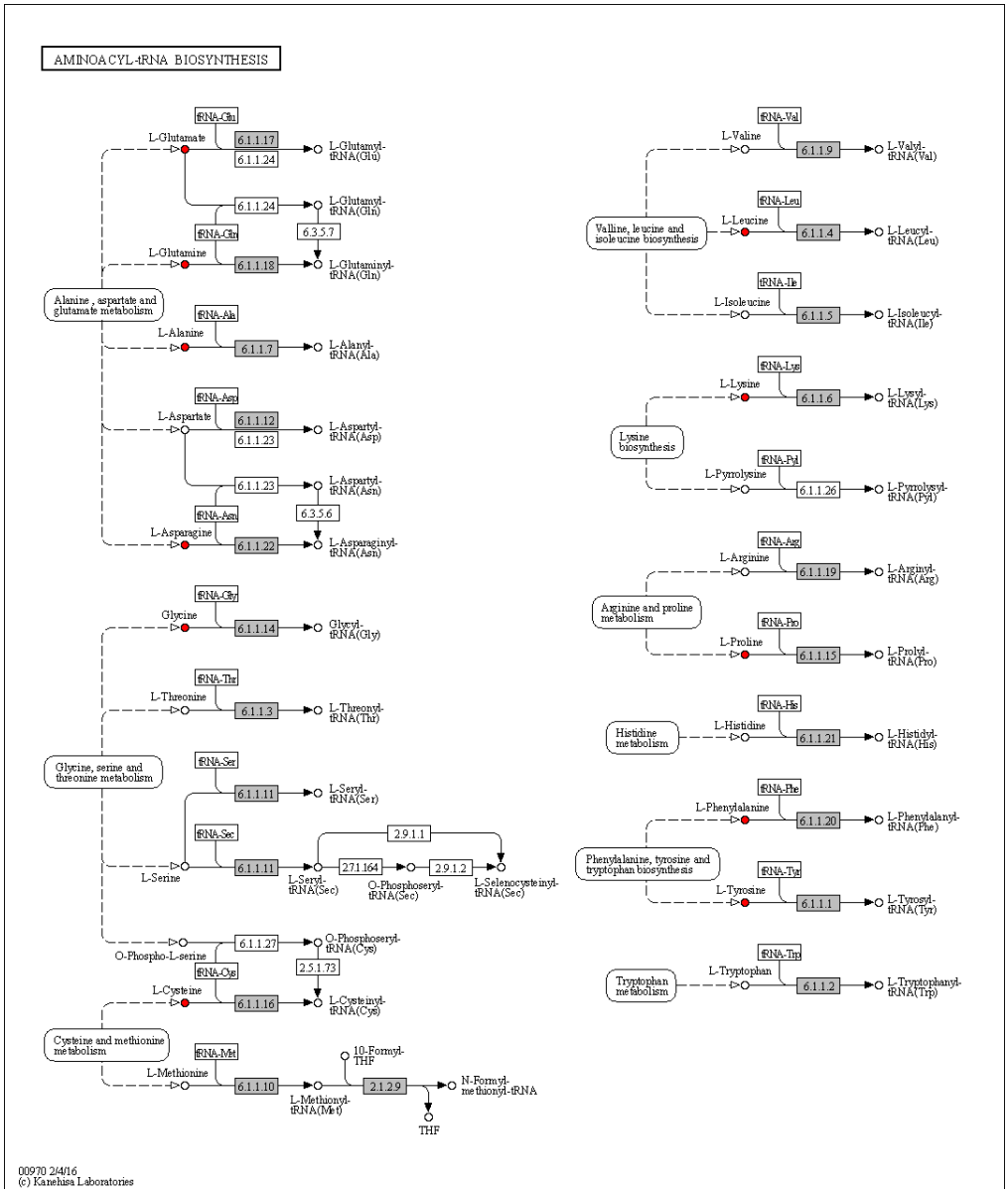

Fig. S1-4. Pathways of GSH metabolism (a) and aa-tRNA biosynthesis (b) in the *Sphingobacterium siyangense* FTD2 (Sph) in response to prolonged exposure to FTD. The genes are marked in gray and the downregulated compounds in red. No upregulated compounds involved in the pathways were observed.

(a) Acb, Ctrl vs NFTs, GSH metabolism

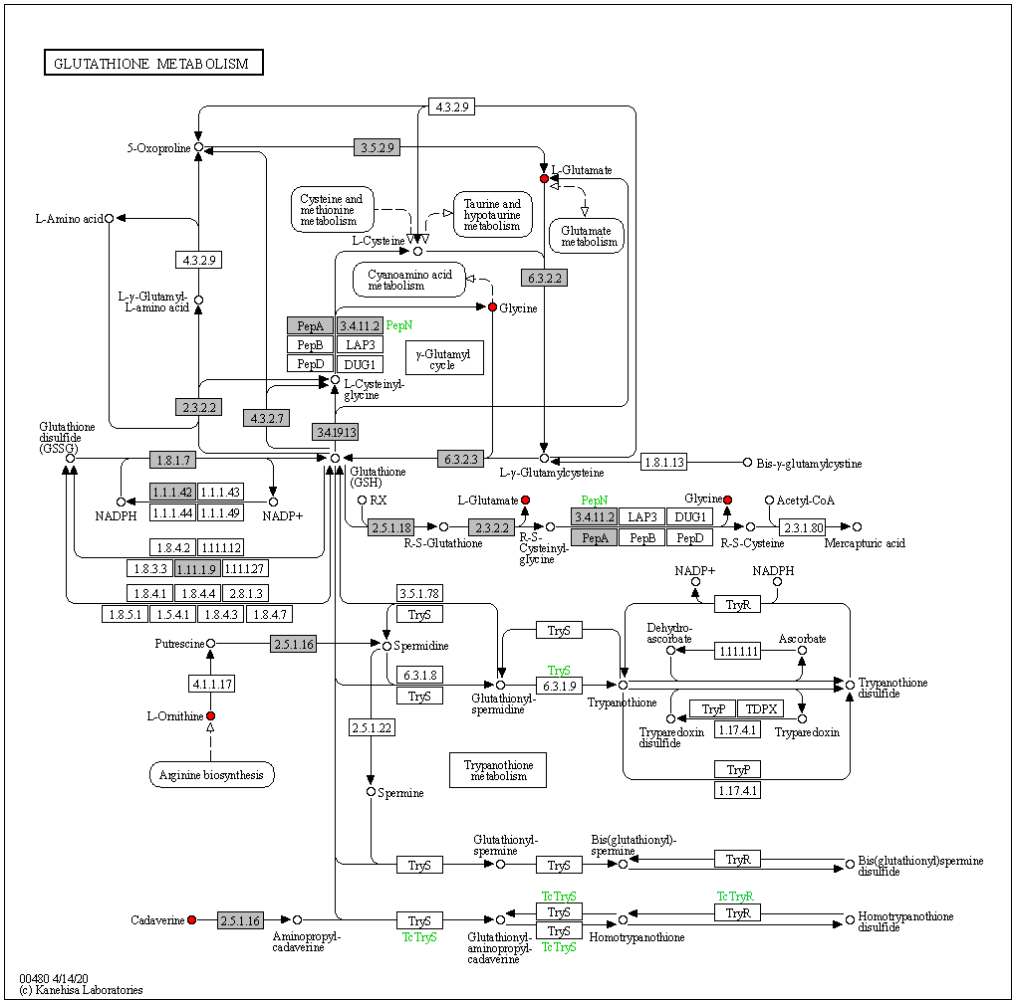

(b) Acb, Ctrl vs NFTs, aa-tRNA biosynthesis

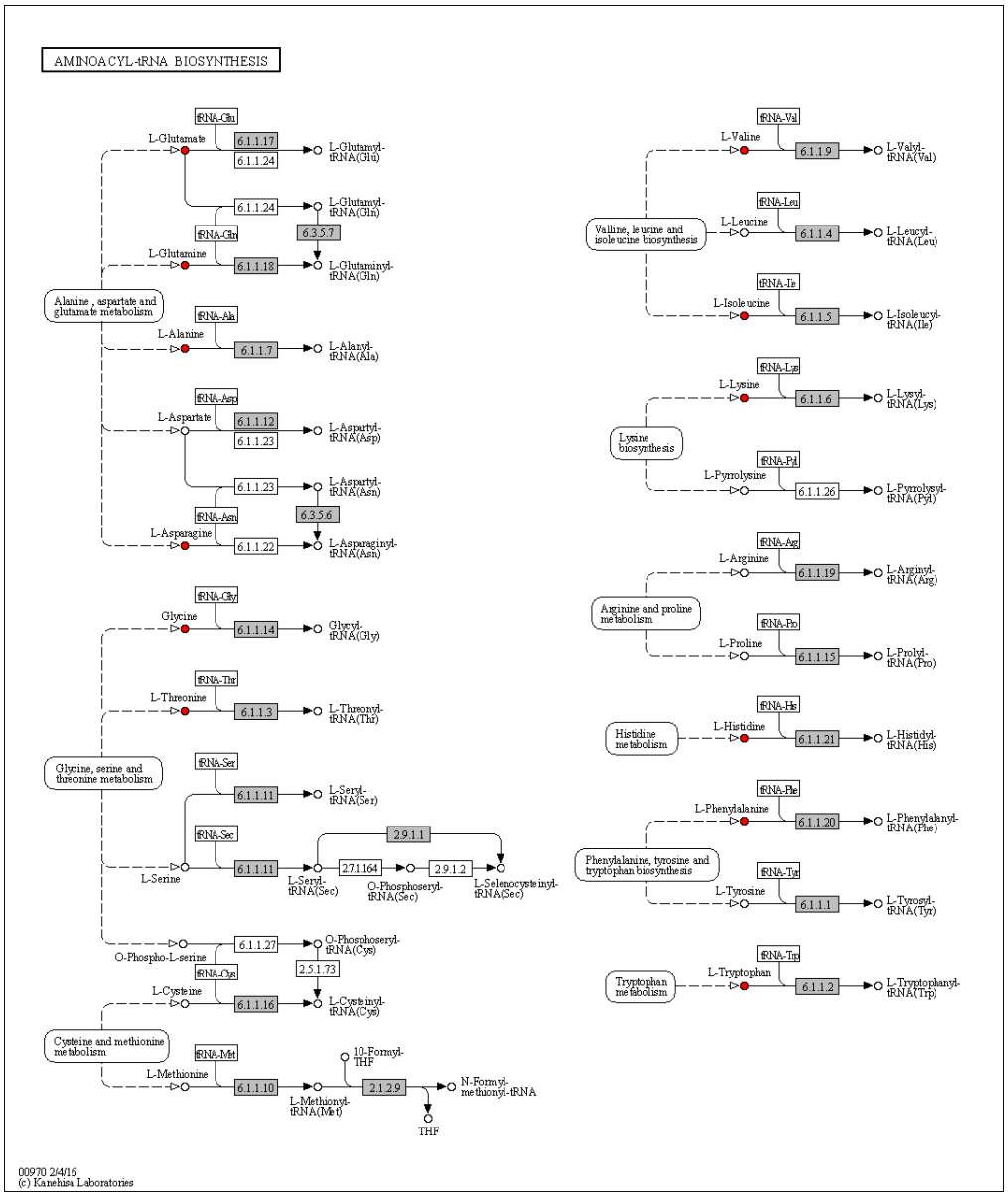

Fig. S1-5. Pathways of GSH metabolism (a) and aa-tRNA biosynthesis (b) in the *Achromobacter pulmonis* NFZ2 (Acb) in response to prolonged exposure to NFT. The genes are marked in gray and the downregulated compounds in red. No upregulated compounds involved in the pathways were observed.

(a) Acb, Ctrl vs FTDs, GSH metabolism

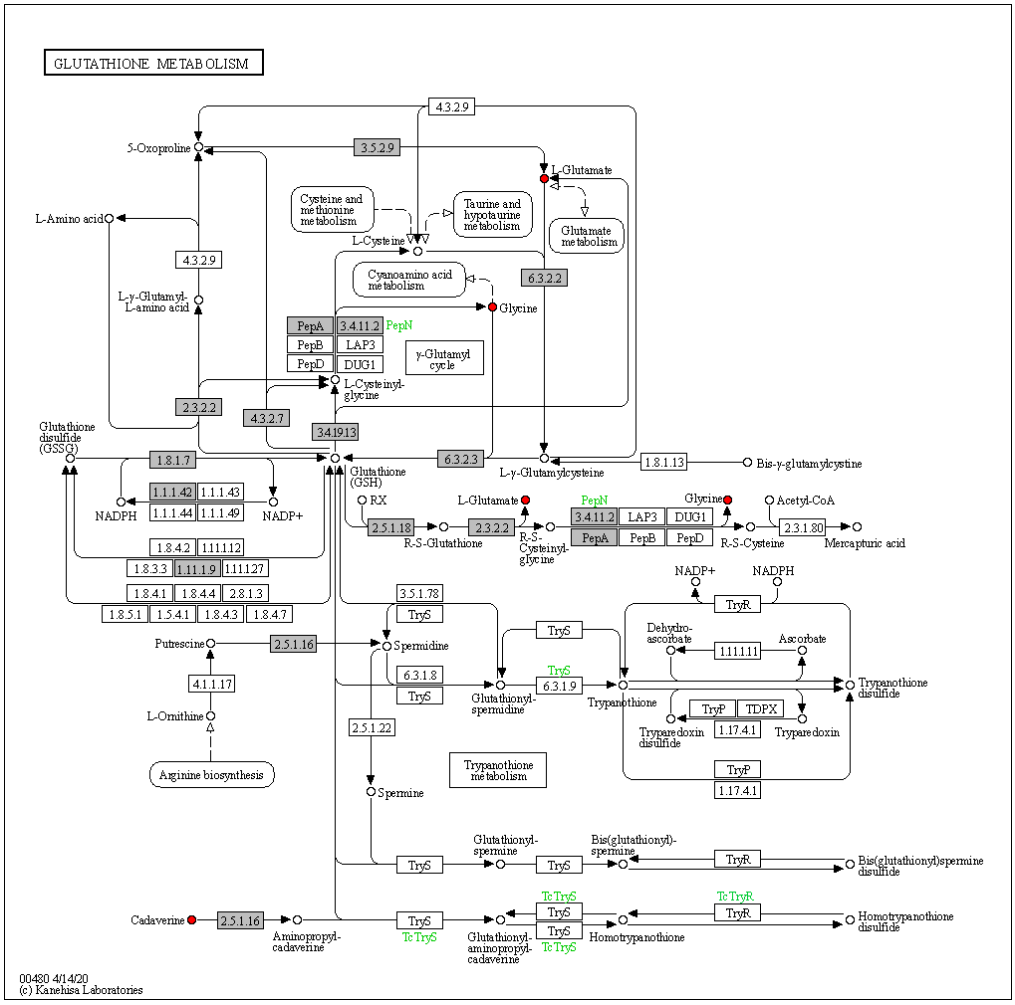

(b) Acb, Ctrl vs FTDs, aa-tRNA biosynthesis

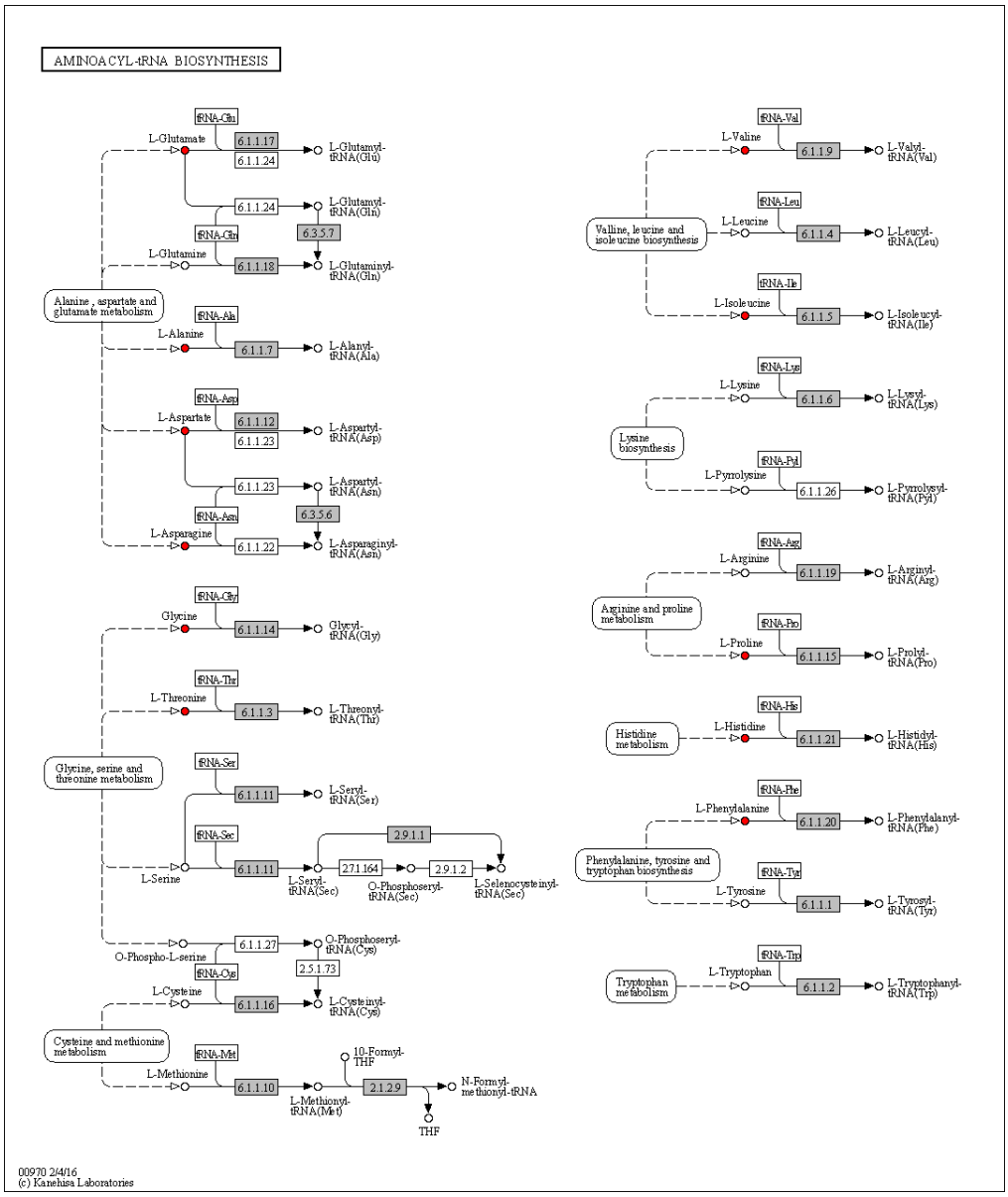

Fig. S1-6. Pathways of GSH metabolism (a) and aa-tRNA biosynthesis (b) in the *Achromobacter pulmonis* NFZ2 (Acb) in response to prolonged exposure to FTD. The genes are marked in gray and the downregulated compounds in red. No upregulated compounds involved in the pathways were observed.

(a) Stm, Ctrl vs NFTs, GSH metabolism

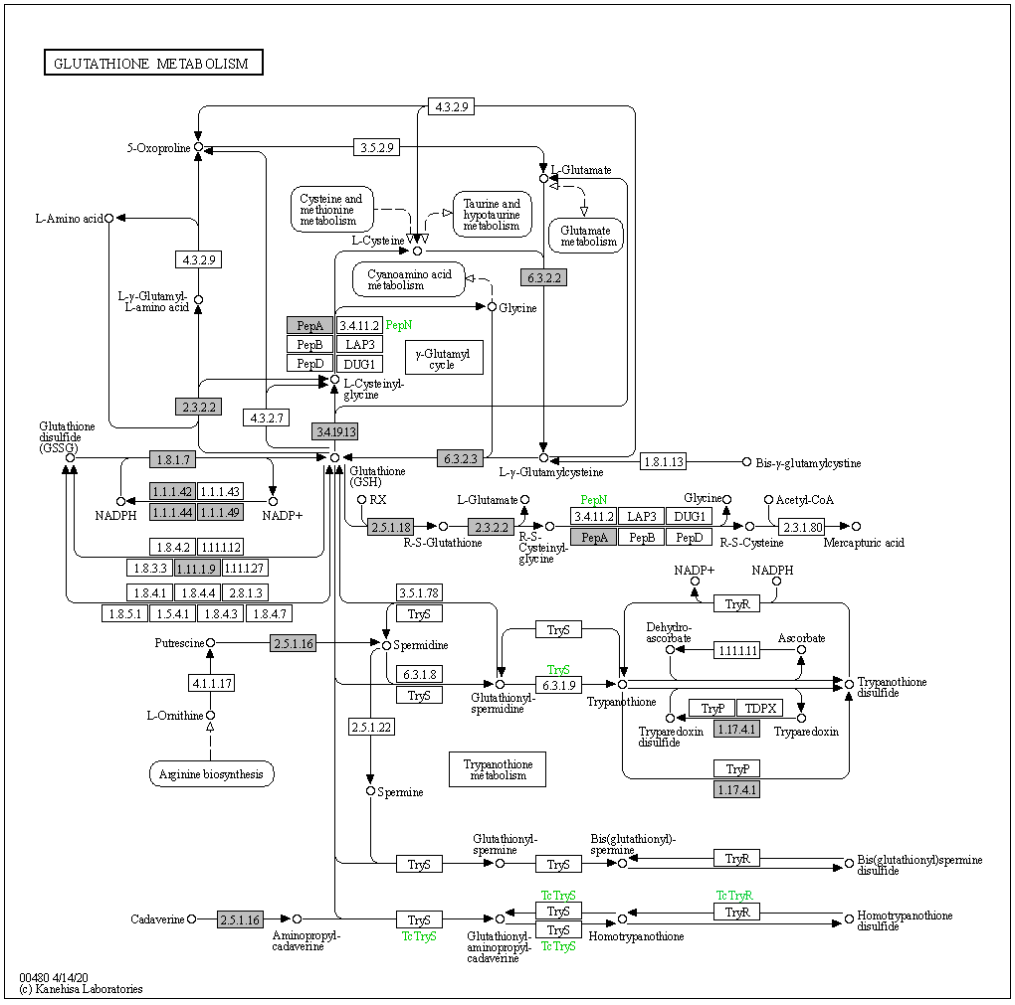

(b) Stm, Ctrl vs NFTs, aa-tRNA biosynthesis

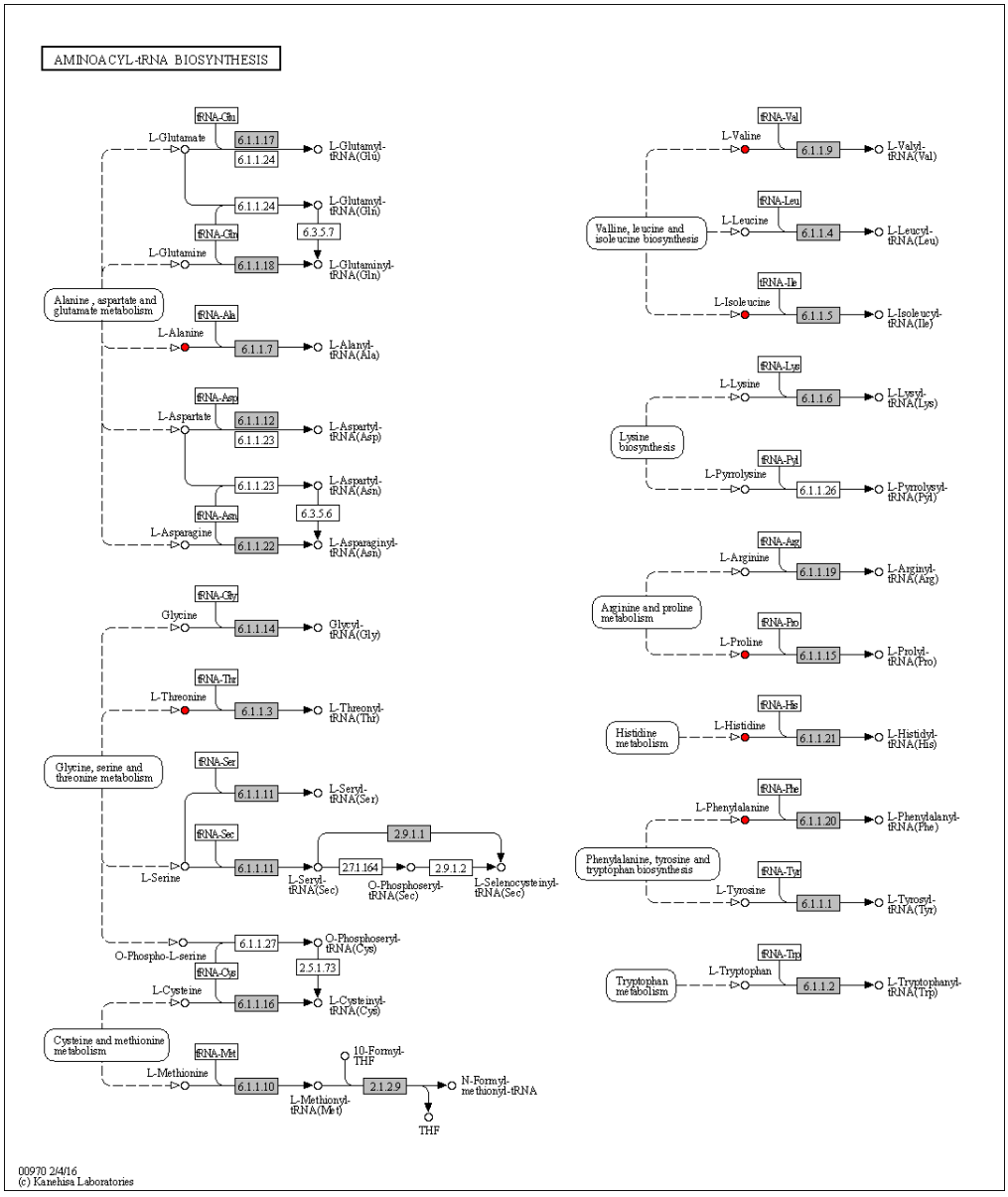

Fig. S1-7. Pathways of GSH metabolism (a) and aa-tRNA biosynthesis (b) in the *Stenotrophomonas maltophilia* FZD2 (Stm) in response to prolonged exposure to NFT. The genes are marked in gray and the downregulated compounds in red. No upregulated compounds involved in the pathways were observed.

(a) Stm, Ctrl vs FTDs, GSH metabolism

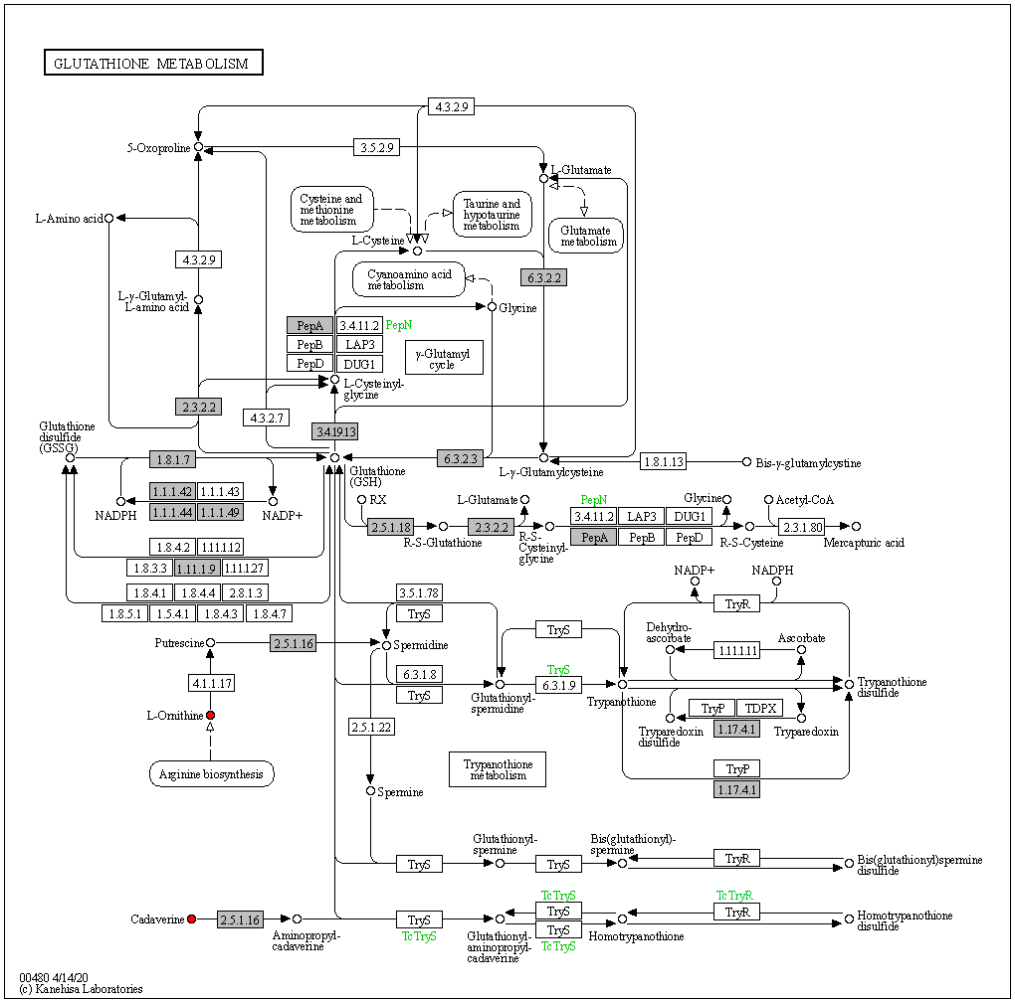

(b) Stm, Ctrl vs FTDs, aa-tRNA biosynthesis

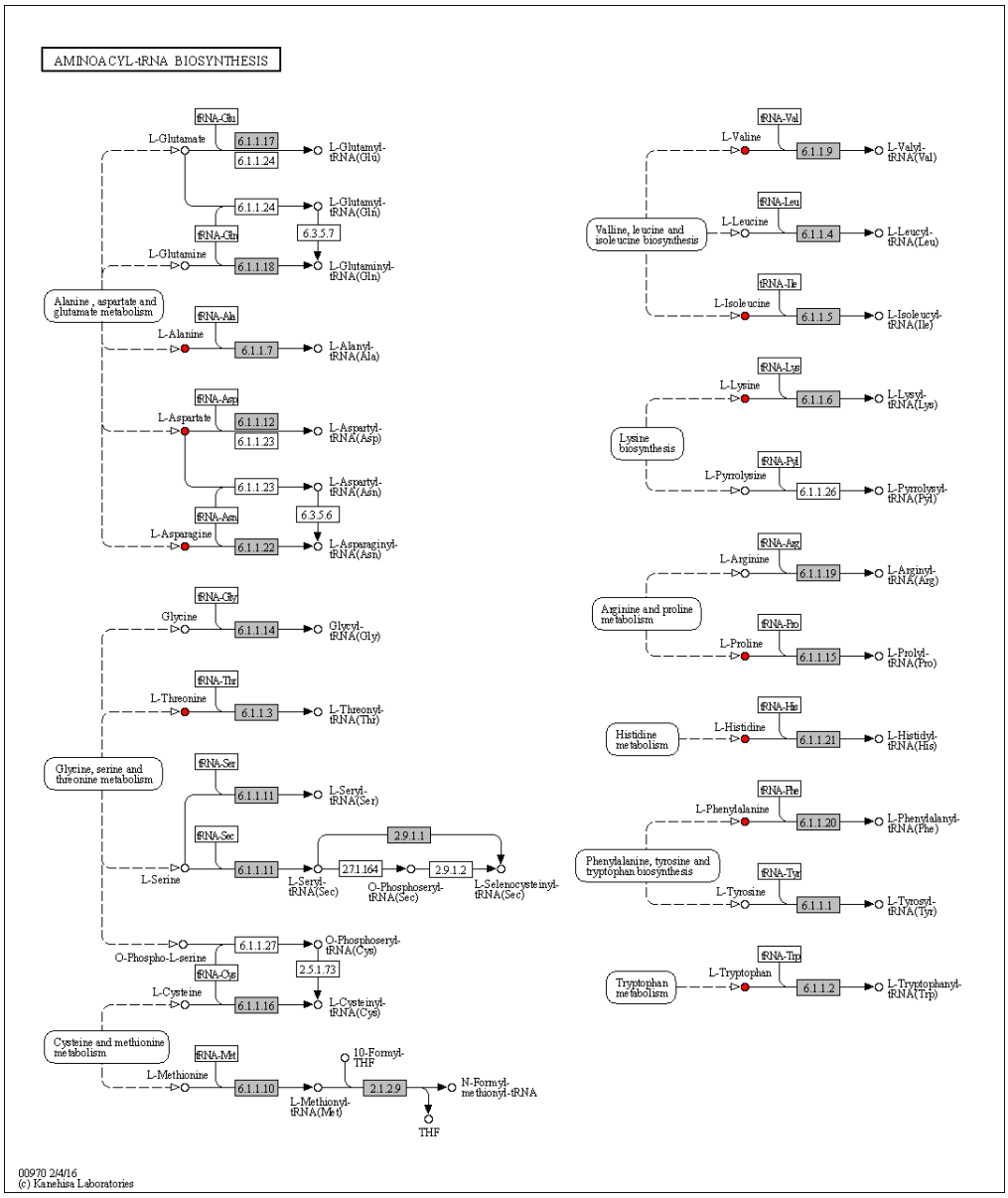

Fig. S1-8. Pathways of GSH metabolism (a) and aa-tRNA biosynthesis (b) in the *Stenotrophomonas maltophilia* FZD2 (Stm) in response to prolonged exposure to FTD. The genes are marked in gray, the downregulated compounds in red, and the enzymes catalyzing the reactions in green. No upregulated compounds involved in the pathways were observed.

2.4. RAPD-PCR

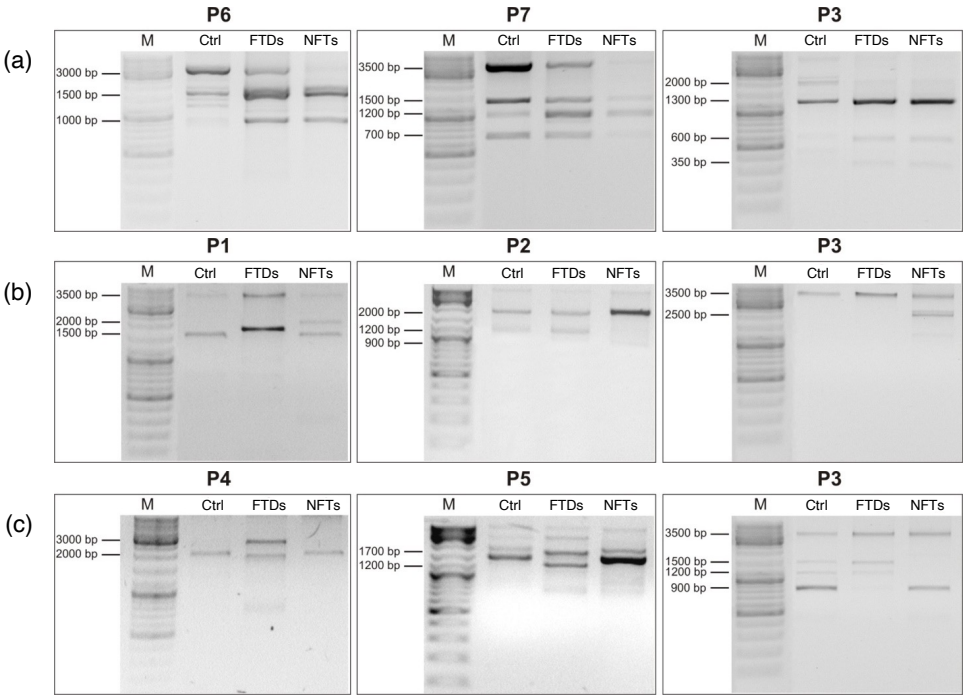

Fig. S1-9. RAPD-PCR patterns generated by *Sphingobacterium siyangense* FTD2 (a), *Achromobacter pulmonis* NFZ2 (b), and *Stenotrophomonas maltophilia* FZD2 (c). Samples labels: Ctrl – control cells, NFTs/FTDs – cells exposed to nitrofurantoin/furaltadone, M - 1 kb DNA Ladder, P1-P7 – primers used in RAPD-PCR reaction.

RAPD-PCR analysis was performed with the kind assistance of Dr. Beata Dudzińska-Bajorek from Hipolit Cegielski State College of Higher Education in Gniezno, Poland.

2.5. Cell metabolic activity

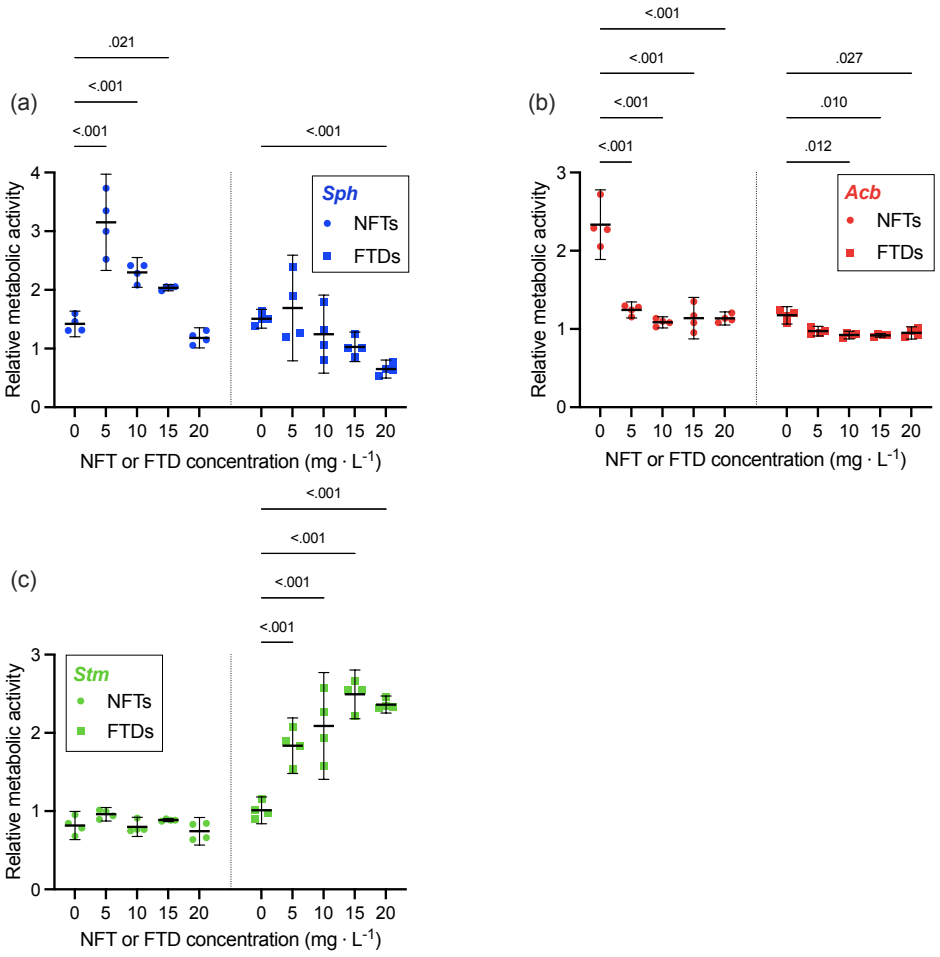

Fig. S1-10. Relative metabolic activity of the strains exposed to various concentrations of NFT or FTD. *Sphingobacterium siyangense* FTD2 (a), *Achromobacter pulmonis* NFZ2 (b), and *Stenotrophomonas maltophilia* FZD2 (c)

Supplementary information 2 (P4)

Supplementary material 2 is an xlsx. file. Document is available at the following link:

https://doi.org/10.1016/j.scitotenv.2023.162199

At the request of the reader, the author or the author's supervisor will send a copy of this document to a personal email address.

Publication P5

Science of the Total Environment 874 (2023) 162422

Contents lists available at ScienceDirect

Science of the Total Environment

journal homepage: www.elsevier.com/locate/scitotenv

Multi-faceted analysis of bacterial transformation of nitrofurantoin

Amanda Pacholak [a,*], Wojciech Juzwa [b], Agnieszka Zgoła-Grześkowiak [c], Ewa Kaczorek [a]

[a] Institute of Chemical Technology and Engineering, Poznan University of Technology, Poznan, Poland
[b] Department of Biotechnology and Food Microbiology, Faculty of Food Science, Poznan University of Life Sciences, Poznan, Poland
[c] Institute of Chemistry and Technical Electrochemistry, Poznan University of Technology, Poznan, Poland

HIGHLIGHTS

- Primary biodegradation of nitrofurantoin by *Serratia marcescens* ODW152 reached 96 %.
- Atomic force microscopy and flow cytometry revealed variations of cell properties.
- Increase in surface roughness of non-active cells was observed.
- Nitrofurantoin biodegradation led to formation of stable transformation products.
- Transformation products affected the physiology and structure of bacterial cells.

GRAPHICAL ABSTRACT

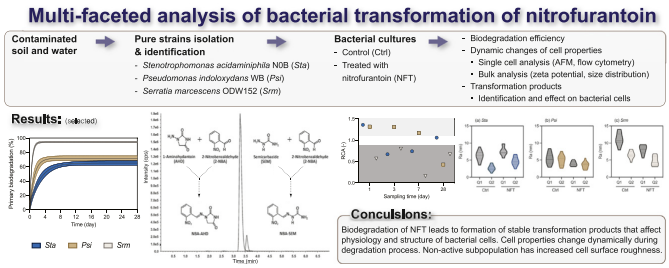

ARTICLE INFO

Editor: Frederic Coulon

Keywords:
Atomic force microscopy
Biotransformation
Metabolites
Single cell microbiology
Toxicity

ABSTRACT

Excessive presence of antibiotics and their residues can be dangerous to the natural environment. To reduce this negative effect, efficient strategies to remove them from the ecosystem are required. This study aimed to explore the potential of bacterial strains to degrade nitrofurantoin (NFT). Single strains isolated from contaminated areas, namely *Stenotrophomonas acidaminiphila* N0B, *Pseudomonas indoloxydans* WB, and *Serratia marcescens* ODW152 were employed in this study. Degradation efficiency and dynamic changes within the cells during NFT biodegradation were investigated. For this purpose, atomic force microscopy, flow cytometry, zeta potential, and particle size distribution measurements were applied. *Serratia marcescens* ODW152 showed the highest performance in removal of NFT (96 % in 28 days). The AFM images revealed modifications of cell shape and surface structure induced by NFT. Zeta potential showed significant variations during biodegradation. Cultures exposed to NFT had a broader size distribution than the control cultures due to increased cells agglomeration or aggregation. 1-Aminohydantoin and semicarbazide were detected as nitrofurantoin biotransformation products. They showed increased cytotoxicity toward bacteria as determined by spectroscopy and flow cytometry. Results of this study suggest that nitrofurantoin biodegradation leads to formation of stable transformation products that significantly affect the physiology and structure of bacterial cells.

1. Introduction

Antibiotics are powerful compounds that play a vital role in curing numerous infections and promoting livestock growth. Nowadays, they are the most produced drugs worldwide (Li et al., 2022a). Among the most important classes of antibiotics, nitrofurans are often used in the excessive quantities, however, they lack enough attention of the scientific community. Nitrofurantoin (NFT), a major representative of the nitrofurans group, is a cyclic amide containing a 5-nitrofuran ring. This synthetic

Abbreviations: AFM, atomic force microscopy; AHD, 1-aminohydantoin; AHD-NBA, 2-nitrobenzaldehyde derivative of 1-aminohydantoin; BHI, Brain Heart Infusion; DPBS, Dulbecco's phosphate-buffered saline; MHA, Mueller Hinton Agar; NBA, 2-nitrobenzaldehyde; NFT, nitrofurantoin; PS, particle size; Ra, roughness average; SEM, semicarbazide; SEM-NBA, 2-nitrobenzaldehyde derivative of semicarbazide; TPs, transformation products; RCA, relative cellular activity; RFI, relative fluorescence units; ZP, zeta potential.

* Corresponding author.
E-mail address: amanda.pacholak@put.poznan.pl (A. Pacholak).

http://dx.doi.org/10.1016/j.scitotenv.2023.162422
Received 18 January 2023; Received in revised form 15 February 2023; Accepted 19 February 2023
Available online 28 February 2023

broad-spectrum antibiotic is used in medicine, livestock, and aquaculture due to effectiveness and low production costs. Despite NFT is an old drug, its mechanism of action against bacteria is not fully understood. Probably it presents multiple mechanisms of action such as inhibition of enzymes involved in DNA and RNA synthesis (Huttner et al., 2015; McOsker and Fitzpatrick, 1994). Utilization of nitrofurans in husbandry and farming has been prohibited in many countries (Commission Regulation (EC), 1995). The illegal use in agriculture and livestock as well as pharmaceutical treatment and manufacturing promote the continuous discharge of nitrofurans into the natural environment (Kumar et al., 2018a; Li et al., 2022b; Sakthivel et al., 2023). Presence of NFT residues in the environment can be hazardous at various trophic levels — from microorganisms, through plants and animals to humans (Bessone et al., 2023; de Oliveira et al., 2020; Lewkowski et al., 2019; Pacholak et al., 2019). The report of the European Food Safety Authority published in 2015 described several aspects of hazardous action on humans and environment of five nitrofuran antibiotics (EFSA Panel on Contaminants in the Food Chain (CONTAM), 2015).

To minimize the negative impact of antibiotics on organisms in the receiving environments, it is essential to remove them from the ecosystems. The main decontamination methods for antibiotics contaminated sites include physical remediation, chemical remediation, bioremediation, and a combination of the above-mentioned technologies. Compared to physical-chemical treatment technologies, biological treatment (phytoremediation or microbial remediation) is more promising because of robustness, cost-effectiveness, and eco-friendly approach (Ye et al., 2017). Microbial bioremediation relies only on natural metabolic processes of microorganisms and their ability to transform hazardous contaminants into simple, less toxic, or non-toxic compounds. According to the OECD guidelines, the total mineralization (ultimate biodegradation) occurs when a compound of interest is completely utilized by microorganisms. As a result, carbon dioxide, water, mineral salts, and biomass are produced. During primary biodegradation (biotransformation) the structural change of a parent compound occurs resulting in the loss of specific properties of that compound (OECD, 1992).

Recently, new, and effective remediation technologies develop successively. The global bioremediation market size was estimated at USD 106 billion in 2019 and is expected to reach USD 335 billion by 2027 (Tran et al., 2021). The bacterial strains that can be used in bioremediation processes are usually isolated from natural bacterial communities inhabiting chronically contaminated sites. A general scheme to isolate pure strains includes four major steps: aseptic environmental sample collection, isolation and screening of pure strains in a medium containing the target compound, identification of single species by 16 sRNA sequencing, and evaluation of biodegradation potential (Pacholak et al., 2019; Tran et al., 2021). It is generally believed that microbial communities have more powerful potential to biodegrade the mixtures of organic compounds than the single strains (Nnabuife et al., 2022; Pacholak et al., 2023). However, bioaugmentation of contaminated sites with autochthonous, highly efficient species capable of directly degrading the pollutants is a promising strategy for bioremediation (Li et al., 2020). The bacterial species recently used for bioremediation include *Bacillus paramycoides* SDB4 (remediation of sulfamethoxazole) (Chen et al., 2022), *Bacillus* sp. LS1 (polychlorinated biphenyls) (Han et al., 2023), *Burkholderia cepacia* (tetracycline) (Hong et al., 2020), *Ochrobactrum* sp. TCC-2 (triclocarban) (Bai et al., 2021). A novel approach also includes augmentation of contaminated sites with non-direct degraders (NDDs). NDDs are organisms unable to directly biodegrade the pollutants of interest but they modify metabolic pathways of target compounds by other organisms and thus their potential contribution can be significant (Li et al., 2020).

Physicochemical parameters of the ecosystem, characteristics of the pollutants, and biological properties of the microbial cells are among crucial factors limiting bioremediation efficiency (Ossai et al., 2020). The latter include, among others, cells tolerance to toxicity, structure of microbial communities, viability, metabolic activity, or surface properties of the cells (Ma et al., 2018; Pacholak et al., 2023). Metabolic activity and viability of cells change dynamically during biodegradation and are important parameters considered when monitoring the bioremediation process. They can be measured using different methods based on either bulk measurement of microbial suspension or single cell measurements that can rapidly provide information about cell function (Nebe-von-Caron et al., 2000). Cell surface properties affect uptake and bioavailability of the contaminants. Therefore, they can play a key role in biodegradation of antibiotics. These properties include, among others, cell surface zeta potential, cell size, ultrastructure, and morphology. To date, dynamic changes occurring within the bacterial cells during biodegradation of antibiotics are not well documented (Ma et al., 2018).

Each degradation process tends to decompose the hazardous pollutant of interest to a harmless state. The processes are usually focused on the parent compounds only, despite they can contribute to formation of hazardous transformation products (TPs) (Vasquez et al., 2013). TPs can remain pharmacologically active in the environment for a long time. Knowledge about them is insufficient, therefore TPs should be monitored and their effect on organisms should be evaluated (López-Serna et al., 2013).

To fulfill the above-mentioned research gaps, this study aimed to isolate the pure bacterial strains from contaminated environments, investigate biodegradation of nitrofurantoin by these novel species, identify biotransformation products, and evaluate their impact on the bacterial cells. As microbiological parameters are essential in monitoring biodegradation process, dynamic changes in the cell surface properties and metabolic activity were investigated during biodegradation of nitrofurantoin. For this purpose, a combination of atomic force microscopy, flow cytometry, zeta potential and particle size distribution measurements was applied. To the authors knowledge, this is the first time that nitrofurantoin biodegradation coupled with evaluation of dynamic changes within the cells is being investigated. This study also aimed to reveal the effects of transformation products identified on the cell membrane permeability and cell metabolic activity determined by spectroscopy and flow cytometry. Results provide new insights into potential ability of indigenous environmental strains to decompose nitrofurantoin and provide information on the possible effect of transformation products on the autochthonous bacterial cells.

2. Materials and methods

2.1. Reagents

M9 minimal salts, organic solvents, standards, and other chemicals were purchased from Merck (Darmstadt, Germany) unless otherwise stated. Mueller Hinton Agar (MHA) and Brain Heart Infusion broth (BHI) were purchased from bioMerieux (Warsaw, Poland). All chemicals were of analytical grade (at least 99 %) and were used as received without further purification. HPLC-grade water used to prepare aqueous solutions was obtained from ultrapure water system (Arium® Pro, Sartorius, Kostrzyn Wlkp., Poland). Glassware and autoclavable solutions were steam sterilized (HMC-Europe, Tüssling Germany). Other solutions were filter sterilized using Captiva 0.22 μm EconoFilters (Agilent, CA, USA). A biological safety cabinet (Labculture® Class II, Esco, Singapore) was used during activities associated with bacterial samples to prevent contamination.

2.2. Bacterial strains and growth conditions

The bacterial strains were isolated from three contaminated sites: two soil types and water reservoir. During the isolation process, which was carried out using a selective culture method, NFT solution acted as a selective agent (Pacholak et al., 2019). After eight weeks of the continuous cultivation, 100 μL of each culture was seeded in triplicate onto the MHA plate and incubated for 24 h at 30 °C. The colonies grown in the largest quantities were selected for biochemical identification and susceptibility testing (Vitek® 2 system, bioMérieux, Warsaw, Poland). The selected strains (one strain from each collected environmental sample) were identified by molecular techniques (Kaczorek et al., 2013). The 16S rRNA gene sequences of the strains have been deposited in the GenBank database

under the following accession numbers: *Stenotrophomonas acidaminiphila* N0B isolated from contaminated soil (hereinafter referred to as *Sta*, GenBank: KY561351.1), *Pseudomonas indoloxydans* WB isolated from water reservoir from the contaminated area (*Psi*, MK503999.1), *Serratia marcescens* ODW152 isolated from contaminated soil (*Srm*, MN960427.1). Phylogenetic tree was constructed by the neighbor joining method using MEGA X software, with bootstrap values set to 1000 replicates. The percentage of replicate trees in which the associated taxa clustered together in the bootstrap test was shown next to the branches. The branch lengths were estimated by the Maximum Likelihood method (Felsenstein, 1985; Kumar et al., 2018b; Saitou and Nei, 1987). To establish the enrichment cultures, three to five colonies of each strain were picked from freshly grown MHA plate and added to 9 mL of the BHI broth. The bacteria were incubated overnight at 30 °C, washed twice with sterile Dulbecco's phosphate-buffered saline (DPBS) and resuspended in this buffer to adjust the optical density at 600 nm to 1.0 ± 0.1 using Multiskan 152 Sky Microplate Spectrophotometer (Thermo Fisher Scientific, Waltham, MA, USA). Such prepared microbial suspensions were used for inoculation to start the bacterial cultures. Media composition and cultures components were described previously (Pacholak et al., 2020a). Cultures of the bacteria without any NFT as well as sterile abiotic samples were also maintained as the controls. The abiotic samples were obtained by autoclaving the biomass for 15 min at 121 °C and adding 2 % sodium azide to inhibit the proliferation of bacteria. Cultures containing NFT at initial concentration of 5 $mg \cdot L^{-1}$ were incubated in the dark at 30 °C with shaking (120 rpm) for 28 days.

2.3. Primary biodegradation and detection of transformation products

The removal efficiency was measured for 28 days according to the guidelines of The Organization for Economic Co-operation and Development. To investigate the ability of the single strains to biodegrade NFT, 1.5 mL samples were collected aseptically from the cultures every few days. Initial samples were collected after 1 h incubation to ensure the equilibration and homogeneity of the sample. The biomass was harvested (13,000 g, 2 min) and stored at −20 °C by the end of the experiment. To calculate the degradation rate, the supernatants were diluted with HPLC-grade methanol and filtered using 0.2 μm PTFE syringe filters (Agilent, Santa Clara, CA, USA). The samples were analyzed qualitatively and quantitatively for the residual content of NFT using LC/MS-MS (UltiMate 3000 LC (Dionex, Sunnyvale, CA, USA)/API 4000 QTRAP (Applied Biosystems/MDS Sciex, Waltham, MA, USA). Removal of NFT during abiotic degradation was subtracted from the results of NFT biological degradation. To identify the degradation products, the supernatants were derivatized. The detailed protocols of metabolites derivatization and LC-MS/MS analysis are presented in the Supplementary Information.

2.4. AFM analysis of the bacterial cell surface

An atomic force microscope Park NX10 from Park Systems (Suwon, South Korea) was used to analyze changes in the cell topography of the bacteria. The changes in the morphology of the cells were analyzed from the surface plots according to the procedure described previously (Pacholak et al., 2020a).

2.5. Zeta potential and size distribution measurements

Zeta potential of the bacterial suspensions during biodegradation of NFT was determined with the Zetasizer Nano ZS (Malvern Panalytical, Malvern, UK). The cells collected from the bacterial cultures were suspended in DPBS and adjusted to OD600 of 0.5 ± 0.1. The polydispersity index (PDI) and particle size distribution of the microbial cultures was determined using the same instrument. Measurements were conducted in a cuvette at 90 degree scattering angle for both untreated and NFT-treated bacterial cells. The Zeta potential and PDI measurements were performed in DPBS buffer solution (pH 7.4) to reduce any influence of pH and conductivity.

2.6. Flow cytometric analysis

Variations in the metabolic activity and viability of the bacterial cells during biodegradation of NFT were determined using BacLight™ Redox Sensor™ Green Vitality Kit from Thermo Fisher Scientific (Waltham, MA, USA) and a flow cytometer (cell sorter) BD FACS Aria™III from Becton Dickinson (San Jose, CA, USA). The configuration of the instrument was as follows: 4 lasers (375 nm, 405 nm, 488 nm, and 633 nm), 11 fluorescence detectors, forward scatter (FSC) and side scatter (SSC) detectors; 70 μm nozzle and 70 psi (0.483 MPa) sheath fluid pressure. Sample preparation and instrument settings were based on the protocol described by Duber et al. (2018). BacLight™ Redox Sensor™ Green Kit contains RedoxSensor Green reagent (RSG), which is a fluorogenic redox indicator dye. This compound is subjected to conversion by microbial reductases involved in electron transport chain. The converted dye, following excitation (maximum = 490 nm) emits a green fluorescence (maximum = 520 nm). The intensity of green fluorescence emission is directly proportional to cellular redox potential (CRP), indicating the levels of microbial cells' metabolic activity (Díaz et al., 2010). The determination of cellular redox potential of the analyzed microorganisms was based on the measurement of green fluorescence intensity (FITC detector) from a redox potential-sensitive reagent (RedoxSensor™ Green reagent from Thermo Fisher Scientific). Data were acquired in a four-decade logarithmic scale as area signals (FSC-A, SSC-A and FITC-A) and analyzed with FACS DIVA software (Becton Dickinson). The discrete subpopulations of non-active (Q1) and active (Q2) cells were defined on bivariate dot plots FITC-A (x axis) vs. SSC-A (y axis) corresponding to cellular redox potential vs. side scatter measurement. Based on percentages of cells from the defined subpopulations (Q1 and Q2) the relative cellular activity (RCA) values were calculated according to Eq. (1).

$$\mathrm{RCA} = \frac{\text{treated sample } \frac{\text{active (\%of Q2)}}{\text{non − active (\%of Q1)}}}{\text{control sample } \frac{\text{active (\%of Q2)}}{\text{non − active (\%of Q1)}}} \quad (1)$$

Three ranges of relative cellular activity (RCA) values were defined: RCA > 1.1 — increase in the number of active cells in the treated sample relative to control; RCA < 0.9 — decrease in the number of active cells in treated sample relative to control; RCA = (0.9–1.1) — no effect of treatment on the cellular activity.

In addition to RCA values, the significant differences among medians of green fluorescence intensity (from RedoxSensor Green reagent) for active cells were also observed. An analogy to Q1 and Q2 percentages-based RCA calculation was used to define RFI (relative fluorescence intensity) values. RFI were calculated as medians of fluorescence intensity emitted by active cells from treated sample relative to control (Eq. 2). RFI were defined as relative fluorescence units (RFU).

$$\mathrm{RFI} = \frac{\text{treated sample (medians of RSG fluorescence (RFU))}}{\text{control samples (medians of RSG fluorescence (RFU))}} \quad (2)$$

2.7. Cell sorting and cell surface roughness analysis

After 28 days of degradation process, cells were sorted using flow cytometry assisted cell sorting into subpopulations representing two physiological states (active and non-active) to analyze them using AFM. The cells from the defined non-active (Q1) and active (Q2) subpopulations were isolated using BD FACS Aria™III cell sorter for the subsequent examination of cellular surface using AFM analysis. Cell sorting preceded doublets discrimination procedure with the use of height versus width scatter signals measurement (SSC-H vs. SSC-W and FSC-H vs. FSC-W) to discriminate single cells from conglomerates allowing high purity sort. The AccuDrop™ beads (Becton Dickinson, San Jose, CA, USA) were used

to setup the drop delay for the best sorting performance. The FACS Aria™III cell sorter settings were established for gaining highest purity level. Cells were sorted to 5 mL cytometric tubes. The cells were subjected to AFM imaging to investigate differences in the average cell surface roughness during biodegradation of NFT. The procedure was adapted from Pacholak et al. (2020a).

2.8. Growth curve measurements

The growth of bacteria treated with NFT and its two transformation products as well as untreated control bacteria was monitored by measuring the optical density of the cell suspensions at the wavelength of 600 nm (OD600) as described by Krishnamurthi et al. (2021). The growth curve measurements were performed with a microplate reader (Multiskan 152 Sky, Thermo Fisher Scientific, Waltham, MA, USA) and the 96-well clear bottom sterile microplates. 200 μL of the prepared bacterial cultures were transferred to the microplate wells. The plates were maintained at 37 °C with pulse shaking. The OD600 of each well were read every 10 min for 24 h.

2.9. Effect of transformation products on bacterial cells

The experiments determining the impact of NFT, SEM, and AHD exposure on bacterial cells include: (i) Modifications of the bacterial membrane permeability — the measurements were based on the Crystal Violet uptake by the cells (Pacholak et al., 2020a); (ii) Relative cytotoxicity of the compounds in question measured with the colorimetric test AlamarBlue® Cell Viability Assay (Pacholak et al., 2022); and (iii) Metabolic activity of cells measured with the flow cytometry. (Duber et al., 2018). TPs used to establish the bacterial cultures were purchased from Merck (Darmstadt, Germany).

2.10. Statistical analysis

Results are reported as the average values calculated from at least three independent biological replicates. For each replicate, at least two technical replicates were performed. A statistical significance of differences between the means of control samples and reference samples was determined by a one-way or two-way ANOVA. Tukey's method was used for *post-hoc* testing with a significance level of 0.05. *P* values calculated report up to three digits after the decimal point, not significant comparisons with *P*-values ≥ 0.05 are not labelled in the graphs. In the violin plots, representing the empirical distribution of the data, midline is plotted at the median and dotted lines represent first and third quartiles. The calculations were performed using GraphPad Prism (GraphPad Software, LLC, San Diego, CA, USA).

3. Results and discussion

3.1. Biodegradation of nitrofurantoin

3.1.1. Strains isolation and nitrofurantoin removal efficiency

In this study, three Gram-negative bacterial strains were isolated and identified from various environmental niches: two types of soil and water. Phylogenetic analysis based on 16S rRNA sequencing was used to identify the strains, namely *Sta*, *Psi*, and *Srm* (as described in Section 2.2). Phylogenetic trees constructed are presented in Supplementary Information, Figs. S1–S3. The *Sta* strain belongs to *Stenotrophomonas acidaminiphila species*, which is a rod-shaped bacterium that widely exists in the environment. *S. acidaminifilia* have been previously isolated by other authors from the long-time contaminated sites for potential use in bioremediation (Li et al., 2022a; Zhang et al., 2023). Li et al. (2022b) isolated *S. acidaminiphila* Y4B strain from the activated sludge which was capable of complete biodegradation of herbicide glyphosate (50 $mg{\cdot}L^{-1}$ was removed within 72 h). Zhang et al. (2023) isolated *S. acidaminiphila* BDBP 071 from contaminated tomato rhizosphere soil. The strain showed a promising biodegradation efficiency of dibutyl phthalate at various concentrations. The *Psi* strain was identified as *Pseudomonas indoloxydans*. *P. indoloxydans* was isolated for the first time in 2008 from a pesticide-contaminated site in India (Manickam et al., 2008). To date, *P. indoloxydans* strains isolated from environmental matrices have been known for their ability to promote plant growth and degrade environmental pollutants (Shahid et al., 2020; Tara et al., 2019). Shahid et al. (2020) proved that inoculation of macrophytes with the bacterial consortium containing *P. indoloxydans* can enhance removal of trace metals from polluted river water. Tara et al. (2019) successfully used *P. indoloxydans* NT-38 strain to support treatment of textile industry wastewater. The *Srm* strains belongs to the *Serratia marcescens* species which is a ubiquitous bacterium in soil, water, plant surfaces, and animals, including humans (Hou et al., 2022). The presented examples prove that the strains can be used in removal of various pollutants. This suggests that they could be also suitable in bioremediation of antibiotic-polluted sites. Further research focused on possible application of the strains in bioaugmentation is necessary to understand the interactions of the pure strain with complex mixture of soil particles and other community members of the ecosystem.

Fig. 1 shows the results of NFT primary biodegradation rate by the *Sta*, *Psi*, and *Srm* strains. The highest removal was observed for the *Srm* strain. The average NFT removal after 24 h of incubation was 82 %. After reaching a peak of 91.3 ± 2.1 % degradation in four days, NFT concentration remained relatively stable by the end of the experiment. Final biodegradation was 96.5 ± 1.4 %. The strains *Psi* and *Sta* showed significantly lower degradation capability than the *Srm* strain. On average, 45 % of NFT was removed from the culture medium in one day and 60 % in four days by the *Psi* strain. A complete removal of NFT has not been achieved, 83.8 ± 4.3 % biodegradation was measured in 28-day cultures (remaining average NFT concentration: 0.81 $mg{\cdot}L^{-1}$). Removal efficiency of the *Sta* strain was significantly lower than that of the *Psi* strain. The highest decrease in NFT concentration was measured on the first day and was followed by steady gradual elimination. The average biodegradation after 24 h was 29 %. This value doubled on the eleventh day. The final removal rate measured after 28 days was 75.6 ± 3.0 % with a residual average NFT concentration of 1.2 $mg{\cdot}L^{-1}$. The concentrations measured in the abiotic samples showed that after 28 days no >5 % of the NFT was abiotically eliminated from the cultures.

Previous studies focused on biodegradation of NFT by both, mixed microbial consortia and single strains indicate that some environmental bacteria are quite capable of degrading NFT (Pacholak et al., 2019, 2020b, 2023; Smułek et al., 2021). For example, *Sphingomonas paucimobilis* K3a and *Ochrobactrum antrophi* K3b were able to degrade on average 90 % of NFT in 28 days (initial concentration of 5 $mg{\cdot}L^{-1}$). That study, however, did not aim to identify biodegradation products generated during the process (Pacholak et al., 2019). This work describes products of NFT biodegradation by single strains for the first time, however, this research area still raises numerous questions and requires further investigation.

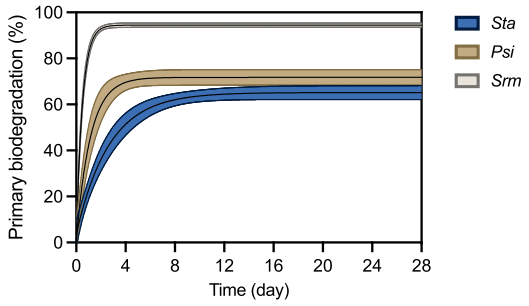

Fig. 1. Nitrofurantoin removal efficiency by three bacterial strains. *Sta* refers to *Stenotrophomonas acidaminiphila* N0B, *Psi* to *Pseudomonas indoloxydans* WB, *Srm* to *Serratia marcescens* ODW152.

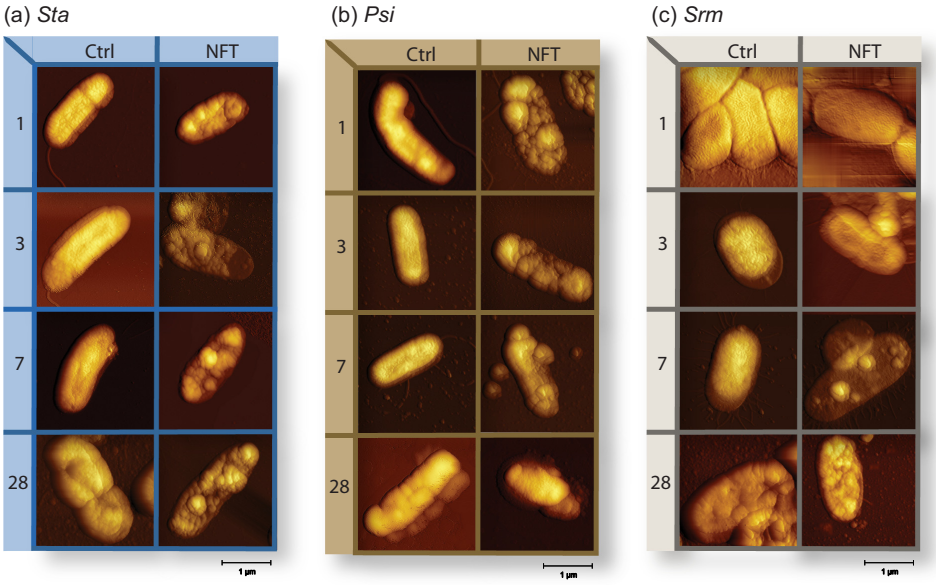

Fig. 2. Representative surface two-dimensional height images illustrating the bacterial topography during biodegradation of nitrofurantoin. The numbers 1, 3, 7, and 28 indicate the sample collection and analysis days. *Sta* refers to *Stenotrophomonas acidaminiphila* N0B, *Psi* to *Pseudomonas indoloxydans* WB, *Srm* to *Serratia marcescens* ODW152. Ctrl denotes bacteria from the control cultures, NFT - bacteria from the cultures containing nitrofurantoin.

3.1.2. Detection of morphological changes during biodegradation

Fig. 2 shows the representative AFM images of the individual cells of the *Sta*, *Psi*, and *Srm* strain. The samples were collected and analyzed after 1, 3, 7, and 28 incubation days. The analyses were performed to investigate morphological changes in cell surface and shape due to potential cell damage. The AFM images of all strains exposed to NFT exhibited substantial modifications of cells shape in comparison to control samples, indicating changes in cells surface structure induced by NFT. Images of the control cells of each strain evidenced a smooth, homogenous surface topography in all directions, especially during the first week of cultivation. Bacteria were homogenous and no apparent damage in the cells was observed (control samples of all strains, observation days 1, 3, and 7). In 28-day cultures, the surface of control cells showed some deformation and corrugation, especially in the *Srm* strain (Fig. 2c). Exposure to NFT had a significant effect on cell surface of each strain as they were completely different in the samples exposed to NFT than the control samples. The presence of NFT resulted in significant deformation of the cells and corrugation of their surface. In particular, the NFT-exposed *Sta* and *Psi* strains (Fig. 2a and b) showed a loss of their original structure. Irregular cells architecture could be attributed to cells damage. A similar but less severe phenomenon was observed in the *Srm* strain after 7 and 28 days. Cells deformation could be due to limited nutrient access or the need to escape xenobiotic substances (NFT and TPs). Cells corrugation could affect attachment of extracellular particles on the bacterial surface (Kämäräinen et al., 2020; Young, 2006). These could indicate activated mechanisms of cell protection. A decrease in the length and width of cells of the *Sta* strain under stress conditions was observed. A slight increase in the length and width of cells of the *Psi* strain under stress conditions was noted at each time point except for 28-day sample. The fewest variations in the cell dimensions caused by NFT were observed for the *Srm* strain. Previous study also revealed considerable modifications of bacterial cells shape and structure indicating calls damage caused by prolonged exposure of bacteria to nitrofurans. However, the cells showed a loss of their original shape and seemed to be vastly inflated upon exposure to antibiotics (Pacholak et al., 2020a). In another study carried out in *Pseudomonas aeruginosa* NFT3, NFT did not have a significant effect on the cell structure, since the treated cells showed the same properties as the control cells (Smułek et al., 2022).

3.1.3. Stability of the microbial suspension during biodegradation

The dispersive properties of the bacterial cultures, including zeta potential (ZP), particle size (PS) and polydispersity index (PdI), were measured for the initial cultures at day zero, and 1-, 3-, 7-, and 28-day cultures (Fig. 3).

All bacteria in this study exhibited a negative ZP. This was due to negatively charged functional groups associated with lipopolysaccharide, phospholipids, and proteins on the surface of the cells (Ferreyra Maillard et al., 2021). ZP of the initial cells of the *Sta* strain was -13.9 ± 1.2 mV (Fig. 3a). ZP of the non-treated *Sta* cells was -16.6 ± 2.1 mV and -16.0 ± 1.2 mV of the treated cells on the first day (significant difference compared to the initial sample, both comparisons $p < 0.001$). Much higher values of ZP were observed during subsequent measurements on days 3, 7, and 28. A statistically significant differences between the control and NFT-treated samples were observed only in 7- and 28-day cultures. The treated samples exhibited lower ZP than the control samples. ZP of the initial cells of the *Psi* strain was lower than that of the *Stm* strain (Fig. 3b). ZP of the non-treated *Psi* cells reduced significantly in 1- and 3-day cultures compared to the initial samples (all p-values < 0.001) indicating increased stability of the bacterial suspension. Differences between the control and NFT-treated samples over time were noted only in 3- and 7-day cultures. The fewest differences in bacterial surface charge between the cultures over time were measured for the *Srm* strain (Fig. 3c). The *Srm* strain was also characterized by the lowest ZP among all strains tested. The initial ZP was -7.9 ± 0.8 mV. Significant differences between the initial sample and control samples over time were measured in 7- and 28-day cultures. A statistical difference between the control (-9.1 ± 1.2 mV) and NFT-treated (-6.3 ± 0.8 mV) cells over time were noted only after seven days of incubation.

(a) *Stenotrophomonas acidaminiphila* N0B (*Sta*)

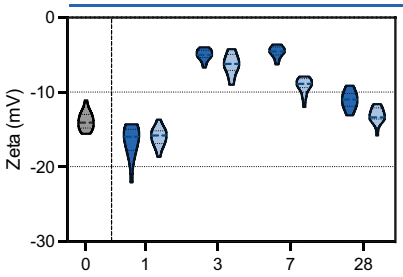

Time (day)	Ctrl		NFT	
	Size Range (nm)	PdI ± SD	Size Range (nm)	PdI ± SD
0	615 → 1484	0.43 ± 0.09	615 → 1484	0.43 ± 0.09
1	615 → 1484	0.42 ± 0.09	615 → 1718	0.55 ± 0.07
3	712 → 1281	0.30 ± 0.04	712 → 1718	0.38 ± 0.08
7	615 → 1484	0.18 ± 0.04	712 → 1484	0.25 ± 0.07
28	615 → 1281	0.13 ± 0.07	712 → 1718	0.24 ± 0.05

(b) *Pseudomonas indoloxydans* WB (*Psi*)

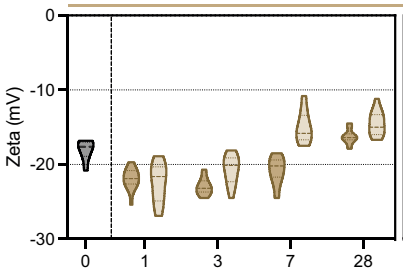

Time (day)	Ctrl		NFT	
	Size Range (nm)	PdI ± SD	Size Range (nm)	PdI ± SD
0	825 → 1718	0.29 ± 0.07	825 → 1718	0.29 ± 0.07
1	615 → 1484	0.33 ± 0.09	825 → 2669	0.59 ± 0.11
3	615 → 1484	0.29 ± 0.07	531 → 1990	0.39 ± 0.03
7	712 → 1281	0.14 ± 0.05	531 → 1484	0.35 ± 0.08
28	615 → 1281	0.25 ± 0.01	342 → 1106	0.29 ± 0.09

(c) *Serratia marcescens* ODW152 (*Srm*)

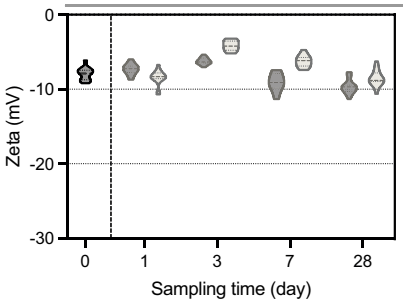

Time (day)	Ctrl		NFT	
	Size Range (nm)	PdI (SD)	Size Range (nm)	PdI (SD)
0	712 → 1281	0.27 ± 0.05	712 → 1281	0.27 ± 0.05
1	615 → 1281	0.36 ± 0.05	615 → 1281	0.36 ± 0.05
3	615 → 1484	0.30 ± 0.05	531 → 1718	0.50 ± 0.05
7	615 → 1281	0.27 ± 0.06	531 → 1106	0.30 ± 0.04
28	458 → 1718	0.44 ± 0.07	531 → 1484	0.38 ± 0.05

Fig. 3. Zeta potential of bacteria and particle size distribution of cell suspensions during biodegradation of nitrofurantoin. The samples were collected and analyzed at the beginning of biodegradation (day 0) and after 1, 3, 7, and 28 days. Ctrl refers to bacteria from the control cultures, NFT to bacteria from the cultures containing nitrofurantoin.

The surface charge of bacteria depends on the metabolic stage of cells. Higher values can be observed for cells at the stationary phase of growth where cellular death is greater, and an elevated leakage of charged molecules into the environment is observed (Ayala-Torres et al., 2014). Zeta potential can provide direct information about many cell properties, such as membrane permeability and viability. This indicates that the fewest modifications were observed for the *Srm* strain, which also showed the highest degradation potential.

Tables in Fig. 3 summarize the ranges of the cell size in every bacterial culture together with the average polydispersity index (PdI). The average size distribution of bacteria in each culture over time presented a unimodal pattern. In the *Sta* strain (Fig. 3a), size range in the control culture was from 615 to 1484 nm, and in the treated culture was from 615 to 1718 nm. In the control cells, PdI decreased from 0.43 ± 0.09 on day zero to 0.13 ± 0.07 on day 28. Higher PdI values indicate that the distribution is broad. The results obtained indicate that monodispersity of the bacterial suspension increased with the incubation time increasing. A similar situation was observed in the NFT-treated cells, however, PdI reached the highest value (0.55 ± 0.07) on day one which was followed by a steady gradual decrease. Suspensions exposed to NFT had always a broader size distribution than the control cultures. This can be due to increased cells agglomeration or aggregation. The control cultures of the *Psi* strain were characterized by size ranging from 615 to 1718 nm. A broader size range (342–2669) accompanied by greater PdI values was observed for NFT-treated cells. For the *Srm* strain, the size distribution was very similar to that of the other strains, however, the differences between the control and treated cells were much smaller.

3.1.4. Metabolic activity determined by flow cytometry during biodegradation

Flow cytometry in combination with specific fluorescent staining enabled the characterization of physiological states of bacterial cells within tested samples (Fig. 4). Interpretation of the flow cytometric results was based on determining the percentages of the defined subpopulations (non-active Q1 and active Q2, Fig. 4b) to assess their distribution within

the entire population of bacterial cells from tested samples. The relative cellular activity (RCA) values (calculated based on the percentages of non-active and active cells evaluated within control and NFT-treated samples) referred to germicidal effect of NFT on tested bacterial strains (Fig. 4a). In fact, the opposite effect indicating the stimulation of metabolic activity of bacterial cells was also observed. The above conclusion emerged from the RCA results of the strain *Srm*. It demonstrated the increase of active cells in treated sample relative to control in three time points (1-, 3-, and 7-day

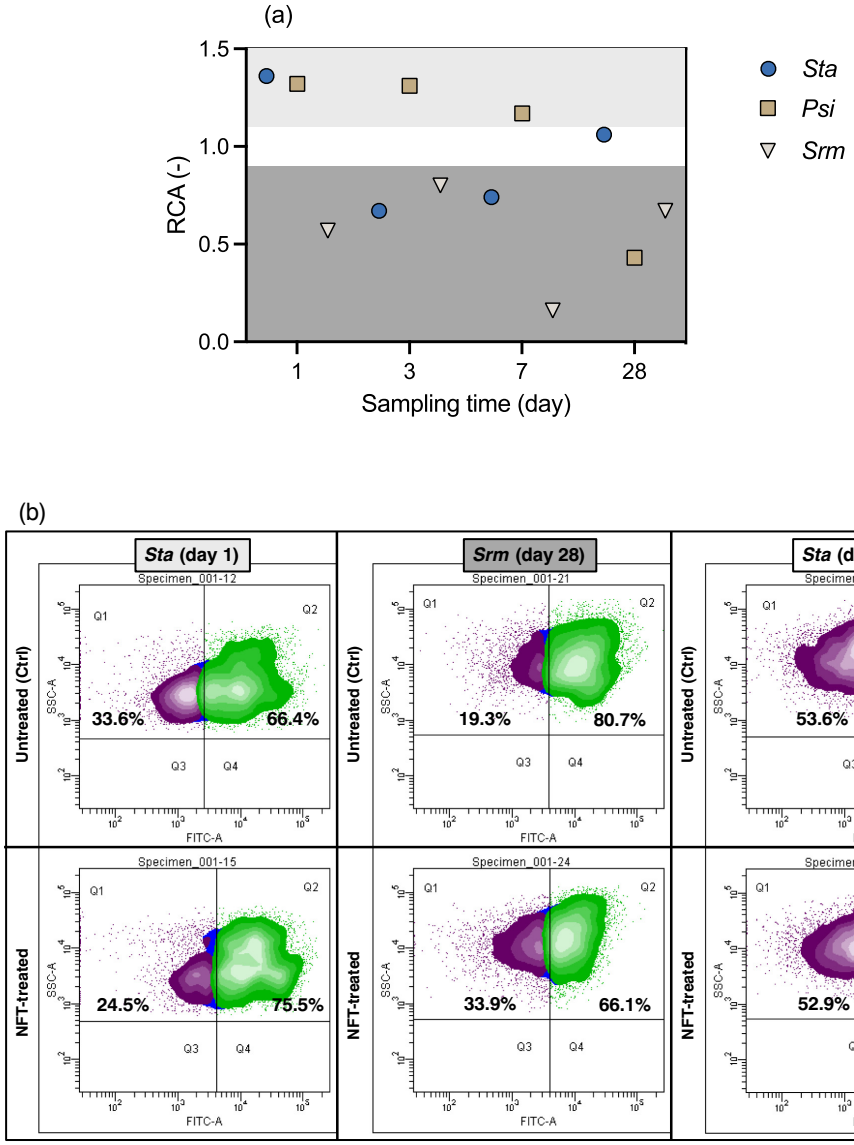

Fig. 4. The relative cellular activity (RCA) of the bacteria treated with NFT over a period of 28 days based on cellular redox potential of microbial cells (a). Flow cytometric analysis of the metabolic activity of microbial cells from NFT-treated and untreated cultures of selected strains (b). Diagrams are examples of the flow cytometric results (Q1 and Q2 correspond to non-active (violet) and active (green) subpopulations) from days 1 and 28 and strains *Sta* and *Srm* representing the 3 ranges of RCA values: RCA > 1.1 — increase of active microbes in treated sample relative to control (light grey colored box with the name of bacterial strain and culture stage); RCA < 0.9 — decrease of active microbes in treated sample relative to control (dark grey colored box with the name of bacterial strain and culture stage); RCA = (0.9–1.1) — no effect to microbes cellular activity after treatment (white colored box with the name of bacterial strain and culture stage). *Sta* refers to *Stenotrophomonas acidaminiphila* N0B, *Psi* to *Pseudomonas indoloxydans* WB, *Srm* to *Serratia marcescens* ODW152. (For interpretation of the references to color in this figure legend, the reader is referred to the web version of this article.)

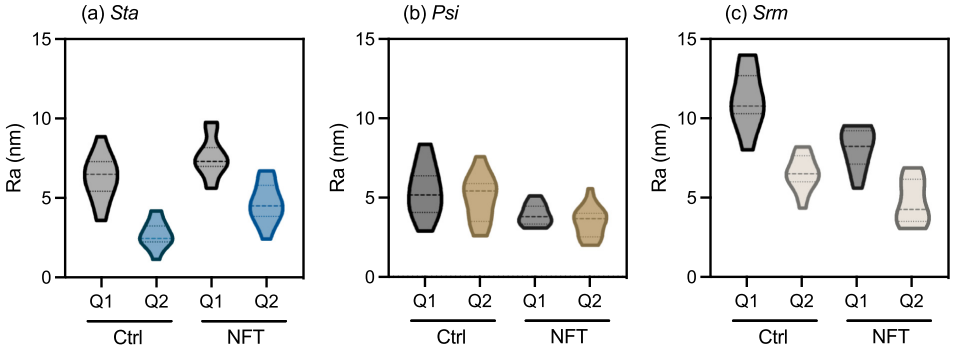

Fig. 5. The average cell surface roughness of the strains: *Sta* — *Stenotrophomonas acidaminiphila* N0B (a), *Psi* — *Pseudomonas indoloxydans* WB (b), *Srm* — *Serratia marcescens* ODW152 (c). Ctrl refers to bacteria from the control cultures, NFT to bacteria from the cultures containing nitrofurantoin. Q1 refers to non-active subpopulation, Q2 to active subpopulation.

cultures) — RCA values were 1.32, 1.31 and 1.17, respectively. The cellular metabolic activity of the *Sta* strain was also stimulated by NFT but this effect was observed only on first day of experiment reaching RCA value of 1.36. *Sta* was the only strain which did not demonstrated the germicidal effect in last day of experiment (day 28) with the RCA value of 1.06 indicating the neutral effect of NFT on cellular metabolic activity. The strain *Psi* occurred the most sensitive to NFT treatment (revealed the highest degree of bactericidal effect) as significant decrease in active bacterial cells was observed for each tested time points (culture age) — RCA values were 0.57, 0.80, 0.16, and 0.67 in 1-, 3-, 7-, and 28-day cultures, respectively. RFI values positively correlated with RCA calculations in all tested 4 time points and all 3 tested strains, demonstrating cellular activity ration of treated vs non-treated bacterial cells above 1 when RCA values indicated the increase of active microbes in treated sample relative to control (RCA > 1.1) and below 1 when RCA values indicated decrease of active microbes in treated sample relative to control (RCA > 0.9). The only exception was strain *Srm* from day 1 revealing RFI of 0.9732, while its RCA value indicated increase of active microbes in treated sample relative to control. The flow cytometric evaluation of microbial cell metabolic activity enabled the characterization of bacterial cells physiology to evaluate the germicidal or stimulant effects based on the calculated relative cellular activity (RCA) values.

3.1.5. Determination of cell surface roughness by AFM

On the last incubation day, bacterial samples were collected and sorted using flow cytometry into two subpopulations representing two physiological states (active and non-active). The sorted cells were analyzed using AFM to calculate modifications in cell surface roughness. Roughness average (Ra) calculated for active and non-active cells of control and treated culture of each strain is summarized in Fig. 5.

Non-active cells in each culture were characterized by substantially higher Ra than the active cells. Specifically, the *Sta* strain showed significant differences between the non-active (Q1 subpopulation) and active (Q2 subpopulation) cells from the control culture (6.2 ± 1.4 vs 2.7 ± 0.8 nm, $p < 0.001$) as well as the NFT culture (7.6 ± 1.2 vs 4.7 ± 1.2 nm, $p < 0.001$) were observed (Fig. 5a). For the *Psi* strain, differences between the two subpopulations in both cultures were not statistically significant (Fig. 5b). For the *Srm* strain, substantial differences between the non-active and active subpopulation of the control culture (11.2 ± 1.8 vs 6.5 ± 1.0 nm, $p < 0.001$) as well as the NFT culture (8.1 ± 1.3 vs 4.8 ± 1.4 nm, $p < 0.001$) were noted (Fig. 5c). Differences between Ra of active and non-active cells has also been observed by Niedźwiedź et al. (2020) who discovered significantly increased Ra of non-active (dead) cells in comparison to active cells. In this study, additional comparisons were made among the same subpopulations of different cultures. Differences between Ra of non-active cells collected from the control and treated cultures were statistically significant for each strain, e.g., in the *Sta* strain a significant increase was observed in NFT-treated cells (6.2 ± 1.4 nm (Ctrl) vs 7.6 ± 1.2 nm (NFT), $p = 0.016$). The two other strains showed decreased Ra in NFT-treated non-active subpopulations (*Psi*: 5.4 ± 1.6 nm (Ctrl) vs 3.9 ± 0.7 nm (NFT), $p = 0.004$; *Srm*: 11.2 ± 1.8 nm (Ctrl) vs 8.1 ± 1.3 nm (NFT), $p < 0.001$). An opposite situation was observed for active subpopulation. An increase in the Ra of the *Sta* strain and a decrease in the two other strains were observed (the Sta strain: 2.7 ± 0.8 nm (Ctrl) vs 4.7 ± 1.2 nm (NFT), $p < 0.001$; the *Psi* strain: 5.0 ± 1.4 nm (Ctrl) vs 3.5 ± 0.9 nm (NFT), $p = 0.003$; the *Srm* strain: 6.5 ± 1.0 nm (Ctrl) vs 4.8 ± 1.4 nm (NFT), $p = 0.004$). Over the years, AFM techniques have been used for imaging bacterial cells at nearly molecular resolution and unravelling the detailed architecture of cell surface. Important feature in in bacterial topography characterization is surface roughness which measures the micro-irregularities on the cell surface (Dufrêne et al., 2021; Paiva et al., 2022). In this study, the highest roughness was calculated non-active subpopulation of control *Srm* cells. Non-active cells always represented higher roughness than active cells suggesting severe membrane damage of the non-active subpopulation. Increased roughness in damaged cells was also observed by other authors (Ahmed et al., 2020; Francius et al., 2008).

3.2. Transformation products and their effect on the cells

3.2.1. Identification of transformation products

In this study, two TPs of nitrofurantoin primary biodegradation by three bacterial strains were identified. To identify TPs, the samples were collected from the microbial cultures at two timepoints (14 and 28 incubation day) and derivatized with 2-nitrobenzaldehyde (NBA). The chromatograms obtained from the LC-MS/MS analysis of the samples are presented in Fig. 6a. TPs were identified at m/z values that correspond to the protonated NBA derivative of 1-aminohydantoin (AHD) and semicarbazide (SEM). NBA-AHD conjugate was found at m/z 249 and NBA-SEM was detected at m/z = 209. AHD was accepted as the primary transformation product, which was next transformed into SEM (secondary TP) as presented in Fig. 6b. Both TPs were detected in liquid medium collected from cultures of all three strains: *Sta*, *Psi*, and *Srm*. This indicates that NFT biotransformation followed similar pathways for every strain and led to the generation of similar TPs. These TPs have been formed because of modification of the side moiety of 5-nitrofuran ring and cleavage at the carbon-carbon bond linking the aromatic ring and the specific tail group in the NFT molecule. Fig. 6c and d shows peak areas of AHD and SEM in samples collected from 14- and 28-day cultures of the *Sta*, *Psi*, and *Srm* strain. The AHD signal increased over in both cultures. The lowest signal was noted for the *Psi* strain. No relationships between primary degradation efficiency and AHD

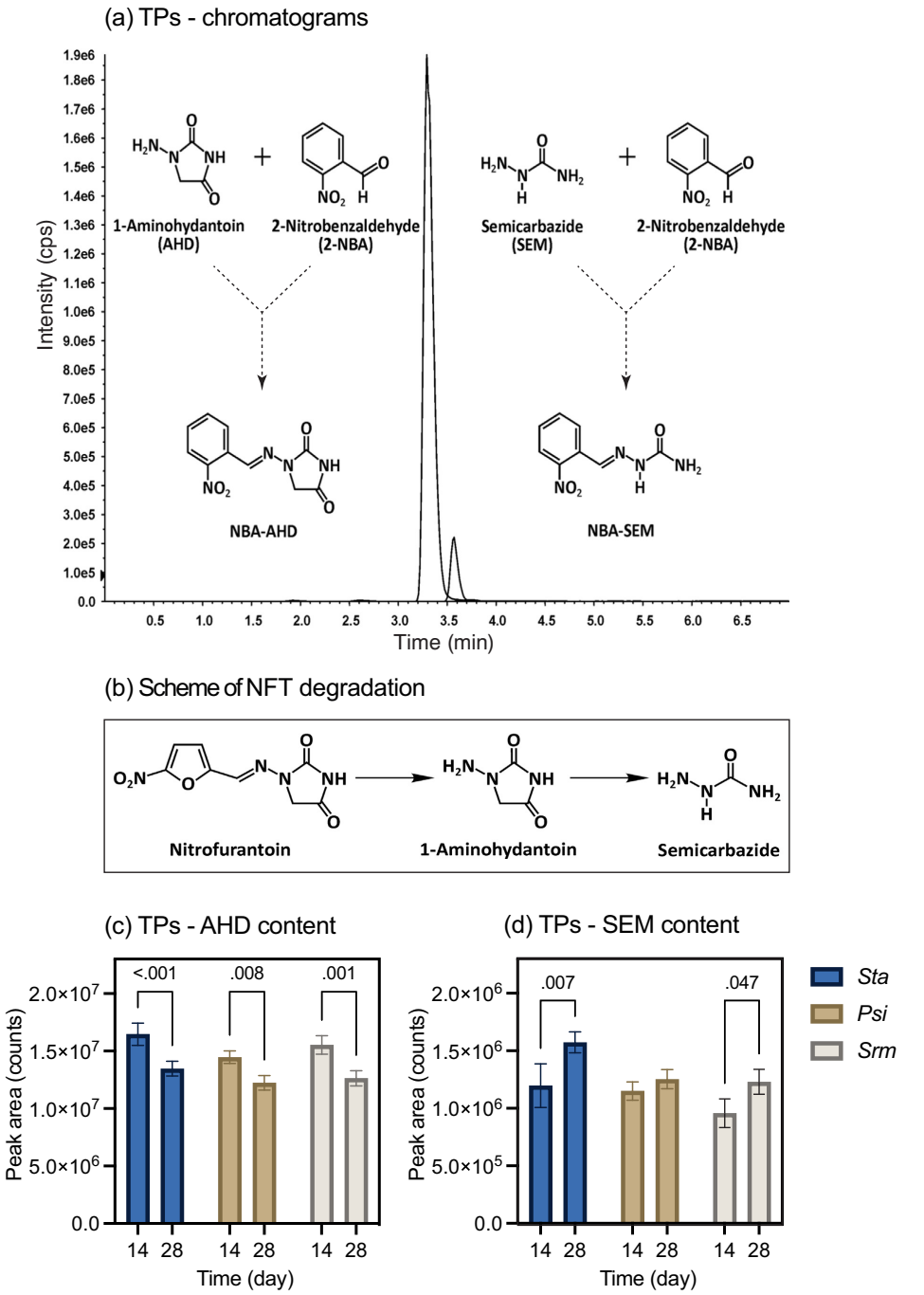

Fig. 6. Identification of transformation products of nitrofurantoin biodegradation (a). Scheme of NFT degradation (b). Changes in the analytical signal of 1-aminohydantoin (AHD) (c) and semicarbazide (SEM) (d) during NFT biodegradation. Numbers 14 and 28 indicate the sample collection days. NBA-AHD refers to 2-nitrobenzaldehyde derivative of AHD, NBA-SEM to 2-nitrobenzaldehyde derivative SEM. *Sta* refers to *Stenotrophomonas acidaminiphila* N0B, *Psi* to *Pseudomonas indoloxydans* WB, *Srm* to *Serratia marcescens* ODW152.

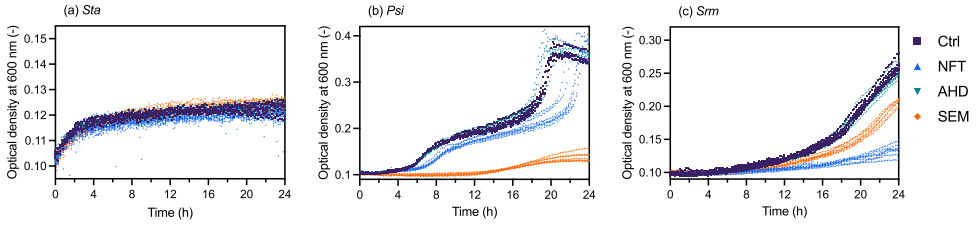

Fig. 7. Growth curve of *Sta* — *Stenotrophomonas acidaminiphila* N0B (a), *Psi* — *Pseudomonas indoloxydans* WB (b), and *Srm* — *Serratia marcescens* ODW152 (c) in the absence (Ctrl, navy squares) and presence of nitrofurantoin (NFT, blue triangles), 1-aminohydantoin (AHD, turquoise inverted triangles), and semicarbazide (SEM, orange diamonds), measured with a 96-well microplate reader at 30 °C. Each dot shows a separate experimental datapoint. (For interpretation of the references to color in this figure legend, the reader is referred to the web version of this article.)

were found. On the contrary, the SEM signal increased over time for the *Sta* and *Srm* strains. For these two strains the highest increase in the SEM signal was noted in the two timepoints. The SEM signal was significantly higher in the *Sta* strain than that in the *Srm* strain. The *Srm* strain showed almost complete primary NFT biodegradation while the final removal rate measured for the *Sta* strain was the lowest among all strains tested and accounted for 75.6 ± 3.0 %. This indicates that the *Srm* strain has transformed NFT to a higher extent and its degradation was more complete. However, both AHD and SEM have been detected in all samples even during the last degradation day. This clearly indicates that NFT was not completely transformed and TPs in question could remain unchanged in the environment for a long time. Results in this study are consistent with our previous research focused on biodegradation of NFT by two microbial consortia. In that study, both AHD and SEM were detected, among others, as NFT transformation products (Pacholak et al., 2023). This shows that biodegradation of NFT leads to formation of stable products and follows similar pathways regardless of the source of microorganisms used for biodegradation study. AHD was also detected by Szabó-Bárdos et al. (2020) as a product of NFT photocatalysis.

3.2.2. Effect of NFT and transformation products on bacteria

We next monitored growth of the *Sta*, *Psi*, and *Srm* strains in absence and presence of NFT, AHD, or SEM (Fig. 7) and assessed modifications in the cell membrane permeability and cell viability (Fig. 8).

As shown in Fig. 7, the shape of a microbial growth curve was different for each strain. None of the strains showed the conventional growth curve that has four discernible stages. Bacteria of the *Sta* strain adjusted to the new environment quickly and started dividing regularly in less than an hour (Fig. 7a). After about 3 h, cells entered the stationary phase. The control cultures showed the same growth rate as the cultures containing NFT, AHD, and SEM. Growth of the *Psi* strain differed significantly depending on the selecting agent used (Fig. 7b). The best growth was observed for the control cultures and the cultures containing AHD. The exponential phase of growth was observed about 4 h after starting the cultures. Bacterial growth in the presence of NFT was delayed (cells entered the log phase after about 5 h), however, the cultures reached the same optical density. Growth of the *Psi* strain in the presence of SEM was significantly inhibited. Substantial differences in bacterial growth were observed also in the *Srm* strain (Fig. 7c). As with the *Psi* strain, the cells showed the best growth in the control cultures and the cultures containing AHD. The greatest reduction in cell density was measured in the presence of NFT. Bacterial growth in cultures containing SEM was greater than NFT cultures but lower than Ctrl and AHD cultures.

Microbial growth curve reflects cellular events that are regulated by metabolic processes occurring within the individual cells. It is worthwhile to note that growth curves provide additional, useful information for evaluating the growth of microbes, however, they do not contain sufficient information to assess the specific processes regulating cells physiological state (Peleg and Corradini, 2011).

Analysis of the cell membrane permeability, cell metabolic activity and viability allowed to assess the effect of NFT and two identified TPs on the tested bacterial strains (Fig. 8). Membrane permeability of the *Sta* strain was the highest in the control sample (45.9 ± 4.1 %) A substantial decrease to 37.0 ± 4.2 % and 36.9 ± 3.2 % was noted for cells exposed to AHD and SEM. Control samples of the *Psi* strain also showed the highest permeability of bacterial membrane (50.0 ± 6.3 %). A substantial reduction by around 25 % was noted for all other samples. Different observations were made for the *Srm* strain which showed significantly increased membrane permeability in the presence of SEM. The *Srm* strain also exhibited the lowest permeability among all strains tested. Permeability of control cells accounted for 5.5 ± 2.5 %, increase to 23.0 ± 3.3 % was measured in cells exposed to SEM. It is worthwhile to note that among all strains tested, the *Srm* strain showed the highest biodegradation potential and the smallest variations in cell properties during degradation process.

The alamarBlue® Assay based on detection of metabolic activity of cells was used to establish relative cytotoxicity of NFT, AHD, and SEM. The average reduction of alamarBlue reagent in NFT-exposed cells of the *Srm* strain was 96.8 % (Fig. 8d). Exposure to AHD resulted in slightly reduced metabolic activity and exposure to SEM resulted in slightly increased metabolic activity. A statistically significant difference was observed between AHD- and SEM-exposed cells only ($p = 0.032$). The greatest changes in the metabolic activity were observed for the *Psi* strain. The highest metabolic activity was measured in the AHD-exposed cells (120.4 ± 7.9 %) and the lowest activity in cells exposed to SEM (43.1 ± 8.1 %). The *Srm* strain was also characterized by the highest metabolic activity in the presence of AHD, however, it was much lower than that of the *Psi* strain (92.4 ± 3.6 %).

Flow cytometry analysis allowed to estimate cellular metabolic activity and viability of the bacterial strains exposed to NFT, AHD, or SEM. The highest proportion of active cells was observed for the *Sta* strain and accounted for 93 % in the controls and cultures exposed to NFT and AHD. The proportion of active cells in culture exposed to SEM decreased significantly to 70.0 ± 2.3 %. This is not consistent with results of alamarBlue assay where metabolic activity of cells was the highest in the SEM sample. Control culture of the *Psi* strain contained 51.8 ± 12.9 % of active cells, an increase to 66.4 ± 12.2 % in the proportion of active cells was observed in culture containing NFT ($p = 0.014$). The proportion of active cells in AHD culture did not change significantly in comparison to control, however, exposure of the *Psi* strain to SEM resulted in dramatically reduced content of active cells (5.8 ± 1.7 %). A very similar direction of changes was observed for the alamarBlue assay results. The *Psi* strain exposed to SEM also showed decreased membrane permeability in comparison to control (Fig. 8b) and its growth was significantly inhibited (Fig. 7b). In general, the lowest proportion of active subpopulation among all strains tested was observed in the *Srm* strain (between 18 and 26 %). However, treatment of the *Srm* strain with NFT, AHD, and SEM did not decrease the abundance of active cells. The average percentage of active cells

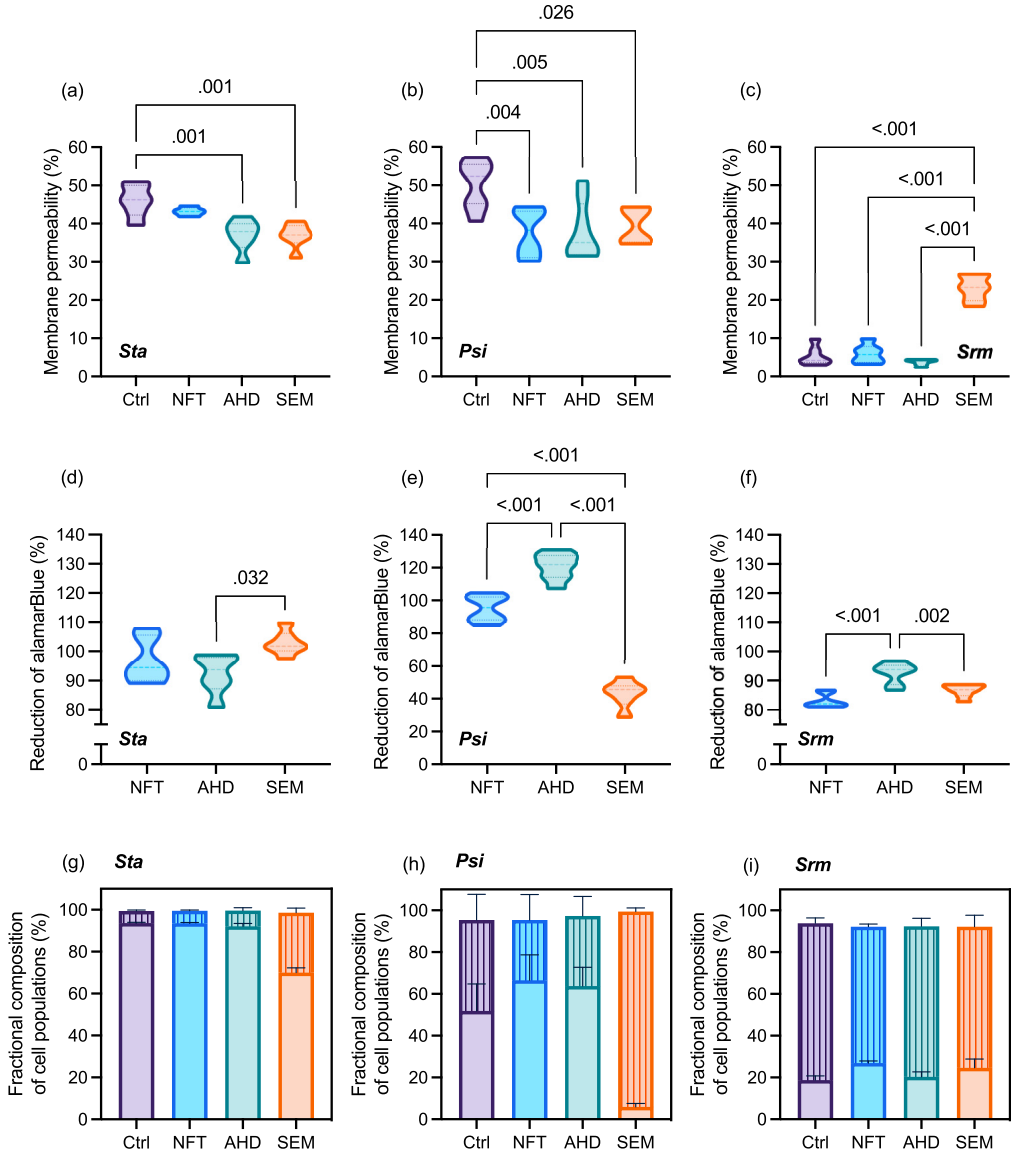

Fig. 8. Cell properties of the *Sta* — *Stenotrophomonas acidaminiphila* N0B, *Psi* — *Pseudomonas indoloxydans* WB, and *Srm* — *Serratia marcescens* ODW152 in the absence (Ctrl, purple color on the graph) and presence of nitrofurantoin (NFT, blue), 1-aminohydantoin (AHD, turquoise), and semicarbazide (SEM, orange). Changes in the cell membrane permeability (a–c). Relative cytotoxicity of NFT, AHD, and SEM measured with the alamarBlue® Assay. The plots show the percentage difference in reduction of the alamarBlue reagent between treated and control cultures (d–f).Cellular metabolic activity of cells measured with the flow cytometry. Bars with pattern are for non-active cells and plain bars are for active cells (g–i). (For interpretation of the references to color in this figure legend, the reader is referred to the web version of this article.)

was 18.7 % in control sample, 26.9 % in NFT-treated sample, 20.3 % in AHD-treated sample, and 24.6 % in SEM-treated sample. *Srm* cells also showed the lowest membrane permeability in the Ctrl, NFT, and AHD cultures. Interestingly, the *Srm* strain showed the best degradation efficiency, and the fewest modifications within other cells features during biodegradation were observed for this strain.

4. Practical applications and future perspectives

Nitrofurans are broad-spectrum synthetic antibiotics. Their major representative is nitrofurantoin. The use of nitrofurans has increased recently because of their multiactivity which contributes to repurposing of these chemicals from growth-promoting substances and basic antibiotics to

efficient pharmaceuticals used to treat other human diseases. Illegal use in agriculture as well as pharmaceutical treatment and manufacturing promote continuous discharge of nitrofurans into the natural environment. This study explored dynamic changes occurring within the cells during biotransformation of nitrofurantoin by pure bacterial strains isolated from contaminated environments. Results indicate that nitrofurantoin biodegradation leads to generation of 1-aminohydantoin and semicarbazide. The occurrence of antibiotic residues in the natural environment is a complex phenomenon which requires global efforts from governments and relevant organizations. Contamination of the environment with antibiotic residues should be reduced starting from regulating antibiotic consumption. In addition, development of novel powerful strategies to remove nitrofurantoin residues from the ecosystem is required. Importantly, environmental impact of nitrofurans is not well-understood. Studies that explain biodegradation of nitrofurantoin and its metabolic pathways are limited. Modifications occurring at the molecular level in the cells of strains biodegrading these drugs remain unknown. This research has contributed to a better understanding of the environmental impact of nitrofurantoin and its intermediates. Results could be helpful in designing the technologies of bioremediation of contaminated sites.

5. Conclusions

Results from this study provide new insights into potential ability of autochthonous bacterial strains isolated from contaminated sites to decompose nitrofurantoin. Results also provide information on the possible effect of transformation products on the isolated bacteria. *Serratia marcescens* ODW152 strain was able to eliminate nitrofurantoin almost completely, however, stable transformation products were formed because of biodegradation. The fewest variations in cell properties were observed for this strain during nitrofurantoin biodegradation. The two other strains were characterized by greater variations during the process. Cell sorting and surface roughness analysis revealed increased roughness of non-active cells relative to active cells. The corresponding subpopulations collected from different cultures were characterized by significant differences in average surface roughness. 1-aminohydantoin was detected as a primary nitrofurantoin biotransformation product and semicarbazide as a secondary product. Semicarbazide showed higher toxicity than nitrofurantoin and 1-aminohydantoin in strains with low degradation potential. Membrane permeability and metabolic activity decreased after exposure to nitrofurantoin, 1-aminohydantoin, and semicarbazide. Taken together, our results suggest that nitrofurantoin biodegradation leads to generation of hazardous transformation products which can remain in the environment for a long time.

CRediT authorship contribution statement

Amanda Pacholak: Conceptualization, Formal analysis, Investigation, Methodology, Resources, Writing – original draft, Writing – review & editing, Validation, Visualization. **Wojciech Juzwa:** Formal analysis, Investigation, Methodology, Writing – review & editing, Validation. **Agnieszka Zgoła-Grześkowiak:** Formal analysis, Investigation, Methodology, Writing – review & editing, Validation. **Ewa Kaczorek:** Conceptualization, Writing – review & editing, Supervision, Project administration, Funding acquisition.

Data availability

Data will be made available on request.

Declaration of competing interest

The authors declare that they have no known competing financial interests or personal relationships that could have appeared to influence the work reported in this paper.

Acknowledgments

This work was supported by National Science Centre, Poland, grant number 2017/27/B/NZ9/01603. The authors are grateful to Filip Jaworski (Institute of Chemical Technology and Engineering, Poznan University of Technology) for technical support during AFM observations and to Artur Piński (Institute of Biology, Biotechnology and Environmental Protection, University of Silesia in Katowice) for building a phylogenetic tree. Amanda Pacholak is grateful for financial support from the Foundation for Polish Sciences.

Appendix A. Supplementary data

Supplementary data to this article can be found online at https://doi.org/10.1016/j.scitotenv.2023.162422.

References

Ahmed, B., Ameen, F., Rizvi, A., Ali, K., Sonbol, H., Zaidi, A., Khan, M.S., Musarrat, J., 2020. Destruction of cell topography, morphology, membrane, inhibition of respiration, biofilm formation, and bioactive molecule production by nanoparticles of ag, ZnO, CuO, TiO 2, and Al 2 O 3 toward beneficial soil bacteria. ACS Omega 5, 7861–7876. https://doi.org/10.1021/acsomega.9b04084.

Ayala-Torres, C., Hernández, N., Galeano, A., Novoa-Aponte, L., Soto, C.-Y., 2014. Zeta potential as a measure of the surface charge of mycobacterial cells. Ann. Microbiol. 64, 1189–1195. https://doi.org/10.1007/s13213-013-0758-y.

Bai, Y., Liang, B., Yun, H., Zhao, Y., Li, Z., Qi, M., Ma, X., Huang, C., Wang, A., 2021. Combined bioaugmentation with electro-biostimulation for improved bioremediation of antimicrobial triclocarban and PAHs complexly contaminated sediments. J. Hazard. Mater. 403, 123937. https://doi.org/10.1016/j.jhazmat.2020.123937.

Bessone, F., Ferrari, A., Hernandez, N., Mendizabal, M., Ridruejo, E., Zerega, A., Tanno, F., Reggiardo, M.V., Vorobioff, J., Tanno, H., Arrese, M., Nunes, V., Tagle, M., Medina-Caliz, I., Robles-Diaz, M., Niu, H., Alvarez-Alvarez, I., Stephens, C., Lucena, M.I., Andrade, R.J., 2023. Nitrofurantoin-induced liver injury: long-term follow-up in two prospective DILI registries. Arch. Toxicol. 97, 593–602. https://doi.org/10.1007/s00204-022-03419-7.

Chen, X., Lin, H., Dong, Y., Li, B., Liu, C., Yin, T., 2022. Mechanisms underlying enhanced bioremediation of sulfamethoxazole and zinc(II) by bacillus sp. SDB4 immobilized on biochar. J. Clean. Prod. 370, 133483. https://doi.org/10.1016/j.jclepro.2022.133483.

Commission Regulation (EC), 1995. 1995/1442/EC (1995). Amending Annexes I, II, III and IV of Regulation (ECC) No 2377/90 laying down a Community Procedure for the establishment of maximum residue limits of veterinary medicinal products in foodstuffs of animal origin. OJ 143, 26–30.

de Oliveira, R.C.S., Oliveira, R., Rodrigues, M.A.C., de Farias, N.O., Sousa-Moura, D., Nunes, N.A., Andrade, T.S., Grisolia, C.K., 2020. Lethal and sub-lethal effects of nitrofurantoin on zebrafish early-life stages. Water Air Soil Pollut. 231, 54. https://doi.org/10.1007/s11270-020-4414-4.

Díaz, M., Herrero, M., García, L.A., Quirós, C., 2010. Application of flow cytometry to industrial microbial bioprocesses. Biochem. Eng. J. 2010 (48), 385–407. https://doi.org/10.1016/j.bej.2009.07.013 Invited Review Issue.

Duber, A., Jaroszynski, L., Zagrodnik, R., Chwialkowska, J., Juzwa, W., Ciesielski, S., Oleskowicz-Popiel, P., 2018. Exploiting the real wastewater potential for resource recovery – n -caproate production from acid whey. Green Chem. 20, 3790–3803. https://doi.org/10.1039/C8GC01759J.

Dufrêne, Y.F., Viljoen, A., Mignolet, J., Mathelié-Guinlet, M., 2021. AFM in cellular and molecular microbiology. Cell. Microbiol. 23. https://doi.org/10.1111/cmi.13324.

EFSA Panel on Contaminants in the Food Chain (CONTAM), 2015. Scientific Opinion on Nitrofurans and Their Metabolites in Food. EFS2 13. https://doi.org/10.2903/j.efsa.2015.4140.

Felsenstein, J., 1985. Confidence limits on phylogenies: an approach using the bootstrap. Evolution 39, 783. https://doi.org/10.2307/2408678.

Ferreyra Maillard, A.P.V., Espeche, J.C., Maturana, P., Cutro, A.C., Hollmann, A., 2021. Zeta potential beyond materials science: applications to bacterial systems and to the development of novel antimicrobials. Biochim. Biophys. Acta - Biomembr 1863, 183597. https://doi.org/10.1016/j.bbamem.2021.183597.

Francius, G., Domenech, O., Mingeot-Leclercq, M.P., Dufrêne, Y.F., 2008. Direct observation of Staphylococcus aureus cell wall digestion by lysostaphin. J. Bacteriol. 190, 7904–7909. https://doi.org/10.1128/JB.01116-08.

Han, Z., Lin, Q., Zhang, S., Zhou, X., Li, S., Sun, F., Shen, C., Su, X., 2023. High PCBs mineralization capability of a resuscitated strain bacillus sp. LS1 and its survival in PCB-contaminated soil. Sci. Total Environ. 856, 159224. https://doi.org/10.1016/j.scitotenv.2022.159224.

Hong, X., Zhao, Y., Zhuang, R., Liu, J., Guo, G., Chen, J., Yao, Y., 2020. Bioremediation of tetracycline antibiotics-contaminated soil by bioaugmentation. RSC Adv. 10, 33086–33102. https://doi.org/10.1039/D0RA04705H.

Hou, J., Mao, D., Zhang, Y., Huang, R., Li, L., Wang, X., Luo, Y., 2022. Long-term spatiotemporal variation of antimicrobial resistance genes within the Serratia marcescens population and transmission of S. Marcescens revealed by public whole-genome datasets. J. Hazard. Mater. 423, 127220. https://doi.org/10.1016/j.jhazmat.2021.127220.

Huttner, A., Verhaegh, E.M., Harbarth, S., Muller, A.E., Theuretzbacher, U., Mouton, J.W., 2015. Nitrofurantoin revisited: a systematic review and meta-analysis of controlled trials. J. Antimicrob. Chemother. 70, 2456–2464. https://doi.org/10.1093/jac/dkv147.

Kaczorek, E., Sałek, K., Guzik, U., Dudzińska-Bajorek, B., 2013. Cell surface properties and fatty acids composition of stenotrophomonas maltophilia under the influence of hydrophobic compounds and surfactants. New Biotechnol. 30, 173–182. https://doi.org/10.1016/j.nbt.2012.09.003.

Kämäräinen, T., Tardy, B.L., Javan Nikkhah, S., Batys, P., Sammalkorpi, M., Rojas, O.J., 2020. Effect of particle surface corrugation on colloidal interactions. J. Colloid Interface Sci. 579, 794–804. https://doi.org/10.1016/j.jcis.2020.06.082.

Krishnamurthi, V.R., Niyonshuti, I.I., Chen, J., Wang, Y., 2021. A new analysis method for evaluating bacterial growth with microplate readers. PLoS ONE 16, e0245205. https://doi.org/10.1371/journal.pone.0245205.

Kumar, J.V., Karthik, R., Chen, S.-M., Chen, K.-H., Sakthinathan, S., Muthuraj, V., Chiu, T.-W., 2018. Design of novel 3D flower-like neodymium molybdate: an efficient and challenging catalyst for sensing and destroying pulmonary toxicity antibiotic drug nitrofurantoin. Chem. Eng. J. 346, 11–23. https://doi.org/10.1016/j.cej.2018.03.183.

Kumar, S., Stecher, G., Li, M., Knyaz, C., Tamura, K., 2018. MEGA X: molecular evolutionary genetics analysis across computing platforms. Mol. Biol. Evol. 35, 1547–1549. https://doi.org/10.1093/molbev/msy096.

Lewkowski, J., Rogacz, D., Rychter, P., 2019. Hazardous ecotoxicological impact of two commonly used nitrofuran-derived antibacterial drugs: furazolidone and nitrofurantoin. Chemosphere 222, 381–390. https://doi.org/10.1016/j.chemosphere.2019.01.144.

Li, J., Chen, W.-J., Zhang, W., Zhang, Y., Lei, Q., Wu, S., Huang, Y., Mishra, S., Bhatt, P., Chen, S., 2022. Effects of free or immobilized bacterium stenotrophomonas acidaminiphila Y4B on glyphosate degradation performance and indigenous microbial community structure. J. Agric. Food Chem. 70, 13945–13958. https://doi.org/10.1021/acs.jafc.2c05612.

Li, J., Peng, K., Zhang, D., Luo, C., Cai, X., Wang, Y., Zhang, G., 2020. Autochthonous bioaugmentation with non-direct degraders: a new strategy to enhance wastewater bioremediation performance. Environ. Int. 136, 105473. https://doi.org/10.1016/j.envint.2020.105473.

Li, Zhe, T., Li, F., Li, R., Bai, F., Jia, P., Bu, T., Xu, Z., Wang, L., 2022. Hybrid structures of cobalt-molybdenum bimetallic oxide embedded in flower-like molybdenum disulfide for sensitive detection of the antibiotic drug nitrofurantoin. J. Hazard. Mater. 435, 129059. https://doi.org/10.1016/j.jhazmat.2022.129059.

López-Serna, R., Jurado, A., Vázquez-Suñé, E., Carrera, J., Petrović, M., Barceló, D., 2013. Occurrence of 95 pharmaceuticals and transformation products in urban groundwaters underlying the metropolis of Barcelona, Spain. Environ. Pollut. 174, 305–315. https://doi.org/10.1016/j.envpol.2012.11.022.

Ma, Z., Liu, J., Dick, R.P., Li, H., Shen, D., Gao, Y., Waigi, M.G., Ling, W., 2018. Rhamnolipid influences biosorption and biodegradation of phenanthrene by phenanthrene-degrading strain pseudomonas sp. Ph6. Environ. Pollut. 240, 359–367. https://doi.org/10.1016/j.envpol.2018.04.125.

Manickam, N., Ghosh, A., Jain, R.K., Mayilraj, S., 2008. Description of a novel indole-oxidizing bacterium pseudomonas Indoloxydans sp. nov., isolated from a pesticide-contaminated site. Syst. Appl. Microbiol. 31, 101–107. https://doi.org/10.1016/j.syapm.2008.02.002.

McOsker, C.C., Fitzpatrick, P.M., 1994. Nitrofurantoin: mechanism of action and implications for resistance development in common uropathogens. J. Antimicrob. Chemother. 33, 23–30. https://doi.org/10.1093/jac/33.suppl_A.23.

Nebe-von-Caron, G., Stephens, P.J., Hewitt, C.J., Powell, J.R., Badley, R.A., 2000. Analysis of bacterial function by multi-colour fluorescence flow cytometry and single cell sorting. J. Microbiol. Methods 42, 97–114. https://doi.org/10.1016/S0167-7012(00)00181-0.

Niedźwiedź, I., Juzwa, W., Skrzypiec, K., Skrzypek, T., Waśko, A., Kwiatkowski, M., Pawłat, J., Polak-Berecka, M., 2020. Morphological and physiological changes in lentilactobacillus hilgardii cells after cold plasma treatment. Sci. Rep. 10, 18882. https://doi.org/10.1038/s41598-020-76053-x.

Nnabuife, O.O., Ogbonna, J.C., Anyanwu, C., Ike, A.C., Eze, C.N., Enemuor, S.C., 2022. Mixed bacterial consortium can hamper the efficient degradation of crude oil hydrocarbons. Arch. Microbiol. 204, 306. https://doi.org/10.1007/s00203-022-02915-9.

OECD, 1992. Test No. 301: Ready Biodegradability, OECD Guidelines for the Testing of Chemicals, Section 3. OECD https://doi.org/10.1787/9789264070349-en.

Ossai, I.C., Ahmed, A., Hassan, A., Hamid, F.S., 2020. Remediation of soil and water contaminated with petroleum hydrocarbon: a review. Environ. Technol. Innov. 17, 100526. https://doi.org/10.1016/j.eti.2019.100526.

Pacholak, A., Burlaga, N., Frankowski, R., Zgoła-Grześkowiak, A., Kaczorek, E., 2022. Azole fungicides: (Bio)degradation, transformation products and toxicity elucidation. Sci. Total Environ. 802, 149917. https://doi.org/10.1016/j.scitotenv.2021.149917.

Pacholak, A., Burlaga, N., Guzik, U., Kaczorek, E., 2020a. Investigation of the bacterial cell envelope nanomechanical properties after long-term exposure to nitrofurans. J. Hazard. Mater., 124352 https://doi.org/10.1016/j.jhazmat.2020.124352.

Pacholak, A., Smułek, W., Zgoła-Grześkowiak, A., Kaczorek, E., 2019. Nitrofurantoin—microbial degradation and interactions with environmental bacterial strains. Int. J. Environ. Res. Public Health 16, 1526. https://doi.org/10.3390/ijerph16091526.

Pacholak, A., Zdarta, A., Frankowski, R., Cybulski, Z., Kaczorek, E., 2020b. Exploring elimination kinetics of four 5-nitrofuran derivatives by microbes pesent in rural and municipal activated sludge. Water Air Soil Pollut. 231, 252. https://doi.org/10.1007/s11270-020-04634-7.

Pacholak, A., Zgoła-Grześkowiak, A., Kaczorek, E., 2023. Dynamics of microbial communities during biotransformation of nitrofurantoin. Environ. Res. 216, 114531. https://doi.org/10.1016/j.envres.2022.114531.

Paiva, T.O., Viljoen, A., Dufrêne, Y.F., 2022. Seeing the unseen: high-resolution AFM imaging captures antibiotic action in bacterial membranes. Nat. Commun. 13, 6196. https://doi.org/10.1038/s41467-022-33839-z.

Peleg, M., Corradini, M.G., 2011. Microbial growth curves: what the models tell us and what they cannot. Crit. Rev. Food Sci. Nutr. 51, 917–945. https://doi.org/10.1080/10408398.2011.570463.

Saitou, N., Nei, M., 1987. The neighbor-joining method: a new method for reconstructing phylogenetic trees. Mol. Biol. Evol. https://doi.org/10.1093/oxfordjournals.molbev.a040454.

Sakthivel, R., Liu, T.-Y., Chung, R.-J., 2023. Bimetallic Cu5Zn8 alloy-embedded hollow porous carbon nanocubes derived from 3D-Cu/ZIF-8 as efficient electrocatalysts for environmental pollutant detection in water bodies. Environ. Res. 216, 114609. https://doi.org/10.1016/j.envres.2022.114609.

Shahid, M.J., Ali, S., Shabir, G., Siddique, M., Rizwan, M., Seleiman, M.F., Afzal, M., 2020. Comparing the performance of four macrophytes in bacterial assisted floating treatment wetlands for the removal of trace metals (Fe, mn, ni, pb, and Cr) from polluted river water. Chemosphere 243, 125353. https://doi.org/10.1016/j.chemosphere.2019.125353.

Smułek, W., Bielan, Z., Pacholak, A., Zdarta, A., Zgoła-Grześkowiak, A., Zielińska-Jurek, A., Kaczorek, E., 2021. Nitrofurazone removal from water enhanced by coupling photocatalysis and biodegradation. IJMS 22, 2186. https://doi.org/10.3390/ijms22042186.

Smułek, W., Rojewska, M., Pacholak, A., Machrowicz, O., Prochaska, K., Kaczorek, E., 2022. Co-interaction of nitrofurantoin and saponins surfactants with biomembrane leads to an increase in antibiotic's antibacterial activity. J. Mol. Liq. 364, 120070. https://doi.org/10.1016/j.molliq.2022.120070.

Szabó-Bárdos, E., Cafuta, A., Hegedűs, P., Fónagy, O., Kiss, G., Babić, S., Škorić, I., Horváth, O., 2020. Photolytic and photocatalytic degradation of nitrofurantoin and its photohydrolytic products. J. Photochem. Photobiol. A Chem. 386, 112093. https://doi.org/10.1016/j.jphotochem.2019.112093.

Tara, N., Arslan, M., Hussain, Z., Iqbal, M., Khan, Q.M., Afzal, M., 2019. On-site performance of floating treatment wetland macrocosms augmented with dye-degrading bacteria for the remediation of textile industry wastewater. J. Clean. Prod. 217, 541–548. https://doi.org/10.1016/j.jclepro.2019.01.258.

Tran, K.M., Lee, H.-M., Thai, T.D., Shen, J., Eyun, S., Na, D., 2021. Synthetically engineered microbial scavengers for enhanced bioremediation. J. Hazard. Mater. 419, 126516. https://doi.org/10.1016/j.jhazmat.2021.126516.

Vasquez, M.I., Hapeshi, E., Fatta-Kassinos, D., Kümmerer, K., 2013. Biodegradation potential of ofloxacin and its resulting transformation products during photolytic and photocatalytic treatment. Environ. Sci. Pollut. Res. 20, 1302–1309. https://doi.org/10.1007/s11356-012-1096-5.

Ye, S., Zeng, G., Wu, H., Zhang, Chang, Dai, J., Liang, J., Yu, J., Ren, X., Yi, H., Cheng, M., Zhang, Chen, 2017. Biological technologies for the remediation of co-contaminated soil. Crit. Rev. Biotechnol. 37, 1062–1076. https://doi.org/10.1080/07388551.2017.1304357.

Young, K.D., 2006. The selective value of bacterial shape. Microbiol. Mol. Biol. Rev. 70, 660–703. https://doi.org/10.1128/MMBR.00001-06.

Zhang, Y., Tang, J., Wu, M., Zhou, X., Wang, S., Ye, H., Xiang, W., Zhang, Q., Cai, T., 2023. Whole genome sequencing exploitation analysis of dibutyl phthalate by strain stenotrophomonas acidaminiphila BDBP 071. Food Biosci. 51, 102185. https://doi.org/10.1016/j.fbio.2022.102185.

Supplementary information (P5)

Multi-faceted analysis of bacterial transformation of nitrofurantoin

submitted to

Science of the Total Environment

by

Amanda Pacholak [a*], Wojciech Juzwa [b],
Agnieszka Zgoła-Grześkowiak [c], Ewa Kaczorek [a]

[a] Institute of Chemical Technology and Engineering, Poznan University of Technology, Poznan, Poland

[b] Department of Biotechnology and Food Microbiology, Faculty of Food Science, Poznan University of Life Sciences, Poznan, Poland

[c] Institute of Chemistry and Technical Electrochemistry, Poznan University of Technology, Poznan, Poland

* Corresponding author:
Email: amanda.pacholak@put.poznan.pl

I. LC/MS-MS analysis for evaluation of NFT biodegradation potential

The samples collected from the bacterial cultures were centrifuged and supernatants were diluted and filtered through a 0.2 μm PTFE syringe filter before their determination on a LC-MS/MS system. The system consisted of an UltiMate 3000 liquid chromatograph from Dionex (Sunnyvale, CA, USA) coupled to an API 4000 QTRAP mass spectrometer from Applied Biosystems/MDS Sciex (Waltham, MA, USA). A Gemini-NX C18 column (100 mm x 2.0 mm, 3 μm) from Phenomenex (Torrance, CA, USA) thermostated at 35°C was used for the chromatographic separation, onto which 5 μL of the sample was applied. A mixture of 5 mM ammonium acetate (A) and methanol (B) was used as the mobile phase. The mobile phase gradient was used for the separation at a flow of 0.3 mL/min. The initial phase composition was 75% B, followed by the increase of component B to 80% in 2 minutes and then to 100% in 1 minute. The eluent flowing from the column was directed to the mass spectrometer using an ESI-type ion source operating in the negative ion mode. The source and spectrometer parameters were set as follows: curtain gas pressure 10 psi, nebulizing gas pressure 40 psi, auxiliary gas pressure 45 psi, temperature 450 °C, electrospray voltage -4500 V, and collision gas was set to medium. NFT was ionized at declustering potential of -60 V. The analytical transition was from m/z 237 to m/z 152 at the collision energy of -17 eV and the collision cell exit potential of -10 V. The confirmatory transition was from m/z 237 to m/z 124 at the collision energy of -20 eV and the collision cell exit potential of -10 V.

II. Protocol of NFT metabolites derivatization

1 mL of 0.1 M HCl and 100 μL of 100 mM NBA methanol solution were added to the Eppendorf tubes containing 1 mL of liquid culture medium. The solutions were incubated for 16 hours at 37 °C. After cooling the tubes to room temperature, 100 μL of 1 M NaOH and 0.5 mL of 0.2 M pH 7 buffer to ensure a neutral environment. Next, the transformation producst were extracted twice with two 2 mL portions of ethyl acetate. The extracts were then combined and evaporated to dryness under a gentle stream of nitrogen. The dry residue was dissolved in 400 μL of methanol and then 600 μL of water was added. After filtering through a 0.2 μm PTFE syringe filter, the samples were analyzed by the LC-MS/MS system described in section I. The same analytical column thermostated at 35°C was used and 5 μL of the sample was injected. A mixture of 5 mM ammonium acetate (A) and methanol (B) was used as the mobile phase at a flow of 0.3 mL/min. The initial phase composition was 30% B held for 1 minute, followed by the increase of component B to 100% in 4 minutes and hold for 2 minutes. The eluent flowing from the column was directed to the mass spectrometer using an ESI-type ion source operating in the positive ion mode. The source and spectrometer parameters were set as follows: curtain gas pressure 10 psi, nebulizing gas pressure 40 psi, auxiliary gas pressure 45 psi, temperature 450 °C, electrospray voltage 4500 V, and collision gas was set to medium. The mass spectrometer was operated in the MRM mode (monitoring of selected ion transition reactions). Additional parameters of the mass spectrometer are presented in Tab. S1.

Tab. S1 – Parameters of the mass spectrometer

Metabolite	DP[a] [V]	Analytical transition	CE[b] [eV]	CXP[c] [V]	Confirmatory transition	CE [eV]	CXP [V]
AHD	70	249 → 134	18	7	249 → 178	22	10
SEM	40	209 → 166	14	9	209 → 192	17	11

a – declustering potential, b – collision energy, c – cell exit potential

III. Phylogenetic tree

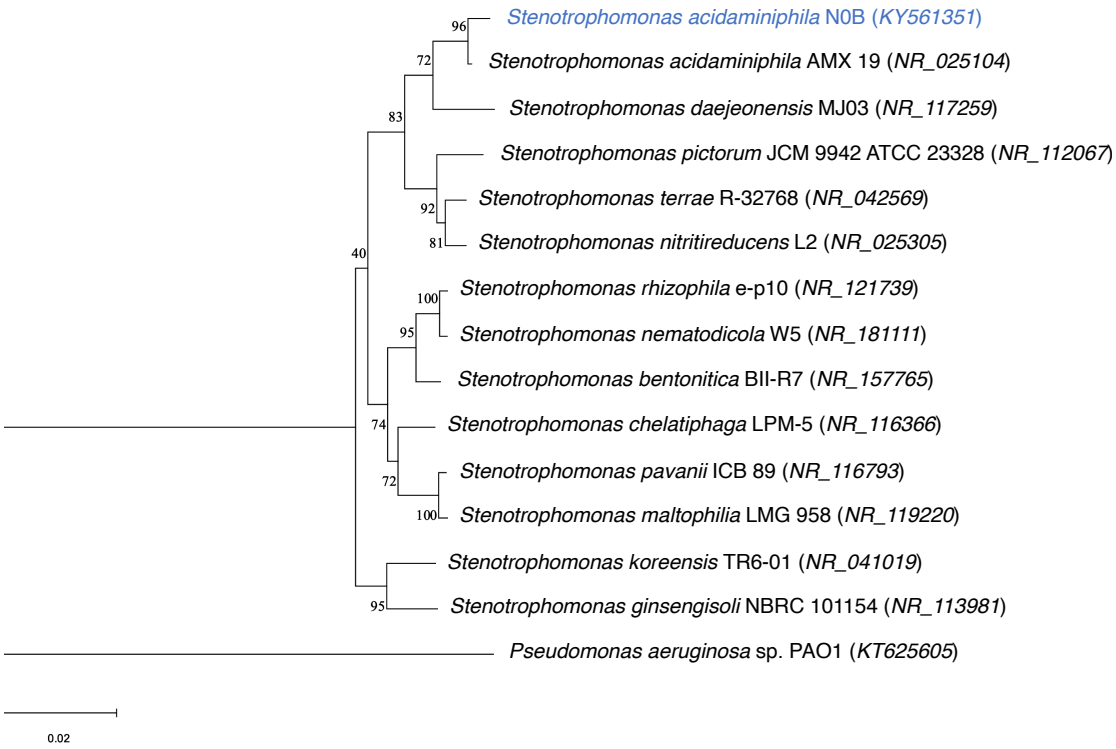

Fig. S1 - Phylogenetic tree of *Stenotrophomonas acidaminiphilia* N0B *(Sta).*
The NCBI accession numbers for the16S rRNA gene sequences are shown in brackets.

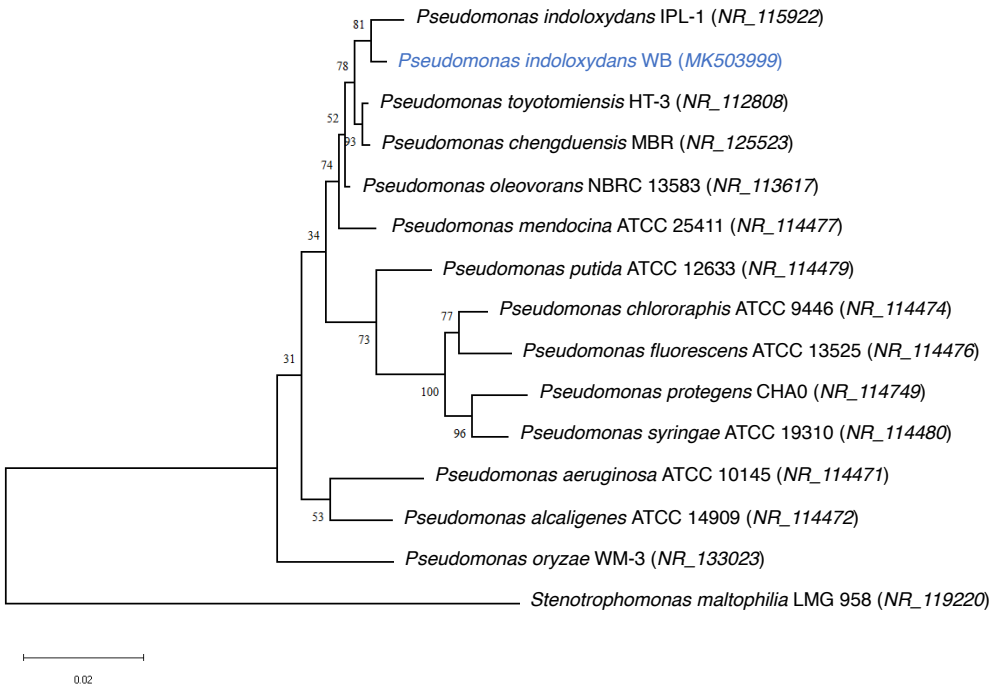

Fig. S2 – Phylogenetic tree of *Pseudomonas indoloxydans* WB (*Psi*).
The NCBI accession numbers for the16S rRNA gene sequences are shown in brackets.

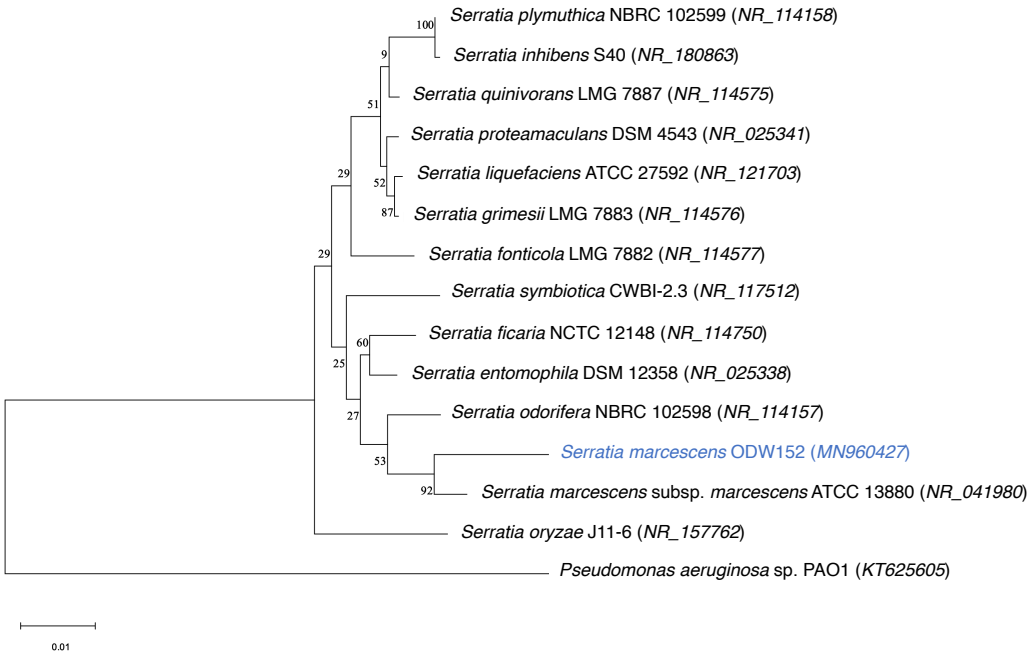

Fig. S3 – Phylogenetic tree of *Serratia marcescens* ODW152 (*Srm*).
The NCBI accession numbers for the16S rRNA gene sequences are shown in brackets.

Appendix B: Author contribution

Publication P1

- Formulation and identification of the scientific problem
- Planning the research concept and experiments
- Development of the methods and conducting the experimental work: isolation of strains, preparation of the bacterial cultures, analysis of cell membrane permeability, cell surface hydrophobicity, and cell viability; collection and preparation of samples for LC-MS/MS analysis
- Conducting the statistical analysis of data
- Main contribution in interpretation of the results, writing the first draft of the manuscript, and finalization of the manuscript
- Main contribution in editing the manuscript and preparing responses to reviewers' comments

Publication P2

- Formulation and identification of the scientific problem
- Planning the research concept and experiments
- Formulation and identification of the scientific problem
- Planning the research concept and experiments
- Development of the methods and conducting the experimental work for strains isolation and cultivation, preparation of the bacterial cultures, preparation of bacterial samples for AFM and TEM analysis, calculation of cell surface roughness and nanomechanical properties, analysis of membrane permeability and cell surface hydrophobicity
- Conducting the statistical analysis of data
- Main contribution in interpretation of the results
- Writing the first draft and finalization of the manuscript
- Editing the manuscript and preparing responses to reviewers' comments,
- Participation in handling the correspondence with the journal

Publication P3

- Formulation and identification of the scientific problem
- Planning the research concept and experiments
- Development of the methods and conducting the experimental work, such as collection of environmental samples, preparation of the bacterial cultures, collection and preparation of samples for LC-MS/MS analysis, DNA isolation
- Conducting the analysis of mNGS
- Main contribution in interpretation of the results
- Writing of the first draft and finalization of the manuscript
- Editing the manuscript and preparing responses to reviewers' comments
- Handling the correspondence with the journal

Publication P4

- Formulation and identification of the scientific problem
- Planning the research concept and experiments
- Development of the methods and conducting the experimental work for strains isolation and cultivation, preparation of the bacterial cultures, DNA isolation, preparation of crude cell extract for metabolomic analysis, analysis of GSTs
- Conducting the statistical analysis of data
- Main contribution in interpretation of the results, writing of the first draft and finalization of the manuscript
- Main contribution in editing the manuscript and preparing responses to reviewers' comments
- Handling the correspondence with the journal

Publication P5

- Formulation and identification of the scientific problem
- Planning the research concept and experiments
- Development of the methods and conducting the experimental work for strains isolation, bacteria cultivation, preparation of the bacterial cultures, collection and preparation of samples for LC-MS/MS analysis, preparation of bacterial samples for AFM and FC, measurements of zeta potential and size distribution, measurements of growth curves, membrane permeability and cytotoxicity
- Conducting the statistical analysis of data
- Main contribution in interpretation of the results,
- Writing of the first draft, editing and finalization of the manuscript, preparing responses to reviewers' comments
- Handling the correspondence with the journal

Appendix C: Co-authors statements

Declarations of co-authorship for articles included in this dissertation are signed by each co-author as below. **Tab. 16** provides a list of co-authors arranged in alphabetical order.

Tab. 16 List of co-authors of publications included in dissertation.

Co-author	P1	P2	P3	P4	P5
Natalia Burlaga		•			
Urszula Guzik		•			
Wojciech Juzwa					•
Ewa Kaczorek	•	•	•	•	•
Marta Ligaj				•	
Magdalena Łuczak				•	
Long Duc Nghiem				•	
Quynh Anh Nguyen				•	
Artur Piński				•	
Wojciech Smułek	•				
Agnieszka Zgoła-Grześkowiak	•		•		•
Joanna Żur-Pińska				•	

POZNAN UNIVERSITY OF TECHNOLOGY

Natalia Burlaga, PhD student
Institute of Chemical Technology and Engineering, Faculty of Chemical Technology
ul. Berdychowo 4, 60-965 Poznan, Poland
phone: +48 (61) 665 3686
e-mail: natalia.burlaga@doctorate.put.poznan.pl

March 31, 2023

Declaration of co-authorship

As the co-author of the following publication:

P2. A. Pacholak, N. Burlaga, U. Guzik, E. Kaczorek, *Investigation of the bacterial cell envelope nanomechanical properties after long-term exposure to nitrofurans*, Journal of Hazardous Materials 407 (2021) 124352, doi:10.1016/j.jhazmat.2020.124352

I solemnly declare that my contribution to this work was:

- Assistance in formal analysis and data curation.
- Assistance in original draft preparation.

Natalia Burlaga

Signature

UNIWERSYTET ŚLĄSKI
W KATOWICACH

March 31, 2023

Dr hab. Urszula Guzik, prof. UŚ

Institute of Biology, Biotechnology and Environmental Protection

Faculty of Natural Science

University of Silesia in Katowice, Poland

email: urszula.guzik@us.edu.pl

Declaration of co-authorship

As the co-author of the following publication:

P2. A. Pacholak, N. Burlaga, U. Guzik, E. Kaczorek, *Investigation of the bacterial cell envelope nanomechanical properties after long-term exposure to nitrofurans*, Journal of Hazardous Materials 407 (2021) 124352, doi:10.1016/j.jhazmat.2020.124352

I solemnly declare that my contribution to this work was:

- Development of the methods for the analysis of fatty acids profile (FAP).
- Conducting the experimental work and interpretation of the FAP results.
- Participating in original draft preparation (assistance in description FAP results).

Signed by / Podpisano przez:
Urszula Guzik
Uniwersytet Śląski w Katowicach
Date / Data: 2023-04-02 12:45

.....

Signature

Poznań University of Life Sciences
ul. Wojska Polskiego 28
60-637 Poznań
tel. +48 61 848 70 01
e-mail: rektorat@up.poznan.pl

FACULTY OF FOOD SCIENCE
and NUTRITION
Department of Biotechnology
and Food Microbiology

March 31, 2023

Dr hab. inż. Wojciech Juzwa, prof. UP
Department of Biotechnology and Food Microbiology
Faculty of Food Science and Nutrition
Poznan University of Life Sciences, Poland
email: wojciech.juzwa@up.poznan.pl

Declaration of co-authorship

As the co-author of the following publication:

P5. A. Pacholak, W. Juzwa, A. Zgoła-Grześkowiak, E. Kaczorek, *Multi-faceted analysis of bacterial transformation of nitrofurantoin*, Science of the Total Environment 874 (2023b) 162422, doi:10.1016/j.scitotenv.2023.162422

I solemnly declare that my contribution to this work was:

- Development of the methods for the flow cytometric analysis (FCA) and cell sorting (CS).
- Conducting the experimental work and participating in interpretation of the FCA and CS results.
- Assistance in manuscript review and editing.

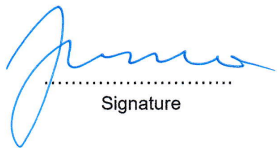

.....
Signature

POZNAN UNIVERSITY OF TECHNOLOGY

prof. Ewa Kaczorek
FACULTY OF CHEMICAL TECHNOLOGY
ul. Berdychowo 4, 60-965 Poznań
Phone: +48 (61) 665 3671
e-mail: ewa.kaczorek@put.poznan.pl

March 31, 2023

Declaration of co-authorship

As the principal supervisor of M. Sc. Eng. Amanda Pacholak, and the co-author of the following publications:

P1. A. Pacholak, W. Smułek, A. Zgoła-Grześkowiak, E. Kaczorek, *Nitrofurantoin – microbial degradation and interactions with environmental bacterial strains*, International Journal of Environmental Research and Public Health 16 (2019) 1526, doi:10.3390/ijerph16091526

P2. A. Pacholak, N. Burlaga, U. Guzik, E. Kaczorek, *Investigation of the bacterial cell envelope nanomechanical properties after long-term exposure to nitrofurans*, Journal of Hazardous Materials 407 (2021) 124352, doi:10.1016/j.jhazmat.2020.124352

P3. A. Pacholak, A. Zgoła-Grześkowiak, E. Kaczorek, *Dynamics of microbial commu-nities during biotransformation of nitrofurantoin*, Environmental Research 2016 (2023) 114531, doi:10.1016/j.envres.2022.114531

P4. A. Pacholak, J. Żur-Pińska, A. Piński, Q. A. Nguyen, M. Ligaj, M. Łuczak, L. D. Nghiem, E. Kaczorek, *Potential negative effect of long-term exposure to nitrofurans on bacteria isolated from wastewater,* Science of the Total Environment 872 (2023a) 162199, doi:10.1016/j.scitotenv.2023.162199

P5. A. Pacholak, W. Juzwa, A. Zgoła-Grześkowiak, E. Kaczorek, *Multi-faceted analysis of bacterial transformation of nitrofurantoin*, Science of the Total Environment 874 (2023b) 162422, doi:10.1016/j.scitotenv.2023.162422

I solemnly declare that Amanda Pacholak is the lead author of these articles. In addition, I affirm that my contribution to these works was:

- Assistance in formulation of the scientific problem, planning the research concept and methodology design (P1 – P5).
- Supervising the research progress (P1 – P5).
- Verification of the original draft and responses to reviewers comments (P1 – P5).
- Handling the correspondence with the journal (P1, P2).

March 31, 2023

Dr hab. Marta Ligaj
Department of Non-Food Products Quality and Packaging Development
Institute of Quality Science
Poznań University of Economics and Business, Poland
email: marta.ligaj@ue.poznan.pl

Declaration of co-authorship

As the co-author of the following publication:

P4. A. Pacholak, J. Żur-Pińska, A. Piński, Q. A. Nguyen, M. Ligaj, M. Łuczak, L. D. Nghiem, E. Kaczorek, *Potential negative effect of long-term exposure to nitrofurans on bacteria isolated from wastewater,* Science of the Total Environment 872 (2023a) 162199, doi:10.1016/j.scitotenv.2023.162422

I solemnly declare that my contribution to this work was:

- Development of the methods for the analysis of electrochemical detection of DNA damage (ED).
- Conducting the experimental work and interpretation of the ED results.
- Participating in original draft preparation (assistance in description of the ED results).

Marta Ligaj

.....
Signature

INSTITUTE OF BIOORGANIC CHEMISTRY
Polish Academy of Sciences

Noskowskiego 12/14, 61-704 Poznań
tel.: +48 61 852 85 03, secretariat +48 61 852 89 19
fax: +48 61 852 05 32, e-mail: ibch@ibch.poznan.pl
REGON 000849327 VAT no. PL 7770002062
http://www.ibch.poznan.pl

Dr hab. Magdalena Łuczak prof. ICHB

Institute of Bioorganic Chemistry

Polish Academy of Sciences

email: magdalu@ibch.poznan.pl

March 31, 2023

Declaration of co-authorship

As the co-author of the following publication:

P4. A. Pacholak, J. Żur-Pińska, A. Piński, Q. A. Nguyen, M. Ligaj, M. Łuczak, L. D. Nghiem, E. Kaczorek, *Potential negative effect of long-term exposure to nitrofurans on bacteria isolated from wastewater,* Science of the Total Environment 872 (2023a) 162199, doi:10.1016/j.scitotenv.2023.162199

I solemnly declare that my contribution to this work was:

- Development of the methods for the metabolomic analysis (MA).
- Conducting the experimental work and statistical analysis of tge MA results.
- Verification of the original draft.

Magdalena Łuczak

Signed by Magdalena Łuczak

March 31, 2023

Prof. Long Duc Nghiem
Centre for Technology in Water and Wastewater
School of Civil and Environmental Engineering
University of Technology Sydney, New South Wales, Australia
email: DucLong.Nghiem@uts.edu.au

Declaration of co-authorship

As the co-author of the following publication:

P4. A. Pacholak, J. Żur-Pińska, A. Piński, Q. A. Nguyen, M. Ligaj, M. Łuczak, L. D. Nghiem, E. Kaczorek, *Potential negative effect of long-term exposure to nitrofurans on bacteria isolated from wastewater,* Science of the Total Environment 872 (2023a) 162199, doi:10.1016/j.scitotenv.2023.162199

I solemnly declare that my contribution to this work was:

- Supervising the research progress.
- Review and editing of the original draft and responses to reviewers comments.

Signature

UTS UNIVERSITY OF TECHNOLOGY SYDNEY

March 31, 2023

Dr Quynh Anh Nguyen
Centre for Technology in Water and Wastewater
School of Civil and Environmental Engineering
University of Technology Sydney, New South Wales, Australia
email: quynhanh.bio.hust@gmail.com

Declaration of co-authorship

As the co-author of the following publication:

P4. A. Pacholak, J. Żur-Pińska, A. Piński, Q. A. Nguyen, M. Ligaj, M. Łuczak, L. D. Nghiem, E. Kaczorek, *Potential negative effect of long-term exposure to nitrofurans on bacteria isolated from wastewater,* Science of the Total Environment 872 (2023a) 162199, doi:10.1016/j.scitotenv.2023.162199

I solemnly declare that my contribution to this work was:

- Assistance in data curation.
- Assistance in review and editing of the original draft.

Signature

UNIVERSITY OF SILESIA
IN KATOWICE

March 31, 2023

Dr Artur Piński, e-mail: artur.pinski@us.edu.pl

Plant Cytogenetics and Molecular Biology Group

Institute of Biology, Biotechnology and Environmental Protection

Faculty of Natural Sciences, University of Silesia in Katowice

28 Jagiellonska Street, 40-032 Katowice, Poland

Declaration of co-authorship

As the co-author of the following publication:

P4. A. Pacholak, J. Żur-Pińska, A. Piński, Q. A. Nguyen, M. Ligaj, M. Łuczak, L. D. Nghiem, E. Kaczorek, *Potential negative effect of long-term exposure to nitrofurans on bacteria isolated from wastewater*, Science of the Total Environment 872 (2023a) 162199, doi:10.1016/j.scitotenv.2023.162199

I solemnly declare that my contribution to this work was:

- Conducting the analysis of data (bacterial genome sequencing, phylogenetic analysis, and secondary metabolite gene clusters prediction)
- Assistance in original draft preparation, review, and editing.

Signed by / Podpisano przez:
Artur Piński
Uniwersytet Śląski w Katowicach
Date / Data:
2023-04-01 22:44

Artur Piński, e-mail: artur.pinski@us.edu.pl
Plant Cytogenetics and Molecular Biology Group
Institute of Biology, Biotechnology and Environmental Protection
Faculty of Natural Sciences, University of Silesia in Katowice
28 Jagiellonska Street, 40-032 Katowice, Poland

POLITECHNIKA POZNAŃSKA

Wojciech Smułek, PhD
Assistant Professor
Institute of Chemcial Technology and Engineering
Faculty of Chemical Technology, Poznan University of Technology
ul. Berdychowo 4, 60-965 Poznań, Poland, Phone: +48 61 665 3671,
e-mail: wojciech.smulek@put.poznan.pl

March 31, 2023

Declaration of co-authorship

As the co-author of the following publication:

P1. A. Pacholak, W. Smułek, A. Zgoła-Grześkowiak, E. Kaczorek, *Nitrofurantoin – microbial degradation and interactions with environmental bacterial strains*, International Journal of Environmental Research and Public Health 16 (2019) 1526, doi:10.3390/ijerph16091526

I solemnly declare that my contribution to this work was:

- Participation in planning the research concept.
- Formal analysis and interpretation of the results (biochemical profile and kinetic calculations).
- Assistance in original draft preparation, review, and editing.

Wojciech Smułek

.....

Signature

POLITECHNIKA POZNAŃSKA

dr hab. inż. Agnieszka Zgoła-Grześkowiak, prof. PP
WYDZIAŁ TECHNOLOGII CHEMICZNEJ
ul. Berdychowo 4, 60-965 Poznań, tel. +48 61 665 2351, -2352, fax +48 61 665 2852
e-mail: office_dctf@put.poznan.pl, www.fct.put.poznan.pl

Poznań, March 31, 2023

Declaration of co-authorship

As the co-author of the following publications:

P1. A. Pacholak, W. Smułek, A. Zgoła-Grześkowiak, E. Kaczorek, Nitrofurantoin – microbial degradation and interactions with environmental bacterial strains, International Journal of Environmental Research and Public Health 16 (2019) 1526, doi:10.3390/ijerph16091526

P3. A. Pacholak, A. Zgoła-Grześkowiak, E. Kaczorek, Dynamics of microbial communities during biotransformation of nitrofurantoin, Environmental Research 2016 (2023) 114531, doi:10.1016/j.envres.2022.114531

P5. A. Pacholak, W. Juzwa, A. Zgoła-Grześkowiak, E. Kaczorek, Multi-faceted analysis of bacterial transformation of nitrofurantoin, Science of the Total Environment 874 (2023b) 162422, doi:10.1016/j.scitotenv.2023.162422

I solemnly declare that my contribution to these works was:

- Development of the methods for the LC-MS/MS analysis.
- Conducting the experimental work and participating in interpretation of the results related to the LC-MS/MS analysis.
- Assistance in manuscript review and editing.

A. Zgoła-Grześkowiak

Signature

Biotechnology Centre

Assistant Professor
Joanna Żur-Pińska, PhD

Gliwice 06.04.2023

Declaration of co-authorship

As the co-author of the following publication:

P4. A. Pacholak, J. Żur-Pińska, A. Piński, Q. A. Nguyen, M. Ligaj, M. Łuczak, L. D. Nghiem, E. Kaczorek, *Potential negative effect of long-term exposure to nitrofurans on bacteria isolated from wastewater,* Science of the Total Environment 872 (2023a) 162199, doi:10.1016/j.scitotenv.2023.162199

I solemnly declare that my contribution to this work was:

- Conducting the experimental work and participating in interpretation of the following results: lipid peroxidation (LPX), superoxide dismutase inhibition rate (SOD), and catalase activity (CAT).
- Participating in original draft preparation (assistance in description of LPX, SOD, and CAT results).

Signed by / Podpisano przez:
Joanna Paulina Żur-Pińska
Date / Data: 2023-04-06 09:31

Silesian University of Technology
Biotechnology Centre

Akademicka 7, 44-100 Gliwice
+48 32 123 45 67 / +48 123 456 789
joanna.zur-pinska@polsl.pl

NIP PL631 020 07 36

Wydział Architektury Politechniki Śląskiej

Copyrights
(publications P2, P4, and P5)

Dear Amanda Pacholak,

Thank you for contacting us.

As an Elsevier journal author, you retain the right to Include the article in a thesis or dissertation (provided that this is not to be published commercially) whether in full or in part, subject to proper acknowledgment; see https://www.elsevier.com/about/policies/copyright for more information. As this is a retained right, no written permission from Elsevier is necessary.

As outlined in our permissions licenses, this extends to the posting to your university's digital repository of the thesis provided that if you include the published journal article (PJA) version, it is embedded in your thesis only and not separately downloadable.

Thank you.

Kind regards,

Thomas Rexson Yesudoss
Copyrights Specialist
ELSEVIER | HCM - Health Content Management

Visit Elsevier Permissions